UNIVERSITA' DEGLI STUDI DI
NAPOLI FEDERICO II

Scuola Politecnica e delle Scienze di Base
Department of Industrial Engineering - Aerospace Division

Doctoral Thesis in Industrial Engineering

Efficient Gas Turbine Modeling for Low Emission Aircraft Preliminary Design Workflows

March 2022

Supervisor
Prof. Fabrizio Nicolosi

Coordinator
Prof. Michele Grassi

Author
Mario Di Stasio
DR993533

Declaration of Authorship

I, Mario Di Stasio, declare that this thesis, titled "Efficient Gas Turbine Engine Modeling for Low Emission Aircraft Preliminary Design Workflows" and the work presented in it are my own. I confirm that:

- This work was done wholly or mainly while in candidature for research degree at this University.
- Where any part of this thesis has previously been submitted for a degree or any other qualification at this University or any other institution, this has been clearly stated.
- Where I have consulted the published work of others, this is always clearly attributed.
- Where I have quoted from the work of others, the source is always given. With the exception of such quotations, this thesis is entirely my own work.
- I have acknowledged all main source of help.
- Where the thesis is based on work done by myself jointly with others, I have made clear exactly what was done by others and what I have contributed myself.

Date: 10^{th} March 2022
Sign: 

Abstract

A major issue, which has prevented aircraft manufacturers from implementing efficient and cost-effective design processes, is the loose integration of engine models into iterative aircraft design workflows.
Modern civil transport aircraft involve several subsystems which are designed, in general, to have the lowest possible weight and the highest possible energy efficiency, so as to minimize their impact on the overall aircraft performance. This same criterion applies to the powerplant system of a modern aircraft, which needs to be specifically designed and built, to meet all the necessary requirements and constraints in terms of performance (thrust and fuel consumption), emissions, noise and costs.
Actually, an effective integration between the design of the aircraft and that of the engines is something which has started to be radically implemented only in recent years. Traditionally, the design of a new aircraft has always been decoupled from the engine design. Even for supersonic military applications, for which the matching between the two designs represents a crucial aspect, an integrated approach supported by dedicated tools has started to be adopted only from the 1990s. For civil transport aircraft, this radical change in the overall design process has been effectively put into practice only for the latest development programs, such as the ones for the Boeing 787 or the Bombardier C Series (now Airbus A220), during which the engine manufacturers, Rolls-Royce/GE and Pratt & Whitney respectively, have been directly involved in the overall design process of the aircraft since the earliest stages.
Based on these observations, the work described in this thesis addresses the following research question:

How to improve preliminary design workflows focused on the optimization of low-emission aircraft by including detailed effects related to changes to the propulsion system?

In order to enable a radical change, aircraft designers should be supported by dedicated tools, allowing to easily and promptly perform, even at conceptual and preliminary design stages, trade-off studies involving information related to the behaviour of the powerplant system in terms of performance, emissions, dry mass, main dimensions, environmental noise, and costs, by linking these changes to key engine design parameters, such as the overall pressure ratio, the bypass ratio, and the burner exit temperature. This type of approach, from one side, would allow aircraft designers to have, since from early design stages, more precise figures on the powerplant, significantly increasing the number and the quality of information available on the aircraft-engine integration process. On the other side, aircraft designers would be allowed to provide important indications to engine designers on which set of design input variables should grant the matching of aircraft requirements, while minimizing mission fuel burn, emissions, noise, or costs.
The generation of a tool with these characteristics, supporting aircraft preliminary de-

sign phases, was the main objective of the collaboration between UNINA and MTU Aero Engines AG for a three-month internship, involving the author of this thesis and engine design experts from MTU. This work was carried out within the context of the Clean Sky 2 project ADORNO (call H2020-CS2-CFP07-2017-02, project number 821043).
The activities related to the tasks of ADORNO served as proving ground of the capabilities in terms of powerplant system modelling of JPAD, a preliminary aircraft design tool designed at UNINA, in whose development the author of this thesis was directly involved. Observations on the gaps and on the margins for improvement related to the implemented modelling of the powerplant characteristics, that emerged during the execution of the project tasks, motivated even further the need for a new tool accounting specifically for the engine.
For this reason, the first section of this thesis is dedicated to the description of the activities carried out by the author for ADORNO. A second section is dedicated to illustrating the work performed for GENESIS, another Clean Sky 2 project (call H2020-CS2-CFP11-2020-01, project number 101007968), for which the author had the possibility to set up a first version of this new tool for preliminary engine design, specifically dedicated to turboprop engines. A detailed description of the implemented methodology is provided in this section. The last chapter of this thesis is dedicated to a generalization of the previously mentioned methodology for preliminary design to the case of turbofan engines, and to a description of its implementation in JPAD. Finally, several examples of application are provided, for an aircraft similar to the Airbus A320neo.

Contents

Nomenclature **xxvi**

1 Introduction **1**

1.1 Identification of the issue 1

1.2 State-of-the-art 9

1.3 Scope of this work and thesis structure 13

2 The experience in ADORNO **15**

2.1 JPAD: a tool for preliminary A/C design 19

2.1.1 The core of the JPAD framework 22

2.1.2 JPAD tools for pre-design and sizing 37

2.1.3 JPAD-*doe* analysis module 38

2.1.4 JPAD module for optimizations 40

2.2 ATTILA++: a tool for preliminary A/C noise analyses 41

2.2.1 Implemented methodologies 42

2.2.2 Implemented noise metrics 47

2.2.3 Input files 47

2.3 ADORNO A/C design activities (WP2) 48

2.3.1 Definition of the set of TLAR 49

2.3.2 Design of the reference A/C model 50

2.3.3 Definition of the set of advanced airframe technologies 65

2.3.4 Design of the advanced turbofan engine model 74

2.3.5 Design of the target A/C model 77

2.4 ADORNO trade factor analyses (WP4) 94

2.4.1 Generation of the set of reference A/C models 94

2.4.2 Description and analysis of the aircraft set 98
2.5 Lessons learnt 105

3 The experience in GENESIS **108**
3.1 Introduction 109
3.2 Methodology 111
3.2.1 Pressure ratios 114
3.2.2 Polytropic efficiencies and basic gas path modelling 114
3.2.3 Cooling air requirements 122
3.2.4 Miscellaneous input variables 125
3.2.5 Dry mass calculation 127
3.2.6 Main dimensions estimation 127
3.2.7 Costs-related estimations 129
3.2.8 Engine limitations 130
3.2.9 Emissions 131
3.2.10 Alternative fuels 132
3.3 Validation 134
3.4 Short-term scenario analysis 136
3.5 Surrogate model and implementation 143
3.6 Conclusions 146

4 Turbofan engine rubberization **149**
4.1 Methodology 150
4.1.1 Pressure ratios 155
4.1.2 Polytropic efficiencies and basic gas path modelling 157
4.1.3 Cooling air requirements 159
4.1.4 Miscellaneous input variables 165
4.1.5 Dry mass calculation 166
4.1.6 Main dimensions estimation 170
4.1.7 Costs-related estimations 171
4.1.8 Engine limitations 171
4.1.9 Emissions 172
4.1.10 Noise 173

4.2 Validation and testing . . . 175
4.2.1 Validation against existing engines data . . . 175
4.2.2 In-depth analysis of effects . . . 181
4.3 Implementation . . . 183
4.3.1 Surrogate model generation . . . 183
4.3.2 Integration in JPAD . . . 185
4.4 Aircraft-integrated tests . . . 189
4.4.1 A320neo-like aircraft model application . . . 189
4.4.2 Advanced A320-like aircraft model applications . . . 197

5 Conclusion **209**
5.1 Recap on the work performed . . . 209
5.2 Considerations and outlook . . . 211

6 Appendix **215**
6.1 Turbofan rubber model in-depth analysis . . . 215

List of Figures

1.1 Future projection on global warming with respect to pre-industrial levels. The shaded area represents uncertainty of the estimation related to the past 30-year average on climate data. The yellow line shows the 1.5 °C upper boundary set out in the Paris agreement [123]. Plot generated with the *Global temperature trend monitor* application, freely available at [64]. . 2

1.2 Passenger transport and global temperature (due to the aviation sector) changes for four different perspectives, including the effect of COVID-19: business-as-usual future technological improvement (BAU), short COVID-19 recovery (3 years), long recovery (15 years), long recovery and behavioural changes (e.g., web conferences instead of face-to-face meetings). Adapted from [77]. 3

1.3 IATA infographic on evolutionary and revolutionary aircraft technologies. Taken from [88] and adapted by IATA on data included in [23]. 5

1.4 Evolution of engine thermal, η_{th}, propulsive, η_{pr}, and overall, η_{o}, efficiencies. Adapted from [166]. 6

2.1 JPAD modules hierarchy 20

2.2 JPAD-*core* set of calculation modules and dependencies. 23

2.3 JPAD complete analysis loop. 24

2.4 JPAD nacelle parameterization 25

2.5 JPAD engine performance deck example: high BPR turbofan engine, Cruise rating. 32

2.6 Complete set of mission phases handled by JPAD for the performance analysis of a civil transport aircraft. 36

2.7 JPAD statistical pre-design tool workflow. 37

2.8 JPAD-*initializer* complete workflow. 39
2.9 JPAD-*doe* module usage example. 40
2.10 Certification points prescribed by ICAO, image taken from [143]. 42
2.11 ATTILA++ main architecture and typical analysis workflow. 43
2.12 Sketch of the set of parameters (angles and distances) taken into account by the airframe noise method of [173]. Image taken from [173]. 44
2.13 Example of ATTILA++ input engine file formatting. 46
2.14 A220-300 front and side view, taken from [18]. 49
2.15 Mission profile for the UM aircraft configurations of ADORNO, based on the set of selected TLAR in terms of speeds, altitudes, durations, and ranges per mission phases. 53
2.16 Class-I weights pie chart for the UM statistical configuration, based on Breguet's equations and statistical OEW-MTOW relationship. 54
2.17 Sizing limitations and sizing point selection for the UM baseline A/C model. 56
2.18 Tail planes geometry and position update loop implemented by JPAD-*doe* module. 57
2.19 Static thrust update process implemented by JPAD multidisciplinary analysis cycle. Objectives: cruise Mach number, take-off field length, and initial cruise service ceiling. 58
2.20 Static thrust update process implemented by JPAD multidisciplinary analysis cycle. Objectives: cruise Mach number and take-off field length. . . . 59
2.21 Flowchart of the process used to assess the best possible variation range of each design variable. 59
2.22 Block fuel and EPNL percent variations with respect to baseline UM A/C model values, accounting to modifications to the wing planform area, aspect ratio, leading edge sweep angle and longitudinal position. 61
2.23 Set of Pareto fronts coming from the MDAO process carried out on the reference UM A/C model. Percentage variations reported in the columns collecting the results of the optimization algorithms are referred to the baseline A/C model resulting from the preliminary sizing activities. 63
2.24 Optimum reference UM A/C model three-view and 3D model. 66
2.25 Comparison between the initial aircraft model and the updated one, allowing to equip the new powerplant system. 78

2.26 MDAO workflow adopted for the single-objective optimizations on fuel burn of the 336 different advanced airframe technologies combinations, considered for the design process of the target UM A/C model. 82
2.27 Summary of the first step to the definition of the UM target A/C model. The light blue boxes represent the workflow implemented for each single set of constraints. 83
2.28 Results of the optimizations carried out with constraints on both the maximum wing span and ACT availability. Minimum block fuel, minimum total DOC and balanced solutions are highlighted and compared with the baseline. 86
2.29 Results of the optimizations carried out with a constraint on the maximum wing span, with an ACT housed in the lower deck of the fuselage. Minimum block fuel, minimum total DOC and balanced solutions are highlighted and compared with the baseline. 86
2.30 Results of the optimizations carried out with no constraint on the maximum allowable wing span, but with no ACT housed in the lower deck of the fuselage. Minimum block fuel, minimum total DOC and balanced solutions are highlighted and compared with the baseline. 87
2.31 Results of the optimizations carried out with no constraint on the maximum allowable wing span and housing an ACT in the lower deck. Minimum block fuel, minimum total DOC and balanced solutions are highlighted and compared with the baseline. 87
2.32 Comparison between minimum block fuel, minimum total DOC and balanced solutions per optimization constraints permutation, also compared with respect to the baseline. 88
2.33 Geometric characteristics in terms of fuel burn optimization design variables of the minimum block fuel, minimum total DOC and balanced solutions, considering the four different sets of constraints. 88
2.34 Optimum target UM A/C model three-view and 3D model. 93
2.35 Cumulative and individual effects of advanced airframe technologies, powerplant system, and geometry modifications on the overall mission fuel burn and CO_2 emissions, based on results summarized in table 2.40 95

2.36 Cumulative and individual effects of advanced airframe technologies, powerplant system, and geometry modifications on the NO_x emissions, based on results summarized in table 2.40 95
2.37 Set of steps for the generation of the response surfaces to be used for the optimization of the A/C models equipped with the BPR 10 and BPR 12 engines. 99
2.38 Set of steps and assumptions of the optimizations on block fuel for the design of the A/C models equipped with the BPR 10 and BPR 12 engines. 99
2.39 Response surface for the optimization of the A/C model equipped with the BPR 10 advanced engine. 103
2.40 Response surface for the optimization of the A/C model equipped with the BPR 12 advanced engine. 103
2.41 Response surface for the optimization of the A/C model equipped with the BPR 13.4 advanced engine. 103
2.42 Nacelle zero-lift drag coefficient growth with increasing engine BPR, for the MDAO process performed on the set of advanced HBPR engines provided for ADORNO WP4. 104
2.43 Engine main parameters and A/C total fuel burn percentage variations with respect to engine BPR, assuming values for the BPR 10 engine and the related optimized A/C model as the references. 104

3.1 Pratt & Whitney PW127 engine configuration. Image taken and adapted from [54]. 112
3.2 Radial compressors polytropic efficiency versus non-dimensional specific speed and technology level. Chart taken and adapted from [181]. 116
3.3 Radial compressors polytropic efficiency EIS correction. Chart taken and adapted from [78]. 116
3.4 HP turbine normalized polytropic efficiency versus mean stage loading and technology level. Adapted from [78]. 118
3.5 LP and free turbine normalized polytropic efficiency versus mean stage loading and technology level. Adapted from [78]. 119
3.6 HP turbine EIS correction for the calculation of the polytropic efficiency. Adapted from [78]. 119

3.7 LP and free turbine EIS correction for the calculation of the polytropic efficiency. Adapted from [78]. 119
3.8 HP turbine relative cooling air correction for the calculation of the polytropic efficiency. Adapted from [78]. 120
3.9 Series of steps implemented in the GasTurb rubber engine model allowing to perform a basic modelling of the flow path (from the combustion chamber onward). 121
3.10 Visual representation of the set of geometrical parameters required for the basic modelling of the gas turbine flow path. 122
3.11 Burner efficiency versus entry into service, according to [117] and to the elaborated extrapolation. 126
3.12 Engine dry mass linear regression law with respect to entry mass flow rate. 128
3.13 Engine overall length linear regression with respect to take-off shaft power. 128
3.14 SFC contour plot for f_{tech} equal to 0.4 and conventional kerosene, resulting from the example parametric analysis carried out for the short-term scenario. 139
3.15 SFC contour plot for f_{tech} equal to 0.4 and 50 % biofuel blending ratio, resulting from the example parametric analysis carried out for the short-term scenario. 139
3.16 SFC contour plot for f_{tech} equal to 0.4 and 100 % biofuel blending ratio, resulting from the example parametric analysis carried out for the short-term scenario. 140
3.17 Dry mass contour plot for f_{tech} equal to 0.4 and conventional kerosene, resulting from the example parametric analysis carried out for the short-term scenario. 140
3.18 Engine maximum diameter contour plot for f_{tech} equal to 0.4 and conventional kerosene, resulting from the example parametric analysis carried out for the short-term scenario. 141
3.19 Production costs contour plot for f_{tech} equal to 0.4 and conventional kerosene, resulting from the example parametric analysis carried out for the short-term scenario. 141
3.20 SFC contour plot for f_{tech} equal to 0.6 and conventional kerosene, resulting from the example parametric analysis carried out for the short-term scenario. 142

3.21 Set of steps elaborated for the development of a new tool for the rubberization of gas turbine engines for turboprop applications. 148

4.1 Set of steps elaborated for the development of a new tool for the rubberization of specific turbofan configurations. 151
4.2 Schematic cross section of the CFM International LEAP-1A turbofan model. 153
4.3 HPC single-stage pressure ratio as a function of EIS, adapted from data included in [78]. 156
4.4 Fan normalized polytropic efficiency as a function of the outer fan pressure ratio and technology level, adapted from data included in [78]. 159
4.5 Booster normalized polytropic efficiency as a function of the mean stage loading and technology level, adapted from data included in [78]. 159
4.6 HPC normalized polytropic efficiency as a function of the mean stage loading and technology level, adapted from data included in [78]. 160
4.7 Fan normalized polytropic efficiency correction for entry into service, adapted from data included in [78]. 160
4.8 Booster normalized polytropic efficiency correction for entry into service, adapted from data included in [78]. 160
4.9 HPC normalized polytropic efficiency correction for entry into service, adapted from data included in [78]. 161
4.10 Fan corrected tip speed as a function of fan outer pressure ratio, adapted from data included in [78]. The intermediate curve (120 %) was selected for the turbofan rubber engine model. 161
4.11 Implemented models for hot and cold nozzle thrust coefficients with respect to nozzle pressure ratio, adapted from [161]. 167
4.12 Implemented models for hot and cold nozzle discharge coefficients with respect to nozzle pressure ratio, adapted from [161]. 167
4.13 Results obtained from the application of equation 4.11 assuming the usage of advanced materials and two different values of core entry mass flow rate. 169
4.14 Set of calibration laws with respect to design/off-design thrust ratio for fan temperature rise, fan rotational speed, and engine entry mass flow rate, for a simplified estimation of fan noise at certification conditions. . . 174

4.15 Set of calibration laws with respect to off-design throttle setting for fan temperature rise, fan rotational speed, and engine entry mass flow rate, for a simplified estimation of fan noise at certification conditions. 175
4.16 Specific fuel consumption of a turbofan engine at cruise condition for constant propulsive efficiency. Adapted from [103]. 182
4.17 Three-view and 3D model of the A320neo-like aircraft modelled with JPAD for the test analyses of the surrogate engine model. 191
4.18 Total CO_2 emissions percentage variations for the application example on the A320neo-like model. Percentage variations refer to aircraft models equipped with engines with different BPRs, assuming the BPR 8 A/C model as the reference. 198
4.19 Comparison of the main characteristics of the engines used in the parametric study on BPR performed on the A320neo-like A/C model. Percentage variations are evaluated with respect to the characteristics of the engine with BPR equal to 8. 199
4.20 Total CO_2 emissions percentage variations for the application example on the advanced A320 (EIS 2030). Percentage variations refer to aircraft models equipped with engines with different BPRs, assuming the BPR 9 A/C model as the reference. 201
4.21 Total CO_2 emissions percentage variations for the application example on the advanced A320 (EIS 2040). Percentage variations refer to aircraft models equipped with engines with different BPRs, assuming the BPR 9 A/C model as the reference. 204
4.22 CO_2 emissions percentage variations of the advanced aircraft (both scenarios) equipped with engines with increasing BPR, calculated with respect to the performance of the reference A320neo-like aircraft, equipped with the BPR 11 engine. 207

5.1 Overview on the set of improvements at aircraft analysis level dictated by the integration of a rubberized, surrogate model of a turbofan engine in JPAD. 212
5.2 Generalized approach for the elaboration and the implementation at aircraft design and analysis level of surrogate model of a gas turbine engine. 214

6.1 Effect of design BPR and T_4 on the ToC SFC. Assumptions on remaining input: EIS 2015, OPR 45:1, Mach 0.78, altitude 35000 ft, ToC net thrust 25 kN, T/O EoR net thrust 94.0 kN, overboard bleed 0.0 kg/s, power off-takes 0.0 kW. 215

6.2 Effect of design BPR and T_4 on the fan diameter. Assumptions on remaining input: EIS 2015, OPR 45:1, Mach 0.78, altitude 35000 ft, ToC net thrust 25 kN, T/O EoR net thrust 94.0 kN, overboard bleed 0.0 kg/s, power off-takes 0.0 kW. 216

6.3 Effect of design BPR and T_4 on the engine dry mass. Assumptions on remaining input: EIS 2015, OPR 45:1, Mach 0.78, altitude 35000 ft, ToC net thrust 25 kN, T/O EoR net thrust 94.0 kN, overboard bleed 0.0 kg/s, power off-takes 0.0 kW. 216

6.4 ToC SFC contour map with respect to different combinations of design BPR and T_4, and for a design OPR value equal to 50:1. Compared with figure 6.1 allows to check the effect of OPR on fuel consumption. With regards to the remaining input: EIS 2015, Mach 0.78, altitude 35000 ft, ToC net thrust 25 kN, T/O EoR net thrust 94.0 kN, overboard bleed 0.0 kg/s, power off-takes 0.0 kW. 217

6.5 NO_x EI at ToC contour map with respect to different combinations of design BPR and T_4, and for a design OPR value equal to 45:1. Assumptions on remaining input: EIS 2015, Mach 0.78, altitude 35000 ft, ToC net thrust 25 kN, T/O EoR net thrust 94.0 kN, overboard bleed 0.0 kg/s, power off-takes 0.0 kW. 217

6.6 NO_x EI at ToC contour map with respect to different combinations of design BPR and T_4, and for a design OPR value equal to 50:1. Compared with figure 6.5 allows to check the effect of OPR on NO_x EI. Assumptions on remaining input: EIS 2015, Mach 0.78, altitude 35000 ft, ToC net thrust 25 kN, T/O EoR net thrust 94.0 kN, overboard bleed 0.0 kg/s, power off-takes 0.0 kW. 218

6.7 ToC SFC contours with respect to different combinations of design BPR and T_4, and for three different assumptions on engine EIS. Assumptions on remaining input: OPR 55:1, Mach 0.78, altitude 35000 ft, ToC net thrust 25 kN, T/O EoR net thrust 94.0 kN, overboard bleed 0.0 kg/s, power off-takes 0.0 kW. 218

6.8 Engine dry mass contours with respect to different combinations of design BPR and T_4, and for three different assumptions on engine EIS. Assumptions on remaining input: OPR 55:1, Mach 0.78, altitude 35000 ft, ToC net thrust 25 kN, T/O EoR net thrust 94.0 kN, overboard bleed 0.0 kg/s, power off-takes 0.0 kW. 219

6.9 ToC SFC contours with respect to different combinations of design BPR and T_4, assuming 0.0 kW power off-takes. With regards to the remaining input: EIS 2015, OPR 55:1, Mach 0.78, altitude 35000 ft, ToC net thrust 25 kN, T/O EoR net thrust 94.0 kN, overboard bleed 0.85 kg/s. 219

6.10 ToC SFC contours with respect to different combinations of design BPR and T_4, assuming 60.0 kW power off-takes. With regards to the remaining input: EIS 2015, OPR 55:1, Mach 0.78, altitude 35000 ft, ToC net thrust 25 kN, T/O EoR net thrust 94.0 kN, overboard bleed 0.85 kg/s. 220

6.11 Engine dry mass contours with respect to different combinations of design BPR and T_4, assuming 0.0 kW power off-takes. With regards to the remaining input: EIS 2015, OPR 55:1, Mach 0.78, altitude 35000 ft, ToC net thrust 25 kN, T/O EoR net thrust 94.0 kN, overboard bleed 0.85 kg/s. 220

6.12 Engine dry mass contours with respect to different combinations of design BPR and T_4, assuming 60.0 kW power off-takes. With regards to the remaining input: EIS 2015, OPR 55:1, Mach 0.78, altitude 35000 ft, ToC net thrust 25 kN, T/O EoR net thrust 94.0 kN, overboard bleed 0.85 kg/s. 221

6.13 ToC SFC contours with respect to different combinations of design BPR and T_4, assuming 0.0 kg/s overboard bleed. With regards to the remaining input: EIS 2015, OPR 55:1, Mach 0.78, altitude 35000 ft, ToC net thrust 25 kN, T/O EoR net thrust 94.0 kN, power off-takes 0.0 kW. 221

6.14 ToC SFC contours with respect to different combinations of design BPR and T_4, assuming 0.8 kg/s overboard bleed. With regards to the remaining input: EIS 2015, OPR 55:1, Mach 0.78, altitude 35000 ft, ToC net thrust 25 kN, T/O EoR net thrust 94.0 kN, power off-takes 0.0 kW. 222

6.15 Engine dry mass contours with respect to different combinations of design BPR and T_4, assuming 0.0 kg/s overboard bleed. With regards to the remaining input: EIS 2015, OPR 55:1, Mach 0.78, altitude 35000 ft, ToC net thrust 25 kN, T/O EoR net thrust 94.0 kN, power off-takes 0.0 kW. . 222

6.16 Engine dry mass contours with respect to different combinations of design BPR and T_4, assuming 0.8 kg/s overboard bleed. With regards to the remaining input: EIS 2015, OPR 55:1, Mach 0.78, altitude 35000 ft, ToC net thrust 25 kN, T/O EoR net thrust 94.0 kN, power off-takes 0.0 kW. . 223

6.17 Fan diameter contours with respect to different combinations of design BPR and T_4, assuming 0.0 kg/s overboard bleed. With regards to the remaining input: EIS 2015, OPR 55:1, Mach 0.78, altitude 35000 ft, ToC net thrust 25 kN, T/O EoR net thrust 94.0 kN, power off-takes 0.0 kW. . 223

6.18 Fan diameter contours with respect to different combinations of design BPR and T_4, assuming 0.8 kg/s overboard bleed. With regards to the remaining input: EIS 2015, OPR 55:1, Mach 0.78, altitude 35000 ft, ToC net thrust 25 kN, T/O EoR net thrust 94.0 kN, power off-takes 0.0 kW. . 224

6.19 Engine dry mass contours with respect to different combinations of design BPR and T_4, assuming a DP net thrust equal to 24.0 kN and a T/O EoR net thrust equal to 94.1 kN. With regards to the remaining input: EIS 2015, OPR 55:1, Mach 0.78, altitude 35000 ft, overboard bleed 0.0 kg/s, power off-takes 0.0 kW. 224

6.20 Engine dry mass contours with respect to different combinations of design BPR and T_4, assuming a DP net thrust equal to 26.0 kN and a T/O EoR net thrust equal to 102.0 kN. With regards to the remaining input: EIS 2015, OPR 55:1, Mach 0.78, altitude 35000 ft, overboard bleed 0.0 kg/s, power off-takes 0.0 kW. 225

6.21 Fan diameter contours with respect to different combinations of design BPR and T_4, assuming a DP net thrust equal to 24.0 kN and a T/O EoR net thrust equal to 94.1 kN. With regards to the remaining input: EIS 2015, OPR 55:1, Mach 0.78, altitude 35000 ft, overboard bleed 0.0 kg/s, power off-takes 0.0 kW. 225

6.22 Fan diameter contours with respect to different combinations of design BPR and T_4, assuming a DP net thrust equal to 26.0 kN and a T/O EoR net thrust equal to 102.0 kN. With regards to the remaining input: EIS 2015, OPR 55:1, Mach 0.78, altitude 35000 ft, overboard bleed 0.0 kg/s, power off-takes 0.0 kW. 226

List of Tables

2.1 Hierarchy of aircraft geometry components in JPAD. 25
2.2 JPAD engine parametric model: list of parameters for piston, turboprop and turbofan engines. 26
2.3 JPAD nacelle parametric model. 27
2.4 List of mission phases accounted by the JPAD performance module. . . . 36
2.5 Set of input variables required by the methodology for engine noise described in [177]. 47
2.6 Set of implemented noise metrics in ATTILA++. 48
2.7 Main geometrical characteristics of the Airbus A220-300. 50
2.8 Design weights and fuel capacity of the A220-300. 50
2.9 Airbus A220-300 engine options [13]. 51
2.10 Set of TLAR selected for the ADORNO design activities of WP2. 51
2.11 Class-I weights analysis results for the UM statistical configuration. 52
2.12 Input data for the sizing module deriving from the statistical pre-design activities carried out on the UM configuration. 55
2.13 Design wing loading and thrust loading, together with updated wing area and engine static thrust, for the statistical UM baseline A/C model. . . . 55
2.14 Summary of the set of dependent and independent design variables of the parametric study carried out for the UM reference A/C model. 56
2.15 MDAO problem definition for the design of the UM reference model. . . . 60
2.16 Comparison between optimum solutions of the MDAO process carried out on the reference UM A/C model. 62
2.17 Results of the multidisciplinary analysis carried out on the optimum reference UM model. 63

2.18 List of airframe technologies selected for ADORNO, along with TRL information (as of 2013) and estimated availability [21]. 67
2.19 JPAD advanced airframe technologies manager implemented fudge factors for HLFC. 70
2.20 JPAD advanced airframe technologies manager implemented fudge factors for riblets. 71
2.21 JPAD advanced airframe technologies manager implemented fudge factors for variable camber wing. 71
2.22 JPAD advanced airframe technologies manager implemented fudge factors for OBS architecture. 71
2.23 JPAD advanced airframe technologies manager implemented fudge factors for materials. 72
2.24 Reference values assumed to trim the impact of the adopted airframe technologies. 72
2.25 Final set of calibration factors and effects levels for HLFC. A calibration equal to 1.0 means full estimated effect. 73
2.26 Final set of calibration factors and effects levels for riblets. A calibration equal to 1.0 means full estimated effect. 73
2.27 Final set of calibration factors and effects levels for wing variable camber trailing edge devices. A calibration equal to 1.0 means full estimated effect. 73
2.28 Final set of calibration factors and effects levels for advanced on-board systems architecture effects. A calibration equal to 1.0 means full estimated effect. 74
2.29 Final set of calibration factors and effects levels for advanced materials. A calibration equal to 1.0 means full estimated effect. 74
2.30 Results of the engine SFC trade factor analysis carried out on a rubberized version of the optimized reference UM A/C and provided to MTU. 75
2.31 Results of the engine dry mass trade factor analysis carried out on a rubberized version of the optimized reference UM A/C and provided to MTU. 75
2.32 Advanced engine requirements at different operating conditions and engine ratings. 76

2.33 Characteristics of the advanced GTF engine designed by MTU for ADORNO WP2 applications. 77
2.34 Set of geometrical modifications applied to the reference UM A/C model for the installation of the new engines and for the generation of the baseline A/C model for the MDAO process of the target UM A/C model. 79
2.35 Set of advanced airframe technologies combinations considered in the optimization study leading to the definition of the best possible target UM A/C model. 82
2.36 Minimum block fuel solutions according to the four combinations of optimization constraints. 89
2.37 Minimum total DOC solutions according to the four combinations of optimization constraints. 89
2.38 Balanced solutions (i.e., compromise solutions between minimum block fuel and minimum total DOC) according to the four combinations of optimization constraints. 89
2.39 Comparative table of multidisciplinary analysis results of the optimized reference and target UM A/C models of ADORNO. 91
2.40 Comparative table of the progressive effect of each technology and update to the geometry on the performance and characteristics of the target UM model. 93
2.41 Main characteristics of the three engines delivered by MTU for the activities of WP2 and WP4 of the ADORNO project. Percentage variations of SFC and mass are provided with respect to BPR 10 engine characteristics. 96
2.42 Percentage variations with respect to BPR 10 of main engines characteristics. 96
2.43 Main landing gear leg length (uncompressed) values for the three reference A/C models designed for the WP4 of ADORNO. 98
2.44 Main results of the optimization study for the design of the A/C models equipped with the set of advanced engines provided by MTU. 102
2.45 Percentage variations of main analysis output of the three optimized target A/C models equipped with the set of advanced turbofan engines with respect to the ADORNO reference UM A/C. 102
2.46 Percentage variations of main analysis output with respect to the ADORNO target UM A/C equipped with BPR 10 engines. 102

2.47 Breakdown of the NO_x emissions contributions per phase for the three optimized target A/C models. 105

3.1 List of input variables of the rubber engine model generated for GENESIS project. 111
3.2 Pratt & Whitney PW127E engine data. 112
3.3 Set of operating conditions assumed for the rubber engine design point. . 114
3.4 Assumptions on Mach number and hub-to-tip ratio values at the inlet and outlet sections of the turbines for the scalable engine model of GENESIS. 120
3.5 Maximum limiting temperature assumptions for the calculation of the required amount of cooling air and for the setting of design boundaries, assumed from data reported in [107][189]. 124
3.6 Cooling factor typical values, according to [75], adopted for the definition of a technological trend inside the GasTurb rubber engine model. 125
3.7 Lower and upper boundaries adopted for the modelling of pressure losses and spool mechanical efficiencies of the GasTurb-implemented rubber engine model of GENESIS. 126
3.8 Collected data for the modelling of the burner efficiency. 126
3.9 Dataset used for the generation of the linear regression model for the engine dry mass. Engines data taken from [121]. 127
3.10 Ratios for engine dimensions with respect to LP impeller and power turbine last stage diameter. 129
3.11 Set of mechanical limitations assumed for the analyses of GENESIS. . . . 131
3.12 EI for CO_2, H_2O, and SO_2 according to [62]. 132
3.13 Input values for the LHV and CO_2 EI of the fuels examined for GENESIS. 133
3.14 Set of input data to the rubber engine model for the validation against known performance of the PW127E engine model. 135
3.15 Design point cycle direct output and derived variables for the PW127E engine, using the GasTurb-implemented rubber engine model. 136
3.16 Effect of alternative fuels on the fuel consumption for f_{tech} equal to 0.4, resulting from the example parametric analysis carried out for the short-term scenario. 140

3.17 Obtained values for the main output variables of a gas turbine engine designed for the short-term scenario, assuming a value for the technology factor equal to 0.4 and conventional jet fuel. 142
3.18 Obtained values for the main output variables of a gas turbine engine designed for the short-term scenario, assuming a value for the technology factor equal to 0.6 and conventional jet fuel. 143
3.19 Effect of alternative fuels on the fuel consumption for f_{tech} equal to 0.6, resulting from the example parametric analysis carried out for the short-term scenario. 143
3.20 Set of input variables of the parametric study carried out for the generation of the surrogate engine model for the short-term scenario of GENESIS. . . 144
3.21 Results of the training for the surrogate engine model of the short-term scenario. 146

4.1 LEAP-1A engine model reference data. 153
4.2 Thrust values for different operating conditions assumed for the reference engine variant. 154
4.3 List of design and off-design conditions considered for the definition of the turbofan rubber engine model. 155
4.4 List of input variables selected for the turbofan rubber engine model. . . . 155
4.5 Mach number and hub-to-tip ratio assumptions for the turbomachineries of the GasTurb-implemented rubber engine model. 161
4.6 Coefficients applied for the conversion of cooling air from multi-stage to the equivalent single-stage model of GasTurb. Table adapted from [161]. . 164
4.7 Set of rubber model input variables involved in the parametric study for the estimation of cooling air requirements. 164
4.8 Results of the training for the models for T/O EoR relative cooling air and maximum temperatures. 164
4.9 Input for maximum allowable material temperature and cooling factor of equation 3.12, adopted for the modelling of cooling air requirements. . . . 165
4.10 Constant values of pressure losses adopted for the modelling of the rubber turbofan engine. 166

4.11 Burner pressure ratios of the rubber turbofan model selected for representative EIS. . . . 166
4.12 Set of input variables of the rubber engine involved in the creation of the regression models for weight-related off-design parameters. . . . 169
4.13 Results of the training for the models of BPR, OPR and core entry mass rate at SLS condition, for the application of the selected weight prediction method. . . . 170
4.14 Reference ratios between maximum nacelle fan cowl diameter and fan size, adapted from [150]. . . . 171
4.15 Set of assumptions for the remaining geometric parameters of the nacelle. 171
4.16 Speed limitations assumed for the turbo components of the turbofan engine model. . . . 172
4.17 Maximum allowable temperatures assumed for the modelling of the turbofan engine. . . . 172
4.18 Set of selected main input values of the rubber engine model for the validation against known data and performance of the LEAP-1A engine model. 176
4.19 Design point cycle direct output, off-design variables and derived variables for the LEAP-1A engine, using the GasTurb-implemented rubber engine model. . . . 177
4.20 Main input variables, design point cycle direct output, off-design variables and derived variables for the CFM56-5B4 engine, using the GasTurb-implemented rubber engine model. . . . 179
4.21 Main input variables, design point cycle direct output, off-design variables and derived variables for the CF34-10E engine, using the GasTurb-implemented rubber engine model. . . . 180
4.22 Main input variables, design point cycle direct output, off-design variables and derived variables for the GE90-94B engine, using the GasTurb-implemented rubber engine model. . . . 181
4.23 Set of input variables, with related lower and upper boundary values, adopted for the full-factorial parametric study for the generation of a surrogate model of the rubber engine. . . . 184

4.24 Results of the training for the surrogate turbofan engine model to be implemented in JPAD. Performance and characteristics of regression models for maximum temperatures and weight estimations have been already reported in table 4.8 and in table 4.13, respectively. 185
4.25 List of input parameters required by the surrogate turbofan engine model implemented by JPAD. 188
4.26 Main geometric parameters of the A320neo-like aircraft modelled in JPAD in order to perform test analyses of the surrogate engine model. Data related to the powerplant geometry already included in table 4.19. 190
4.27 Set of assumptions for the design mission of the A320neo-like aircraft model. 193
4.28 Set of assumptions for the estimation of the DOC of the A320neo-like aircraft model analyzed with JPAD. 194
4.29 Results of the multidisciplinary analysis on the A320neo-like aircraft model equipped with the set of engines sized by the surrogate turbofan model and comparison with data from the real aircraft. 195
4.30 Results of the parametric study on engine BPR performed on the A320neo-like aircraft model. 197
4.31 Characteristics of the engines automatically generated with the surrogate turbofan model implemented in JPAD for the application example on the A320neo-like aircraft. 198
4.32 Results of the parametric study on engine BPR performed on the advanced A320 with EIS in 2030. 201
4.33 Characteristics of the engines automatically generated with the surrogate turbofan model implemented in JPAD for the application example on the advanced A320 aircraft with 2030 EIS. 202
4.34 Results of the parametric study on engine BPR performed on the advanced A320 with EIS in 2040. 203
4.35 Characteristics of the engines automatically generated with the surrogate turbofan model implemented in JPAD for the application example on the advanced A320 aircraft with 2040 EIS. 204
4.36 Comparative table of the performance of the best (i.e. minimum fuel burn) aircraft for each investigated time perspective: current level of technology, EIS 2030, and EIS 2040. 207

4.37 Comparative table, in terms of percentage and delta differences, of the performance of the best (i.e. minimum fuel burn) aircraft for each investigated time perspective: current level of technology, EIS 2030, and EIS 2040. 208
4.38 Comparative table of the performance and characteristics of the engines equipped on the best (i.e. minimum fuel burn) aircraft of each investigated time perspective: current level of technology, EIS 2030, and EIS 2040. . . 208
4.39 Comparative table, in terms of percentage differences, of the performance and characteristics of the engines equipped on the best (i.e. minimum fuel burn) aircraft of each investigated time perspective: current level of technology, EIS 2030, and EIS 2040. 208

Nomenclature

The next list describes several symbols and acronyms that will be later used within the body of the document.

Acronyms and abbreviations

A/C	Aircraft
ACT	Auxiliary Central Tank
ADP	Aerodynamic Design Point
AEO	All Engines Operating
APR	Auxiliary Power Reserve
APU	Auxiliary Power Unit
AR	Aspect Ratio
BFL	Balanced Field Length
BPR	Bypass Ratio
BRF	Body Reference Frame
BWB	Blended Wing-Body
CAD	Computer Aided Design
CAS	Calibrated Air Speed
CFD	Computational Fluid Dynamics
CFRP	Carbon Fiber Reinforced Plastic

CG	Center of Gravity
CS2	Clean Sky 2
DLL	Dynamic-Link Library
DOC	Direct Operating Costs
DOE	Design Of Experiments
DP	Design Point
ECS	Environmental Control System
EIS	Entry Into Service
EI	Emission Index
EoL	End of Life
EoR	End of Rotation
EPNL	Effective Perceived Noise Level
FCS	Flight Control System
FE	Finite Element
FI	Flight Idle
FT-SPK	Fischer-Tropsch Synthetic Paraffinic Kerosene
GA	Genetic Algorithms
GI	Ground Idle
GTF	Geared Turbofan
GUI	Graphical User Interface
HBPR	High Bypass Ratio
HEFA-SPK	Hydro-processed Esters and Fatty Acids Synthetic Paraffinic Kerosene
HLFC	Hybrid Laminar Flow Control

HPC	High-Pressure Compressor
HPT	High-Pressure Turbine
HP	High-Pressure
IAS	Indicated Air Speed
IPS	Ice Protection System
ISA	International Standard Atmosphere
IT	Information Technology
JAR	Java Archive
LFL	Landing Field Length
LHV	Lower Heating Value
LPC	Low-Pressure Compressor
LPT	Low-Pressure Turbine
LP	Low-Pressure
MAC	Mean Aerodynamic Chord
MCL	Maximum Climb
MCR	Maximum Cruise
MCT	Maximum Continuous
MDAO	Multidisciplinary Analysis and Optimization
MEA	More-Electric Aircraft
MLW	Maximum Landing Weight
MRW	Maximum Ramp Weight
MTOW	Maximum Take-Off Weight
MTO	Maximum Take-Off

MZFW	Maximum Zero Fuel Weight
NSGA	Non-dominated Sorting Genetic Algorithm
OASPL	Overall Sound Pressure Level
OBS	On-Board Systems
ODE	Ordinary Differential Equation
OEI	One Engine Inoperative
OEW	Operating Empty Weight
OMOPSO	Optimized Multi-Objective Particle Swarm Optimization
OOP	Object-Oriented Programming
OPR	Overall Pressure Ratio
PNLT	Tone-corrected Perceived Noise Level
PNL	Perceived Noise Level
PPS	Powerplant System
PSO	Particle Swarm Optimization
PT	Power Turbine
RMSE	Root-Mean-Square Error
RM	Rear-Mounted (Engines)
RNI	Reynolds Number Index
RPK	Revenue Passenger Kilometer
SAF	Sustainable Aviation Fuel
SAR	Specific Air Range
SEL	Sound Exposure Level
SFC	Specific Fuel Consumption

SHP	Shaft Horse Power
SLS	Sea-Level Static
SL	Sea-Level
SOT	Stator Outlet Temperature
SPD	Shaft Power Delivered
SPK	Synthetic Paraffinic Kerosene
SPL	Sound Pressure Level
SSM	Static Stability Margin
T/O	Take-Off
TLAR	Top-Level Aircraft Requirements
ToC	Top-of-Climb
TOFL	Take-Off Field Length
TRL	Technology Readiness Level
UHBPR	Ultra-High Bypass Ratio
UM	Underwing-Mounted (Engines)
VTOL	Vertical Take-Off and Landing
WP	Work Package

Glossary

ACARE	Advisory Council for Aeronautics Research in Europe, is a public-private partnership between the European Commission and aeronautical industry leaders, launched in 2001 during the Paris Airshow, targeting the improvement of European aeronautical industries both in terms of competitiveness and environmental friendliness.

ADORNO Clean Sky 2 funded project focusing on allowing fast and reliable estimation of aircraft environmental noise and gaseous emissions at different mission phases, through the implementation of a flexible aircraft model which provides requirements for the engine platform in terms of thrusts and offtakes at different power settings and flight conditions.

AEA Association of European Airlines, was an organization (dissolved in 2016) bringing together more than 20 major airlines, working to ensure the growth of the European airline industry.

ATAG Air Transport Action Group, is an independent coalition of aeronautical industries and organisations including partners from all over the world.

ATA Air Transport Association of America, today known as Airlines for America (A4A) is an organization representing major North American airlines.

ATTILA++ Abbreviation of AircrafT noise predicTion IncLuding performAnce (programmed in C++), is the tool for preliminary aircraft noise calculations developed within the context of ADORNO by UNINA and Lead Tech, according to requirements and specifications provided by MTU.

CSJU A public-private partnership between the European Commission and the European aeronautics industry, working to make the achievement of ambitious environmental targets possible. It manages the Clean Sky (CS) and the Clean Sky 2 (CS2) Programmes.

CSV Abbreviation of Comma Separated Values. Is a widely used file format for large data sharing.

DAF UNINA research group focused on the development of new aircraft design methodologies and technologies. The author of this thesis has been part of this research group during his doctoral years.

DLR Deutsches Zentrum fur Luft- und Raumfahrt, is the German national center for research on aerospace, energy and transportation topics. Its headquarter is located in Cologne, but it accounts for approximately thirty research sites distributed throughout Germany.

ECAC Acronym of European Civil Aviation Conference, is an intergovernmental organization established by the ICAO and the Council of Europe, working to ensure flight safety, security and sustainability.

ESDU Acronym of Engineering Science Data Unit, is an engineering organization of the United Kingdom providing methodologies, equations and computer programs covering several engineering branches and disciplines.

FAA Federal Aviation Administration, is an agency of the United States of America in charge of regulating civil aviation, emanating rules for the certification of aircraft and air personnel, setting standards for airports and ruling the air traffic management.

GENESIS Clean Sky 2 funded project focusing on determining the environmental sustainability over the 2025-2055 timeframe of electric aircraft, making use of life-cycle analyses and by taking advantage of prospective analyses on propulsive technologies.

IATA International Air Transport Association, is an association of world's airline founded in 1945 in Havana, contributing to the formulation of industry policies and standards. It currently comprises 290 airlines from more than 100 countries.

ICAO International Civil Aviation Organization, is an agency of the United Nations working on setting the principles and techniques of air navigation, while ensuring flight safety and sustainable growth.

JPAD Abbreviation of Java API for Aircraft Design. It is a new software supporting multidisciplinary preliminary design workflows developed in-house at UNINA.

TCDS Abbreviation of Type Certificate Data Sheet, is a document produced by the the FAA or the EASA, concerning aircraft/engine/propeller characteristics and limitations in terms of weight, airspeed, thrust, etc.

UNINA University of Naples Federico II.

XML Abbreviation of eXtensible Markup Language. Is a markup language that specifies a set of rules which allow to produce documents that can be easily read both by humans and machines.

Symbols

$\Delta\eta_{cool}$ Cooling air polytropic efficiency correction

$\Delta\eta_{EIS}$ EIS polytropic efficiency correction

$\Delta\eta_{RNI}$ Reynolds number polytropic efficiency correction

$\Delta\eta_{size}$ Size polytropic efficiency correction

ΔH Generic turbo component specific work

$\dot{m}$ Generic turbo component entry mass flow rate

$\dot{m}_2$ Engine entry mass flow rate

$\dot{m}_{25}$ HPC entry mass flow rate

$\dot{m}_{cool}$ Cooling air flow

$\dot{m}_{cool}/\dot{m}_{25}$ Relative cooling air flow

$\dot{m}_{cool}^{r,eq}$ Equivalent HPT rotor cooling air

$\dot{m}_{cool}^{s,eq}$ Equivalent HPT stator cooling air

$\dot{m}_{core}$ Engine core entry mass flow rate

$\dot{m}_{corr}$ Generic turbo component corrected entry mass flow rate

$\dot{m}_{r1}^{cool}$ First HPT stage rotor cooling air

$\dot{m}_{r2}^{cool}$ Second HPT stage rotor cooling air

$\dot{m}_{s1}^{cool}$	First HPT stage stator cooling air
$\dot{m}_{s2}^{cool}$	Second HPT stage stator cooling air
η_{cool}	Cooling effectiveness
η_{is}	Generic turbo component isentropic efficiency
η_{pol}	Generic turbo component polytropic efficiency
η_{pol}^{***}	Generic turbo component normalizedpolytropic efficiency
η_{prop}	Propeller efficiency
$\frac{h}{t}$	Generic turbo component hub-to-tip ratio
γ	Gas specific heat capacity ratio
$\left(\frac{V_{18}}{V_8}\right)_{ideal}$	Ideal jet velocity ratio
$\overline{\Psi}$	Mean stage loading
$\overline{U}^2$	Generic turbo component averaged circumferential speed
A_i	Annulus area at the i$^{\text{th}}$ turbo component station
C_F	Nozzle thrust coefficient
C_f	Skin friction coefficient
c_p	Gas specific heat capacity at constant pressure
c_{cool}	Cooling factor
C_{D0}	Zero-lift drag coefficient
C_{D0}^{nac}	Nacelle zero-lift drag coefficient
C_{dev}	Engine development costs
C_{Dis}	Nozzle discharge coefficient
C_D	Drag coefficient
C_L	Lift coefficient

C_{prod}^{1}	Production costs 1st engine
C_{prod}^{375}	Production costs 375th engine
CO	Carbon monoxide
CO_2	Carbon dioxide
D_m	Generic turbo component average diameter
D_{fan}	Fan diameter
D_{in}	Nacelle inlet diameter
D_{in}^{ratio}	Nacelle inlet diameter ratio
$D_{m,i}$	Average turbo component diameter at the ith station
$D_{max,nac}$	Nacelle maximum diameter
D_{out}	Nacelle outlet diameter
D_{out}^{ratio}	Nacelle outlet diameter ratio
D_{prop}	Propeller diameter
e	Oswald factor
f_{cost}	Turboprop gas turbine costs fudge factor
$F_{P\ input}$	Power input factor
F_{slip}	Slip factor
f_{tech}	Technology factor
FF	Nacelle form factor
h	Enthalphy
H_2O	Water
HC	Hydrocarbon
L_{nac}	Nacelle length

M	Mach number
M_{MO}	Maximum operating Mach number
N	Generic rotational speed
N_{blades}	Number of blades of the propeller
n_{stg}	Generic turbo component number of stages
NO_x	Nitrogen oxides
NS	Non-dimensional specific speed
P	Generic total pressure
$P0$	Engine static power
PL	Generic engine pressure loss
PR	Generic turbo component pressure ratio
Re	Reynolds number
S_{NO_x}	NO_x severity index
S_{wing}	Wing planform surface
SO_x	Sulphur oxides
T	Generic total temperature
T/W	Thrust loading
$T0$	Engine static thrust
T_3	HPC exit total temperature
T_3^{EoR}	T/O EoR HPC total exit temperature
$T_{4.1}$	HPT rotor inlet temperature
$T_{4.3}$	LPT inlet temperature (turboprop application)
$T_{4.4}$	HPT exit temperature (turbofan application)

T_{45}^{EoR}	T/O EoR LPT turbine entry temperature (turbofan application)
T_4	Burner exit temperature
T_4^{EoR}	T/O EoR burner exit temperature
T_{CA}	Cooling air total temperature
T_{dev}	Engine development time
T_{HG}	Hot gas total temperature
T_M	Allowable bulk metal temperature
U_{ex}	Exducer tip speed
U_{hub}	Generic turbo component circumferential hub velocity
U_{tip}	Generic turbo component circumferential tip velocity
V_2	Minimum take-off safety speed
V_{stall}	Stall speed
VW	Volumetric inlet flow
W	Generic component weight
W/S	Wing loading
W_{dry}	Engine dry mass
war	Water-to-air ratio
$X_{max,nac}$	Nacelle maximum diameter longitudinal position
$X_{max,nac}^{ratio}$	Nacelle maximum diameter longitudinal position ratio
Z_{out}	Nacelle outlet offset
Z_{out}^{ratio}	Nacelle outlet offset ratio

Chapter 1

Introduction

1.1 Identification of the issue

Environmental issues have become during the last three decades the central topic of many national and international meetings, requiring specific resolutions to be activated in the shortest time possible, in order to effectively contrast the negative impact of human activities on the biophysical environment. The higher life-quality standards achieved from the end of the Second World War onward in most of the Western nations, and the continuous economic growth during the last 20 years of new emerging countries, such as China, India, and Brazil, have determined a severe alteration of our ecosystem. The emission in the atmosphere deriving from human-related activities of large quantities of greenhouse gases, such as carbon dioxide (CO_2), has already provoked a 1.2 °C global warming with respect to pre-industrial levels, which will soon reach (by 2033) 1.5 °C if today's pace will be kept [63], as reported in figure 1.1. Such a value should remain an upper boundary: going higher would mean to trigger even more frequent and harsher natural disasters, with permanent effects on our lives and our habits.
The aviation, as many other modes of transport, is responsible for this climate change. According to [110], the aviation sector accounts for around 2.5 % (according to data estimated in 2018) of global CO_2 emissions. This contribution is higher (raises up to 3.5 %) if non-CO_2 effects on climate are also considered. In fact, the engine of an aircraft does not only emit CO_2, but many other gases and pollutants, such as nitrogen oxides (NO_x), unburnt hydrocarbons (HC), sulphur oxides (SO_x), water vapor (H_2O), and soot. The overall effect of these additional emissions (formation of contrail cirrus, ozone decrease, aerosol-radiation and cloud interactions) is a further increase in the impact of aviation on the global warming [110].
These numbers might seem quite low, and could lead to thinking that focusing on the aviation sector too in order to reduce the overall impact of human-related activities on the climate might not be so relevant. However, air transport has been growing rapidly during the last decades in many countries. As stated in [77], both the total number of flights and the passenger load factor have increasingly grown during last years. Airbus and Boeing predicted, before the COVID pandemic, 4.4 % and 4.6 % average annual growths in revenue passenger kilometer (RPK) for the next decades, respectively. Even the effects of the COVID situation are not expected to drastically impact on these scenarios. As reported in figure 1.2 (which was adapted from [77]), even assuming the most pessimistic scenario in terms of aviation sector recovery from the pandemic, air transport would still be responsible for a large contribution to global warming for the coming years. This is

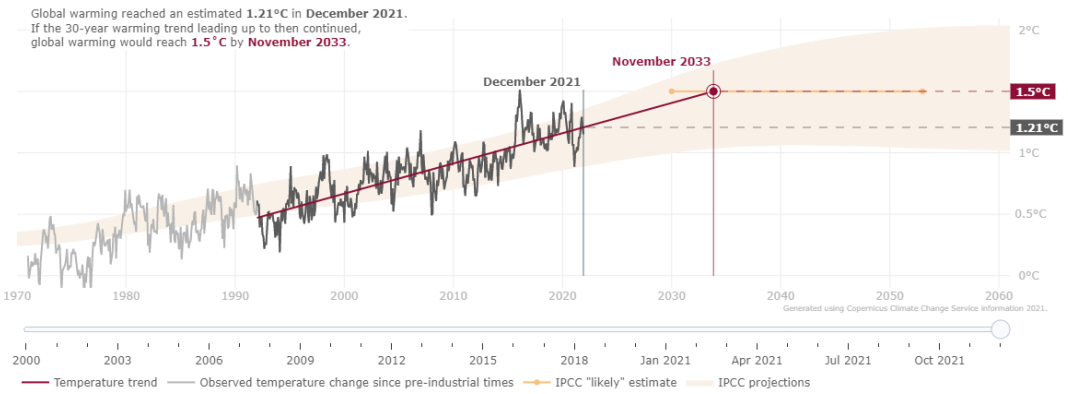

Figure 1.1: Future projection on global warming with respect to pre-industrial levels. The shaded area represents uncertainty of the estimation related to the past 30-year average on climate data. The yellow line shows the 1.5 °C upper boundary set out in the Paris agreement [123]. Plot generated with the *Global temperature trend monitor* application, freely available at [64].

linked to the fact that, as explained in [152], it is particularly difficult to decarbonize the aviation sector. We currently have the technology which is necessary, for example, to drastically reduce the emissions of the power and road transport sectors. While, on the aviation side, we still do not have proven concepts allowing to reach zero, or close to zero, emissions.

The necessity to keep aviation emissions under control has led to the definition, mainly during the last two decades, of several important resolutions, aiming at reducing the environmental footprint of the air transport by fixing precise objectives in terms of CO_2, NO_x, and noise emissions abatement. A brief recap on the main actions and commitments in this sense is provided in the following. Some of these are actually outdated and the latest resolutions are provided at the end.
The Advisory Council for Aeronautics Research in Europe (ACARE) set in 2001 through its Strategic Research Agenda challenging and ambitious environmental objectives for new designed aircraft: 50 % reduction in CO_2 emissions, 80 % cut in terms of NO_x emissions, and 50 % perceived noise abatement by 2020, with respect to 2000 best aircraft models [72]. In 2008, the Air Transport Action Group (ATAG) promoted the establishment of a long-term plan in order to reduce the impact of aviation on the environment [24]. This was the first time that industry leaders of a global transport sector converged towards such a an important commitment. This plan provided actions to be undertaken in three steps over time:

- an average improvement in fuel efficiency of 1.5 % per year from 2009 to 2020;
- a cap on net aviation CO_2 emissions from 2020, implying carbon-neutral growth;
- a reduction in net aviation CO_2 emissions of 50 % by 2050, with respect to 2005 levels.

Also in 2008, the Clean Sky Joint Undertaking (CSJU), a partnership between the European Commission and the European aerospace industry, started the Clean Sky (CS)

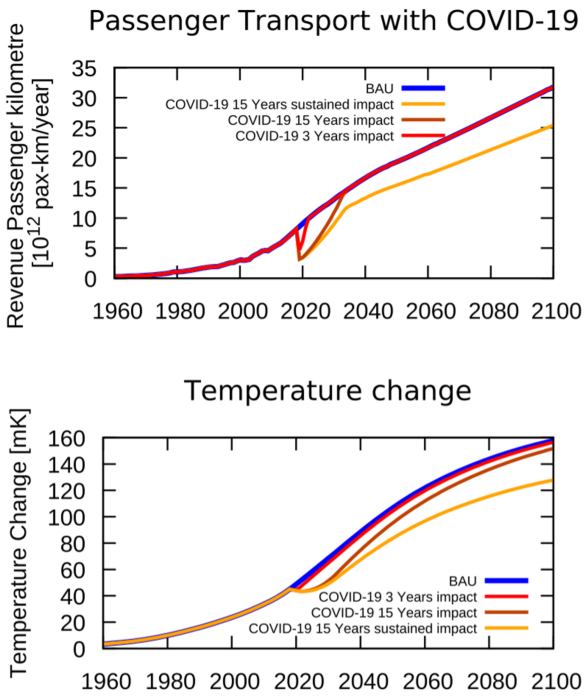

Figure 1.2: Passenger transport and global temperature (due to the aviation sector) changes for four different perspectives, including the effect of COVID-19: business-as-usual future technological improvement (BAU), short COVID-19 recovery (3 years), long recovery (15 years), long recovery and behavioural changes (e.g., web conferences instead of face-to-face meetings). Adapted from [77].

Programme [124], to tackle the ambitious objectives set by ACARE in 2001 and to improve the competitiveness of the European aircraft industry and supply chain at global level. In 2014, following the success of its predecessor, the Clean Sky 2 (CS2) Programme was launched [114] aiming at further accelerating the process towards greener aviation in the 2025-2035 timeframe, through the integration, demonstration and validation of new aircraft technologies, allowing to reduce CO_2, NO_x, and noise emissions by 20 to 30 % with respect to 2014 state-of-the-art aircraft models. These ambitious goals followed the update of the ACARE Strategic Research and Innovation Agenda in 2012, aiming at: -75 % CO_2, -90 % NO_x, and -65 % noise emissions by 2050, with respect to 2000 levels [73].
In order to match these targets, both new airframe and propulsion solutions are required. In 2013, the International Air Transport Association (IATA), together with the contribution of the German Aerospace Center (DLR), produced a Technology Roadmap to 2050 [21][22], providing an overview on all the possible technologies to be implemented in order to achieve the objectives of the ACARE Agenda. These technologies were split in two lists, depending on their technology readiness level (TRL), with revolutionary technologies such as novel aircraft configurations (blended wing-body, truss-braced/strut-braced wing) and advanced propulsion concepts (open rotor engine, hybrid-electric/full-electric aircraft) more likely to be sufficiently mature and applicable for the long-term scenario (2035-2050 timeframe). For the short/medium-term perspective (2015-2035 scenario), evolutionary airframe and engine technologies, such as hybrid laminar flow control (HLFC), riblets, and morphing wing on one side, and advanced high/ultra-high bypass ratio (BPR) turbofans and new engine core concepts on the other, were identified, with the latter assessed to allow for the greatest impact on CO_2 reduction wit respect to a 2015 aircraft: -20 to -25 % from advanced turbofan concepts, -25 to -30 % from new engine core designs (figure 1.3).
In October 2021, IATA further updated its environmental roadmap, by setting as an updated objective the matching of net zero carbon contribution of aviation industry by 2050 [90]. A resolution called Fly Net Zero was passed by IATA members, committing them to achieve this ambitious objective by the half of the 21st century, in accordance with the Paris agreement on keeping global warming below 1.5 °C. On this occasion, IATA also provided an updated version of its vision on the impact of new aircraft technologies [89], which, in terms of new engine solutions for the short/mid-term scenario, reported a further 15 to 25 % fuel efficiency improvement with respect to current levels.

The quantity of CO_2 emissions of an engine is tightly coupled with the fuel burn: a certain reduction in terms of fuel consumed by the engine means the same reduction in terms of CO_2. In order to drastically decrease the specific fuel consumption (SFC), all the latest turbofan developments feature high bypass ratios. The reason for this is linked to the propulsive efficiency of such a configuration: the higher the bypass ratio, the lower the jet velocity and the energy wastage as jet kinetic energy, for a given net thrust. Lower fuel consumption can also be achieved by improving the thermal efficiency of the engine, which in turn depends on the turbine entry temperature, on the overall pressure ratio (OPR), and on the efficiencies of the turbomachineries. The SFC of a turbofan is a function of the product between these two efficiencies, which is the overall efficiency of the engine. Figure 1.4 shows the development over time of these quantities, and how did they allow to achieve today's level of specific fuel consumption.
The increase in engine BPR, however, differently from the core improvements which impact on the thermal efficiency, has several downsides, which need to be adequately

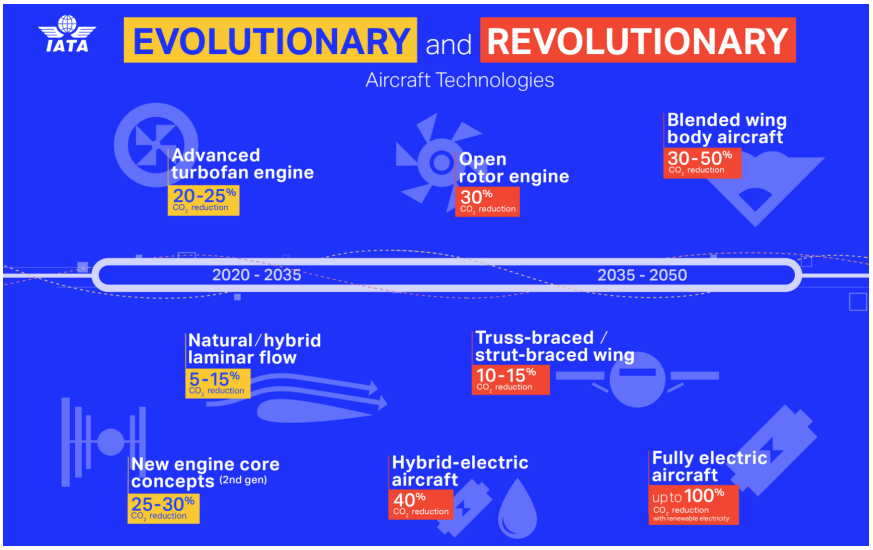

Figure 1.3: IATA infographic on evolutionary and revolutionary aircraft technologies. Taken from [88] and adapted by IATA on data included in [23].

accounted in order to correctly assess the benefit of higher bypass ratios at aircraft level [181]. In fact, an increase in BPR determines, for a fixed core technology and for a selected engine concept:

- A growth of the engine frontal area, due to bigger fan tip diameter and to the consequently bigger nacelle fan cowl maximum diameter. This, of course, negatively affects the drag (both skin friction and form contributions) of the engine nacelle.
- A growth of the dry mass of the engine, and of the powerplant weight as a consequence, which is strictly related to the increased overall size of the motor, and to the necessity to increase the number of low-pressure turbine (LPT) stages, in order to achieve reasonable performance values of this turbo component. This may also represent a manufacturing and installation issue: turbomachineries with a too high number of stages might be difficult to be produced and the tip diameter of the last stage of the LPT could be so big to require specific solutions for the installation and the assembly with the other components of the engine.
- The production cost of the engine generally increases, mainly due to materials costs.

For these reasons, the optimum engine bypass ratio is not something that can be selected arbitrarily by an engine manufacturer. Instead, it should be the result of trade-off analyses performed at aircraft level, allowing to detect which solution best fits a given aircraft platform. This process may also imply, in the conceptual/preliminary design phase of a new aircraft, when the main characteristics and geometric parameters of an airplane are still not precisely determined, changes to the wing (in terms of dihedral angle or relative positioning with respect to the fuselage) or to the landing gear system (by modifications to main and nose landing gear struts length).
More in general, an integrated design approach, such as the one described above, could be always adopted when dealing with the propulsive system of a new aircraft concept. During the conceptual design phase of a hybrid-electric aircraft several levels of hybridization

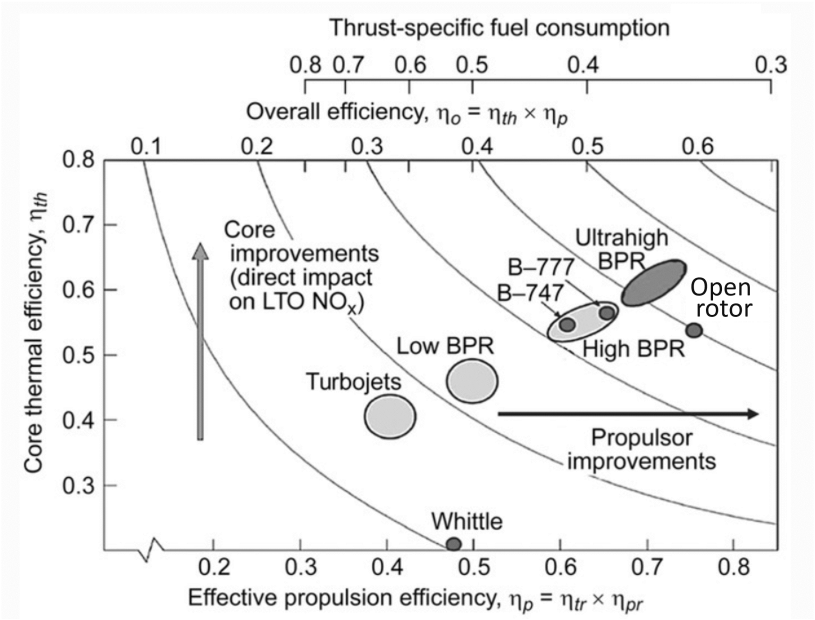

Figure 1.4: Evolution of engine thermal, η_{th}, propulsive, η_{pr}, and overall, η_{o}, efficiencies. Adapted from [166].

are typically investigated, based on technological assumptions and future trends for the performance of batteries and fuel cells [142]. The requirement in terms of gas turbine shaft power at this point is still not precisely set, but it is adjusted during parametric analyses, in order to detect the best promising combinations of conventional and advanced propulsive solutions. Typically, during these studies, the characteristics of the gas turbine in terms of size, weight, and performance are simply scaled based on thrust ratios and semi-empirical calibrations. However, a more systematic approach, including physics-based considerations derived from actual gas turbine performance models would surely lead to more accurate results.
It is evident that in order to match vital objectives in terms of emissions reduction, engine models should be integrated in aircraft design workflows, in order to assess the effective benefits deriving from the adoption of new propulsive systems. However, there are still some gaps in this sense.
In classical aircraft design workflows, reported for example by [167] and [101], the engine is simply selected off-the-shelf during (quite at the end) of the conceptual design phase, allowing to start the parametric analyses of the preliminary design phase, leading to the definition of the main geometric characteristics of the aircraft before the detailed design stage begins. A more contemporary design approach is reported in [168]. Here, three options are provided when dealing with the powerplant during the conceptual/preliminary design phase of a new aircraft:

- A new aircraft design is conceived after that a new powerplant system becomes available. In this case the airframe can be adapted to the new engine by considering minor modifications to its geometry and characteristics, but with little or no margin for optimization.

- An engine is adapted to an already existing airframe by scaling up or down its characteristics in terms of thrust, SFC, size, and weight following indications provided

by the engine manufacturer. In this case the engine is already almost defined, but with more margin for optimization with respect to the previous case.

- Several engine cycles are considered in order to determine the best fitting engine characteristics (in terms of design cycle parameters, including BPR) for a given aircraft platform. In this case the engine manufacturer should provide for each combination of engine parameters a detailed description of the performance, dimensions, and weight, or precise scaling factors with respect to a reference dataset.

This last approach is the closest to the one actually applied during the development programs of modern aircraft such as the Airbus A220 (previously known as Bombardier CS), the Airbus A350 XWB, and the Boeing 787. All these aircraft mount engines with BPR values much higher than those of the previous generation of turbofans, and ranging from 8 to 12. The selection of the definitive engine cycle for these aircraft went through a closer interaction between aircraft and engine design expert, including several iterations on engine characteristics and airframe modifications.
Based on these observations, it is legitimate to ask:

Do modern tools supporting aircraft conceptual and preliminary design activities implement a consistent and effective modelling of the propulsion system? Which characteristics should they include?

In light of the above discussion, the following features are essential for a modern preliminary aircraft design tool aiming at an improved modelling of the gas turbine characteristics and performance:

- It should include a simplified modelling of the most common gas turbine engine configurations for aviation use (such as turbofan and turboprop), allowing to already perform trade-off analyses at conceptual and preliminary design stages involving engine design parameters. These models should be more preferably implemented through a simplified parameterization of the thermodynamic cycle of the engine, in order to encourage the use even by non-experts of engine preliminary and detailed design.

- This simplified modelling should be implemented in a consistent way: the behaviour of the performance of the engine with respect to a certain set of input parameters should reflect the characteristics of a feasible engine cycle. General engine design laws, as well as thermal and mechanical limitations, should be accounted by this simplified model.

- Not only information strictly related to the gas turbine cycle (thrust, power, specific fuel consumption, etc.) are essential. These models should also provide, based on the output of the thermodynamic cycle, important indications on weight and size of the engine. Trade-off analyses at aircraft level would obviously benefit from these information.

- Fuel consumption is tightly related to CO_2 emissions, as recalled before, but this does not apply to all the gaseous emissions of an aircraft engine. An efficient modelling of the behaviour of pollutant species such as NO_x, HC, and CO with respect to engine characteristics and operating conditions would be for sure an added value to a tool for preliminary aircraft design, allowing to perform significant landing and take-off (LTO) cycle analyses at early design stages.

- The ACARE Agenda tackles not only aircraft gaseous emissions. Environmental noise abatement is another fundamental topic to be addressed by aircraft designers shaping tomorrow's aircraft models. The addition of a simplified but effective modelling of the noise spectra of a modern gas turbine engine would be for sure an important bonus to an aircraft design tool, enabling to carry out noise simulations for certification purposes.

- In order to match the important targets set by the aviation environmental agenda, it is necessary to equip the airframe with greener technologies. Some of these technologies, such as HLFC and more-electric aircraft (MEA) concepts, impact directly on the requirements to the engine. Some MEA concepts (such as the one adopted on the Boeing 787 [134]) are bleedless, meaning that no air is extracted from the engine to be delivered to the cabin or to any other external system working with air delivered by the powerplant. This has a positive effect on the fuel consumption and on the weight of the engine. On the opposite side, advanced airframe systems such as HLFC require power to work. If this power is not provided by external generators but is directly taken from the high-pressure compressor of the engines, it is necessary to take into account its effect on the specific fuel consumption. It is clear that for a modern pre-design tool it is not only important to provide a modelling of these advanced airframe solutions in terms of their impact on disciplines such as aerodynamics, weights, off-takes, and direct costs, but it is also necessary that it correctly links these off-takes requirements to the powerplant system.

- Sustainable aviation fuels (SAF) are another available means to reduce emissions. Several biofuels have been already approved and are going to be more widely adopted by civil aviation very soon [147][91][119]. Most of the emissions reduction directly derives from the production process of these drop-in fuels. Moreover, some of them allow both to decrease fuel consumption, thanks to slightly higher fuel heating values (i.e., higher produced energy per unit mass), and to generate less kilograms of CO_2 per kilograms of fuel burn [187]. In order to take into account their effect on the emissions of the aircraft, it is necessary to model their impact at engine cycle level.

- Last but not least, one of the major challenges in the transport sector is to make economic growth compatible with sustainability and environmental constraints. Applying changes to the aircraft in order to match specific environmental objectives impacts negatively on its production costs and on those of its sub components, and the powerplant system is equally affected. Increasing the thermal and the propulsive efficiency of a turbofan engine, for example, has a strong influence on the final production cost. Including in this refined engine model an estimation of the costs of the engine would allow to check whether the beneficial effect on the fuel consumption of a higher overall efficiency allows to counteract the detrimental effect on the aircraft direct operating costs produced by the increased engine price.

All these features require the development of specific methodologies or the collection of already available empirical and semi-empirical approaches from the literature.
The next section provides an overview on the capability in terms of engine modelling and integrated design approach of some of the main and most recent software supporting aircraft conceptual and preliminary design, in order to further highlight the previously mentioned gap and motivate the work carried out for this thesis. An overview on a feasible approach to overcome these issues is also provided.

1.2 State-of-the-art

The last two decades have seen the development of several tools supporting aircraft conceptual and preliminary design workflows. This was caused by the request to analyse during these design phases the highest possible number of different aircraft configurations, in order to ensure the fulfillment of an ever-growing number of certification requirements, environmental constraints, and customer demands. At the same time, the increased calculation capability of modern computers has allowed the development of complex design frameworks supporting multidisciplinary analysis and optimization (MDAO) workflows [169]. The following are the most remarkable examples of this family of tools. For each software, greater emphasis is given on the modelling of the powerplant system and its integration in the aircraft analysis and design work chain.

- **AAA** - AAA [53] stands for Advanced Aircraft Analysis and it is a tool conceived for typical conceptual and preliminary aircraft design tasks and developed by DARcorporation. It supports calculations for all the main disciplines involved in the aircraft design process, from weights to detailed aerodynamics and static stability and control analyses. It is mainly based on the design methodology reported in [153] and developed by Dr. Jan Roskam and Dr. C.T. Lan, but it also incorporates several methods from NACA/NASA, and methods elaborated by DARcorporation engineers, which allow to analyze unconventional configurations such as tilt rotor and tilt wing designs [52]. With regards to powerplant modelling, it provides the possibility to select between several different engine configurations (piston engines, turboprop engines, turbojet engines, turbofan engines, propfan engines) and the impact of different installations (wing-mounted or rear-mounted engines) is well accounted by the other calculation modules. Characteristics of the engines in terms of thrust and fuel consumption for different operating conditions and throttle settings are based on data reported in [153]. The approach included in the same reference for the calculation of installed thrust and power from engine manufacturers data and based on considerations on the effect of the air induction system, of the power extraction (including bleed air), and of the effect of the exhaust nozzle is also implemented by this tool [52][153].

- **FLIGHT** - Developed at the University of Manchester starting from 2006 under the direction of Dr. Antonio Filippone, FLIGHT is a remarkable example of aircraft preliminary analysis tool capable to provide important indications in terms of pollutant emissions and environmental noise estimations [140]. It was specifically designed for fixed-wing aircraft powered by conventional gas turbine engines (turbofan and turboprops), to perform multidisciplinary analyses involving geometric modelling of the external shapes of the aircraft, main components weights estimation, static trim (in air and on the ground) calculations, characterization of the aerodynamics at all flight conditions, propulsion modelling for the gas turbine engines, flight mechanics calculations, and environmental (emissions and noise) analyses [67]. Since it includes a vast database of commercial aircraft and routes, it can be used in order to help air traffic control and airline authorities to determine the best flight paths allowing to minimize the noise footprint of incoming and departing airplanes, as well as to investigate accidents [139]. Dealing with the powerplant and its characteristics, FLIGHT implements the capability to read essential information to carry out aircraft performance and environmental noise analyses from dedicated engine decks. These decks contain

performance charts representing the full envelope of the engine over a large range of atmospheric conditions [67], and are generated by means of a dedicated engine module, for which [68] provides theoretical backgrounds. Essentially, this module relies on basic engine data available from public documents (such as type certificates or data included in emissions databanks) and mainly consisting in thrust ratings, speed limitations, maximum permissible temperatures and fuel flows, to carry out the determination of the design point of the engine as the intersection of constant thrust and constant turbine temperature lines at the nominal engine rotational speed. Then the complete flight envelope is built and stored in the engine deck file. Dealing with pollutant emissions, it allows to perform predictions of LTO cycles for HC, CO, and NO_x pollutant species, as well as an estimation of the total and by segment emissions of CO_2. Moreover, it also allows contrail analyses [67]. For environmental noise estimations, it allows to take into account several individual contributions of engine components, such as the noise generated by the fan, by the compressors, by the combustor, by the turbine, and by the nozzles. The effect of jet-by-jet shielding (i.e., the mutual shielding of two parallel and identical exhaust jets) is accounted as well [67].

- **MICADO** - Developed at the Institute of Aerospace Systems (ILR) of RWTH Aachen University since 2008 and first presented to the public in 2012, MICADO (standing for Multidisciplinary Integrated Conceptual Aircraft Design and Optimization Environment) is a conceptual/preliminary design tool allowing to perform fast and significant assessment and optimization of new aircraft designs [135][17]. One of the key feature of MICADO is to allow a fast preliminary sizing of a new conceptual aircraft starting from the definition of a limited set of top-level aircraft requirements (TLARs) and design specifications. This preliminary sizing can be performed by the tool in an automated way, by following a precise workflow which evaluates the convergence to a satisfactory design (i.e., compliant with user-defined requirements in terms of maximum take-off weight, operating empty mass, etc., and, of course, with the set of TLARs and design specifications) at the end of each aircraft component sizing and multidisciplinary analysis [17]. Moreover, the tool allows to include the effect of advanced airframe technologies such as HLFC during this iterative design cycle, by performing an automatic modelling of the system during the detailed design phase [135][17]. Dealing with the description of the powerplant system, conventional turboprop, turbojet and turbofan engines are modelled by the tool. In order to carry out the performance analysis of the aircraft, an engine deck must be linked to the input file managed by MICADO in order to collect information on the powerplant. This engine deck includes fundamental data dealing with the thrust and the required fuel flow for different operating conditions, but also detailed information on the values of thermodynamic variables (such as total pressures and total temperatures) for each meaningful station of the engine [151][17]. Furthermore, the effect of different overboard bleed and power off-takes requests on the engine thermodynamic cycle and fuel flow is accounted as well [151]. During the sizing loop, the tool is capable to select the most suited engine deck between the ones available in the software database. This deck is then eventually scaled, in order to adequately fit to the sizing point characteristics: a scaling factor depending on the sea-level static (SLS) thrust of the baseline engine, on the estimated maximum take-off weight (MTOW) of the aircraft, and on the thrust-to-weight ratio provided by the sizing point selection, is applied to the deck and to the

geometry of the baseline engine, whereas semi-empirical regression laws are applied in order to determine an updated dry mass too [17]. More recently, in order to enable MICADO to investigate hybrid-electric aircraft concepts, it was equipped with an advanced new module enabling the modelling of the powertrain. With regards to the gas turbine modelling, the same scaling procedure is still applied [17].

- **Piano** - Piano [163] is a professional software developed by UK-based Lissys company since 1990. It is a widely used tool to accomplish preliminary aircraft sizing and performance assessment. Throughout the years, it was adopted by many different users, ranging from airframe and engine manufacturers to aviation research centers and governmental institutions. It features all the basic modules that are necessary to carry out a multidisciplinary analysis of an existing aircraft, or of a new concept: weights, balance, aerodynamics, static stability, performance, emissions, and costs can be all evaluated with the help of this tool. The engine is modelled by Piano as a simple data matrix, providing information in terms of thrust and fuel flow for different operating conditions. The tool provides a database of 30 engines, which can be eventually expanded by the user by providing additional engine files, adequately formatted according to the standard of Piano. These engine data matrices can be eventually scaled if a higher SLS thrust value with respect to the one of the baseline is selected by the user [163]. With regards to gaseous emissions, Piano provides an estimation of NO_x, CO, and HC emitted during the overall mission or during specific flight manoeuvres, based on the model provided by [29], on reference emission indices (EIs) available from public emissions databank released by aviation authorities, and on performance results in terms of fuel flow derived from the engine deck [163].

- **PrADO** - PrADO (Preliminary Aircraft Design and Optimization program) is a framework of tools developed by the Institute of Aircraft Design and Lightweight Structures (IFL) of the Technical University of Braunschweig starting from the late 1980s [146]. It comprises several design sub modules, each dealing with precise tasks, which can be conveniently arranged according to the design, analysis, and optimization workflow to be implemented. Due to its modularity, it can support a wide range of aircraft configurations, and it can also deal with unconventional ones, such as blended wing-body (BWB) aircraft [146][184]. One of the key features of PrADO is the support for finite element (FE) analysis, which can be exploited, for example, to estimate the operating empty weight (OEW) of the aircraft, and to carry out structural, aerodynamic, and aeroelastic analyses [184]. This is an essential feature when investigating unconventional designs, for which there is lack or there is no semi-empirical method available. With regards to engine characteristics implementation, PrADO provides a simplified thermodynamic cycle, which allows to estimate engine thrust and specific fuel consumption as a function of flight altitude and speed. As said in [146], this implemented engine model is *rubberized*, meaning that it scales according to design requirements, but no additional information is available on its actual application. PrADO also features a basic sub module for noise estimations, which, however, is independent of aircraft parameters (it relies on a description of the aircraft spectra that should be provided by the user) and it is only sensitive to the thrust setting [184].

- **SUAVE** - SUAVE (Stanford University Aerospace Vehicle Environment) is an

open-source environment allowing to accomplish design tasks related to both conventional and unconventional aircraft configurations [178]. It is completely written in Python and consists in several collections of classes which can be conveniently used and adapted in order to implement the desired design framework. The most significant feature of SUAVE is to include both low-fidelity and high-fidelity methodologies, with the first allowing to perform design and analysis of conventional configuration, while the second are particularly suited to the investigation of breakthrough designs. The great flexibility in terms of definition of the powerplant system offered by this design environment allows for the modelling of the most diverse propulsive solutions, ranging from conventional turboprop, turbojet and turbofan designs to battery-electric, solar-electric and hybrid systems [112]. The modelling of *energy networks* (this is how powerplant or powerplant components are referred to in SUAVE) is implemented in such a way to support both conventional and unconventional propulsive systems. In order to generate the model for a turbofan engine, for example, the user is required to put together all the necessary components (i.e., inlet, fan, compressors, turbines, combustor, nozzles) by adding them to a generic new instance of the *Turbofan* class of SUAVE, which represents the engine. Each of these components include evaluation methods (one-dimensional flow equations) allowing to compute the energy transfer between one component and the next one [112]. These calculations are based on user-provided values in terms of pressure ratios, efficiencies, and total exit temperature (for the combustor). To perform the sizing of the engines based on the provided cycle characteristics, the user is required to provide the design net thrust (which sets the mass flow rate of the engine at full throttle) as well as design point conditions (Mach number and flight altitude). Once sized, the characteristics of the engine are set (also in terms of specific fuel consumption) and it can be inserted in a generic SUAVE class instance for an aircraft, called *Vehicle*, and used to perform analyses. A typical workflow like this one is described in [179]. With respect to environmental noise, SUAVE implements the model described in [137] in order to estimate the noise produced by the jet of a turbofan engine, comprising the contributions from the core, from the fan exhaust and the from the mixed jet [35].

Chapter 2 provides an overview on an additional aircraft conceptual and preliminary design tool, which saw the author directly involved in the development, together with other colleagues from the University of Naples (UNINA). This in-house built tool was used to carry out design and analysis tasks related to an European research project, dealing with an integrated aircraft-engine design process. The capability of this tool to support such an activity will be highlighted in the next chapter.

A feasible approach to the fulfillment of at least part of the requirements listed in the previous section was provided by [161]. In order to integrate in an ad hoc and simplified aircraft design and optimization framework the design of conventional (high bypass ratio turbofan engine) and unconventional (open rotor) propulsive systems, a methodological approach was elaborated. This approach consisted in the selection of a limited number of essential engine design parameters per engine configuration, and in the implementation in a tool for the simulation of the performance of gas turbine engines of a selected set of engine design laws and update rules, allowing to generate a parametric model of the gas turbine. This scalable model was applied to carry out parametric analyses and to generate design and off-design point results, which were used to train a neural network

and to produce a surrogate model of the engine behaviour in terms of thrust and fuel consumption, depending on basic design characteristics (BPR, core technology level, design point requirements, etc.). Empirical correlations were used in order to account for the effect of these basic design characteristics on the overall size of the nacelle, while the engine weight was assessed through an accurate mapping of the weight of all the turbo components, which in turn required a basic modelling of the gas flow path, including considerations on the diameters, lengths and materials of the turbomachineries. All these models were then integrated in an aircraft design and optimization framework generated specifically for this application. It was tested that such a modelling allowed to efficiently perform aircraft optimizations on fuel burn including changes to both the airframe and the powerplant system

1.3 Scope of this work and thesis structure

The scenario outlined in this chapter underlines the motivations behind this research work:

How to improve preliminary design workflows focused on the optimization of low-emission aircraft by including detailed effects related to changes to the propulsion system?

An answer to this question was already given at the end of section 1.1, where several considerations were provided in light of current and future design scenarios, in which engineers of all the disciplines involved in the aircraft design process are and will be called to include ever-increasing factors and constraints in their analyses.
In order to fill the existing gap on the integration of engine-related considerations in the conceptual and preliminary design process of a new aircraft it is necessary to adopt a new approach. As shown in section 1.2, many current design tools adopt a static or almost static description of the powerplant. In many cases, empirical and semi-empirical scaling laws are applied in order to adapt an existing baseline engine to new aircraft requirements. On the opposite, it would be preferable to enrich a conceptual/preliminary aircraft design tool with a more realistic and reliable sizing of the engine, but without the need to define too many additional input quantities, in order to keep the total number of available parameters down. Moreover, it would be important to always include in this scalable engine model considerations on environmental noise, gaseous emissions, and costs, and linking them to its input and output parameters.
The following chapters aim at providing a description of the possible methodological approach to the fulfillment of all these requirements, and to give practical examples of its application for different typologies of gas turbine engines.
Specifically, this work is structured as follows:

- **Chapter 2** provides a detailed description of the research context from which part of the considerations included in this chapter originated. ADORNO is a Clean Sky 2 project focusing on a more effective integration of airplane and engine models during conceptual and preliminary aircraft design stages, involving personnel from UNINA as aircraft design experts, and MTU Aero Engines engineers as gas turbine specialists. After a short introduction on the project, details are provided on the aircraft design tools that were implemented and developed to perform planned tasks. Major emphasis is given on the description of JPAD, the aircraft design framework developed in-house at UNINA, on which the the author actively worked

during his PhD and on which he tested the abovementioned approach for a more effective modelling of gas turbine engines. Details are provided for all the sub modules of JPAD dealing with the characteristics of the powerplant. After that, the work performed for the project is described, focusing on aircraft design activities and highlighting each aspect of the interaction with MTU for the modelling and integration at aircraft level of new advanced engine models. The last section provides a recap on the main outcomes of this project in terms of aircraft and engine design specialists interaction, focusing on the detection of those aspects that particularly slowed down the integrated design process, and trying to make a synthesis on all the gaps that emerged during the project activities. These considerations add to the ones already listed in this chapter and are part of the premises of the work described in the remaining sections.

- **Chapter 3** provides a first application of the abovementioned novel approach to the modelling and description of gas turbine engines, applied within the context of another European, Clean Sky 2 funded project: GENESIS. GENESIS deals with perspective analyses, including life-cycle considerations, of innovative hybrid/full-electric aircraft configurations. For the second work package of this project, the author was deeply involved in the development, validation, testing and implementation of an efficient approach to the modelling of a scalable gas turbine engine for a turboprop application. First, a detailed description of the adopted methodology is provided. Then the approach is validated against real engine data and the model is tested for different input, in order to check consistency of the results. Finally, an efficient approach for the implementation of this model in the aircraft design framework of GENESIS is provided.

- **Chapter 4** describes the application of the approach developed for GENESIS to turbofan engines, thus proving the applicability of this methodology to a wide range of engine types and configurations. Since, of course, this application required for some aspects different assumptions, due to inherent differences between turbofan and turboprop engines, major details are provided first regarding these changes. Following the same pattern of chapter 3, validation and testing are provided for this further application. The last sections deal with a detailed description of the implementation of this scalable turbofan engine model in the JPAD aircraft design work chain, and with its testing at aircraft level, finally providing proof of the consistency of the adopted approach.

- **Chapter 5** provides a recap on the main results achieved and includes considerations for further improvements.

Chapter 2

The experience in ADORNO

ADORNO (**A**ircraft **D**esign and n**O**ise **R**ati**N**g for regi**O**nal aircraft) is a Clean Sky 2 project (call H2020-CS2-CFP07-2017-02, project number 821043) which started in November 2018 and will end in October 2022, and sees the collaboration between the German aircraft engine manufacturer MTU Aero Engines AG (Topic Manager of the project), the University of Naples Federico II UNINA (Project Coordinator), and the Italian engineering company Lead Tech. The high-level objective of ADORNO is to allow a fast and reliable estimation of aircraft environmental noise and gaseous emissions at different mission phases, through the implementation of a flexible aircraft model, providing requirements for the engine platform in terms of thrusts and off-takes at different power settings and flight conditions. The aim of the ADORNO project is to reduce design times in the conceptual and preliminary design phases of a new aircraft, allowing aircraft and engine manufacturers to maintain and strengthen competitiveness in the short/medium range market. Competitiveness is closely linked to fuel burn reduction. On one hand, reductions in terms of consumed fuel imply reductions in terms of certain pollutant emissions, allowing to match important environmental objectives. On the other hand, fuel burn is one of the main drivers of aircraft direct operating costs, whose reduction is essential for the industry competitiveness.
The activities of the project are organized in four work packages, of which UNINA is the lead beneficiary. The WP1 focuses on dissemination, communication and exploitation activities, providing the plan for management and publication of conference/journal papers, and defining the strategy for the communication of the major outcomes of the project.
The remaining WP deal with technical activities. The WP2 is focused on the design activities of reference (year 2014) and target (year 2025+) A/C models, both with underwing-mounted (UM) and rear-mounted (RM) engines. The target models feature new turbofan engines, designed by MTU following indications and requirements provided by UNINA, as well as advanced evolutionary airframe technologies, selected and modelled by UNINA. The main outcome of this work package is the assessment in terms of pollutant emissions and environmental noise of the target models with respect to the reference, to check the achievement of the ambitious targets set by CS2: 20 to 30 % reduction in terms of CO_2 and NO_x emissions, 20 to 30 % reduction in terms of environmental noise (with respect to 2014 best aircraft).
The third WP deals with the design and coding of a new software for preliminary aircraft noise assessment. This tool, produced by UNINA with the support of Lead Tech (especially for the documentation), and designed according to the set of requirements

and specifications provided by MTU, is going to be implemented by the German aircraft engine manufacturer in its IT-framework, to perform preliminary engine noise estimations including the contribution of the airframe. Moreover, it will be used by UNINA to carry out the assessment of the WP2 aircraft models in terms of noise.
Finally, the fourth work package addresses the development of an advanced trade factor methodology. This WP comprises several sub tasks, dealing with:

1. The elaboration of fuel burn trade factors for weight, drag and SFC.
2. The design of a set of A/C models, corresponding to an engine parameter study defined by MTU.
3. The check on the applicability of a conventional trade factor methodology.
4. The development of design methods for major aircraft elements (such as nacelles, landing gears, wing, etc.) most significantly influenced by the design of the propulsion system.
5. The development of an improved trade factor methodology, accounting for major A/C geometry changes driven by changes to the characteristics of the engine.

Section 2.1 and section 2.2 give information on the tools that were developed and used in order to carry out the activities of ADORNO, highlighting those features more closely related to engine modelling and integration. Section 2.3 and section 2.4 provide an insight on the tasks that were performed, focusing more on those activities that required an interaction and an exchange of information between aircraft and engine design specialists. Finally, section 2.5 includes author's considerations on the technical activities that were performed for ADORNO and provides the motivations that led to the development of a preliminary engine design methodology to be included in a typical civil aircraft design work chain.
Despite several delays on the delivery of the data necessary to carry out some of the tasks and analyses planned for the project, mostly related to the COVID-19 pandemic, the project is close to its conclusion, without any of the activities initially included in the Description of Action of the project getting cancelled. These delays have particularly affected the activities of WP2 and WP4, for which recovery actions have been already planned for 2022. These activities are related to the design of the RM target model of WP2, and to the development of advanced A/C design methods and of an advanced trade factor methodology for WP4. For this reason, these topics will not be addressed in the following work. For the same reason, results coming from the analyses performed for WP2 will be reported only for the UM A/C configurations, since only for those a comparative assessment has been already concluded. However, missing information from these tasks would have not altered the considerations included in section 2.5.

Author contribution

The author of this thesis work was active on all the work packages of ADORNO. For the first WP, he was directly involved in the writing of three conference papers [40][133][57] and one extended abstract, all four submitted to international conferences and dealing with the main outcomes of the project. Moreover, a journal paper related to the main outcomes of the activities of WP2 for the design of the

UM target A/C model is in preparation and will be submitted to an international journal by the first half of 2022.
He worked on the definition of the set of TLARs of WP2, leading to the design of both reference and target A/C models. He worked on the implementation of a pre-design module in the A/C design framework adopted by UNINA for ADORNO, namely JPAD, which was used to carry out the design of the reference A/C. For this purpose, he was responsible for the programming of such a module in Java language, and for the definition of part of the statistical pre-design laws implemented by this tool. He was the author of the statistical pre-design activities leading to the definition of the A/C models (both UM and RM configurations) to be used as baseline models for the parametric analyses and the subsequent optimizations of the reference A/C models of ADORNO. Moreover, he collaborated with other colleagues of the DAF research group (in the persons of Doc. Vittorio Trifari and Prof. Pierluigi Della Vecchia) for the definition of the strategy (i.e., the setting of the independent and dependent variables of the parametric study, and the definition of the set of constraints and objectives of the optimization) allowing to generate the optimized reference models. Still for WP2, he was responsible for the definition of the set of advanced airframe technologies to be equipped on the target A/C models, carrying out the necessary literature review allowing to perform a first order estimation of the impacts of these technologies on aircraft design disciplines such as weights, aerodynamics, performance, and costs. Along with Vittorio Trifari, he worked on the implementation in JPAD of a new module dedicated to the modelling of these airframe technologies. For the generation of the UM target A/C model, he worked along with Vittorio Trifari to define a reasonable optimization strategy, including both changes to the geometry of the aircraft and to the set of airframe technologies.
For WP3, he supported the development of the noise tool, namely ATTILA++, and the generation of its user manual. For the first, he worked together with other members of the DAF research group (Eng. Valerio Marciello) and experts from UNINA (Prof. Francesco Marulo, Prof. Tiziano Polito, and Eng. Caludio Casale) on the setting of the specifications of the software and helped in the definition of its final architecture. With respect to the user manual, he collaborated with experts from Lead Tech (in the persons of Eng. Raffaele Bianco and Eng. Luigi Staibano) by providing descriptions of the methodologies included in the noise tool and a detailed account on the set of C++ classes, together with their related attributes and methods, implemented by ATTILA++. He was also deeply involved in the validation of this tool: he was responsible for the validation of ATTILA++ and of its calculation modules against aircraft noise experimental data, and against results provided by other preliminary noise calculation tools. Moreover, he was responsible for the implementation of ATTILA++ in the UNINA aircraft design and analysis framework adopted for ADORNO.
For WP4, he carried out the design of the set of A/C models equipped with the set of turbofan engines provided by MTU and resulting from a parametric study on BPR. For the same work package, he also performed the check on the applicability of the linear trade factor methodology for the prediction of fuel burn changes.
For each WP, he worked together with colleagues from UNINA and partners from Lead Tech involved in the project on the submission of Deliverables and on the

production of all the documentation required by the project.

List of publications related to ADORNO and involving the author

Conference papers

- C. Casale, T. Polito, V. Trifari, **M. Di Stasio**, P. Della Vecchia, F. Nicolosi, and F. Marulo. Implementation of a noise prediction software for civil aircraft applications. In *AIDAA XXV International Congress*, 9-12 September 2019, Rome, Italy. DOI: 10.5281/zenodo.3943793.

  The candidate performed for this paper the modelling of the Airbus A220-like A/C model used for the noise tool validation in the aircraft design and analysis framework of ADORNO. Moreover, he contributed to the writing of the section dedicated to the description of JPAD, as well as of the section describing the case study.

- F. Nicolosi, P. Della Vecchia, V. Trifari, **M. Di Stasio**, F. Marulo, A. De Marco, V. Marciello, and V. Cusati. Noise, emissions and costs trade factors for regional jet platforms using a new software for aircraft preliminary design. In *AIAA AVIATION Forum 2020*, 15-19 June 2020, virtual meeting. DOI: 10.2514/6.2020-2638.

  The candidate was responsible for the generation of the baseline A/C model, used later as the starting point for a full-factorial design of experiment, involving changes to the aircraft geometry. Moreover, he was responsible for the description of the methodologies and approaches adopted for the analyses, as well as for the account on the results achieved from the statistical pre-design of the baseline aircraft.

- **M. Di Stasio**, V. Trifari, F. Nicolosi, A. De Marco, S. Fuhrmann, and R. Schaber. Multidisciplinary optimization of a regional jet including advanced airframe and engine technologies. In *AIAA AVIATION Forum 2021*, 2-6 August 2021, virtual meeting. DOI: 10.2514/6.2021-2424.

  The author performed the necessary literature review, to determine the effects on aircraft weights, aerodynamics, power off-takes, and direct operating costs related to the implementation of advanced airframe technologies. He contributed to the definition of a reasonable strategy for aircraft optimization (on fuel burn). He was responsible for the description of the airframe technologies set, for the description of the technologies implementation in the aircraft preliminary design framework (JPAD), and collaborated to the writing of the sections illustrating the optimization strategy and the main achievements.

Journal papers

- (*In preparation*) **M. Di Stasio**, V. Trifari, F. Nicolosi, and A. De Marco. Optimization of an advanced regional aircraft based on HBPR turbofan engine characteristics.

A paper collecting the main achievements linked to the fourth WP of ADORNO will be submitted during the second half of 2022 to a an internationally respected journal (e.g., Aerospace Science and Technology). This paper will mainly deal with the work carried out by the author on the optimization of a UM target A/C, equipped with innovative airframe solutions, based on the characteristics of three different HBPR engines, designed (at preliminary level) by the German engine manufacturer MTU.

2.1 JPAD: a tool for preliminary A/C design

JPAD is a Java framework developed in-house at the University of Naples Federico II by the DAF research group and by the university spin-off SmartUp Engineering, allowing to perform multidisciplinary analyses and optimizations of civil transport aircraft. It is the result of the efforts of the DAF group during several years of involvement in European research projects, which have allowed to gather a solid experience in aircraft design techniques and in the development of novel methodologies supporting the design process [129][130][132][126][128][44].
Nowadays the preliminary design phase of an aircraft has become very challenging due to increasingly demanding requirements. The goal of first design stages is to search for the configuration that best fits all the requirements among the results of a great number of multidisciplinary analyses. This task must be accomplished as fast as possible and, preferably, with a certain degree of accuracy. JPAD has been designed meeting all these requirements, relying on semi-empirical methods which allow a fast estimate of all the most significant aircraft quantities and performance. A comprehensive study of the methods available in literature has been firstly carried out, followed by a period of testing against experimental data, to select the most accurate ones or to perform a merge between different available approaches. In addition, several in-house developed methods [131][44] have also been implemented in the JPAD framework, providing a significant advantage with respect to most of the current competitors in the aircraft design software scenario. Particular attention has been paid for aerodynamics and performance estimation methodologies, for which the classical semi-empirical approaches have been complemented (or in some cases even substituted) with more refined and higher fidelity techniques [155][169], such as vortex lattice method and simulation-based approaches.
The JPAD framework has been organized as an interconnected ecosystem of software modules, each one dedicated to a specific task. The root of the JPAD framework is the JPAD-*core* module, which allows to manage the aircraft parameterization and the performing of all available analyses. On top of that, several other modules provide other important features (figure 2.1).

- JPAD-*cad* - This module oversees the automatic computer aided design (CAD) modelling, based on the aircraft parameterization provided and managed by the JPAD-*core* module [55].
- JPAD-*commander* - The dedicated graphical user interface (GUI) of the JPAD framework. Completely written using JavaFX[1] along with the support of Gluon Scene Builder[2], this powerful tool allows users to easily define a JPAD-parametrized

[1] https://openjfx.io/
[2] https://gluonhq.com/products/scene-builder/

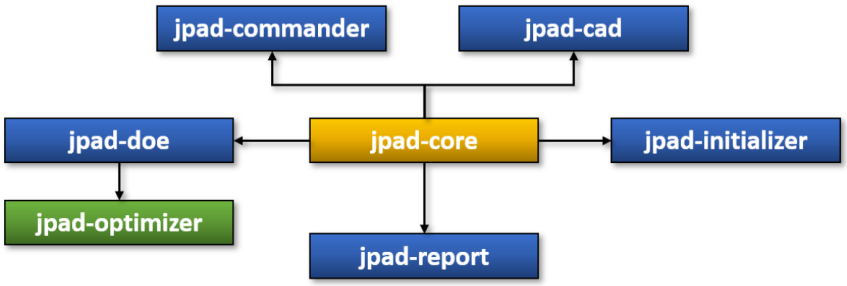

Figure 2.1: JPAD modules hierarchy

aircraft model, to generate its CAD model, to run a prescribed set of analyses, and to visualize results.

- JPAD-*doe* - This module is in charge to perform sensitivity studies, as well as full-factorial design of experiments (DOE), by managing changes to geometrical and/or analysis-related design parameters, thus generating a population of aircraft to be analyzed. It makes use of the JPAD-*core* module to perform a set of multidisciplinary analyses for each aircraft included in the population. The output of the JPAD-*doe* module is a response surface, which is suitable for both built-in optimizations and external optimization tools.

- JPAD-*initializer* - Starting from a set of user-defined TLARs and a limited amount of information regarding the aircraft category, such as general layout and powerplant type, the JPAD-*initializer* allows to easily generate a baseline A/C to be used, for example, to perform sensitivity studies. The JPAD-*initializer* relies on a statistical database. Throughout the years, those have been enriched by the DAF research group, by gathering data from several renowned aircraft design textbooks, aircraft manufacturers, and online available material.

- JPAD-*optimizer* - This standalone module can be used to perform single-objective as well as multi-objective optimizations by means of the state of the art in terms metaheuristic optimization algorithms based on computational intelligence, like genetic algorithms (GA) and particle swarm optimization (PSO).

- JPAD-*report* - Conceived for fast and efficient output visualization, this module allows to automatically generate a complete aircraft report mixing text, figures and tables, both in Microsoft Word and PDF file formats.

The following sub sections provide a more detailed description of the JPAD modules which have been more extensively used for the activities of ADORNO. In addition, attention will be focused on those aspect related to the description, parameterization and management of the powerplant system.

Author contribution

As a member of the DAF research group and as a Java developer, the author of this thesis work was directly involved during his doctoral years in the development of many of the abovementioned modules.
He was responsible for the development of the CAD module and of the overall system of Java classes, allowing to automate the generation of a high-fidelity 3D model of the external shape of a conventional civil aircraft starting from the geometry parameterization provided by JPAD. During his PhD, he focused in particular on the modelling of aircraft movables (i.e., control and high-lift devices) and of the powerplant system, including the automatic generation of pylons. Work was performed in order to ensure that the aircraft 3D models produced with JPAD through this CAD module were actually suitable for high-fidelity analyses with CFD tools, and the candidate also worked on the generation of the instruments, i.e., Java macros and Java archives (JAR), allowing to automate the import, the meshing, and the analysis of aircraft 3D shapes in a CFD software such as STAR-CCM+[a].
He also provided several contributions to the work of the other members of the DAF research group involved in the development of JPAD (Prof. Agostino De Marco, Doc. Vittorio Trifari, Doc. Manuela Ruocco, and Doc. Vincenzo Cusati): in particular, the author supported:

- the development of the graphical user interface (GUI) of JPAD,
- the implementation of a pre-design initializer (described in section 2.1.2),
- the addition of a module dedicated to the implementation of advanced airframe technologies (described in section 2.3.3),
- and the re-design of the core module dedicated to the management of the cabin layout.

Moreover, he was responsible for the implementation of a module dedicated to the preliminary modelling of gas turbine engines, as it was already mentioned in chapter 1 and which will be shown in details in chapter 4.

[a] https://www.plm.automation.siemens.com/global/en/products/simcenter/STAR-CCM.html

List of publications related to JPAD and involving the author

Conference papers

- (*Extended abstract sent and accepted*) V. Trifari, A. De Marco, **M. Di Stasio**, M. Ruocco, F. Nicolosi, G. Grazioso, V. Ahuja, R. Hartfield. An aircraft design workflow using the automatic knowledge-based modelling tool JPAD Modeller. In *AIAA AVIATION Forum 2022*, 27 June - 1 July 2022, Chicago, IL, USA.

  The candidate contributed by developing the CAD module dedicated to the automatic generation of movables 3D shapes. He also supervised and

managed the linkage between JPAD output in terms of aircraft geometry and its import in the analysis software FlighStream[a].

Journal papers

- A. De Marco, **M. Di Stasio**, P. Della Vecchia, V. Trifari, and F. Nicolosi. Automatic modeling of aircraft external geometries for preliminary design workflows. *Aerospace Science and Technology*, Volume 98, 2020, 105667, ISSN 1270-9638, DOI: 10.1016/j.ast.2019.105667.

  For this journal paper, the candidate contributed by developing most of the Java classes and algorithms, dealing with the automation of lifting surfaces, fuselage, fairings, engines, and pylons 3D shapes production. Moreover, he carried out the work on interfacing JPAD with a CFD software (STAR-CCM+) and managed and supervised the work presented in the final test case.

[a] https://www.darcorp.com/flightstream-aerodynamics-software/

2.1.1 The core of the JPAD framework

The JPAD-*core* module manages both the aircraft parameterization and the analyses managers related to the following implemented disciplines: weights, balance and ground stability, aerodynamics and static stability, performance, pollutant emissions, environmental noise, and costs (figure 2.2). Input for both the geometry and the analyses, in the format of XML files, have been organized forming a hierarchical structure, following a pattern similar to the one adopted for the Java classes. With regards to the aircraft geometry, for example, the main aircraft file (*aircraft.xml*) collects all the components positions with respect to the body reference frame (BRF) along with their related XML file name (i.e., *fuselage.xml*, *wing.xml*, etc.). These, in turn, contain all the geometrical data related to that specific component.
To enhance the framework flexibility, the core has been conceived to allow both a complete analysis loop, involving all the disciplines shown in figure 2.2, and standalone use of any of its analysis modules. Since the obvious interconnections between the core disciplines, in the last case the user must directly provide all the necessary input for the analysis to be carried out.
In case the user wants to perform a complete multidisciplinary analysis cycle, a preliminary iterative loop on mission fuel mass can be performed. In this case a first estimation of weights is carried out, along with a balance analysis to determine the center of gravity excursion. For each considered center of gravity position (e.g., maximum forward, maximum afterward, and operative), the aerodynamics and stability module estimates trimmed drag polar curves and lift curves for the take-off, climb, cruise, and landing conditions. Then the performance module uses the results coming from the aerodynamics and static stability analysis to perform a detailed simulation of the mission profile, estimating a new amount of fuel needed to cover the mission. Thus, an iterative process is carried out, until the fuel mass considered for the estimation of the weights of the aircraft is equal to the one calculated by the mission profile analysis. In addition, during this first preliminary analysis phase users can require the aircraft to match specific performance requirements in terms of take-off field length, maximum cruise Mach number, and minimum cruise service ceiling. In case one of the abovementioned require-

ments is not fulfilled, the engines static thrust is automatically updated. As a result, all dimensional thrusts (i.e., at different power settings and flight conditions) provided by the non-dimensional engine deck on which the JPAD performance analysis module relies are scaled as well. More information on the JPAD engine deck will be provided in the following paragraph dedicated to the description of the performance calculation module. It is important to highlight that, to account for the snow-ball effect provided by an increased value of the engine static thrust, JPAD calculates for each updated aircraft new values for the engine dry mass and main nacelle dimensions, using a dedicated statistical database developed by the DAF research group. In this way, effects of the engine update process influence all the disciplines involved in the analysis cycle.
Once the preliminary iterative loop has converged, the JPAD-*core* reads from the XML input file information on the analyses to be carried out according to the user's request, and performs a call to those analysis modules. An overview of JPAD complete analysis cycle is provided in figure 2.3.
The following paragraphs provide a brief overview of the geometry and analysis modules implemented by JPAD-*core*, along with references to the adopted methodologies. Since the focus of the activities presented in the following chapters (chapter 4 mainly) is on engine-related aspects, some additional details will be provided for the parameterization of the nacelles and on the assumptions performed for the calculation of nacelle and powerplant system (PPS) mass, and of the nacelle drag. Since JPAD noise module relies on ATTILA++, a more detailed description of it will be provided in section 2.2. For a more comprehensive overview of the calculation modules of JPAD, the reader should refer to the works described in [169][155][50].

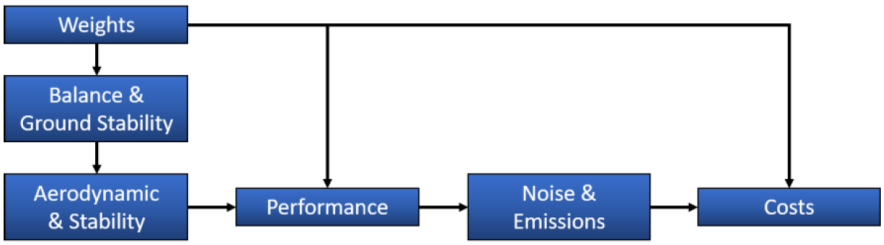

Figure 2.2: JPAD-*core* set of calculation modules and dependencies.

Geometry

JPAD allows the management of the geometry of the aircraft and its components through several input files in the XML format. These files are organized according to a precise and reasoned hierarchy. The *aircraft.xml* is on the top of this hierarchy: it collects information on the set of components constituting the aircraft model in terms of apex position (e.g., for a generic lifting surface, the position of the leading edge point on the root airfoil) in the BRF, and XML filename. For each sub component, a dedicated XML file named accordingly with the represented aircraft element collects information on the geometry, according to a well-established parameterization. This parameterization, on one hand, aims at reducing the number of information required to describe a certain component, while on the other hand it ensures that the amount and the type of information still allows for the application of most of the semi-empirical and medium-fidelity methodologies available in literature for the estimation of weights, aerodynamic

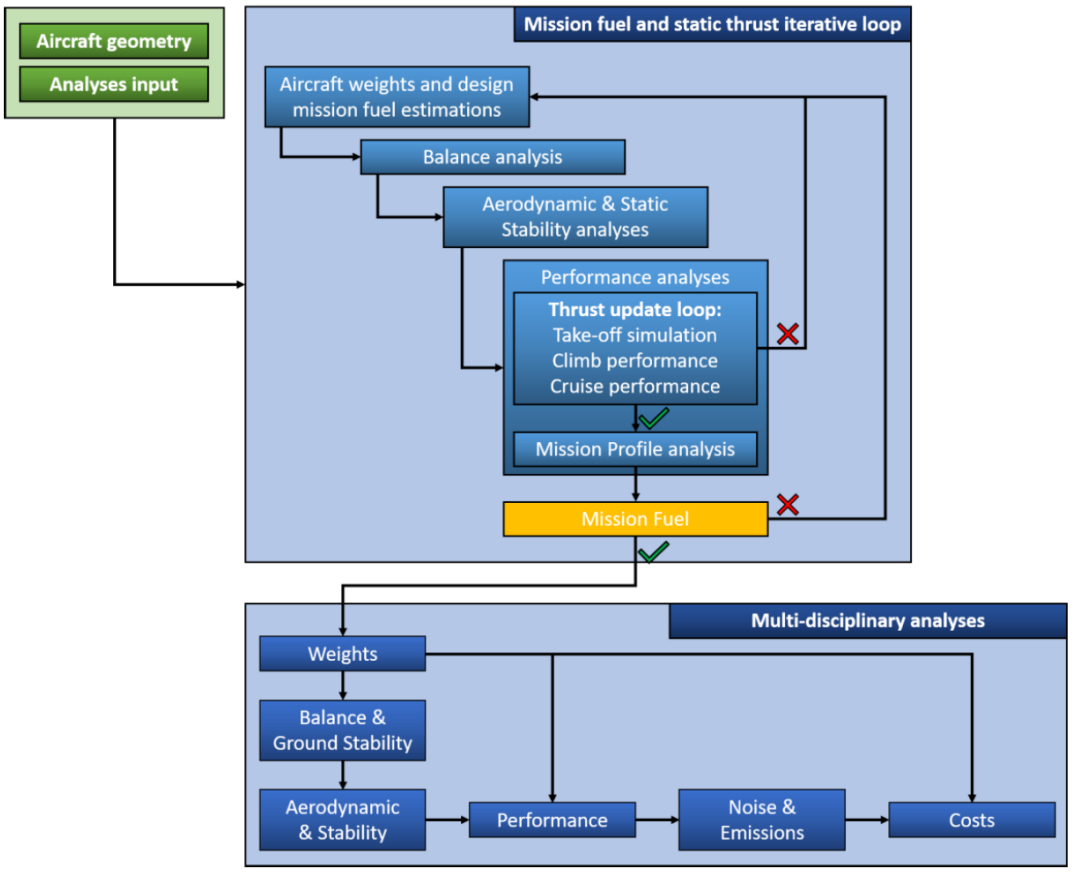

Figure 2.3: JPAD complete analysis loop.

behaviour, performance, noise, and costs of the aircraft. Not to mention the necessity to provide satisfactory 2D and 3D representations of the external shapes of the airplane, as well as a preliminary CAD model, to be used to perform high-fidelity analyses on the aircraft model with the aid of an external tool. Table 2.1 provides an overview on the aircraft components accounted by the analysis methods that can be managed with JPAD, as well as indications on the hierarchy relations between them. Regarding the powerplant system, JPAD allows to model each engine individually. A nacelle component, describing the external shape of the engine, must be always linked to the engine. According to the selected engine type, an adequate set of information must be provided, as reported in table 2.2: not all the parameters listed in table 2.2 are required, but only those pertaining to the engine type selection. Moreover, the linked engine deck file should be consistent with this selection too. The dry mass of the engine can be both assigned, if data is available from an engine manufacturer, or estimated, by means of available regression laws. For a turbofan engine, a formula elaborated by the DAF research group based on available engine data and making use of information on the engine in terms of BPR and static thrust has been implemented. Table 2.3 and figure 2.4, instead, provide information on the set of parameters of the nacelle. This simple parameterization is functional to the application of semi-empirical approaches for the estimation of the nacelle drag.

Table 2.1: Hierarchy of aircraft geometry components in JPAD.

Component	Level	Linked to
Aircraft	0	none
Fuselage	1	Aircraft
Cabin	2	Fuselage
Lifting surface	1	Aircraft
Airfoil	2	Lifting surface
Engine	1	Aircraft
Nacelle	2	Engine
Landing gears	1	Aircraft

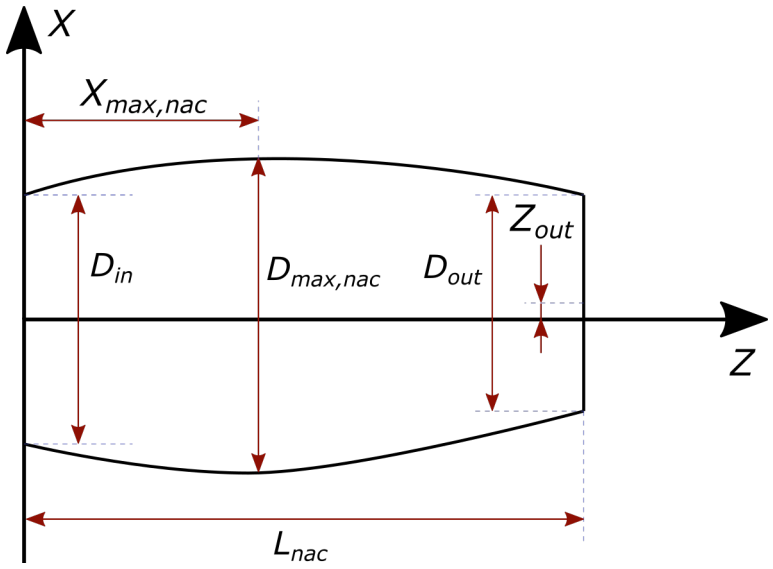

Figure 2.4: JPAD nacelle parameterization

Weights analysis

This module is in charge of performing a Class-II estimation in order to assess all main aircraft weights data starting from a detailed mass breakdown of all its components. Each component mass is calculated using several semi-empirical equations retrieved from the literature [167][97][86][101][149][157][125][162][168]. The user is allowed to choose, for each aircraft component, whether to use a specific calculation method or a mean value provided by the application of all the available methods. In addition, the weights analysis manager provides the user with the possibility to manually calibrate each component weight by means of a dedicated set of calibration factors, in order to simulate technological trends.
For the estimation of the PPS mass, the formulations suggested by [167][97][101] have all been implemented. According to these approaches, the PPS mass is equal to the engine dry mass multiplied by a constant, which slightly varies according to the different formulations. In this case too, the user can both select to apply one formulation in particular, or to calculate an averaged value between the results provided by the different formulas. Regarding the dry mass instead, the user can both provide an estimated/verified value,

Table 2.2: JPAD engine parametric model: list of parameters for piston, turboprop and turbofan engines.

Parameter	**Symbol**	**Definition**
Engine type	-	Defines the engine type (piston, turboprop, turbofan).
Database file name	-	Sets the name of the engine deck to be retrieved from the JPAD database folder in order to carry out aircraft performance analyses.
Dry mass	W_{dry}	Sets the dry weight of the engine, which is used to calculate the PPS mass.
Static thrust	T0	The sea-level static thrust of the engine (this option is only available for turbofan engines).
Static power	P0	The sea-level static power of the engine (this option is only available for piston and turboprop engines).
Bypass ratio	BPR	The engine bypass ratio (this option is only available for turbofan engines).
Propeller diameter	D_{prop}	The engine propeller diameter (this option is only available for piston and turboprop engines).
Number of blades	N_{blades}	The number of propeller blades (this option is only available for piston and turboprop engines).
Propeller efficiency	η_{prop}	The efficiency of the propeller (this option is only available for piston and turboprop engines).

or, in case of turbofan engines, can proceed to estimate it directly with JPAD, by using the previously mentioned model, based on an online turbofan database and on engine characteristics in terms of BPR and static thrust.
Concerning the nacelle weight, an estimation is carried out by JPAD using the formulas suggested in the same references listed above for the PPS mass. Basically these formulas require information on the static thrust and, eventually, on the BPR for turbofan engines, and the static power value for turboprop and piston engines. Moreover, some of the formulas for turboprop and piston engines require also information regarding the mounting position (e.g., under the wing, on the fuselage, etc.).

Balance and Ground Stability analyses

The balance module allows to calculate: the aircraft center of gravity position at different weight conditions (e.g., operating empty, maximum zero fuel, maximum take-off, etc.); the center of gravity of each component; the boarding diagram; the maximum forward, the maximum afterward and the operative center of gravity (CG) positions; aircraft inertia moments and inertia products. With regards to inertia calculation, a semi-empirical

Table 2.3: JPAD nacelle parametric model.

Parameter	Symbol	Definition
Nacelle length	L_{nac}	Defines the length of the nacelle cowl for turbofan engines, and the overall nacelle length for piston and turboprop engines.
Maximum diameter	$D_{max,nac}$	Sets the maximum nacelle diameter.
Inlet ratio	D_{in}^{ratio}	Defines the ratio between the nacelle inlet diameter and the maximum diameter. Sets D_{in} of figure 2.4
Outlet ratio	D_{out}^{ratio}	Defines the ratio between the nacelle outlet diameter and the maximum diameter. Sets D_{out} of figure 2.4
Max. diameter relative position	$X_{max,nac}^{ratio}$	Sets the ratio between the nacelle maximum diameter longitudinal position and the nacelle length. Sets $X_{max,nac}$ of figure 2.4
Outlet center relative position	Z_{out}^{ratio}	Defines the offset, relative to the nacelle maximum diameter, between the outlet and the inlet section centers. Sets Z_{out} of figure 2.4

approach, based on the formulas proposed in [167][162], has been implemented. This module also allows to include in the modelling of the aircraft the center of gravity positions of systems components/groups, such as the auxiliary power unit (APU), the ice protection system (IPS), the control surfaces, etc. Those can either be manually assigned by the user or can be automatically estimated by JPAD, by means of a procedure based on statistical on-board systems typical positions, retrieved from [162].
JPAD also allows to manage several ground stability and operability analyses/checks, which allow to ensure that the chosen aircraft configuration fulfills all the following requirements.

- The possibility to safely rotate the aircraft during take-off and landing phases, e.g., the main landing gear strut length and the fuselage upsweep angle have been adequately sized/selected, allowing to avoid tail strike during take-off and nose or tail tip during touchdown.

- An adequate engine clearance from ground is guaranteed. Information are produced by JPAD ground stability module on the minimum distance between the powerplant (nacelles or propellers) and the ground, when the aircraft is in the taxi phase.

- Aircraft stability at touchdown and during taxiing must be always guaranteed. This check is performed by JPAD using the approach suggested in [167], which uses information on the aircraft center of gravity position and on the geometry of the aircraft to detect whether the selected positioning of the nose and main landing gears is sufficient to ensure aircraft stability during the abovementioned conditions.

- The aircraft turning radius should be lower than half of the runway total width (which in turn depends on the airplane design group), in order to ensure that it can be adequately maneuvered on ground, when moving from the airport runway to the passengers terminal.

Aerodynamics and Static Stability analyses

The aerodynamics module of JPAD estimates all the aerodynamic characteristics concerning lift, drag and moment coefficients, at different operating conditions (take-off, climb, cruise and landing) both for the complete aircraft and for each airframe component (wing, tails, fuselage and nacelles). Furthermore, the stability module provides useful data regarding longitudinal and lateral-directional stability of the whole aircraft, taking also into account non-linear effects (i.e., pendular stability, non linear downwash gradient, etc.).
Each analysis is carried out using one (or a mix) of the following approaches:

- low-fidelity (e.g., semi-empirical equations from literature);
- medium-fidelity (e.g., vortex lattice method for lifting surface loading, corrected for non-linear effects);
- high-fidelity surrogate models developed by UNINA DAF research group [131][127][56];

In terms of lifting surfaces, the starting point is the definition of all airfoils characteristics. Users may choose to manually assign each aerodynamic parameter required to model the lift curve, the drag polar and the pitching moment curve of the generic airfoil, or to assign an external set of curves (coming from CFD analyses, for example) to provide for a higher analysis accuracy. A third option is to select a generic NACA airfoil from a dedicated internal database, based on the data reported in [1], by choosing just the series/family and the thickness ratio. In the first two cases, the user must assign all data at a low speed condition, then the aerodynamic module performs all the required Mach and Reynolds numbers corrections to scale aerodynamic data according to the specific operating condition.
With regard to the airfoil database, it currently allows to manage airfoils from the following families: NACA 4-digit, NACA 5-digit, NACA 6^{th} series, supercritical airfoils. From the database, all necessary values to automatically produce the curves of lift, drag and pitching moment are collected, starting just from user-provided airfoil family name and information in terms of airfoil thickness and curvature. The database has been built by digitalizing data from [1] and by re-elaborating them with the support of MATLAB[3].
One of the main features of JPAD aerodynamic module consists in implementing an improved methodology for lift estimation. One of the main issues of classical vortex methods, such as the one proposed in [32], is their reliability only in the linear range of lift curve and the fact that they tend to ignore actual airfoil lift coefficient slope, by considering it simply equal to 2π, which is the value from Glauert theory. The method currently implementd by JPAD modifies the load distribution obtained using the NASA-Blackwell approach of [32], taking into account actual airfoil lift characteristics and extending results up to the stall. The implemented methodology follows a two-step approach. First, airfoil input curves are modified in order to take into account 3D effects such as cross-flow. Due to this effect, airfoil lift slope is slightly reduced. Once that input airfoil curves have been modified, the following steps take place.

[3] https://www.mathworks.com/products/matlab.html

- The inviscid lift distribution is evaluated using the NASA-Blackwell method.
- For each lifting surface section, for which the local lift coefficient is known, it is possible to enter in the corresponding airfoil chart, the one accounting for 3D effects, and obtain the local angle of attack at which the airfoil is working.
- This angle of attack can be used in viscid airfoil lift charts, in order to obtain updated values of local lift coefficients, this time accounting for viscous effects too.
- A new lift distribution along the semispan is obtained, which considers also 2D non-linearity.
- This updated lift coefficient distribution results in a new distribution of induced angle of attack, which produces, in turn, a new 2D lift coefficient distribution. So an iterative process is needed.
- Once the updated distribution of induced angle of attack is known, the implemented algorithm calculates the new angle of attack and lift coefficient distributions.
- The lifting surface lift coefficient is obtained integrating the lift coefficient distribution once that the convergence has been reached.

This calculation procedure is then repeated for each angle of attack requested by the user.
An improved methodology for high-lift devices has been implemented too. In order to take into account the presence of these devices, the method works using the flapped airfoil aerodynamic characteristics where needed, replacing the clean wing geometric parameters with the flapped ones, i.e., modifying the wing planform geometry, to which the modified vortex-lattice method described above is applied. The wing with high-lift devices deployed is generated from the clean wing by substituting the following parameters:

- chord distribution,
- zero lift angle of attack distribution,
- wing leading edge longitudinal position distribution,
- airfoil maximum lift coefficient distribution.

These updated values are the input values for the method, and can be both automatically calculated by JPAD aerodynamic module by following a semi-empirical approach (as the one suggested in [167]), or can be externally provided, being the result of high-fidelity computational fluid dynamics (CFD) analyses.
Concerning drag estimation for isolated lifting surfaces in clean configuration, the following contributions are taken into account to estimate the drag coefficient at different angles of attack:

- Parasite drag coefficient, which is the sum of skin friction and form drag contributions, and is calculated starting from airfoil drag polar and integrating drag coefficient distribution along lifting surface semispan.
- Gap drag coefficient, which is the contribution to total drag coming from gaps and slots due to the presence of control surfaces and/or high-lift devices. Its contribution is estimated through the formulas reported in [167].

- Wave drag coefficient, which is due to air compressibility, and is estimated though formulas provided in [83][45].
- Vortex drag coefficient (angle of attack dependent), which is the drag that results from the generation of a trailing vortex system downstream of a lifting surface of finite aspect ratio, and whose value is calculated from Prandtl theory [118].

Regarding the drag produced by the nacelles, this consists in two contributions: an induced contribution, which depends on the angle of attack of the aircraft and is calculated according to the approach suggested in [186], and a lift-independent contribution. This latter accounts for both skin friction and form drag. The calculation of the skin friction contribution relies on previous estimation of skin friction coefficient, C_f, and nacelle form factor, FF, according to the following equations:

$$C_f = \frac{0.455}{log(Re)^{2.58}}(1 + 0.144M^2)^{0.165} \tag{2.1}$$

$$FF = 1.165 + 0.91\frac{D_{max,nac}}{L_{nac}} \tag{2.2}$$

in which Re and M are the flight Reynolds and Mach number, respectively. Form drag contribution is calculated using the equations suggested by [100][125], with the usage of one specific formula with respect to the others depending on the engine type. The form drag calculated according to these equations depends on the skin friction drag, on the nacelle maximum diameter, and on the nacelle outlet diameter. Finally, an interference contribution is considered if the engines/nacelle are mounted on the wing of the aircraft. In this case, the following contribution is added to the total zero-lift drag coefficient, C_{D0}, of the aircraft:

$$\Delta C_{D0}^{nac} = 0.0033\frac{D_{max,nac}^2}{S_{wing}} \tag{2.3}$$

where S_{wing} is the wing reference planform surface.

Performance

The performance module of JPAD has been completely developed using a simulation-based approach for each mission phase. It has been divided in several sub-modules to allow the user to perform a single performance analysis (e.g., a detailed take-off or landing simulation), a complete mission profile analysis, or a combination of them.
In the overall *jpad-core* dependency map, the performance module requires some weight data as well as trimmed aerodynamic data concerning polar drag curves and lift curves for every flight condition (take-off, climb, cruise, landing). The user can both manually provide this data, or make the module inherit them from previously performed analyses. In the first case, two possible approaches have been conceived:

- working with parametrically defined parabolic drag polar curves;
- using points from externally generated drag polar curves, if the user has higher fidelity data.

In any case, lift curves data must be provided using only the following parameters in clean, take-off and landing configurations: lift curve slope, lift coefficient at zero angle of attack, and maximum lift coefficient. In addition, also the rudder effectiveness coefficient

must be specified, in case of standalone usage, to allow the performance module to carry out the estimation of the minimum control speed.
The performance module allows to carry out the following analyses: take-off, landing, take-off and landing noise trajectories, climb, cruise, descent, mission profile, payload-range, V-n diagram. Part of these analysis is described in the following sub sections. Moreover, information are provided on the engine performance file required by these modules.

Engine performance file In terms of input data, the performance module requires also an engine deck, which must be provided together with each engine input file, storing all necessary information regarding engine characteristics in terms of thrusts and emissions.
The JPAD engine performance database is a non-dimensional (in the sense of thrust) rubberized engine deck built up as an Excel file which collects thrust ratios, SFC values and pollutant emission indexes at different altitudes, Mach numbers, ISA deviations and throttle settings. These values are provided for each of the following engine ratings: maximum take-off (MTO), auxiliary power reserve (APR), maximum climb (MCL), maximum continuous (MCT), cruise, flight idle (FI), and ground idle (GI). The maximum take-off rating is used for take-off and take-off noise trajectory simulations, the maximum continuous and APR ratings can be used for in air minimum control speed calculation, the maximum climb setting is used for climb performance analyses, the cruise rating is used for analyses during cruise and descent phases, the flight idle setting mainly drives the descent and landing simulations along with landing noise trajectory analyses, and the ground idle rating is the one used for the on-ground phase of the landing simulation.
In order to enable the use of this rubberized file during the performance analyses, the thrust ratios are multiplied by the value of static thrust, which is an information that must be included by the user in the JPAD input file dedicated to the engine. JPAD provides several rubberized engine decks, which are representative of different engine types (e.g., piston, turboprop and turbofan engines), but the use of custom decks different from the default ones is allowed, as long as they comply with the required format. For example, the analyses carried out for ADORNO concerning the reference aircraft models involved the use of a new custom built engine deck for a high BPR engine, similar, in terms of performance, to the Pratt & Whitney PW1500 model (i.e., the one equipped on the Airbus A220). For the design of the target aircraft models, instead, a new engine deck, representative of an advanced high BPR engine, was produced by MTU, and successively adapted by UNINA to the format required by JPAD (i.e., convert the file to non-dimensional thrust ratios, by dividing all the thrust values by the value of engine static thrust).
Moreover, only for turbofan engines, the user can select to adapt one of the default engine decks or even a custom-built one to a different BPR value with respect to the one specified in the deck file, by providing a distinct bypass ratio value in the XML input file of the engine. In this case, the SFC information included in the deck are automatically updated, by means of scaling factors obtained from [97]. Although this implemented strategy tested well against some reference engines, the user is still recommended to use custom-built engine deck, when they are available.
Figure 2.5 provides an example of JPAD engine deck for a turbofan engine. The data reported in this figure refer to the Cruise rating. As can be deduced from this figure, information on thrust ratio, fuel consumption and pollutant emissions (in the form of

EI) are provided for each different combination of flight altitude and Mach number, deviation from ISA temperature and throttle setting. Since information on the EI of some pollutant species might be difficult to be retrieved or assumed, these can be left blank, and the tool will automatically skip the calculation of the total emission (i.e., during the aircraft mission simulation) for those species.

Altitude	Mach	delta Temperature	Throttle Setting	T/T0	TSFC	EI NOx	EI CO	EI HC	EI soot	EI CO_2	EI SOx	EI H_2O
ft	none	°C	none	none	lb/(lb*hr)	g/kg	g/kg	g/kg	g/kg	g/kg	g/kg	g/kg
0	0.1	0	0.2	0.1128	0.522004	27.9945				3162		1250
0	0.2	0	0.2	0.1032	0.564267	29.52861				3162		1250
0	0.3	0	0.2	0.0947	0.630691	30.82524				3162		1250
0	0.4	0	0.2	0.0839	0.726688	31.89739				3162		1250
0	0.5	0	0.2	0.0752	0.831878	33.04731				3162		1250
0	0.6	0	0.2	0.0668	0.955855	34.53034				3162		1250
0	0.7	0	0.2	0.0571	1.143477	35.65959				3162		1250
0	0.74	0	0.2	0.0534	1.233026	36.14356				3162		1250
0	0.78	0	0.2	0.0498	1.335554	36.64219				3162		1250
0	0.8	0	0.2	0.0479	1.392711	36.89664				3162		1250
0	0.82	0	0.2	0.0462	1.45723	37.05535				3162		1250
0	0.85	0	0.2	0.0435	1.561193	37.31351				3162		1250
5000	0.1	0	0.2	0.1012	0.524878	25.72771				3162		1250
5000	0.2	0	0.2	0.0971	0.528552	27.29677				3162		1250
5000	0.3	0	0.2	0.0894	0.589339	28.62154				3162		1250
5000	0.4	0	0.2	0.0798	0.674941	29.72464				3162		1250
5000	0.5	0	0.2	0.0717	0.770923	31.01037				3162		1250
5000	0.6	0	0.2	0.0645	0.878615	32.39108				3162		1250
5000	0.7	0	0.2	0.0579	0.998087	33.6838				3162		1250
5000	0.74	0	0.2	0.0536	1.088813	34.19555				3162		1250
5000	0.78	0	0.2	0.0504	1.168062	34.62276				3162		1250
5000	0.8	0	0.2	0.0491	1.203508	34.9438				3162		1250
5000	0.82	0	0.2	0.0465	1.261793	35.09586				3162		1250
5000	0.85	0	0.2	0.0428	1.349698	35.36275				3162		1250

Figure 2.5: JPAD engine performance deck example: high BPR turbofan engine, Cruise rating.

Take-off simulations The take-off calculation module computes all the take-off performance using a simulation-based approach. The analysis procedure expects to solve an appropriate set of ordinary differential equations (ODE), which describes the aircraft equations of motion during all the take-off phase up to the obstacle. The strategy is to find out all the fundamentals variables of motion, which completely describe the aircraft state during this phase, and then study the dynamic system in exam in a state-space representation. The dependent variables of this system of equations are the following: aircraft position, aircraft air speed, flight path, center of gravity altitude from the ground, aircraft mass. These variables form the vector of state variables, while the input is a given function of time that corresponds to an assumed time history of the angle of attack. Information regarding engine related parameters, such as thrust and fuel flow rate, is directly retrieved from the engine deck and adequately interpolated. The total drag and lift forces as functions of airspeed, altitude, flight path angle, aircraft mass and angle of attack are given by conventional classic formulas, involving lift and drag coefficients estimated for the trimmed aircraft condition, with flaps (and eventually slats) deflected. Ground effect contribution is also taken into account, as suggested in [87]. During all the simulation the maximum allowed rotation angle is constantly monitored to ensure the absence of tail strike and, in case this happens, a warning message is issued to the user. The take-off calculation module also simulates the take-off phase in case of one engine inoperative (OEI) condition, by reproducing a discontinuity in total engine thrust and a little drag increment due to the failed engine. The procedure followed and replicated to adequately simulate the take-off in OEI condition is the one proposed in [162]. Both take-off with one failed engine and aborted take-off are simulated, at different critical velocities (i.e., the velocity at which action is taken in case of one engine inoperative), in

order to calculate the balanced field length (BFL). Several minimum control speed (i.e., the calibrated air speed below which directional or lateral control of an airplane, on the runway or in the air, can no longer be maintained by the pilot after the failure of the most critical wing-mounted engine) are also monitored during OEI take-off simulations. These estimations are carried out also thanks to the Vertical tail DESign Stability and Control tool (VeDSC) [56], embedded in JPAD aerodynamics module.

Landing simulations Similar to the take-off, also for the landing phase a simulation-based approach, involving the resolution of an ODE system, has been implemented inside the JPAD performance module. In this case the starting point of the simulation has been assumed as the beginning of the approach phase at 1500 ft above the runway. From the landing obstacle altitude (50 ft) the aircraft begins the final approach down to the initial flare rotation altitude, assumed to be at 20 ft above the ground, as suggested in [148] as averaged value for transport aircraft. In this phase the aircraft speed must be kept almost constant and the overall thrust is calculated using the flight idle setting for each engine rather than calculating the amount of thrust needed to ensure the 3 degrees glide path as for the initial approach phase. As a consequence, the angle of attack begins to rise to provide for the amount of lift needed to keep the flight path angle constant. The flare rotation plays a very important role in the landing simulation, since it must provide a reasonable value of the vertical speed at touchdown as well as to ensure that the aircraft effectively touches the ground with a value of the flight path angle almost equal to zero. The key parameter is the angle of attack time derivative which is unknown. Thus, an iterative process has been implemented to define the best angular velocity to comply with all the required conditions for the terminal phase of the landing. The aircraft drag coefficient, calculated from the input drag polar curve in landing configuration and taking also into account ground effect, is incremented during the ground roll phase to include also the effect of spoilers deflection. This additive contribution is calculated as proposed in [156], using each spoiler at maximum deflection angle. In a similar way, also the lift coefficient during the ground roll phase is affected by the spoilers deflection, reducing it of an amount depending on each spoiler span ratio.

Take-off and landing noise trajectories Concerning the take-off noise trajectory, the procedure is the same as the all engines operating (AEO) normal take-off, with the difference that all the simulations are carried out considering an ISA deviation equal to +10 °C. Landing gears retraction once the aircraft passes the obstacle at 35 ft is simulated by linearly reducing the aircraft overall drag coefficient (derived from the trimmed drag polar in take-off configuration), of a quantity equal to the landing gears overall drag coefficient. The input law for the angle of attack (previously discussed for the normal take-off simulation) is still used here up to the obstacle altitude. From there, the instant at which the acceleration reaches a value close to zero (due to the induced drag) is monitored in order to estimate the aircraft speed to be maintained during all the simulation. This velocity must fall into a very specific range, which depends on the aircraft estimated stall speed at take-off. In order to ensure this condition, an iterative process is carried out on the take-off rotation speed, ensuring at the same time that it complies with all the limitation for normal take-off. Thus, if the calculated climb speed is lower than the lower bound of the abovementioned interval, the rotation speed is increased to allow the aircraft to accelerate more during the ground roll phase. Otherwise, the rotation speed is reduced. Another iterative process is carried out during

the simulation to ensure that the calculated climb speed is kept constant:

- the last calculated angle of attack is used to predict the acceleration at the next simulation step;
- if the acceleration is positive, the angle of attack is increased to provide more deceleration, otherwise its value is reduced in order to increase the acceleration.

At this point two different scenarios are considered: a 100 % take-off thrust simulation, and another one with a thrust cutback at a specific altitude prescribed by the Federal Aviation Administration (FAA). The cutback thrust setting is selected according to [3]. Upon reaching the cutback altitude, the aircraft thrust must not be reduced below that required to maintain either of the following, whichever is greater:

- a climb gradient of 4 %,
- in case of multi-engine airplanes, level flight with one engine inoperative.

In both cases (100 % thrust and cutback) the simulation continues until the aircraft reaches a user-defined horizontal distance from the starting point, set by default at 8000 m.
The landing noise trajectory simulation is performed in the same way as the normal landing phase. However, the need to only model the trajectory up to the end of the final approach allows to completely ignore the iterative process needed to simulate the flare rotation phase.

Climb, cruise and descent simulations The performance module of JPAD allows to carry out the detailed analysis of climb, cruise and descent segments. For each of them a simulation-based approach is still used but with several modifications. First, no ODE system is solved, and, in second place, fewer discrete time steps are considered for the simulation.
With regard to the climb segment, the analysis is carried out taking into account both AEO and OEI conditions in order to estimate the following quantities:

- the rate of climb, the climb angle and the climb gradient as function of true and calibrated airspeed, as well as the Mach number, at different altitudes;
- the aerodynamic efficiency as function of true and calibrated airspeed, as well as the Mach number, at different altitudes;
- maximum rates of climb, climb angles and climb gradients envelopes at different altitudes;
- absolute and operative ceilings;
- time to climb at the maximum rate of climb speed;
- time to climb at the user-defined calibrated climb speed.

Required user-defined parameters are the initial climb altitude, the final climb altitude, and the reference calibrated airspeed for the climb simulation. The simulation considers five intermediate altitudes, from the initial one to the final one, at which all calculation must be made. At each altitude step, the calculation module evaluates also the amount

of fuel used per step by retrieving the value of the SFC from the engine deck at given altitude, Mach number and ambient temperature. The Maximum Climb engine rating is used for the AEO case, while in OEI condition the engine rating is assumed to be the Maximum Continuous.
With reference to the cruise simulation, cruise performance are evaluated only in a steady state, straight flight condition, assuming a symmetrical thrust as well. The cruise analysis is focused on the evaluation of the following quantities:

- aircraft drag, aircraft aerodynamic efficiency, aircraft power needed and overall thrust as functions of the true airspeed, the calibrated airspeed and the Mach number, at different altitudes and for different weight conditions;
- cruise flight envelope as a function of the Mach number;
- aircraft specific air range (SAR) at different weight conditions (cruise grid chart).

For each altitude and weight condition, with the first being provided by the user and the second estimated directly by the software, the JPAD performance module calculates the aircraft drag, the aircraft lift, the overall thrust, the power needed and the power available. Then the aerodynamic efficiency is estimated.
Concerning the descent analysis, the implemented simulation approach is similar to the one described for the climb phase. Users are required to provide initial descent altitude, final descent altitude, reference calibrated airspeed for the descent simulation, and the desired rate of descent. The descent path is first divided in five intermediate altitudes between the initial and final ones. Then for each of them, an iterative procedure, consisting of two iterative loops, is applied. These iterative loops aim at ensuring that the calculated rate of descent differs from the desired one by less than 5 %, and at making sure that the calculated rate of climb differs from the desired one by less than 5 % too. For the engine thrust calculation, a weighted average between Cruise and Flight Idle ratings is used.

Mission profile In addition to the standalone analysis of a single ground or flight phase, JPAD also allows the user to carry out a complete mission profile simulation. The mission profile analysis has the key-role of investigating the behaviour of the aircraft during a specific mission by calculating and reporting time histories of the main physical quantities of interest, as well as to estimate whether or not the designed aircraft is able to cover a given mission range. Table 2.4 and figure 2.6 provide an overview on the set of flight and ground phases accounted by JPAD for the mission performance analysis of a civil transport aircraft.

Emissions

The JPAD emissions tool provides the user with the possibility to estimate pollutant emissions at mission level. The estimation procedure is tightly linked with the output of the mission analysis module, from which it retrieves fuel consumption for each flight phase. These data are then used to assess each pollutant emission using emission indexes provided by the engine deck (the same used for performance assessment). The following species are considered by the emission tool: NO_x, CO, HC, soot, CO_2, SO_x, H_2O.

Table 2.4: List of mission phases accounted by the JPAD performance module.

Phase number	Description
1	Take-off
2	Climb
3	Cruise
4	First descent down to 1500 ft
5	Second climb from 1500 ft up to alternate cruise altitude
6	Alternate cruise
7	Second descent down to holding altitude
8	Holding
9	Approach and landing

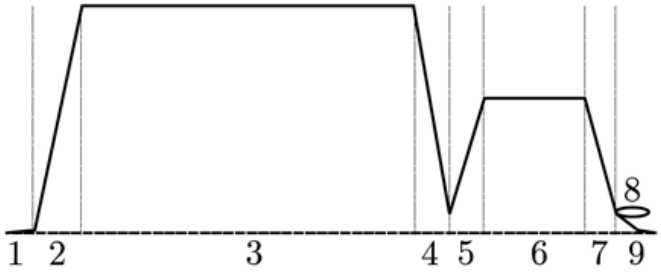

Figure 2.6: Complete set of mission phases handled by JPAD for the performance analysis of a civil transport aircraft.

Noise

Environmental noise calculation are carried out by JPAD by means of ATTILA++. The noise tool, developed during the course of the project, has been linked to the JPAD framework, so that the same calculations that can be normally performed by means of a standalone use of the tool can be also performed in a multidisciplinary environment, with input to the tool in terms of aircraft geometry and flight trajectories directly deriving from the previous analyses. A more detailed description of this tool is provided in section 2.2.

Costs

The last analysis module of JPAD is the one in charge of estimating direct operating costs. The estimation of the DOC breakdown concerns flight operations and considers the following items: capital costs (depreciation, interest, insurance), crew costs (flight and cabin), fuel cost, charges (landing, navigation, ground handling, environmental noise, emissions), direct maintenance (airframe and engine). To estimate those cost items, the methodologies defined by the Association of European Airlines (AEA) for capital, fuel, charges (landing, navigation and ground-handling) and crew costs have been implemented [138], while the method proposed by the former Air Transport Association of America (ATA, today A4A) has been used for direct maintenance costs [136]. Noise charges are calculated by using the formulation recommended in [46][47]. The emissions

charges instead are estimated using the approach prescribed by ICAO in [144].

2.1.2 JPAD tools for pre-design and sizing

JPAD-*initializer* provides the baseline A/C model from which a new design process can start. The baseline A/C is automatically produced in two steps. The first step consists in defining the base geometry of a novel aircraft design starting from a set of top-level aircraft requirements (e.g., number of passengers, design range, cruise Mach number, take-off field length, landing field length, etc.), and basic requests in terms of aircraft type (e.g., general aviation, commuter, business jet, regional jet, regional turboprop, medium-haul jet, long-haul jet, etc.) and configuration (e.g., low wing, high wing, conventional tail, T-tail, wing-mounted engines, rear-mounted engines). Starting from this limited set of information, the module performs an aircraft statistical pre-design. Most of the statistics currently employed by the tool have been developed throughout the years by the DAF research group, while some others have been simply collected from some of the most popular aircraft design books. Pre-design activity by the tool is performed in a stepwise fashion. The first component to be shaped is the fuselage, whose pre-design requires the aircraft type and configuration, and the number of passengers. Next component to be pre-designed is the wing, whose design requires information about the fuselage geometry, besides necessary information regarding TLARs. The pre-design of the wing is followed by the definition of the shapes of the tail components, for which basic information regarding the geometry and the positioning of the wing with respect to the fuselage are essential. For last, engines and landing gears are designed, according to the results at the previous steps. Figure 2.7 synthesizes the statistical pre-design tool workflow. Since the statistics on which the methods implemented by the code rely are based on existing airplanes, with some of them being particularly old designs, several calibration factors have been defined as input to the tool, in order to enable the user to introduce some kind of entry into service or technology level factor for certain selected variables, such as the wing aspect ratio.

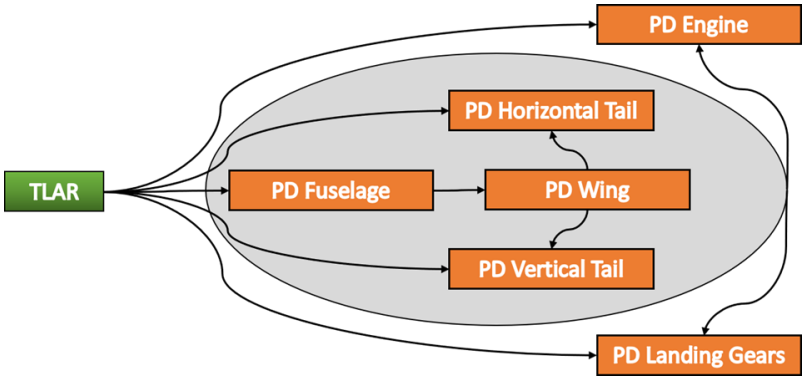

Figure 2.7: JPAD statistical pre-design tool workflow.

Once the geometry of the aircraft has been defined, the pre-design tool performs a Class-I weight estimation based on the fuel fraction method. This low-fidelity calculation allows to have, even at such an early stage, a first estimate of the max take-off weight, of the fuel weight and of the operative empty weight of the pre-designed airplane. The fuel fraction method involves the use of the Breguet formulas in order to estimate the fuel fractions for the cruise, holding, and alternate phases of the design mission, for which

duration, spatial extent and aircraft speed have been provided through the starting set of TLARs. Fuel fractions for the remaining phases of the design mission are not directly calculated, but constant values set according to the available literature [153] and based on the aircraft type and configuration provided through the set of top-level requirements are assumed. For last, in order to actually estimate the abovementioned design weights, the method necessitates of a statistical law linking the max take-off weight and the operative empty weight. Several DAF in-house prepared statistical laws, covering different airplane categories, provide the coefficients of the linear relationship between the logarithms of the two weights.
In a second step, JPAD-*initializer* allows to perform the sizing of the newly created aircraft and to select a sizing point, permanently fixing the geometry and the static thrust of the baseline A/C. The adopted methodology is the one described in [153]. The application of such a procedure ensures that, in addition to meet the range and endurance objectives, the newly designed aircraft also fulfils the following performance targets fixed by the TLARs: take-off field length, landing field length, climb rate, and cruise speed. The application of the sizing method results in the determination of a range of values of wing loading (W/S) and thrust loading (T/S) within which a specific set of performance requirements are met, allowing to derive a design space in which the combination of the highest possible wing loading and lowest possible thrust loading results in an airplane with the lowest weight and the lowest cost. In order to perform such a task, several input variables should be provided:

- weight ratios (e.g., cruise start over maximum take-off weight ratio, landing over maximum take-off weight ratio),
- drag coefficients (e.g., zero lift drag coefficient, landing gear and flap zero lift drag coefficient delta),
- Oswald factors (e.g., clean Oswald factor, landing and take-off Oswald factors),
- maximum lift coefficients (e.g., clean, take-off and landing max lift coefficients).

The sizing tool automatically selects the most suitable values for the abovementioned variables based on the input at pre-design level in terms of aircraft type and configuration. For this purpose, several statistics have been collected from some of the most renowned aircraft design textbooks. As with the pre-design tool, also the sizing tool allows to perform a tune on some variables estimated from statistics, in order to introduce some kind of technology trend factor. Once the sizing activities have been performed and the sizing point has been selected, updated values for the engine static thrust and the wing planform surface are calculated. The latter is then used to perform an update through the pre-design tool of all the components whose geometry directly depends on the wing planform surface (mainly the horizontal and vertical tail) and to update the wing geometry of course. The entire JPAD-*initializer* workflow has been summarized in figure 2.8. The output produced by this module is ready to be used to carry out a multidisciplinary analysis, according to the workflow illustrated in section 2.1.1, or to be used as the starting point for a full-factorial DOE, as demonstrated in section 2.1.3.

2.1.3 JPAD-*doe* analysis module

The JPAD-*doe* module allows to perform aircraft parametric analyses, paving the way to the set-up of multidisciplinary analysis and optimization (MDAO) workflows. In order

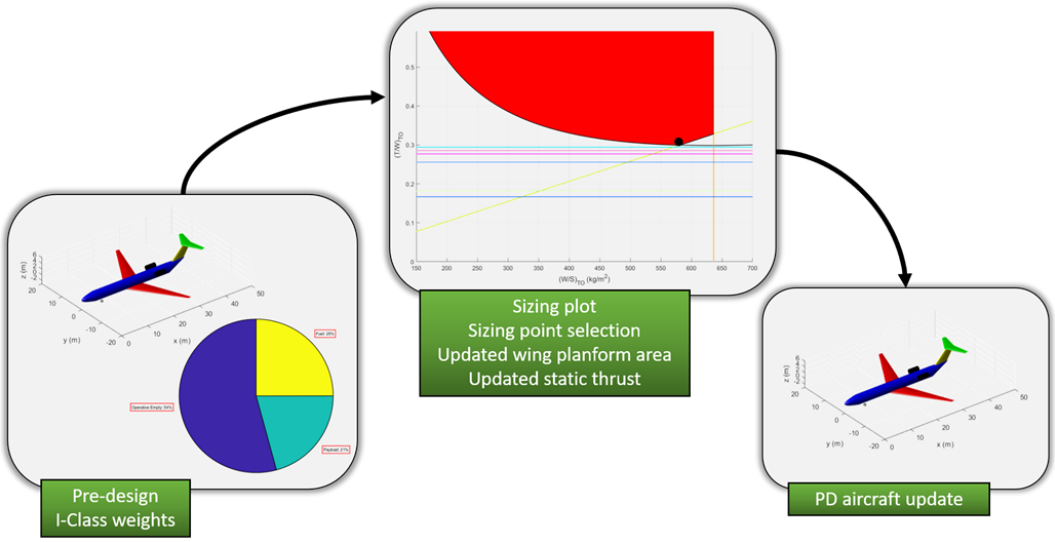

Figure 2.8: JPAD-*initializer* complete workflow.

to carry out such a task, the JPAD-*doe* relies on all the features implemented inside the core module. Because of this, the JPAD-*doe* module can be seen as a general analysis manager, allowing users to easily analyze a large number of different aircraft models, searching for one or more optimum configurations thanks to the optimization module described in section 2.1.4.
Speaking of the JPAD-*doe* module, it allows users to have access to all possible input variables needed to define both the aircraft parametric model and main analysis input parameters (e.g., cruise operating conditions, calibration factors to simulate technological trends, etc.), giving the possibility to specify which ones have to be changed and within which range of values. The final number of aircraft models generated by the module is equal to the total number of possible combinations between all the design parameters, in a full-factorial combination.
In order to ensure the feasibility of each generated aircraft model, several consistency checks are performed. These consist in a series of geometrical checks used to assess that there are no overlapped or floating components. For example, the module is capable to inspect lifting surfaces and to check whether their positioning with respect to the fuselage is not consistent (i.e., lifting surfaces are not attached to the fuselage), or to perform a check on the cabin and on its estimated dimensions and positioning with repect to the fuselage, in order to assess its feasibility.
In addition to feasibility checks, the JPAD-*doe* module allows the user to assign one or more geometry update strategies to differentiate the DOE aircraft population from the baseline A/C model. These update strategies mainly concern the geometry of the fuselage, the planform shape of the lifting surfaces, and the positioning of tail surfaces. Dealing with the fuselage, all geometry update strategies are focused on the management of nose, cylinder and tail trunks parameters, as well as cylinder trunk section dimensions. One fuselage update strategy, for instance, allows to update the overall fuselage length while keeping constant nose and tail trunks ratios along with the cylinder trunk section diameter, while another one allows to update the length of the nose trunk with the overall length and diameters kept constant. Each lifting surface planform shape can be modified and updated as well by adopting specific strategies allowing to manage both

equivalent lifting surface parameters (area, span, aspect ratio, etc.) and single panel data (inner and outer chords, panel spans, etc.). For example, users can perform an update of the value of the aspect ratio of a lifting surface while keeping constant panels relative span and chord ratios. Concerning horizontal and vertical tail planes, users can also choose whether to scale and (eventually) move the tail surface in order to keep the volumetric ratio constant and equal to the one of the baseline A/C. If the surface scaling provides for an unfeasible tail position (e.g., the tail plane is no more attached to the fuselage) the latter is also modified, starting an iterative loop to match the target volumetric ratio. Obviously, the adoption of such an update strategy precludes the use of any aforementioned procedure for lifting surfaces. Figure 2.9 provides an example of JPAD-*doe* application for a generic A/C model.
Once the aircraft population has been generated, each aircraft is analyzed by means of a combination of JPAD-*core* analysis modules. At the end of each analysis cycle, JPAD stores in an external dataset all the output variables that the user has decided to monitor, defining in this way a cloud of solution points (one per aircraft). All these data can be then passed to JPAD-*optimizer* module. This one, conceived as a standalone tool usable both within the JPAD framework and as an independent application, is described in section 2.1.4.

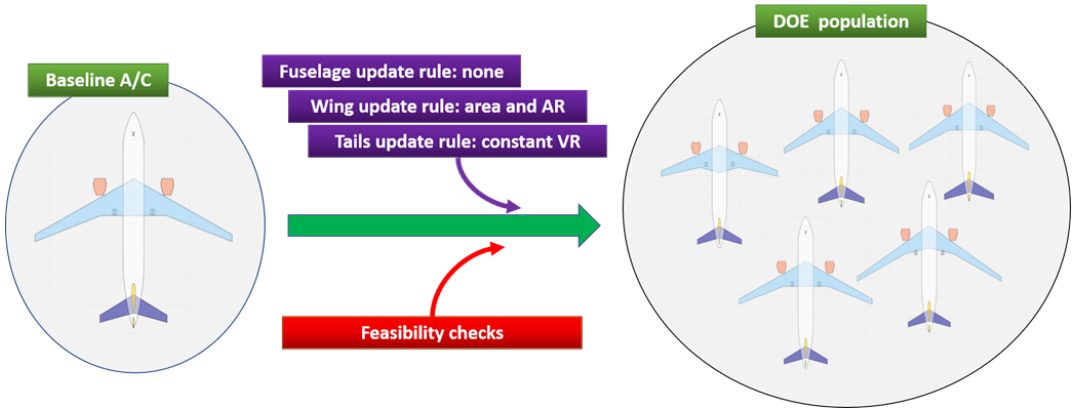

Figure 2.9: JPAD-*doe* module usage example.

2.1.4 JPAD module for optimizations

The JPAD module for optimizations is based on well-known metaheuristic algorithms, among which the most commonly used are Genetic Algorithms (GA) and Particle Swarm Optimization (PSO) algorithms. The use of metaheuristic algorithms allows to easily manage complex optimization problems with a reduced amount of calculations if compared with classical deterministic algorithms (i.e., gradient based like Newton-Raphson). In addition, since they do not rely on derivatives but only on objective function values, they easily manage complex and even discontinuous response surfaces [188].
JPAD-*optimizer* is provided with all the current state-of-the-art metaheuristic optimization algorithms thanks to the use of a dedicated external library, named MOEA Framework[4]. Although the JPAD optimization module can use every algorithm provided by this library, two of them have been typically used in recent research activities due to better results in terms of quality and computational efforts: ϵ-NSGA-II, which is an

[4]http://moeaframework.org/

extension of NSGA (Non-dominated Sorting Genetic Algorithm); and OMOPSO (Optimized Multi-Objective Particle Swarm Optimization). Using both these algorithms, the JPAD optimization module can easily solve complex MDAO problems reading all the following required instructions from a dedicated configuration file:

- the number of design variables, objectives and constraints;
- whether an objective has to be minimized or maximized;
- upper and lower boundaries for the values of the design variables;
- constraints in terms of values and type of violating condition (e.g., constrained variable value falling outside a prescribed interval)
- the algorithm to be used.

Together with this information, the complete set of points of the response surface generated by the JPAD-*doe*, or by an external application, is passed to the module as a comma separated value (CSV) file. Before the optimization process starts, all response surface points are interpolated using radial basis function interpolation.

2.2 ATTILA++: a tool for preliminary A/C noise analyses

ATTILA++ (AircrafT noise predicTion IncLuding performAnce) is the tool for preliminary aircraft noise calculations developed within the context of ADORNO. This tool is particularly suited for the estimation of environmental noise produced by turbofan driven civil aircraft at the three certification points prescribed by ICAO [143] and represented in figure 2.10:

- Approach (landing) condition:
  - Measuring point positioned 2000 m away from the beginning of the landing strip.
  - Descent angle for the approach trajectory equal to 3 degrees.
- Flyover (take-off cutback, i.e., reduced engine thrust) condition:
  - Measuring point positioned 6500 m away from the beginning of the take-off run.
  - Thrust or power not reduced below that required to maintain:
    - A climb gradient equal to 4 %, or, for multi-engine airplanes.
    - Level flight in case of OEI conditions.
- Lateral (take-off sideline, i.e., maximum engine thrust):
  - Maximum engine speed.
  - Measuring performed on two sidelines, 450 m away from the take-off runway.
  - Reference effective perceived noise level (EPNL) value equal to the maximum measured along the sidelines.
- Prescribed ambient conditions (valid for all the certification points):

- Sea-level atmospheric pressure (101.325 kPa).
- Air temperature equal to 25 °C.
- 70 % of relative humidity.
- Zero wind.

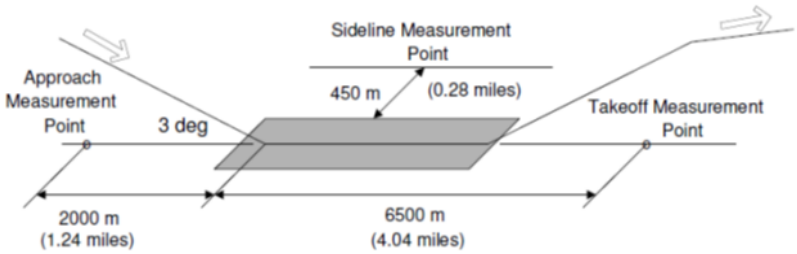

Figure 2.10: Certification points prescribed by ICAO, image taken from [143].

In order to make the tool compliant with the list of requirements set by MTU, it has been written in C++ language, following an object-oriented programming (OOP) approach. This choice has been guided by the necessity to link this tool to the existing MTU IT-framework. Moreover, OOP paradigms allow to easily pursue several software engineering goals, such as reusability, extensibility and flexibility, which should ease code maintenance tasks and future updates.
Engineering Science Data Unit (ESDU) methodologies and equations have been implemented in order to include the contribution to the overall aircraft noise of both airframe components and engines, as well as the effects related to the propagation of the noise towards the receiver microphone. Calculations can be performed for the three certification points and/or for a user-defined case, for which a completely arbitrary trajectory and array of receivers can be assigned. A limited amount of information is required in order to run the calculations, including data on the geometry of the aircraft, on the flight trajectories and on the aircraft configuration during flight (i.e., high-lift devices deployed, landing gears extended, etc.). An engine noise deck, appropriately formatted and including information on engine noise spectra for different values of the polar emission angle (i.e., the angle set by the noise source and the receiver with respect to a horizontal line) should be provided too, in order to include the engines contribution in the overall aircraft noise calculation.
Figure 2.11 provides an overview on the general architecture of the software and on the typical ATTILA++ workflow. In this figure, the set of C++ classes and the sets of input and output files on which ATTILA++ is built are highlighted, along with their usage during an ATTILA++ noise analysis. The following sub sections provide a brief overview on the methodologies implemented by ATTILA++, on the included noise metrics, and on the set of input files managed by the tool.

2.2.1 Implemented methodologies

Airframe noise

The calculation of airframe noise relies on the methodology reported in [173]. This methodology allows to take into account the environmental noise produced by the following components of the aircraft: wing, horizontal tail, vertical tail, nose and main landing gears, flaps and slats. Airframe noise results from air flowing over the surfaces

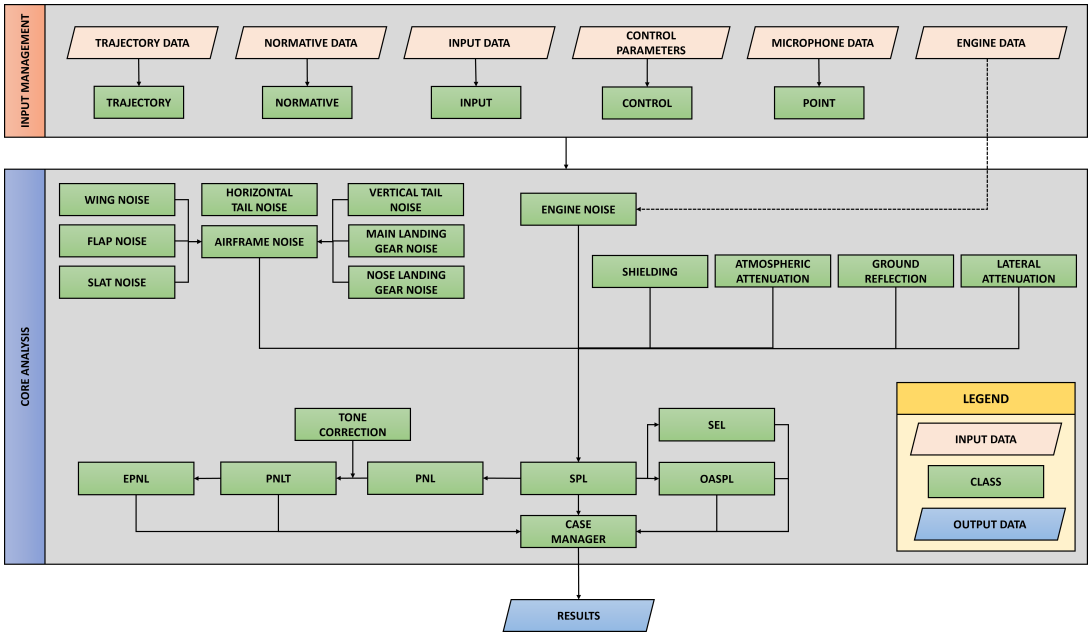

Figure 2.11: ATTILA++ main architecture and typical analysis workflow.

of the airplane. It does not include the contribution of the powerplant, thus setting a lower boundary for engine noise reductions, below which any further decrease in terms of noise produced by the engines would not have any noticeable impact on the overall noise of the aircraft. The configuration of the aircraft has of course an effect on the airframe noise. An aerodynamically clean configuration (i.e., with no high-lift devices deployed and landing gears extended) generates less noise than an aircraft in landing or take-off configuration.
The methodology reported in [173] is semi-empirical and has been developed starting from that proposed in [70][192], but including new or updated information. The sound pressure level (SPL) values produced by the application of this method are for free-field and still, lossless atmospheric conditions. Each of the abovementioned components is modelled by the method as an elementary source or a source distribution. Analitical and/or empirical approaches have been adopted to model the directivity and spectral characteristics of each source. Moreover, this method assumes that no interaction occurs between different sources. The SPL at the receiver location is estimated using the following equation, depending on the ambient density and sound speed at aircraft location (ρ and c, respectively), on a reference pressure (p_{ref}, equal to 20 μPa), on the ambient pressure at source and receiver location (p_l and p_0, respectively), and on the dimensionless mean square acoustic pressure (p^2):

$$SPL = 10log(p^2) + 10log(\frac{\rho^2 c^4}{p_{ref}^2}) - 20log(\frac{p_l}{p_0}). \tag{2.4}$$

The dimensionless mean square acoustic pressure, p^2, is given by the following general equation, which depends on the characteristics of the airframe component to be modelled in terms of directivity function $D(\phi_f,\theta)$, spectral function F(Sr) and geometry, through

the Pb_w^2 term:

$$p^2 = \frac{Pb_w^2 D(\phi_f, \theta) F(Sr)}{4\pi r^2 (1 - Mcos(\theta))^4} \tag{2.5}$$

in which r is the radial distance between the source and the receiver, θ is the polar emission angle, ϕ_f is the azimuthal angle (figure 2.12 provides an explication on these angles), M is the flight Mach number, and Sr is the Strouhal number. The term Pb_w^2 is a function of the Mach number and of the geometry of the component, through the k_1, k_2, and k_3 constants:

$$Pb_w^2 = k_1 M^{k_2} k_3. \tag{2.6}$$

For each of the abovementioned airframe components, [173] provides several tables allowing to calculate directivity functions, spectral functions, and geometry-dependent constants.

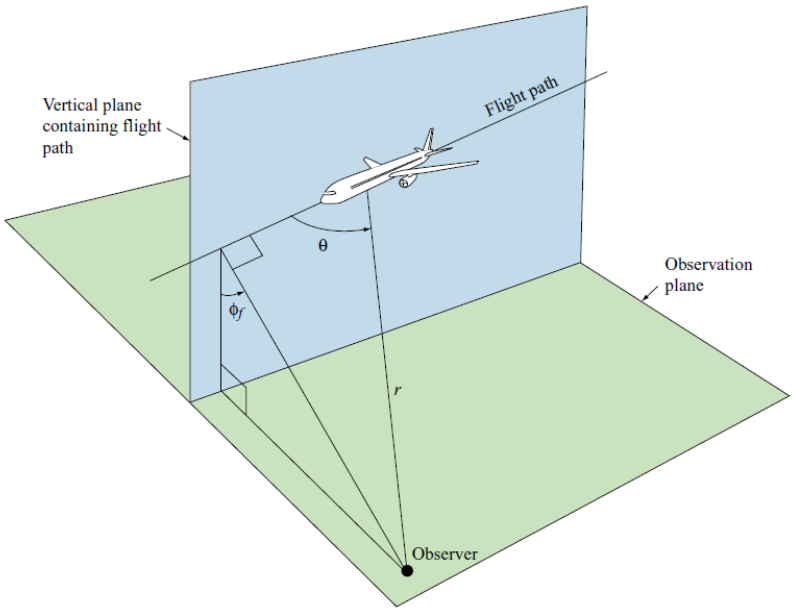

Figure 2.12: Sketch of the set of parameters (angles and distances) taken into account by the airframe noise method of [173]. Image taken from [173].

Propagation effects

In order to include the effects of atmospheric attenuation, the methodology proposed in [171] has been implemented. Several processes, in general, can lead to the loss of acoustic energy of a sound wave propagating through the atmosphere. These are mainly the spherical spreading and the gaseous absorption. The effect of spherical spreading is already accounted by the method reported in [173], while the methodology reported in [171] allows to include the effects of gaseous absorption. This methodology relies on a series of tabulated data of the rate of atmospheric attenuation at discrete frequencies for a still homogeneous atmosphere, for different conditions in terms of temperature, relative humidity, and pressure. In order to ease the calculation, the reference also provides interpolating functions.
The procedure described in [175] allows to estimate the effect of noise measurements affected by the reflection of the sound wave by the ground. When ground reflection occurs,

reflected waves will reach the receiver following a different (longer) path with respect to direct waves. The interference between direct and reflected waves determines the necessity for ground reflection corrections. The correction given by this method could be both subtracted from a measured spectrum, providing a free-field spectrum, or added to the free-field spectrum, in order to get a measured spectrum, which is the case of ATTILA++. Besides information on the reciprocal positions of source and receiver, this method also requires a basic description of the characteristics of the ground (in order to derive an impedance value) and those of the air (in terms of average turbulence). The ground is simply described as a porous layer structure, using a two-parameter model (the reference also provides typical values of these parameters for several ground surfaces), while the presence of air turbulence is accounted by considering its effect on the coherence between direct and reflected waves, assuming a value for the fluctuating index of refraction of the surrounding air.
Lateral attenuation data in terms of one-third octave band values provided in [172] has been adopted in ATTILA++. This data accounts for the effect of any additional attenuation factor occurring when the receiver is not directly under the flight path of the aircraft. The reference provides two separate sets of data: one for civil jet-powered aircraft with engines mounted below the wing, the other one for civil jets with rear-mounted engines. In this case too, data is provided in terms of several carpets. For generic values of propagation distance, elevation angle and frequency, interpolation is carried out.
An approach for the estimation of noise shielding by lifting surfaces has been developed and implemented too, starting from the methodology described in [174]. A barrier placed between a sound source and a receiver forces the sound to reach the observer by diffraction over the edges of the barrier, which is the shielding effect. The method proposed in [174] is based on a series of geometric considerations on the relative position of source and receiver. When there is no line of sight, the path of the acoustic rays around the edges of the barrier is considered and the diffraction effect is taken into account. The methodology presented in [174] has been conceived for semi-infinite barriers in non-aeronautical applications. This has implied the need to adapt the methodology and to perform several assumptions, in order to ease the modelling of airplane components as potential noise barriers. Wing, horizontal tail and vertical tail are the only aircraft elements considered as potential acoustic barriers, while the engines are considered as the only source to which the shielding effect is applicable. The method is valid for a generic wedge-shaped barrier, but, for a practical integration in ATTILA++, only flat barriers have been supposed for the modelling of lifting surfaces. Moreover, to preserve the simplicity and the limited amount of information required by the input files, the lifting surfaces have been modelled as flat rectangles in 3D space. Effects of warping, airfoil curvature and sweep angle cannot be captured by the shielding calculation module of ATTILA++.

Engine noise

ATTILA++ has been implemented with the capability to read via input interface a given dataset of engine noise spectra to compute the contribution of engine noise to the overall aircraft noise, for a specific flight condition. After reading a given engine noise dataset, ATTILA++ performs a linear interpolation or extrapolation of the data, depending on the specific request and on the provided dataset in terms of polar directivity angles and engine throttle values. The aircraft SPL spectra are calculated by energetically adding the noise contribution of the engine to that of the airframe, once that engine noise spectra have been corrected for spherical spreading, Doppler shift, and, eventually, for the

TAKEOFF_RATING							
DISTANCE	50						
RATE	1.0						
ALFA	50	63	80	100	125	...	One-third octave bands
20	59	62.9	66.6	69.9	...	...	
30	59	62.9	66.7	69.9	...	...	SPL spectra for TO rating
40	59.1	62.9	66.7	69.9	...	...	
...	...	...	...	...	...	...	
...	...	...	...	...	...	...	
APPROACH_RATING							
DISTANCE	50						
RATE	1.0						
ALFA	50	63	80	100	125	...	One-third octave bands
20	59	62.9	66.6	69.9	...	...	
30	59	62.9	66.7	69.9	...	...	SPL spectra for App. rating
40	59.1	62.9	66.7	69.9	...	...	
...	...	...	...	...	...	...	
...	...	...	...	...	...	...	

Figure 2.13: Example of ATTILA++ input engine file formatting.

additional propagation effects requested by the user (e.g., atmospheric attenuation and ground reflection). It is important that the engine input file is formatted as shown in figure 2.13. It must be a comma separated values file, and SPL spectra should be provided as one-third octave band spectra, ranging from 50 to 10,000 Hz. Moreover, spectra must be provided for a single fixed distance (preferably equal to 150 ft), and for different values of the polar emission angle, possibly ranging from 0 (corresponding to engine inlet direction) to 180 degrees (on the same direction of the engine exhaust). Data should be provided for both the engine ratings considered by ATTILA++ during the noise calculations: take-off (for the flyover and sideline certification points) and approach (for the certification condition with the same name). Moreover, SPL spectra corresponding to different throttle ratios should be provided for both the engine ratings, in order to allow data interpolation/extrapolation, depending on the input in this sense coming from the trajectory input files.
Since no data on reference engine noise was provided in ADORNO, the methodology described in [177] was used in order to generate an engine noise deck like the one required by ATTILA++, to be used for the noise assessment of the reference (year 2014) aircraft models. The one included in [177] is a simple semi-empirical methodology allowing to generate a noise engine deck from a limited set of information, involving both geometrical and thermo-fluid dynamic parameters. It consents to calculate the noise produced by axial-flow fans or compressors in turbofan and turbojet engines. Components with multiple stages (e.g., multi-stage fan) can be also modelled with this approach. Table 2.5 provides the list of input variables required by the application of this method. It is possible to include in the calculation of the engine noise spectra only the fan/compressor noise contribution coming from the inlet or the discharge ducts, or eventually consider both of them. It requires a basic description of the geometry of the fan/compressor, in terms of number of blades of rotors and stators and in terms of minimum distance between them. Information on blade row attenuation can be also provided, if available. Information on the total temperature rise, on the mass flow rate, on the rotational speed, and on the rotor tip Mach number (both at design and operating point conditions), might be difficult to retrieve from a simple online research on a specific engine model, but they can be quite simply estimated by using a third-party calculation tool for engine performance, as it will be discussed later in chapter 4. This was done, for example, for the generation

of the engine noise deck used for the analyses described in section 2.3.2. Starting from a reliable engine model of the PW1500 engine implemented in a well-known engine performance tool, thermo-fluid dynamic parameters listed in table 2.5 were derived for that engine, and a new engine noise deck was built.

Table 2.5: Set of input variables required by the methodology for engine noise described in [177].

Number	Variable description
1	Fan/compressor noise from inlet and discharge ducts: only inlet, only discharge, both ducts.
2	Number of stages.
3	Number of stator blades (one value for each stage).
4	Number of rotor blades (one value for each stage).
5	Minimum rotor-stator spacing, divided by rotor blade chord (percentage, one value for each stage).
6	Total temperature rise across stage (one value for each stage).
7	Blade row attenuation in forward arc.
8	Blade row attenuation in rear arc.
9	Rotor shaft rotational speed.
10	Mass flow rate through fan/compressor.
11	Rotor tip relative inlet Mach number at design point.
12	Rotor tip relative inlet Mach number at operating point.
13	Rotor tip Mach number at operating point.
14	Inlet guide vanes (present or absent).
15	Air pressure at fan location.
16	Air pressure at receiver location.
17	Ambient air temperature.
18	Receiver locations (in radial coordinates).

2.2.2 Implemented noise metrics

ATTILA++ provides aircraft noise calculations according to the metrics listed in table 2.6. All the metrics are expressed in dB, or in A-weighted dB (dBA), depending on the user's request. OASPL is calculated from SPL by logarithmic addition of all the discrete spectral sound pressure levels. PNL, the tonal correction, PNLT and EPNL are calculated according to the formulation described in [3].

2.2.3 Input files

Input files of ATTILA++ contain comma separated data and are assigned by means appropriate labels, which identify each input variable. When not all the data necessary for a certain calculation have been included, default values are assumed by the tool. The calculation proceeds, but the user is notified about this issue in the output log file, produced by the tool at the end of the execution.
Several input files must be provided and eventually modified to perform the desired calculations:

Table 2.6: Set of implemented noise metrics in ATTILA++.

Number	Noise metric
1	Sound Pressure Level (SPL) in one-third octave band frequencies
2	Overall Sound Pressure Level (OASPL)
3	Perceived Noise Level (PNL)
4	Tone-corrected Perceived Noise Level (PNLT)
5	Effective Perceived Noise Level (EPNL)
6	Sound Exposure Level (SEL)

- *Input.csv* - It contains input data related to the aircraft type, airframe components characteristics and geometry, airframe components relative positions with respect to the engine (which are eventually required by the noise shielding module), and some additional parameters related to the calculation of the effects of ground reflection.
- *Trajectory.csv* - It includes data related to the aircraft trajectory and, optionally, ambient conditions at noise source locations (if not provided through this input file, they are automatically assumed by ATTILA++, by means of an integrated atmosphere model). Separate files should be provided for the three certification points and for the user-defined case.
- *Receivers.csv* - It contains input data related to receiver's positions and, eventually, ambient conditions at receivers' locations (automatically calculated if not present). Separate files should be provided for the three certification points and for the user-defined case.
- *ControlParameters.csv* - It includes input data related to analysis directives (e.g., which analyses should be carried out, which noise sources should be included in the calculations, according to which noise metrics, etc.) and the verbosity of the output files.
- *Engine.csv* - It includes engine noise data to be used to carry out aircraft noise calculations including the contribution of the engines.

2.3 ADORNO A/C design activities (WP2)

The following sections provide a detailed description of the work carried out for the WP2 activities of ADORNO by the author and by his colleagues of the DAF research group. The WP2 focused on the design of reference (year 2014) and target (year 2025+) A/C models, the latter equipped with CS2 airframe technologies and with advanced turbofan engines, designed by MTU. The design and the comparison of UM and RM configurations for both the time horizons was planned at the beginning of the project. Since the design of the target RM configuration is still ongoing (the submission of the dataset is expected by the first quarter of 2022), the following sections will be focused on the design and analyses performed on the UM configurations.

2.3.1 Definition of the set of TLAR

The Airbus A220-300 (figure 2.14) was selected as the reference A/C model for project activities. The A220-300 is a narrow-body, single-aisle, twin engine, medium-haul jet airliner, previously known as CS300. Newly designed from ground up, it was initially produced by Bombardier Aerospace, but is currently marketed by Airbus and built by CSeries Aircraft Limited Partnership joint venture (CSALP). It belongs to the Airbus newly branded A220 family, in which the A220-100 (previously called CS100) offers a smaller option. It features a 38.7 m overall length, a wingspan of 35.1 m, and a 11.5 m height [6]. It can accommodate from 130 (in a 2-class configuration) up to 160 passengers (single-class high-density layout) with two-by-three seating, and it offers one of the highest overhead bin volume per passenger and one of the widest aisle, allowing for faster boarding and disembarkment operations [6]. Being a clean sheet design, the A220-300 features the latest generation flight deck, fly-by-wire, and a large use of composites (both for the fuselage and the wings, to the point to be nicknamed *the plastic airplane*) along with aluminium-lithium alloys, which help managing target operating weights [108]. It comes equipped with two Pratt & Whitney's new fuel-economising PurePower geared turbofan (GTF) engines (PW1521G and PW1524G variants), providing a static thrust (measured at sea level, flat rated to ISA +15 °C) going from 93.4 kN (PW1521G engine variant) up to 103.6 kN (PW1524G) [11][13]. The use of high bypass ratio (HBPR) geared turbofan engines, along with the aforementioned use of advanced materials and aerodynamic devices (such as winglets), allow for an improved saving on fuel (20 % compared with Airbus A320neo and Boeing 737NG, according to Bombardier) and operating costs (12 % with respect to the latest-generation competitors and 15 % with respect to current market-leading models) [108]. Range reaches up to 3750 nmi (ferry range), while for a design mission with 140 passengers range goes to 3100 nmi [7].

Figure 2.14: A220-300 front and side view, taken from [18].

Tables 2.7, 2.8 and 2.9 provide information and data regarding the geometry, the design weights, and the powerplant options of the A220-300. These data were mainly gathered using technical documents provided by the manufacturer, official brochures, and certification documents (type certificate data sheets, TCDS). Table 2.10, instead, provides information on the set of TLARs that, starting from the available information on the A220-300, were selected as the main requirements guiding the design process of the aircraft models of WP2. These data were mainly derived from the same set of technical documents listed above. Additional information on climb speed and rate of climb per flight level interval, available at the online Eurocontrol database[5], were assumed, and have not been reported in table 2.10 for the sake of brevity. Moreover, requirements on alternate and holding phases were assumed based on information on similar aircraft.

[5] https://contentzone.eurocontrol.int/aircraftperformance/default.aspx?

Table 2.7: Main geometrical characteristics of the Airbus A220-300.

Main geometric data and cabin arrangement [6][7][5]	
Cockpit crew	2 pilots
Cabin crew	3 (minimum)
Passengers	130 (2-class) - 160 (1-class)
Seats configuration	Two-by-three
Seat pitch	81.3 cm (economy)
Seat width	47-48 cm (economy)
Cargo volume	31.6 m^2
Overall length	38.71 m
Wing span	35.1 m
Wing area	112.3 m^2
Overall height	11.5 m
Fuselage diameter	3.7 m
Cabin width	3.28 m
Cabin height	2.13 m

Table 2.8: Design weights and fuel capacity of the A220-300.

Main weight data and fuel capacity [7][11]	
Maximum Ramp Weight (MRW)	68039 kg
Maximum Take-Off Weight (MTOW)	67585 kg
Maximum Landing Weight (MLW)	58740 kg
Maximum Zero Fuel Weight (MZFW)	55792 kg
Operating Empty Weight (OEW)	37081 kg
Max Payload	18711 kg
Max Fuel Tank Capacity	21508 l

2.3.2 Design of the reference A/C model

In this section all the activities related to the definition of the reference UM aircraft model are summarized, highlighting the optimization process used to select the best set of geometrical design parameters, as well as the main results coming from the complete multidisciplinary analysis cycle of the final configuration.

Preliminary sizing of the baseline model

Section 2.1 has provided an overview on the MDAO framework put in place in order to produce results for the ADORNO WP2 design activities in terms of year 2014 reference A/C models and year 2025+ target A/C configurations. In order to provide the design framework with a plausible and, most importantly, feasible baseline A/C, JPAD-*initializer* capabilities were employed, together with the set of top-level requirements shown in table 2.10, which was the main input of the tool in this phase, together with information on the powerplant system (e.g., engine type and number of propulsive units) and on the aircraft configuration (e.g., wing position, tail type, engines location). The

Table 2.9: Airbus A220-300 engine options [13].

Engine	**PW1521G**	**PW1524G**
Bypass ratio	12:1	12:1
Overall length	3.184 m	3.184 m
Diameter fan tip	185.42 cm	185.42 cm
Dry weight	2177 kg	2177 kg
Sea-level static thrust	93.4 kN	103.6 kN

Table 2.10: Set of TLAR selected for the ADORNO design activities of WP2.

ADORNO set of reference TLAR	
Accommodation	140 passengers (1-class) [5]
Range (140 passengers)	3100 nmi [5]
Take-Off Field Length (MTOW, ISA SL, dry)	1890 m [6]
Landing Field Length (MLW, ISA SL, dry)	1509 m [6]
Approach speed (IAS)	136.5 kn [7]
Cruise Mach number	0.78
Cruise altitude	37000 ft
Alternate Mach number	0.65
Alternate altitude	20000 ft
Alternate range	200 nmi
Holding Mach number	0.55
Holding duration	30 min
Fuel reserve	5 %

first steps performed with the A/C initializer were, as mentioned in section 2.1.2, the statistical pre-design of the baseline UM model, the definition of the mission profile, and the Class-I weight estimation. The following parameters were used in order to perform the first of the task listed above, and guide the definition of the geometry of the baseline model, along with the characterization of some basic aerodynamic parameters, such as Oswald factors, zero-lift drag coefficients, and maximum lift coefficients:

- aircraft type,
- number of design passengers,
- design range,
- landing field length,
- take-off field length,
- cruise Mach number,
- number of engines,
- engines type,

- aircraft configuration.

On the other hand, top-level requirements in terms of ranges, speeds, rates of climb/descent, durations, and fuel reserve, contributed to the definition of the mission profile and to the weights estimation. In section 2.1.2 it was mentioned that the statistical pre-design tool allows the user to perform calibrations on some selected variables, in order to simulate technological trends for some specific design parameters. In this case, tweaks were performed on the following variables managed by the tool:

- wing aspect ratio,
- maximum lift coefficient at take-off,
- maximum lift coefficient at landing.

This was performed to allow for values of the wing aspect ratio closer to the ones for modern aircraft such as the Airbus A220, and to have slightly higher values for the maximum lift coefficients, in line with those of similar modern airliners.
The main output of this pre-design activities were a preliminary aircraft geometry (to be subjected to changes according to the results coming from the sizing activity, as already mentioned in section 2.1.2), along with the mission profile (reported in figure 2.15) and a preliminary weight estimation (reported in figure 2.16 and in table 2.11). In order to perform a first weight estimation, the statistical pre-design tool made use of Breguet's formulas for range and endurance calculations, together with statistical weight fractions for mission phases such as take-off and landing, in order to implement the weight fraction method described in [153]. As already mentioned in section 2.1.2, this applied methodology relies also on statistical laws linking the aircraft maximum take-off weight to the operating empty weight. In this case, an in-house developed regression law for modern (2000+) regional jets/narrow-body airliners was employed by the tool, in order to perform a much more suiting first estimate of the design weights.

Table 2.11: Class-I weights analysis results for the UM statistical configuration.

Description	**Value**
Maximum Take-Off Weight	68018 kg
Operating Empty Weight	36018 kg
Payload Weight	14288 kg
Fuel Weight	16759 kg
Crew Weight	612 kg
Maximum Zero Fuel Weight	51258 kg

The output from the statistical pre-design was then provided to the sizing module, in order to ensure that the UM baseline A/C fulfilled top-level requirements in terms of take-off field length, landing field length, climb rate and cruise speed. Main input to the sizing coming from the statistical pre-design module, apart from geometry-related quantities, is summarized in table 2.12.
The sizing limitations and the design point selected for the UM baseline A/C from the pre-design output are shown in figure 2.17, while table 2.13 reports thrust and wing loading data for the selected sizing point. As can be deduced from figure 2.17, design point selection was limited by cruise, take-off and landing requirements. In order to have

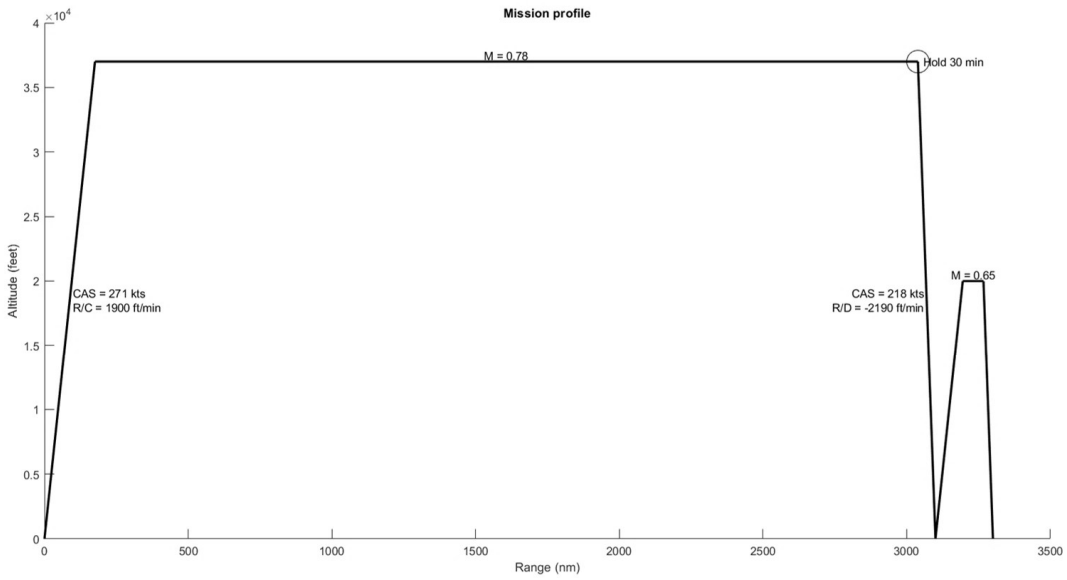

Figure 2.15: Mission profile for the UM aircraft configurations of ADORNO, based on the set of selected TLAR in terms of speeds, altitudes, durations, and ranges per mission phases.

the lowest possible wing surface along with the lowest possible engine static thrust, the entire segment between the intersection of the cruise and take-off limitations and the intersection of the take-off and landing limitations would have been suitable, with the final design point selected being a good compromise between the two abovementioned objectives, which, in this specific case, could not be simultaneously satisfied. Design point selection was also limited by the available reference engine dataset at the time these analyses were carried out. An engine deck, elaborated by UNINA, and to be used to perform aircraft detailed performance assessment, had already been checked and validated by MTU for an engine with characteristics similar to those of the Pratt & Whitney PW1524G. Since just small variations around the original static thrust value (103.6 kN) were agreed with MTU in order for the engine performance dataset to be considered still reliable, the baseline A/C model design point selection was driven by an additional constraint.
As previously anticipated, once that the sizing analysis had been carried out, the statistical pre-design module was used again, this time using updated data on wing planform area and engine static thrust coming from the sizing, and reported in table 2.13. Wing planform area was updated by using the MTOW obtained from the Class-I weight analysis. This step is quite important since it allows to update horizontal and vertical tails accordingly with the updated wing area.

UM reference model MDAO process

Starting from the baseline aircraft model defined in the previous section, a complete MDAO process was carried out to investigate the effect of some of the main geometrical design parameters of the aircraft model on mission-related output objectives linked to CO_2 and NO_x emissions, as well as to the environmental noise. The outcome of this activity was the assessment of the best possible A/C configuration to be used as reference

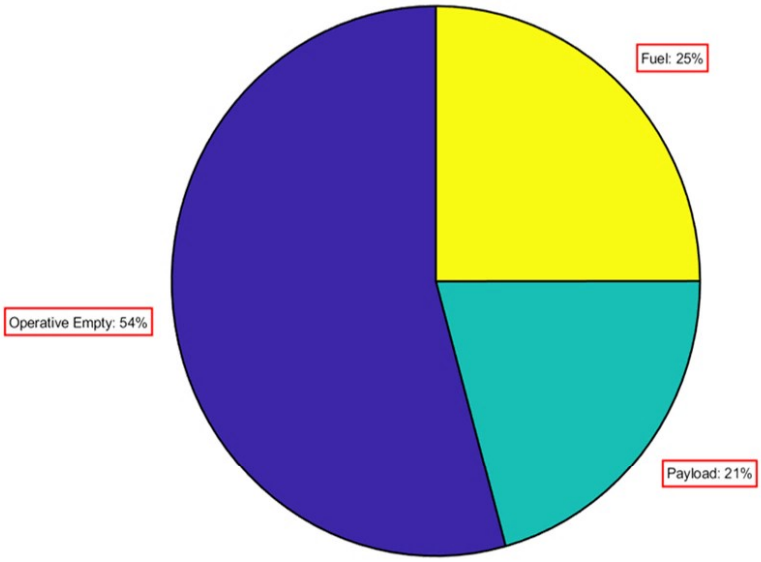

Figure 2.16: Class-I weights pie chart for the UM statistical configuration, based on Breguet's equations and statistical OEW-MTOW relationship.

2014 UM aircraft model for the WP2.
Since an engine performance deck provided by UNINA had been already verified by MTU for the ADORNO reference A/C configurations, its characteristics in terms of performance and main geometry were not included in the set of design parameters driving the optimization study. However, according to the possibility implemented by JPAD to modify the static thrust of each engine during a complete multi-disciplinary analysis cycle aimed at matching some prescribed TLARs (as explained in section 2.1.1), a maximum allowed static thrust variation was set for the MDAO process and assumed equal to +3 % with respect to the baseline value. Each case related to a higher thrust variation, however, was penalized in the following optimization process, in order to eventually discard those configurations from the set of optimum aircraft models.
In terms of design variables used to generate the A/C population of the parametric study, main wing geometrical parameters were selected together with the wing longitudinal position. It must be noted that the fuselage was not modified at all in this process to keep the same number of passengers and the same seat abreast of the Airbus A220-300, assumed as reference A/C for the set of TLARs.
Parallel to the definition of the set of design variables, a dedicated list of A/C geometry update rules was generated to feed the DOE module of the JPAD software. This list is reported below.

- Each lifting surface planform geometry was modified by assigning panel chords and the overall span.
- Lifting surfaces chords were scaled using the ratio between updated and baseline lifting surface planform areas.
- Wing fuel tank dimensions were scaled according to the ratio between updated and baseline lifting surface planform areas.

Table 2.12: Input data for the sizing module deriving from the statistical pre-design activities carried out on the UM configuration.

Sizing input data from the statistical pre-design

Weight ratios	
Description	**Value**
$W_{\text{cruise}}/W_{\text{take-off}}$	0.975
$W_{\text{landing}}/W_{\text{take-off}}$	0.850
$W_{\text{climb OEI}}/W_{\text{take-off}}$	1.000
$W_{\text{climb AEO}}/W_{\text{take-off}}$	1.000

Drag coefficients	
Description	**Value**
$\Delta C_{\text{D0 landing gears}}$	0.0200
$\Delta C_{\text{D0 flap landing}}$	0.0650
$\Delta C_{\text{D0 flap take-off}}$	0.0150
C_{D0}	0.0195

Oswald factors	
Description	**Value**
e_{approach}	0.75
e_{landing}	0.72
$e_{\text{take-off}}$	0.78
e_{clean}	0.83

Lift coefficients	
Description	**Value**
$C_{\text{L max take-off}}$	2.40
$C_{\text{L max landing}}$	2.90
$C_{\text{L approach}}$	2.65
$C_{\text{L clean}}$	1.45

Table 2.13: Design wing loading and thrust loading, together with updated wing area and engine static thrust, for the statistical UM baseline A/C model.

Description	Value
Wing loading, $(W/S)_{T/O}$	605 kg/m^2
Thrust loading, $(T/W)_{T/O}$	0.310
Updated wing area	112.3 m^2
Updated static thrust per engine	103.6 kN

- A/C control surfaces and high-lift devices areas were scaled according to updated lifting surfaces planform areas.
- Engines, nacelles, and main landing gears were supposed to be linked to the wing position by means of fixed longitudinal and lateral offsets. Thus, their positions in the BRF were modified according to each wing position considered in the parametric analysis.
- Landing gears leg lengths were kept fixed.
- Horizontal and vertical tail planes planform shapes and positions were updated assuming constant values of volumetric ratios and aspect ratios. These values were assumed from the baseline A/C model. Each tail plane geometry update process was carried out according to the iterative loop shown in figure 2.18.
- In case of static thrust variation, nacelle maximum diameter, cowl length and dry mass were updated using a dedicated statistical model developed by UNINA and implemented by the JPAD software. This model takes as input data the

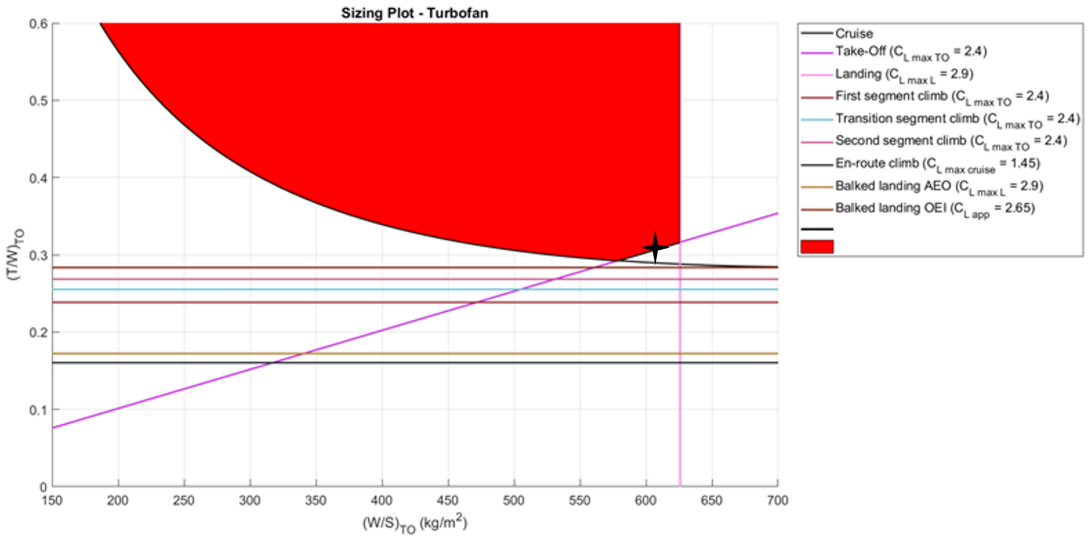

Figure 2.17: Sizing limitations and sizing point selection for the UM baseline A/C model.

engine static thrust and the BPR to estimate the abovementioned engine/nacelle parameters.

In terms of engine static thrust update strategy, for each analysis of the parametric study, a first attempt was made aiming at matching both the take-off field length and the cruise Mach number reported in the set of TLARs. Then, a second attempt was made also adding the cruise service ceiling to the set of target values within the process, as exemplified in figure 2.19. However, due to quite similar results, the first strategy was selected in order to reduce the amount of computational time needed to carry out the complete analysis. A visual representation of the finally selected engine static thrust update process is shown in figure 2.20.
To fully understand the interconnection existing between main A/C geometry variables used to define a generic JPAD parametric A/C model, table 2.14 reports the list of design variables selected for the MDAO process as well as the list of all the dependent variables. Those are also related to the abovementioned set of geometry update rules.

Table 2.14: Summary of the set of dependent and independent design variables of the parametric study carried out for the UM reference A/C model.

Design variables	**Dependent variables**
Wing area	Wing span
Wing aspect ratio	Wing fuel tank volume
Wing leading edge sweep angle	Wing control surfaces and high-lift devices area
Wing apex longitudinal position	Tail planes areas
Engines static thrust (MDAO process-related variable)	Main landing gears positions in the BRF
	Engines/nacelles positions in the BRF
	Nacelles dimensions
	Engines dry masses

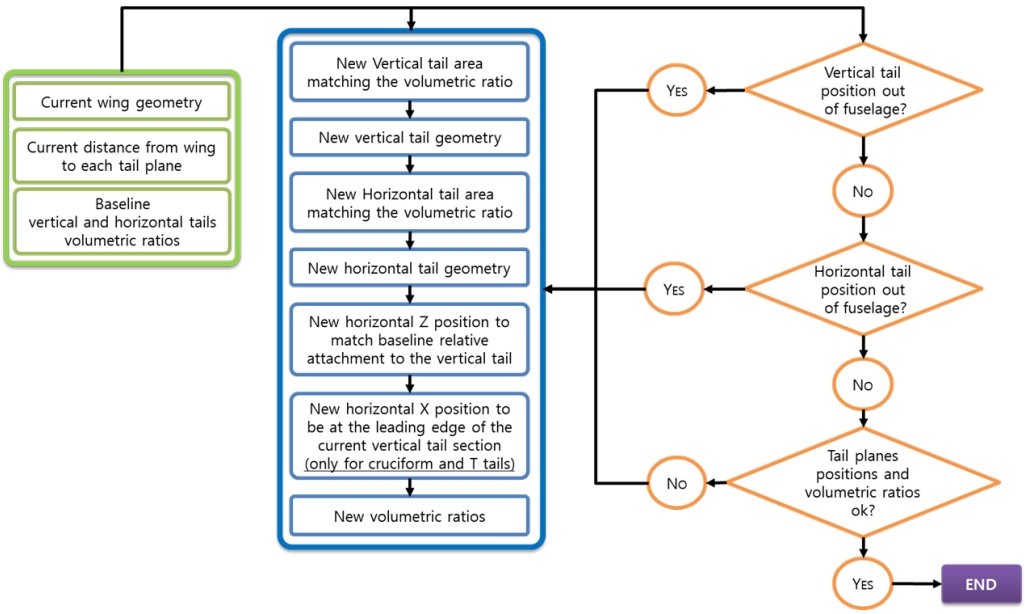

Figure 2.18: Tail planes geometry and position update loop implemented by JPAD-*doe* module.

The exploration of the design space was carried out by means of a full-factorial DOE approach. This expects to analyse each single aircraft model coming from the combination of all design variables values to define a response surface. Thus, the higher the number of values for each design parameter, the more precise the final response surface will be. However, this approach can surely result in a huge amount of computational time required to perform all the analyses. Furthermore, having large design space boundaries surely leads to a significant number of unfeasible solutions, which will be later discarded by the optimization tool.
To optimize both the analysis time and the accuracy of the response surface, avoiding the need for a large number of analyses, a preliminary sensitivity study was carried out, for each design variable, to evaluate their effect on the baseline A/C model. The obtained set of trend curves was used to assess the best variation range of each design variables, aiming at achieving the best trade-off between response surface accuracy and computational time.
A visual representation of this process is provided in the flowchart of figure 2.21. Here, a configuration is considered to be feasible if it passes all the following checks:

- The wing span is below the upper bound of 36 m prescribed by ICAO for aircraft belonging to category C [145].
- Each engine static thrust variation is below 3 %. This to allow the use of the same performance engine deck for each A/C model.
- The design mission fuel mass is lower than the maximum fuel mass storable in the wing fuel tanks.
- All ground stability and ground operation checks must pass:
  - Possibility to rotate the aircraft during take-off and landing phases at a given rotation angle.

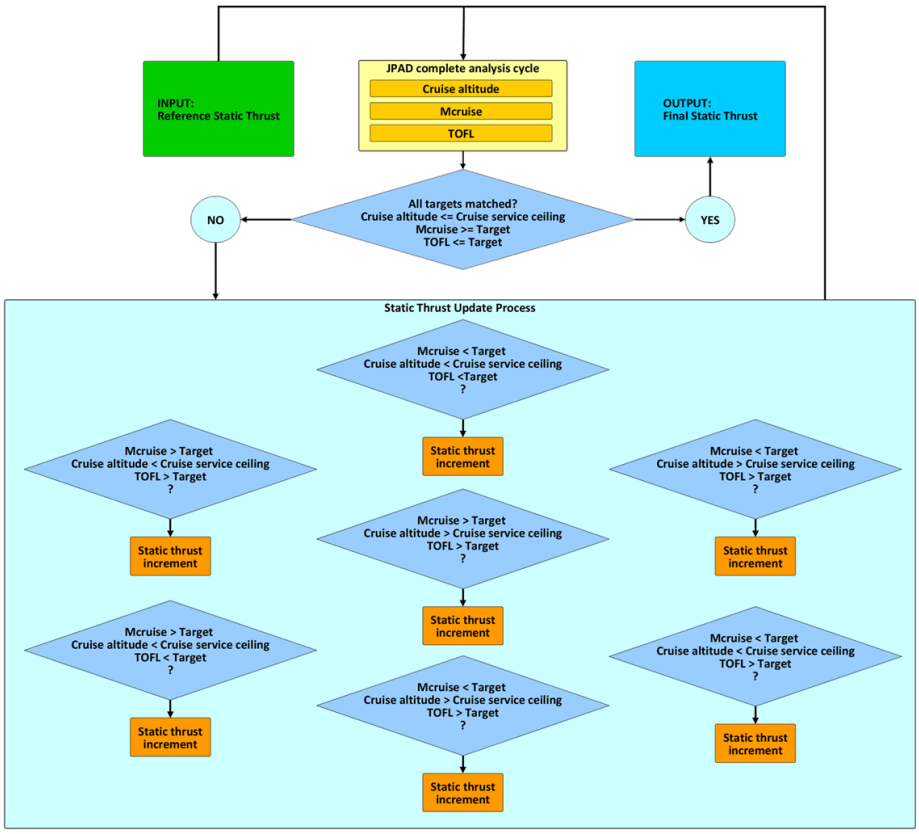

Figure 2.19: Static thrust update process implemented by JPAD multidisciplinary analysis cycle. Objectives: cruise Mach number, take-off field length, and initial cruise service ceiling.

  - Sufficient engines clearance from ground.
  - The maximum bank angle during ground operations is lower than the maximum turning bank angle.
  - The minimum sideways turnover angle is lower than the maximum value of 63 degrees [49].
  - The turning radius is lower than the maximum allowed value prescribed by regulations [84].
  - Main and nose landing gears positions are in line with their limit values, calculated as suggested in [167].

- The static stability margin (SSM) at the most afterward center of gravity position is negative (i.e., the aircraft is longitudinally stable).
- No tail strike during take-off and landing phases. For the landing phase, the check is applied to the nose strike too.
- The minimum take-off safety speed, V_2, during OEI take-off is at least 1.13 times the take-off stall speed, as prescribed by regulations.
- The initial cruise service ceiling is above the 37000 ft cruise altitude (prescribed by the set of TLARs).

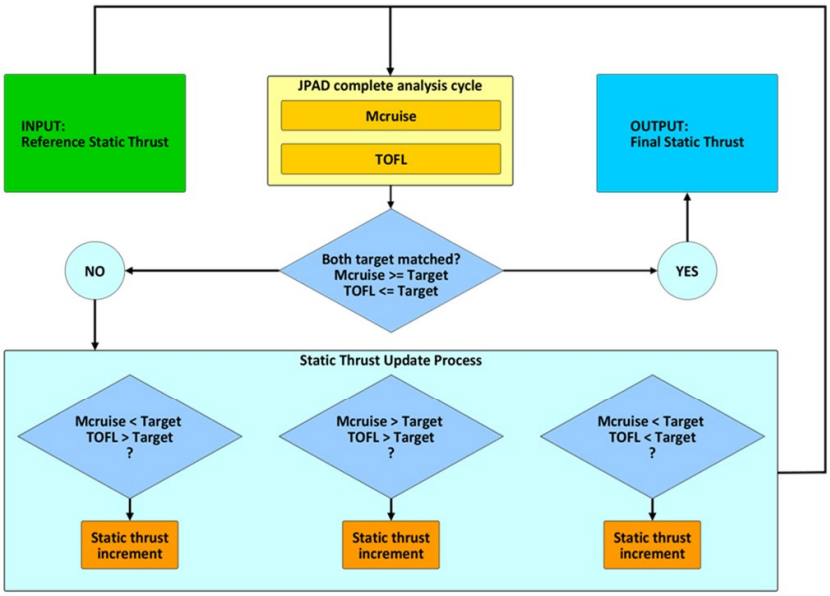

Figure 2.20: Static thrust update process implemented by JPAD multidisciplinary analysis cycle. Objectives: cruise Mach number and take-off field length.

- The number of passengers allowed for the design mission is equal to the TLARs design passengers number.
- The climb speed for both full-power and cutback take-off noise trajectories falls in the V_2 + 10 kn, V_2 + 20 kn interval, as prescribed by regulations [3].

Once the variation range of each design variable was assessed, the best number of values for each variable was selected considering variation sensitivity of main aircraft output data in terms of weights, aerodynamic characteristics, performance, DOC, and noise, with respect to the set of design variables under investigation. The lower the effect of the variable, the larger the step inside the variation range.

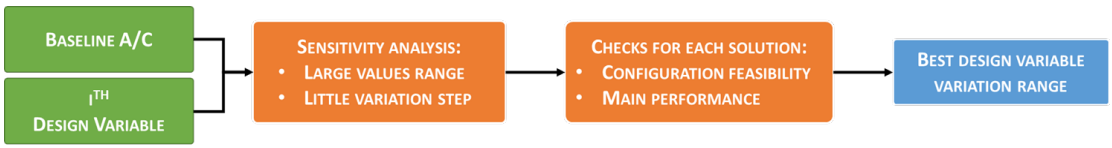

Figure 2.21: Flowchart of the process used to assess the best possible variation range of each design variable.

The MDAO problem for the UM reference A/C is summarized in table 2.15. The selection of the block fuel as one of the two objectives of the MDAO process was mainly linked to the tight relationship between this parameter and the amount of pollutant emissions produced by the aircraft during the design mission. In fact, these are calculated by the JPAD software as the product of the fuel burn times the emission index of a certain pollutant species (if available), retrieved from the engine performance deck. The calculation of the cumulative EPNL value (i.e., the algebraic sum of the EPNL values obtained at the three certification points prescribed by regulations) was carried out using an early

version of ATTILA++, the ADORNO aircraft noise tool for preliminary analyses.
A visual representation of both block fuel and cumulative EPNL response surfaces is provided in figure 2.22, in which variations in terms of design objectives are expressed as percent variations with respect to baseline A/C values. In figure 2.22a and figure 2.22b the wing area and the wing aspect ratio were selected as independent variables, while the wing leading edge sweep angle and the wing longitudinal position in the BRF were kept equal to baseline A/C values. On the other hand, figure 2.22c and figure 2.22d show the effects on block fuel and cumulative EPNL of the sweep angle and wing apex position, with the wing aspect ratio and planform area kept constant and equal to the values for the baseline A/C model. It is important to highlight that these response surfaces do not include the effect of the constraints listed in table 2.15.

Table 2.15: MDAO problem definition for the design of the UM reference model.

Minimum:	
Objectives	Block fuel, kg
	Cumulative aircraft EPNL, dB
with respect to:	
Constraints	Wing span less than 36 m
	Single engine static thrust variation less than 3 %
	Design mission fuel less than maximum storable fuel
	Ground stability and ground operability checks passed
	Negative SSM at maximum aft CG
	$V_2/V_{stall\ T/O}$ in OEI condition less than 1.13
	Tail and nose strike check at landing and take-off passed
	Take-off noise trajectory climb speed check passed
	Initial cruise service ceiling greater than 37000 ft
	Allowed passengers number equal to 140
	Maximum cruise Mach number equal to 0.82
	Take-off field length lower than 1890 m
by varying:	
Design variables	Wing area, from −2.5 % to +10 % with respect to the baseline value (112.3 m^2), using 5 values.
	Wing aspect ratio, from −10 % to +30 % with respect to the baseline value (11.0), using 5 values.
	Wing sweep at leading edge, from −10 % to +10 % with respect to the baseline value (30.0 degrees), using 3 values.
	Wing longitudinal position, from −5 % to +5 % with respect to the baseline value (12.0 m, from the fuselage nose), using 3 values.
for 225 A/C models analyzed in total	

To carry out the MDAO process defined in table 2.15, five different algorithms, all included in the package described in section 2.1.4, were used, to compare different sets of optimum solutions as well as to monitor the convergence of each algorithm towards a shared optimum region:

- ϵ-NSGA-II, an extension of NSGA that uses ϵ-dominance archive and randomized

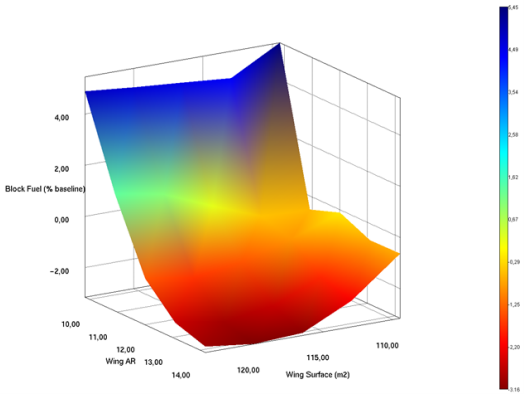

(a) Block fuel versus wing planform area and aspect ratio.

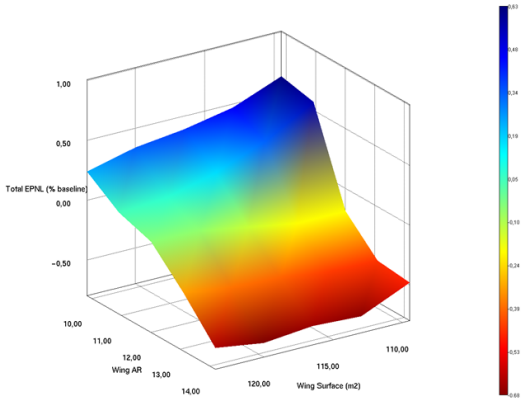

(b) Cumulative EPNL versus wing planform area and aspect ratio.

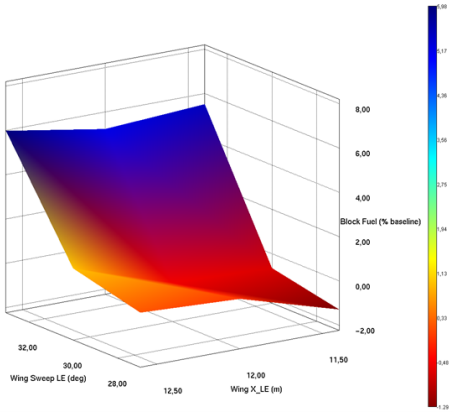

(c) Block fuel versus wing leading edge sweep angle and longitudinal position.

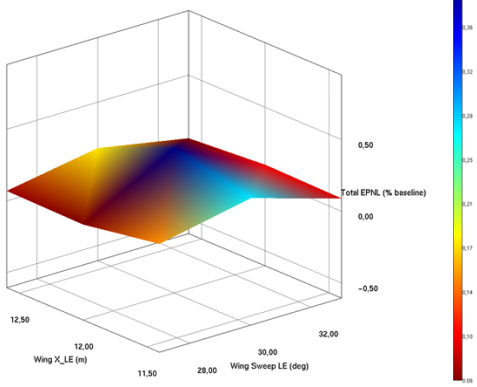

(d) Cumulative EPNL versus wing leading edge sweep angle and longitudinal position.

Figure 2.22: Block fuel and EPNL percent variations with respect to baseline UM A/C model values, accounting to modifications to the wing planform area, aspect ratio, leading edge sweep angle and longitudinal position.

restarts to enhance search and find a diverse set of Pareto optimal solutions.

- OMOPSO, which is a multi-objective particle swarm optimization algorithm also adopting ϵ-dominance.
- SMPSO (Speed-Constrained Particle Swarm Optimization).
- MOEA/D, a relatively new optimization algorithm based on the concept of decomposing the problem into many single-objective formulations.
- ϵ-MOEA, a steady-state multi-objective evolutionary algorithm using ϵ-dominance too.

Using these algorithms, the set of Pareto fronts shown in was figure 2.23 obtained. Here, the baseline values in terms of both block fuel and cumulative EPNL are also reported, showing the optimization margin for each objective function. Furthermore, the selected optimum solutions for each algorithm are highlighted. These are also reported in table 2.16 for greater clarity. As can be deduced from figure 2.23, some Pareto fronts show discontinuities. Those regions are related to unfeasible solutions for which one or more

Table 2.16: Comparison between optimum solutions of the MDAO process carried out on the reference UM A/C model.

	Baseline	**ϵ-NSGA-II**	**OMOPSO**	**SMPSO**	**MOEA/D**	**ϵ-MOEA**
Wing area, m^2	112.98	115.55 (+2.91 %)	109.76 (−2.24 %)	109.76 (−2.24 %)	109.76 (−2.24 %)	115.55 (+2.91 %)
Wing aspect ratio	10.92	11.026 (+0.97 %)	11.79 (+7.97 %)	11.79 (+7.97 %)	11.79 (+7.97 %)	11.026 (+0.97 %)
Wing LE sweep, degree	30.0	30.0 (+0.0 %)	27.0 (-10.0 %)	27.0 (−10.0 %)	27.0 (−10.0 %)	30.0 (+0.0 %)
Wing position, m	12.0	12.0 (+0.0 %)	12.6 (+5.0 %)	12.6 (+5.0 %)	12.6 (+5.0 %)	12.0 (+0.0 %)
Interpolated block fuel, kg	-	14123 (+0.24 %)	13570 (−3.68 %)	13570 (−3.68 %)	13570 (−3.68 %)	14123 (+0.24 %)
Interpolated EPNL, dB	-	264.05 (−0.30 %)	263.96 (−0.34 %)	263.96 (−0.34 %)	263.96 (−0.34 %)	264.05 (−0.30 %)
Calculated block fuel, kg	14089	14093 (+0.03 %)	13801 (−2.04 %)	13801 (−2.04 %)	13801 (−2.04 %)	14093 (+0.03 %)
Calculated EPNL, dB	264.85	264.6 (−0.09 %)	263.47 (−0.52 %)	263.47 (−0.52 %)	263.47 (−0.52 %)	264.6 (−0.09 %)

than one constraint were violated. The effect of the constraints is also highlighted by the quite narrow optimum design space identified by the optimization process. Two groups of optimum solutions can be found in 2.23. The first one, characterized by better overall objective values, is related to OMOPSO, SMPSO and MOEA/D algorithms. The second one is related to the genetic algorithm ϵ-NSGA-II and to the evolutionary algorithm ϵ-MOEA. Since this last set of optimum objectives provided less Pareto efficient solutions, both ϵ-NSGA-II and ϵ-MOEA were not considered in the selection of the final optimum aircraft. However, for the sake of completeness, 2.23 provides information on optimum solutions related to those algorithms too.

When working with multi-objective optimizations and Pareto fronts, it is not possible to define an overall optimum solution in a deterministic way. Each point of the best Pareto front is a feasible optimum solution to the MDAO problem. It is up to the aircraft designer to use his/her experience and common sense to select one or more optimum solutions. Focusing on OMOPSO, SMPSO and MOEA/D algorithms, and taking into account the variation range of each objective function, the reduction in block fuel was assumed as the driving parameter for the definition of the optimum aircraft model, and the best block fuel solution highlighted in figure 2.23 (the yellow triangle) was selected as the optimum UM reference aircraft.

Since the optimization process was carried out by means of a linear interpolation of the response surface resulting from the parametric study, interpolated results were slightly different from the calculated values, obtained at the end of a complete multidisciplinary analysis cycle, due to interpolation approximation. Table 2.16 provides information on the interpolated values (the ones produced by the optimization algorithms) and on the calculated ones (generated by a complete analysis cycle, starting from the aircraft geometry defined at the end of the optimization process), for both the block fuel and the cumulative EPNL. It is important to highlight that differences between interpolated and calculated values never exceeded 1.64 %.

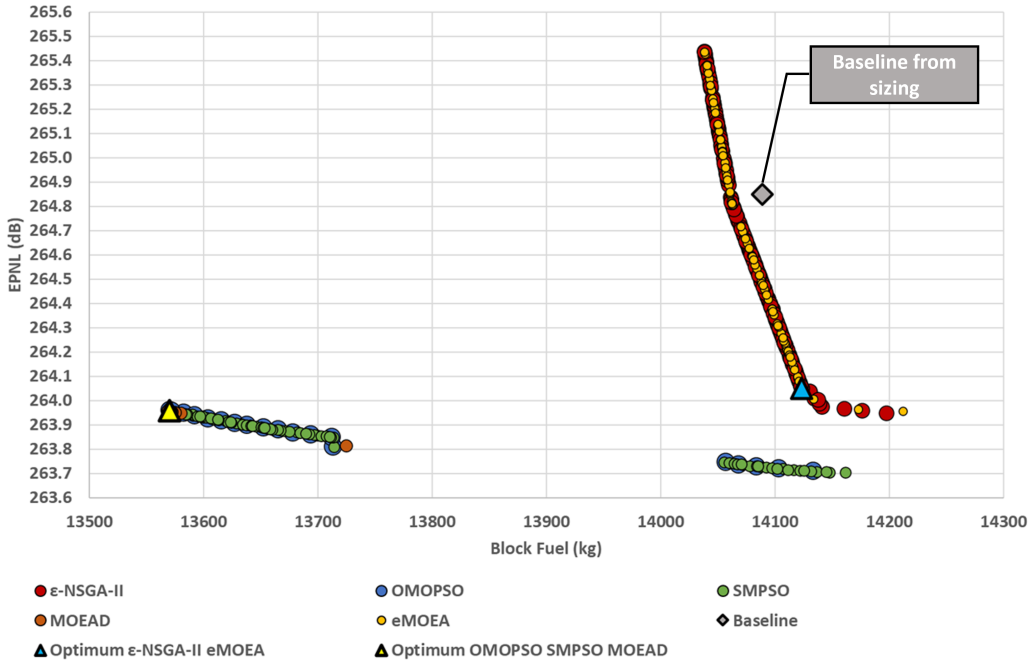

Figure 2.23: Set of Pareto fronts coming from the MDAO process carried out on the reference UM A/C model. Percentage variations reported in the columns collecting the results of the optimization algorithms are referred to the baseline A/C model resulting from the preliminary sizing activities.

Multidisciplinary analysis of the optimum UM model

Table 2.17 provides more details, with respect to those reported in table 2.16, on the results obtained from the multidisciplinary analysis carried out on the optimum UM reference A/C model, which was one of the main outcome of the activities carried out for Deliverable 2.1 of ADORNO. It is immediate to notice that the block fuel and the total EPNL values reported in table 2.17 slightly differs from those reported in table 2.16 for the optimum solutions provided by the OMOPSO, SMPSO and MOEA/D algorithms. In light of the activities concerning Deliverable 2.2 and the design of a target (year 2025+) UM A/C model, featuring both advanced airframe technologies and a new powerplant system designed by MTU, the optimum reference UM A/C was analyzed again. Especially following the application of bug fixes and minor improvements to both JPAD and ATTILA++, the results in terms of performance and noise assessment were slightly different with respect to those included in Deliverable 2.1. For this reason, an amendment section was included in Deliverable 2.2, to finally set the characteristics of the reference model to be compared, mainly in terms of emissions and noise performance, with respect to an advanced target configuration.
Figure 2.24 provides a visual representation of the optimum UM reference A/C model.

Table 2.17: Results of the multidisciplinary analysis carried out on the optimum reference UM model.

Geometry	
Wing area, m^2	109.76
Wing aspect ratio	11.79

Table 2.17 continued from previous page

Wing leading edge sweep angle, degrees	27.0
Wing apex X position (BRF), m	12.5
Wing apex Z position (BRF), m	-1.25
Horizontal tail area, m^2	26.34
Horizontal tail span, m	11.58
Horizontal tail aspect ratio	5.09
Horizontal tail leading edge sweep angle, degrees	32.0
Horizontal tail apex X position (BRF), m	33.0
Horizontal tail apex Z position (BRF), m	1.0
Vertical tail area, m^2	23.17
Vertical tail span, m	6.19
Vertical tail aspect ratio	1.65
Vertical tail leading edge sweep angle, degrees	45.0
Vertical tail apex X position (BRF), m	31.0
Vertical tail apex Z position (BRF), m	1.52
Powerplant	
Single engine SL static thrust, kN	103.6
Weights	
Maximum take-off weight, kg	68177
Maximum landing weight, kg	57950
Operating empty weight, kg	36684
Maximum fuel mass, kg	17049
Design payload, kg	14462
Balance	
Maximum forward X CG, % mean aerodynamic chord (MAC)	10.1
Maximum afterward X CG, % MAC	36.64
Operative X CG, % MAC	26.73
Aerodynamics and static stability	
Maximum clean lift coefficient, at operative X CG	1.52
Maximum take-off lift coefficient, at operative X CG	2.47
Maximum landing lift coefficient, at operative X CG	2.96
Cruise zero-lift drag coefficient	0.0209
Cruise SSM, at maximum afterward X CG	18.9
Maximum cruise aerodynamic efficiency	17.98
Performance and emissions	
Take-off field length, MTOW, ISA SL, m	1814
Landing field length, MLW, ISA SL, m	1568
Time to climb at 270 KCAS from 1500 ft to 37000 ft, min	18
Absolute OEI ceiling, ft	21263
Service OEI ceiling, ft	20817
Typical cruise Mach number	0.78
Maximum cruise Mach number	0.82
Typical cruise altitude, ft	37000
Block time, min	424
Block fuel, kg	14139
Total NO_x emissions, kg	287.43

Table 2.17 continued from previous page

Total CO_2 emissions, kg	51222
Environmental noise	
Approach EPNL, dB	92.6
Flyover (cutback) EPNL, dB	82.4
Lateral EPNL, dB	86.7
Cumulative EPNL, dB	261.7
Costs	
Cash DOC, cent/(nmi*seat)	6.774
Total DOC, cent/(nmi*seat)	12.703

2.3.3 Definition of the set of advanced airframe technologies

One of the objectives of ADORNO WP2 was the design of target (with EIS expected in the 2030-2035 timeframe) UM and RM aircraft configurations, equipped with both advanced airframe and engine technologies, to be compared in terms of pollutant emissions and environmental noise with respect to reference (2014 EIS) aircraft models, in order to check the matching of ambitious Clean Sky 2 targets:

- -20 to -30 % CO_2 emissions,
- -20 to -30 % NO_x emissions,
- -20 to -30 % environmental noise.

UNINA carried out the definition of the list and the modelling in the JPAD analysis and design framework of the advanced airframe technologies, while MTU generated the dataset for an advanced geared turbofan engine.
The selection of advanced airframe technologies was carried out starting from the list of technologies to be developed and demonstrated during the course of the Clean Sky 2 program presented in [170]. Since the Clean Sky 2 development plan is continuously updated, based on the annual results coming from the different topics, it was hard to set a list of most promising technologies capable to reach a sufficient technology readiness level (TRL) before the selected EIS timeframe for the ADORNO target aircraft. Hence, technology selection was also supported by IATA aircraft technology roadmap [21][22][23], in which a distinction is made between:

- evolutionary technologies, i.e., technologies that can be equipped on a conventional aircraft configuration (tube-and-wing) and that are ready to be adopted on new generation A/C models entering into service in the next 10-15 years.
- revolutionary technologies, i.e., novel airframe configurations, such as strut-braced wing, blended wing body, flying V, double-bubble fuselage, etc.

Technologies that were selected for the ADORNO target A/C all come from the first of these two lists, with a planned TRL at least equal to 6 (i.e., technology demonstrated in relevant environment) by 2025 (as reported in table 2.18).
In the following sub sections the implementation, and the eventual calibration, of each technology effect in the UNINA analysis framework is presented. First, the set of technologies selected for the target UM A/C is illustrated, and general assumptions

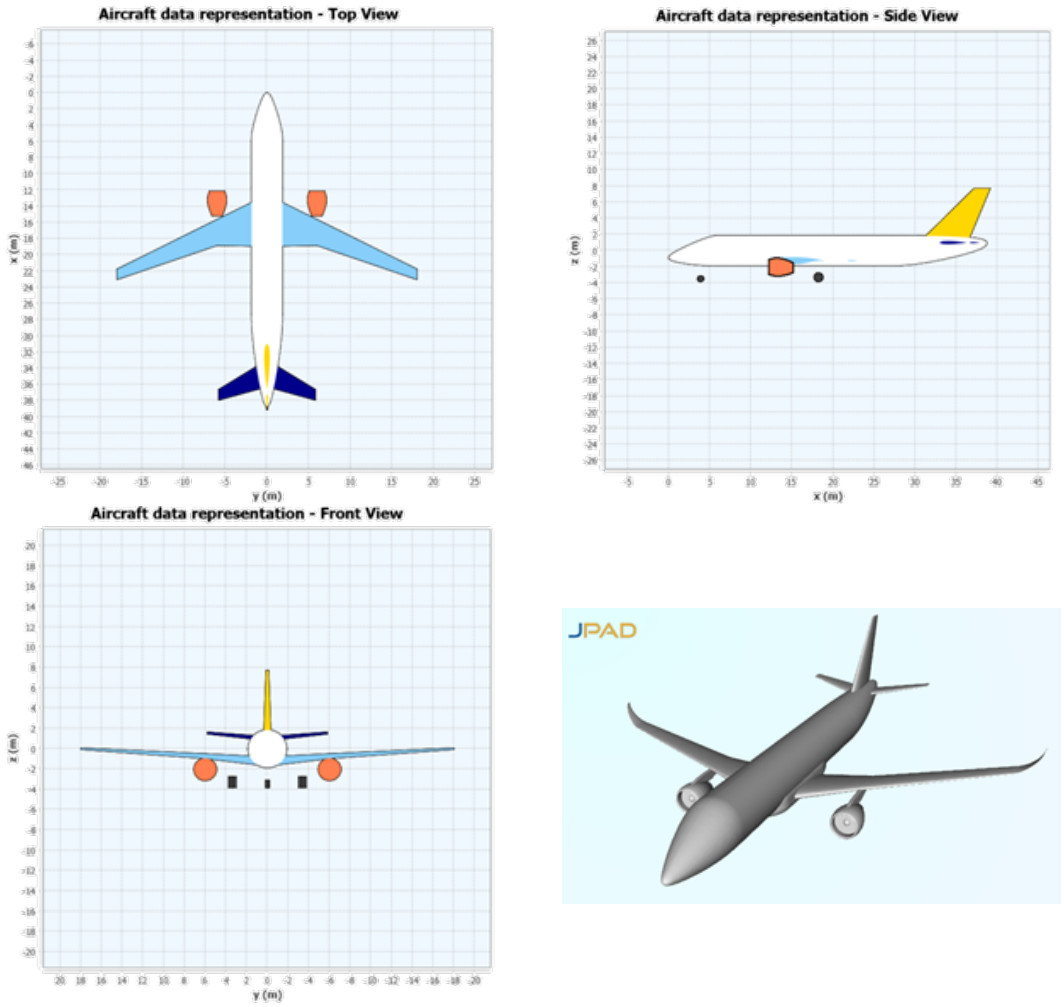

Figure 2.24: Optimum reference UM A/C model three-view and 3D model.

Table 2.18: List of airframe technologies selected for ADORNO, along with TRL information (as of 2013) and estimated availability [21].

Technology	**TRL (2013)**	**Availability (estimated)**
Hybrid Laminar Flow Control (HLFC)	7	2022
Riblets	8	2015
Variable camber wing with high-lift devices	5	2024
More-Electric Aircraft (MEA) architecture	8	2015
Composite primary structure	9	2012
Advanced alloys	8	2015

performed on the impact of each technology on aircraft aerodynamics, weights, power off-takes and costs are presented. These assumptions came directly from an in-depth literature review that was carried out for each mentioned technology. For each involved advanced airframe solution, a check and, if necessary, a trim on the original assumptions on the effects was performed, in order to try to match the expected beneficial/detrimental effects in terms of fuel burn and annual operating costs provided by IATA in [21][22].

Technologies assumptions and implementation

To implement each technology in the UNINA design and analysis framework, a strategy making use of calibration factors and calibration offsets was elaborated, to consider the impact on aerodynamics, weights, engines power off-takes and costs. For this purpose, a new module was implemented in the JPAD framework, dedicated to the definition of technologies calibrations, starting from literature-based default values. Table 2.19, table 2.20, table 2.21, table 2.22, and table 2.23 provide the default assumptions made for the calibration factors to be used to carry out the design and the analyses on the target A/C models of ADORNO. Assumptions on the power off-takes are the only exception in this sense. Concerning the values assumed for the MEA concept, these were not used to perform any kind of calibration, but were directly provided to MTU to perform the design of the advanced GTF engine to be fitted on the target A/C. The assumptions for the power off-takes deriving from the use of HLFC devices, instead, were set to be used to estimate the amount of additional power to be extracted from the engine in cruise condition, which is the flight condition in which these devices are designed to be operative. This amount of power was meant to be scalable: it should change with the dimensions of the lifting surfaces on which the system is equipped. The impact of additional power off-takes was modelled by adequately scaling engine data. An increase in terms of power off-takes, in fact, should have an impact on both engine SFC and powerplant system mass. For this purpose, the JPAD manager for advanced technologies was provided with two possible strategies:

- users can use hard-coded scale factors for fuel consumption and powerplant mass, based on assumptions from literature;
- users can define custom scale factors.

The second option, in particular, was used to carry out the analyses on the target UM A/C, since the MTU engine dataset for the advanced engine, described in section 2.3.4, had been provided including information on powerplant mass and specific fuel

consumption scale factors.
It should be noted that for certain technologies, the JPAD technologies manager was provided with the option to select between three different levels of intensity of a specific effect (namely *Low*, *Medium* and *High*). In most of the cases, these options adjusting the level of intensity were introduced for those effects for which the literature review provided not just a single value, but a plausible interval of variation. Moreover, most of the modelled effects were paired with additional calibration attributes which allow to better trim each effect, further increasing tool flexibility, as it is demonstrated in the next sub section.
Speaking of assumptions for costs, these were mainly driven by suggestions included by IATA in [22]. IATA, in fact, provided for both evolutionary and revolutionary aircraft technologies a forecast in terms of effect on annual operating costs, on-aircraft investment costs, and impact on maintenance costs. For the first two quantities, tables included in [22] provide a plausible range of variation. For most of the technologies involved in the ADORNO design activities, a mid-range value was assumed for the default impact. With regards to maintenance costs, [22] provides just an indication in terms of impact by means of six different indices: weak detrimental/beneficial effect, mild detrimental/beneficial effect, and strong detrimental/beneficial impact. To perform, therefore, quantitative assumptions on maintenance costs variations, the following values were assumed:

- To a weak beneficial/detrimental effect according to [22] corresponds a ± 1 % in maintenance costs, with respect to a baseline value.
- To a mild beneficial/detrimental effect according to [22] corresponds a ± 10 % in maintenance costs, with respect to a baseline value.
- To a strong beneficial/detrimental effect according to [22] corresponds a ± 25 % in maintenance costs, with respect to a baseline value.

It is important to remark that assumed values for impact on annual operating costs were used in a second stage to eventually calibrate these assumptions, as explained in the following section.
Dealing with environmental noise, a remarkable impact could not be assumed for any of the advanced airframe technologies involved, at least for the three certification conditions prescribed by ICAO and for which a noise assessment was carried out in ADORNO. For this reason, impact on aircraft noise of the technologies listed in table 2.18 was neglected, and no calibration factors were included in the JPAD technologies manager to model their effects on the airframe noise predicted by ATTILA++.
The following paragraphs provide a more detailed explanation on the assumptions performed for each involved airframe technology and included in the tables of this section.

On-board systems (OBS) architecture The MEA architecture that was assumed for the target A/C is the concept presented in [71] and called MEA2. The main characteristics of this architecture are:

- Bleed-less configuration, external compressors, powered by the electric system, feed the environmental control system (ECS), while the ice protection system (IPS) is totally electrified.
- The electric system powers the electric pumps of the hydraulic system, which in turn supplies the flight control system (FCS), the actuators for the landing gears, and the wheel brakes.

Required mechanical power off-takes for such an architecture were estimated starting from the data reported in [71] and performing a linear interpolation. These data were later delivered to MTU for the design of the advanced GTF engine, along with additional necessary information, about which more details are provided in section 2.3.4.
Moreover, two additional advanced OBS architectures, the ones indicated in [71] as MEA1 and AEA, were also implemented in the JPAD technologies manager, providing different requirements in terms of power off-takes and bleed air extraction. The first one is a solution closer to a conventional one, with air being extracted from the engines to feed the ECS and less electrification with respect to the MEA2. The last one is an all-electric solution.
For all three configurations, impact on weights was also assumed starting from information available in [71], while no costs assumptions were included regarding the maintenance contribution. In fact, according to [22], relevant impact in terms of maintenance costs should not be expected.

Variable camber wing with trailing edge devices The system concept presented in [39] (i.e., variable camber wing with new trailing edge devices) was assumed. With respect to the aerodynamics, assumptions were made on the impact of this technology starting from the work performed in [113]. Here, the authors tried to quantify the benefits arising from the adoption of a morphing trailing edge wing for a medium /long range aircraft similar to the Boeing 777-200.
No assumptions were made in terms of impact on weights and power off-takes. According to [22], no additional mass should be accounted for such a system, especially when dealing with advanced light materials. As regards power off-takes, no studies were retrieved from literature providing information on the required amount of power per flight phase for such a technology.

Hybrid Laminar Flow Control With respect to the assumptions made for the impact on aerodynamics, these were essentially gathered from several reports of actual flight tests, performed both on business jets and short to medium-haul airliners [98][159][122]. In particular, [98][159] provided data on transition delay over wings and tail group thanks to the application of a HLFC system on those components. In general, a transition beyond the 30 % of chord length and up to 50 % can be reasonably assumed.
The effect of this delay was simulated by means of JPAD aerodynamics module, by manipulating the transition option available for the airfoils of the lifting surfaces. By setting the transition over the upper and lower surfaces of wings beyond the 40 % of chord length, a 40 % reduction in skin friction drag was observed, which was in line with data reported in [22]. With regards to the impact on the aerodynamics of nacelles, a 35 % reduction in terms of skin friction drag was assumed, considering results reported in [122].
Hypotheses on the effects on weights were made starting from data reported in [109], a study performed by Lockheed to evaluate the application of HLFC technology to a global range military transport aircraft. Here, a breakdown of weight increments had been reported, accounting weight changes for wing, tails, powerplant, and systems.
Speaking of power off-takes, indications in terms of power required by the systems were retrieved from [190], in which a computer performance model for an aircraft similar to the Boeing 757 had been used to study the application of a HLFC system. This study provided assumptions in terms of power required when applying a HLFC system on

Table 2.19: JPAD advanced airframe technologies manager implemented fudge factors for HLFC.

HLFC	**Disciplines**						
	Aerodynamics			**Weights**			
Component	Low	Medium	High	Low	Medium		High
Wing	−27 %	−36 % skin friction drag	−45 %	-	+1 %		-
Hor. tail	−27 %	−36 % skin friction drag	−45 %	-	+2.5 %		-
Ver. tail	−27 %	−36 % skin friction drag	−45 %	-	+2.5 %		-
Nacelles	−35 %	−35 % skin friction drag	−35 %	-	+5.5 %		-
Systems	-	-	-	-	+4 %		-
	Disciplines						
	Power off-takes			**Costs**			
Component	Low	Medium	High		Low	Medium	High
Wing	-	+0.56 kW/m^2	-	A/C price	+10 M$	+50 M$	+100 M$
Hor. tail	-	+0.44 kW/m^2	-	Maintenance	+0 %	+1 %	+5 %
Ver. tail	-	+0.77 kW/m^2	-				
Nacelles	-	+0.76 kW/m^2	-				
Systems	-	-	-				

different aircraft components, such as wing, tails and nacelles. To scale the values included in the reference for their use in different applications, such as the ones involved in ADORNO, they were divided by the wetted of their respective aircraft component, in order to derive scale factors to be used independently from the application.
Finally, dealing with the costs, it was assumed that the data reported in [22] was related to a full HLFC configuration (i.e., HLFC applied simultaneously on the upper and lower surfaces of wing, tails and nacelles). In case of a different configuration, the following rule was designed and implemented in the analysis framework: predicted aircraft price and maintenance increments are divided by the total potential wetted area available to HLFC systems (wing, tails and nacelles) and multiplied by the actual wetted area, on which HLFC systems are applied for a specific application.

Riblets Impact on aerodynamics was assumed starting from indications provided in [41][120][180][48], which included results from flight tests and wind tunnel tests too. Effects on aircraft weights were assumed to be negligible, while the same assumptions made for full and non-full HLFC configurations was applied for riblets-related costs.

Advanced materials Assumptions on weight reduction linked to the use of carbon fiber reinforced plastic (CFRP) materials for the fuselage and for the wings were made starting from data reported in [2] and [165], respectively. A 25 % weight reduction was assumed for the fuselage with respect to a conventional full-alloy one, and a 20 % for the wing and for the tail group. A 30 % weight reduction for the landing gears was assumed starting from the data reported in [76], assuming that advanced titanium-based alloys were used instead of conventional steel.
Dealing with the costs, for the use of advanced composites on the aircraft main structures, a strategy similar to the one for HLFC and riblets was implemented, based this time on components weights rather than wetted areas.

Calibration of technologies assumptions

Prior to the beginning of the design activities for the UM target A/C, work was performed to check if the assumed set of calibrations for the characterization of the advanced airframe technologies was compliant with the expected beneficial/detrimental effects in

Table 2.20: JPAD advanced airframe technologies manager implemented fudge factors for riblets.

Riblets	**Disciplines**					
	Aerodynamics			**Weights**		
Component	Low	Medium	High	Low	Medium	High
Wing	−5 %	−7.5 % skin friction drag	−10 %	-	-	-
Horizontal tail	−5 %	−7.5 % skin friction drag	−10 %	-	-	-
Vertical tail	−5 %	−7.5 % skin friction drag	−10 %	-	-	-
Fuselage	−5 %	−7.5 % skin friction drag	−10 %	-	-	-
	Disciplines					
	Power off-takes			**Costs**		
Component	Low	Medium	High		Low	Medium	High
Wing	-	-	-	A/C price	+1 M$	+5 M$	+10 M$
Horizontal tail	-	-	-	Maintenance	+0 %	+1 %	+5 %
Vertical tail	-	-	-				
Fuselage	-	-	-				

Table 2.21: JPAD advanced airframe technologies manager implemented fudge factors for variable camber wing.

Variable camber	**Disciplines**					
	Aerodynamics			**Weights**		
Flight condition	Low	Medium	High	Low	Medium	High
Climb	-	−4.9 % aerodynamic drag	-	-	-	-
Cruise	-	−2.5 % aerodynamic drag	-	-	-	-
	Disciplines					
	Power off-takes			**Costs**		
Flight condition	Low	Medium	High		Low	Medium	High
Climb	-	-	-	A/C price	+1 M$	+5 M$	+10 M$
Cruise	-	-	-	Maintenance	+0 %	+1 %	+5 %

Table 2.22: JPAD advanced airframe technologies manager implemented fudge factors for OBS architecture.

OBS		**Disciplines**						
		Aerodynamics			**Weights**			
A/C type		Low	Medium	High	Low	Medium		High
Reg. jet 90 pax	MEA1	-	-	-	-	−6.95 % OBS mass		-
	MEA2	-	-	-	-	−0.99 % OBS mass		-
	AEA	-	-	-	-	−5.53 % OBS mass		-
Med. Haul 160 pax	MEA1	-	-	-	-	−2.51 % OBS mass		-
	MEA2	-	-	-	-	−1.92 % OBS mass		-
	AEA	-	-	-	-	−2.95 % OBS mass		-
		Disciplines						
		Power off-takes			**Costs**			
A/C type		Low	Medium	High		Low	Medium	High
Reg. jet 90 pax	MEA1	-	−3.80 %	-	A/C price	+100 k$	+500 k$	+1 M$
	MEA2	-	+175.41 %	-	Maintenance	-	-	-
	AEA	-	+171.61 %	-				
Med. Haul 160 pax	MEA1	-	−2.27 %	-				
	MEA2	-	+186.74 %	-				
	AEA	-	+181.65 %	-				

Table 2.23: JPAD advanced airframe technologies manager implemented fudge factors for materials.

Advanced materials	**Disciplines**					
	Aerodynamics			**Weights**		
CFRP	Low	Medium	High	Low	Medium	High
Wing	-	-	-	-	−20 %	-
Horizontal tail	-	-	-	-	−20 %	-
Vertical tail	-	-	-	-	−20 %	-
Fuselage	-	-	-	-	−25 %	-
Ti-based alloys						
Landing gears	-	-	-	-	−30 %	-
	Disciplines					
	Power off-takes			**Costs**		
CFRP	Low	Medium	High		Low	Medium	High
Wing	-	-	-	A/C price	+1 M$	+5 M$	+10 M$
Horizontal tail	-	-	-	Maintenance	+5 %	+10 %	+15 %
Vertical tail	-	-	-				
Fuselage	-	-	-				
Ti-based alloys				A/C price	+100 k$	+500 k$	+1 M$
Landing gears	-	-	-	Maintenance	+0 %	+1 %	+5 %

Table 2.24: Reference values assumed to trim the impact of the adopted airframe technologies.

	Expected impact	
Technology	**Annual operating costs impact [22]**	**Fuel burn impact [21]**
Hybrid Laminar Flow Control	[+1.0, +10 %]	[−10, −15 %]
Riblets	[+0.1, +1.0 %]	−1 %
Variable Camber wing	[+0.1, +1.0 %]	[−1.0, −2.0 %]
More-Electric system architecture	[−0.1, −1 %]	-
Composite primary structures	[+1.0, +10 %]	[−1.0, −3.0 %]
Advanced alloys	[+0.1, +1.0 %]	[−1.0, −3.0 %]

terms of fuel burn and annual operating costs reported in [21][22]. For the sake of clarity, these are reported in table 2.24 too.
Assuming, therefore, an initial set of user-defined calibrations and effect magnitude levels, equal to 1.0 and *Medium*, respectively (the addition of supplementary user-defined calibration factors and intensity level selectors is explained in the previous section), an iterative process was carried out, allowing to obtain the final trimmed set of fudge factors reported in table 2.25, table 2.26, table 2.27, table 2.28, and table 2.29.
It is important to highlight that the effects related to the impact of the advanced onboard systems architecture on the SFC were not considered in this analysis, since they were already included in the new engine performance dataset provided by MTU. In addition, having assumed the Airbus A220 as the reference aircraft model for the design of the year 2014 reference UM aircraft, all advanced materials effects related to lifting surfaces were also neglected, since the reference aircraft already makes an extensive usage of advanced composite materials for the wing and for the empennages structures. Composite materials are also used for the rear portion of the fuselage of the A220. Therefore, to consider the effect of a full-composite fuselage for the ADORNO target aircraft, a calibration factor equal to 0.75 was assumed for the fuselage weight calibration of table 2.29, lowering the hard-coded 25 % weight reduction to 18.75 %.

Table 2.25: Final set of calibration factors and effects levels for HLFC. A calibration equal to 1.0 means full estimated effect.

HLFC		
Wing	Weights	Effect calibration → 1.0
	Aerodynamics	Effect level → High Effect calibration → 1.1
	Off-takes effect on cruise SFC	Effect calibration → 1.0
Horizontal tail	Weights	Effect calibration → 1.0
	Aerodynamics	Effect level → High Effect calibration → 1.1
	Off-takes effect on cruise SFC	Effect calibration → 1.0
Vertical tail	Weights	Effect calibration → 1.0
	Aerodynamics	Effect level → High Effect calibration → 1.1
	Off-takes effect on cruise SFC	Effect calibration → 1.0
Powerplant	Weights	Effect calibration → 1.0
	Aerodynamics	Effect calibration → 1.0
	Off-takes effect on cruise SFC	Effect calibration → 1.0
Systems weights		Effect calibration → 1.0
Aircraft price		Effect level → Low Effect calibration → 1.0
Maintenance costs		Effect level → High Effect calibration → 1.0

Table 2.26: Final set of calibration factors and effects levels for riblets. A calibration equal to 1.0 means full estimated effect.

RIBLETS	
Wing aerodynamics	Effect level → Medium Effect calibration → 1.0
Horizontal tail aerodynamics	Effect level → Medium Effect calibration → 1.0
Vertical tail aerodynamics	Effect level → Medium Effect calibration → 1.0
Fuselage aerodynamics	Effect level → Medium Effect calibration → 1.0
Aircraft price	Effect level → Medium Effect calibration → 1.0
Maintenance costs	Effect level → High Effect calibration → 1.0

Table 2.27: Final set of calibration factors and effects levels for wing variable camber trailing edge devices. A calibration equal to 1.0 means full estimated effect.

VARIABLE CAMBER	
Aircraft aerodynamics (climb condition)	Effect calibration → 1.0
Aircraft aerodynamics (cruise condition)	Effect calibration → 1.0
Aircraft price	Effect level → Low Effect calibration → 1.0
Maintenance costs	Effect level → High Effect calibration → 0.75

Table 2.28: Final set of calibration factors and effects levels for advanced on-board systems architecture effects. A calibration equal to 1.0 means full estimated effect.

MEA	
Powerplant weight	Effect calibration → 0.0
Aircraft price	Effect level → Low Effect calibration → 1.0
Off-takes effect on cruise SFC	Effect calibration → 0.0
Bleed-less effect on cruise SFC	Effect calibration → 0.0

Table 2.29: Final set of calibration factors and effects levels for advanced materials. A calibration equal to 1.0 means full estimated effect.

ADVANCED MATERIALS	
Wing weight	Effect calibration → 0.0
Horizontal tail weight	Effect calibration → 0.0
Vertical tail weight	Effect calibration → 0.0
Fuselage weight	Effect calibration → 0.75
Landing gears weight	Effect calibration → 1.0
Aircraft price	Effect level → Low Effect calibration → 1.0
Maintenance costs	Effect level → Low Effect calibration → 0.5

2.3.4 Design of the advanced turbofan engine model

MTU oversaw the generation of the dataset (dimensions, weights, performance and emissions) for an advanced GTF engine, to be equipped on ADORNO target A/C models. To enable MTU to perform the design of this engine, and to optimize it for the selected A/C platform of ADORNO, a trade factor analysis on mission fuel burn was preliminarily performed by UNINA.
This trade factor analysis was carried out on the optimized UM reference A/C model (the one described at the end of section 2.3.2, considering the following parameters:

- single engine dry mass, made vary from the baseline value up to +300 kg;
- engine specific fuel consumption, made vary from the baseline value up to +5 % with respect to it.

Each variation of these variables was analyzed individually, to investigate their direct effect. Therefore, no cross-correlation effect was considered. The design block fuel of the reference UM A/C was assumed as the reference value for this study.
The aircraft model adopted for these analyses was conveniently rubberized. For each parameter variation, the aircraft geometry was updated to ensure that the performance of the aircraft in terms of take-off and landing field lengths, cruise Mach number, and time to climb, were the closest possible to the ones of the baseline A/C model.
The geometrical parameters assumed as independent variables in this update process were the wing area and the wing aspect ratio, with the latter being actually modified only if strictly required. In addition, positions in the BRF and planform parameters of the horizontal and vertical tails were considered as dependent variables to be automatically updated, to ensure constant volumetric ratios with respect to the optimized reference UM A/C.

Table 2.30: Results of the engine SFC trade factor analysis carried out on a rubberized version of the optimized reference UM A/C and provided to MTU.

	SFC (Δ%)	**Wing Area (m^2)**	**Wing Area (Δ%)**	**Wing AR**	**Wing AR (Δ%)**	**Block Fuel (Δ%)**
Reference UM A/C (baseline)	-	109.76	-	11.79	-	-
Mod. Reference UM (+1 % SFC)	+1 %	110.86	+1.00 %	11.79	-	+1.20 %
Mod. Reference UM (+5 % SFC)	+5 %	118.54	+8.00 %	12.38	+5.00 %	+5.33 %

Table 2.31: Results of the engine dry mass trade factor analysis carried out on a rubberized version of the optimized reference UM A/C and provided to MTU.

	Engine Dry Mass (kg)	**Engine Dry Mass (Δ%)**	**Wing Area (m^2)**	**Wing Area (Δ%)**	**Block Fuel (Δ%)**
Reference UM A/C (baseline)	2299	-	109.76	-	-
Mod. Reference UM (Engines +100 kg)	2349	+2 %	110.86	+1.00 %	+0.26 %
Mod. Reference UM (Engine +200 kg)	2399	+4 %	113.43	+3.34 %	+0.63 %
Mod. Reference UM (Engine +300 kg)	2449	+7 %	115.25	+5.00 %	+0.95 %

For each modification to the aircraft model, the wing area was manually altered (by keeping the same original aspect ratio and consequently modifying the overall wing span value) to match both target (according to the performance of the optimized reference A/C model and to the original set of TLARs) take-off and landing field lengths. In case the cruise or climb performance were not in line with target values, or in case the initial cruise service ceiling was not compatible with an operative cruise altitude of 37000 ft, the wing aspect ratio was manually adjusted as well. It is important to highlight that, for all the analyses of this trade factor study, the overall mission range was kept constant, while the maximum take-off weight was automatically adjusted to match the reference design mission.
Fuselage dimensions, as well as landing gears parameters, were kept constant in this study, and no modifications were applied to the position of the wing with respect to the main body of the aircraft. The reference engine dataset used for the analyses was the same adopted to carry out the design of the optimized reference UM A/C.
The results of these trade factor analyses are reported in table 2.30 and in table 2.31. In these tables, block fuel variations for the design mission specified by the TLAR of table 2.10 are reported, along with the set of modifications to the wing planform geometry (area plus, eventually, aspect ratio).
In addition to the trade factor analysis, the definition of the system architecture of the aircraft (implying the setting of power off-takes and customer bleed air, per flight phase), as well as thrust requirements and maximum dimensions constraints, were also provided to MTU.
Regarding the thrust requirements, these were assessed by UNINA using the performance module of JPAD-*core*, using the results coming from the analyses of the optimized reference UM model. The effect of airframe technologies on thrust demand was not accounted, in order to allow for the analyses of different combinations on technologies, in order to eventually define the best suitable set for the aircraft platform considered in ADORNO.

Table 2.32: Advanced engine requirements at different operating conditions and engine ratings.

	Altitude ft	Mach -	Delta ISA °C	Single Engine Thrust kN	Power Off-takes (per engine) kW	Customer Bleed kg/s
Cruise AEO	37000	0.78	0	19.500	173	0.0
Cruise OEI	20000	0.47	0	46.896	377	0.0
Climb AEO	35000	0.78	10	27.477	140	0.0
Climb OEI	20000	0.6	10	44.944	312	0.0
Take-off AEO	0	0.2	15	80.186	64	0.0
Take-off OEI	0	0.2	15	83.916	128	0.0

Power off-takes and customer bleed requirements were assessed once the final systems architecture of the target UM A/C model was set. This was the bleed-less, more-electric architecture reported in [71] and already described in section 2.3.3. The amount of power off-takes required per flight condition was estimated by using information included in [71][34][66], using linear interpolation between data for different aircraft platforms with respect to the one examined in ADORNO when necessary. Requests for additional power off-takes coming from the adoption of advanced systems such as hybrid laminar flow control were not directly included in the requirements provided to MTU. Nevertheless, a supposed range of variation, with respect to the power off-takes concerning the systems architecture only, was delivered to the engine manufacturer, to enable further evaluations.
No particular constraints were provided to MTU in terms of maximum allowed dimensions of the engine/nacelle. It was stated that, except for special cases (e.g., particularly high values of the maximum nacelle diameter), engine installation issues could be handled by adequately adjusting the characteristics of the landing gears and by modifying the wing shape and position with respect to the main body of the aircraft.
The set of engine requirements delivered by UNINA to MTU for the design of the advanced engine of ADORNO WP2 is summarized in table 2.32.
Table 2.33 provides the main characteristics of the advanced GTF engine designed by MTU. It should be noted that, along with the information included in this table, MTU also provided a dimensional engine performance deck, according to the JPAD-required formatting illustrated in section 2.1.1. This deck was later non-dimensionalized in terms of thrust by UNINA, using information on take-off SL static thrust included in the same deck. The engine dataset also included information on scaling factors for SFC and PPS mass, that were used by UNINA in order to account the effect of additional power off-takes, linked to the application on the target A/C of advanced airframe technologies.
Information in terms of weight, dry engine and PPS masses, were both used, by including the first in the set of input data managed by JPAD for the description of the characteristics of the engine, and the second one to adequately calibrate the result coming from the combined (averaged) usage of the equations provided by [167][97][101], as explained in section 2.1.1.
For the modelling of the external shapes of the nacelle, information on the maximum fan cowl diameter and length were directly assigned to the same variables managed by the JPAD aircraft parameterization. The remaining attributes required by the modelling of the nacelle provided by JPAD were arbitrarily assigned, using typical ratios for HBPR turbofan engines. It must be said that these parameters only have a minor impact on the calculation of the nacelle drag, according to the implemented methodology (which was reported in section 2.1.1).

Table 2.33: Characteristics of the advanced GTF engine designed by MTU for ADORNO WP2 applications.

Description	Value
Bypass Ratio (ADP)	13.4:1
Overall Pressure Ratio (Max. Climb)	51.5:1
Powerplant System Mass	3390 kg
Dry Engine Mass	2366 kg
Nacelle Fan Cowl Length	3.65 m
Max. Nacelle Fan Cowl Diameter	2.704 m
Fan Diameter	1.997 m
SFC calibration per 100 kW additional power off-takes	1.0157
PPS mass calibration per 100 kW additional power off-takes	1.0157

It is also important to remark that no information were included in this engine dataset regarding noise. This type of information is usually quite strategic for the engine manufacturer, making it quite difficult to disclose to those outside the company. For this reason, UNINA was not able to directly carry out a comparative assessment on environmental noise between the optimized reference and target UM configurations, as it is explained in section 2.3.5. However, a noise assessment will be carried out on the target A/C models later on in the project. UNINA will provide MTU with the necessary data on airframe noise spectra at certification points, allowing the engine manufacturer to carry out an overall aircraft noise assessment by including its own information on engine noise in the ATTILA++ analysis framework.
The new engine dataset did not include any information on engine price or maintenance, that could be used in order to perform a more accurate analysis on aircraft direct costs. Moreover, no information were included on the design and maximum temperatures endured by the engine, that could be used to perform more reasonable assumptions. For this reason, engine cost and maintenance charges adopted for the assessment of target aircraft direct costs were simply assumed by UNINA, following a statistical approach for the first one (using public available information on turbofan engines prices and by assuming a linear regression law with respect to EIS) and by assuming the same charges adopted for the reference for the latter. However, at least for ADORNO WP2 activities, a correct estimation of the engine effect on the aircraft direct costs was not essential, since for the MDAO process on the target UM A/C model the engine dataset was considered fixed.

2.3.5 Design of the target A/C model

The following sub sections provide information on the activities carried out for the design of the target UM A/C model. Details are provided on the set of modifications applied to the optimized reference UM configuration, in order to fit the advanced engine designed by MTU and to define the baseline A/C model adopted for the MDAO process leading to the definition of the optimized target UM model. The general approach to the MDAO process is outlined too, by highlighting the set of assumptions and constraints considered throughout the analyses. Finally, the main results deriving from the multidisciplinary

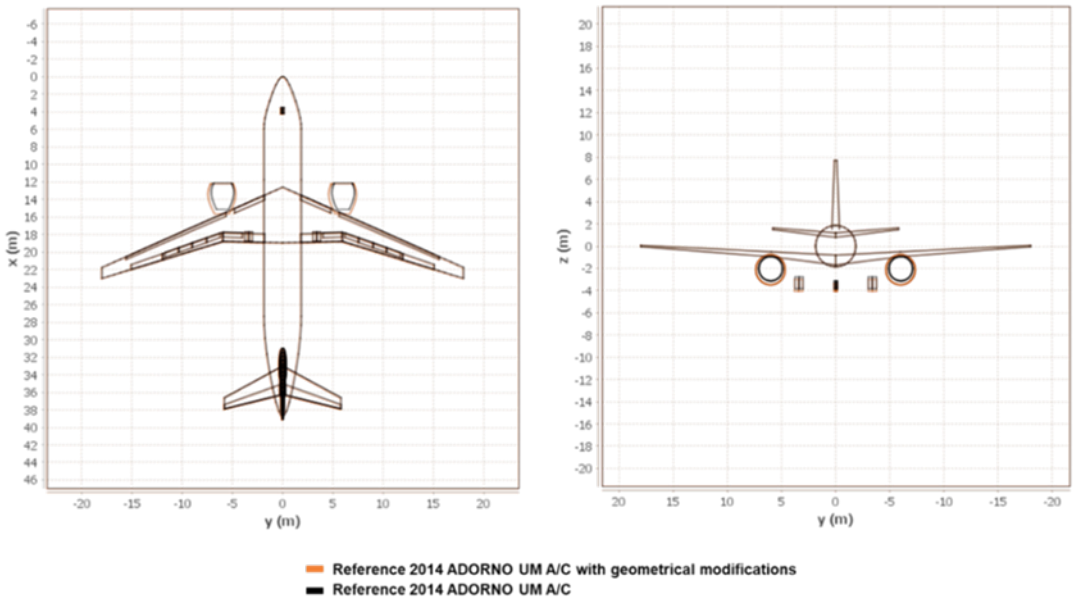

Figure 2.25: Comparison between the initial aircraft model and the updated one, allowing to equip the new powerplant system.

analysis of the optimized target UM A/C are reported and commented, by also including a breakdown of the effects of all the advanced technologies applied to this model. These results are also compared to those of the optimized reference UM configuration, in order to check the matching of CS2 objectives on emissions reduction.

Fixing of engine installation issues

The new engine provided by MTU was characterized by an increased bypass ratio with respect to the reference engine. The larger fan diameter, maximum nacelle fan cowl diameter and nacelle cowl length required to apply some geometrical modifications to the aircraft, aiming at providing a feasible engine installation. In fact, these modifications were applied with all ground stability and ground operation limitations, as well as to provide an adequate amount of engine ground clearance, a correct positioning of the landing gears, and the possibility to retract the main landing gears in the aircraft wing-body fairing.
A visual comparison between the initial aircraft model (i.e., the optimized reference UM model) and the updated one is provided in figure 2.25. This update process was mainly driven by the need to not lose the beneficial effect provided by the lower cruise SFC value of the new engine. For this reason, several attempts were made to define the best possible set of modifications, represented by the one including the lowest possible number of adjustments applied to the wing planform geometry and positioning with respect to the main body of the aircraft. A summary of the geometrical modifications applied to the optimized reference UM A/C is reported in table 2.34. It was tested that this set of modifications provided a negligible effect on the design mission block fuel, using the same engine dataset adopted for the optimized reference UM model performance analysis.

Table 2.34: Set of geometrical modifications applied to the reference UM A/C model for the installation of the new engines and for the generation of the baseline A/C model for the MDAO process of the target UM A/C model.

	Reference UM A/C	**Updated UM A/C (target A/C baseline)**
Engine apex vertical offset from wing attachment	−1.3 m	−1.4 m
Main landing gear leg length	2.56 m	2.85 m
Main landing gear wheel track	6.73 m	6.78 m

Target UM A/C MDAO process

Starting from the updated reference UM aircraft described in the previous sub section, a complete MDAO process was carried out, to investigate the effects on mission-related objectives, such as the block fuel and the total DOC, of both the selected set of advanced airframe technologies and main aircraft geometrical parameters, like the wing area and the wing aspect ratio. The advanced engine dataset provided by MTU was considered fixed at this stage and was only manipulated in terms of scale factors for engine power-plant mass and SFC, to account different power off-takes demands with respect to the ones considered in the preliminary engine design process.
It is important to highlight that, differently from the optimization carried out for the reference UM model, aircraft cumulative EPNL was not considered as one of the driving objectives of the optimization, along with mission block fuel. Results from the design and analysis activities carried out on the reference A/C clearly highlighted that even significant variations in terms of wing planform parameters, had only a minor impact on aircraft cumulative EPNL. In addition, the Pareto fronts used for the reference A/C optimization showed that the best solutions in terms of minimum block fuel were pretty close to the best solutions in terms of minimum cumulative EPNL. Based on these considerations, and to speed up the target A/C optimization problem, mission block fuel was selected as the only optimization objective.
With regards to costs, these did not drive the optimization process, since they were not among the list of disciplines to be investigated within the context of ADORNO. Nevertheless, results in terms of total DOC are reported in the analyses presented in this sub section, in order to highlight the impact that advanced airframe technologies could have on aircraft costs, according at least to the approach implemented in JPAD and in the technologies manager. Of course, the considerations on engine costs and maintenance discussed in section 2.3.4 also apply.
The multidisciplinary optimization of the target UM aircraft model was carried out by following a two-step approach. First, a single-objective optimization on the mission block fuel was performed, by implementing the procedure shown in figure 2.26 for each of the 336 advanced airframe technologies combinations reported in table 2.35. The reduced number of combinations concerning the use of advanced composite materials was already explained in section 2.3.3. With regards to the remaining combinations, a preliminary selection aiming at considering only the most relevant combinations was performed, in order to reduce the total number of permutations. This drastically reduced the necessary computational time.
To generate the aircraft population for each of the 336 single-objective optimizations, wing planform parameters, represented by the wing area and the wing aspect ratio, were

included in the set of independent design variables. No variation were applied to the geometry of the fuselage, to be sure to comply with prescribed top-level requirements in terms of accommodation, neither to the relative position of the wing with respect to the fuselage or the position of the engines with respect to the wing (i.e., spanwise non-dimensional position was kept constant and equal to the baseline value, as well as the vertical and longitudinal offset of the engine with respect to the wing leading edge). In addition, the same main landing gear leg length of the baseline A/C model was considered for all the performed analyses.
It is important to remark that variations just to the wing planform geometry implied modifications to other aircraft main and secondary components, according to a set of pre-selected updated strategies. The overall set of modifications applied to the aircraft for the generation of the DOE population for each airframe technology combination can be summarized as follows:

- The wing aspect ratio and the wing area were changed from -20 % to $+20$ % with respect to baseline values (11.79 and 109.76 m^2, respectively), using 5 equally spaced values. An upper limit was set on the maximum reachable value of wing aspect ratio (slightly higher than 14), in order to not incur in structural problems and to not stress too much the range of applicability of the semi-empirical equations adopted for the estimation of the weight of the wing. A total number of 25 permutations was considered, and for each of them wing panel chords (both inner and outer) and spans were subsequently updated: chords were multiplied by the ratio between updated planform surface and baseline surface, while spans were updated by keeping the same ratios with respect to the overall span of the baseline configuration.

- The dimensions of the fuel tank were updated according to the ratio between the updated and the baseline planform area.

- Planform geometries and positions in the BRF of the horizontal and vertical tails were automatically updated, to keep the same volumetric ratios and the same aspect ratios of the baseline model.

- Dimensions and positions of the control surfaces and high-lift devices were automatically updated too, by keeping the same definitions in terms of non-dimensional parameters (e.g., inner and outer spanwise positions along lifting surfaces, as well as chordwise positions and chord ratios) of the baseline A/C model.

In addition to these geometry updates, it is important to remark that, depending on the implemented set of airframe technologies, the advanced engine was updated in terms of SFC and powerplant mass, by using the scale factors for additional power off-takes provided by MTU together with the engine dataset. No thrust update strategies (as reported in figure 2.26 were applied in this case to match specific design mission requirements.
For each combination of airframe technologies, a full-factorial design of experiments was carried out, leading to 336 different response surfaces, and to 8400 different aircraft being analyzed. These response surface were successively fed to the JPAD-*optimizer* module, to perform single-objective optimizations on fuel burn (block fuel). A set of constraints was provided to the optimization sub-module, in addition to the response surface, in order to ensure the feasibility of each of the optimum A/C models generated by the tool. This set of constraints is quite similar to the one already included in section 2.3.2,

which was adopted for the MDAO process of the reference UM A/C. The complete list is repeated here again for the sake of clarity, and to better specify some modifications that were applied to it.

- All ground stability and ground operation checks should be successfully passed.
- The static stability margin at the most afterward center of gravity position should ensure aircraft longitudinal stability.
- No tail-strike should occur during take-off simulation, no nose and tail-strike should occur during landing simulation.
- The minimum safety speed during OEI take-off should be at least equal to the take-off stall speed, multiplied by 1.13.
- The cruise altitude (flat cruise) should be above 35000 ft, adopting a 2000 ft tolerance with respect to the value prescribed in the TLARs.
- The take-off field length should be lower than 1950 m, adopting a 60 m tolerance with respect to the reference value prescribed by the set of TLARs.

In addition to these constraints, two additional ones were included in the set and alternatively imposed:

- The overall wing span should be below the current limitation (36 m) set by ICAO Annex 14 for aircraft belonging to C category.
- The mission fuel mass should be lower than the maximum storable in the wing fuel tank.

The last constraint, in particular, was slightly softened, when switched off, by assuming to allocate an auxiliary central tank (ACT) in the lower deck of the fuselage, allowing to board an additional fuel mass equal to 2132 kg. The dimensions of this additional tank, and the maximum quantity of additional fuel storable, were estimated starting from the geometry of the lower deck of the fuselage of the baseline model.
With this set of constraints, and by considering all the possible permutations, four different single-objective optimizations on block fuel were carried out per airframe technology set, leading to a total of 1344 optimizations. This first step in the optimization process towards the final target UM aircraft model is summarized in figure 2.27.
Following this first step, the results coming from the 1344 optimizations on block fuel were used to perform a further analysis, aiming at providing, for each combination of constraints, three possible solutions: one for minimum block fuel, one for minimum total DOC, and a balanced solution, representing a compromise between minimum costs and block fuel. For this analysis, each of the optimum aircraft obtained at the previous step were analyzed again by means of the complete multidisciplinary analysis cycle reported in figure 2.3, in order to have more reliable results than those obtained by means of an interpolation of the response surfaces (although it was tested that these differences were quite limited). The results of these additional analyses are reported in figure 2.28, figure 2.29, figure 2.30, figure 2.31, figure 2.32, figure 2.33, and in table 2.36, table 2.37, table 2.38.
These figures provide a direct comparison between the characteristics of the optimized reference UM aircraft in terms of mission block fuel and total DOC, and those of the

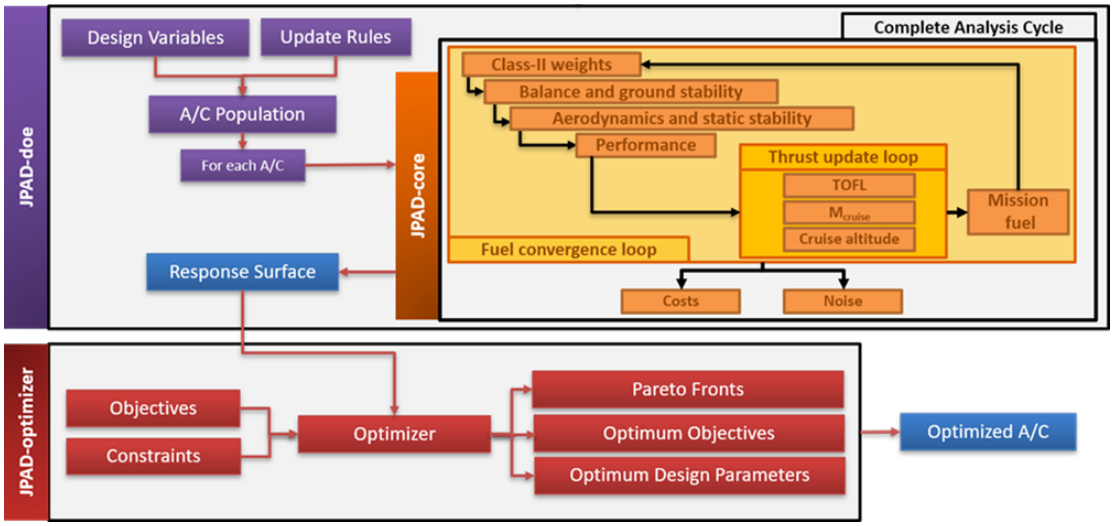

Figure 2.26: MDAO workflow adopted for the single-objective optimizations on fuel burn of the 336 different advanced airframe technologies combinations, considered for the design process of the target UM A/C model.

Table 2.35: Set of advanced airframe technologies combinations considered in the optimization study leading to the definition of the best possible target UM A/C model.

TECHNOLOGIES				
HLFC	**Riblets**	**Variable Camber**	**OBS Architecture**	**Advanced Materials**
None	None	None	MEA2	None
Wing	Wing	Wing		Fuselage
Tails	Tails			Landing gears
Wing+Tails	Fuselage			LG+Fuselage
Tails+Nacelles	Wing+Tails			
Wing+Tails+Nacelles	Tails+Fuselage			
	Wing+Tails+Fuselage			
6 combinations	7 combinations	2 combinations	1 combination	4 combinations
336 total combinations				

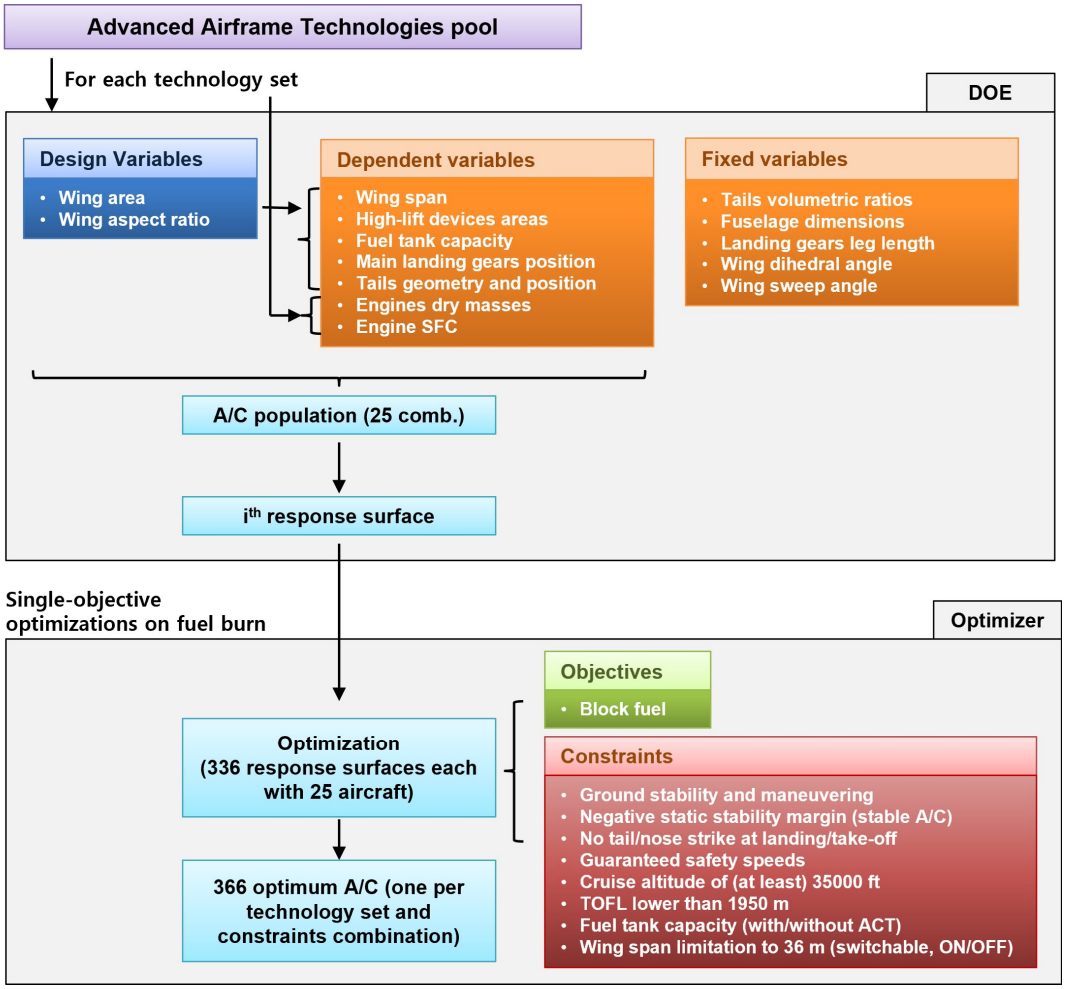

Figure 2.27: Summary of the first step to the definition of the UM target A/C model. The light blue boxes represent the workflow implemented for each single set of constraints.

optimized aircraft deriving from the MDAO process previously described. Each point reported in these figures represents an optimum (i.e., minimum block fuel) solution for a certain combination of airframe technologies (those reported in table 2.35) and optimization constraints. Figures from 2.28 to 2.31 are related to different combinations of optimization constraints, respectively:

- constrained wing span (i.e., the wing span can not assume values higher than 36 m), constrained maximum available fuel mass (i.e., there is no additional central tank in the lower deck of the fuselage).
- constrained wing span, unconstrained maximum available fuel mass, i.e., the design mission fuel can exceed the maximum fuel storable in the wing tank (which, in turn, depends on the dimensions of the wing, set by the parametric study as described in the previous section) by 2132 kg, at most.
- unconstrained wing span, constrained design mission fuel mass.
- unconstrained wing span, unconstrained design mission fuel mass.

In these figures, overall (considering all the possible permutations of airframe technologies) minimum block fuel, overall minimum total DOC, and balanced solutions are highlighted and compared with the baseline solution. Moreover, figure 2.32 allows to simultaneously compare this set of three solutions for each combination of optimization constraints. Finally, figure 2.36 provides information on the geometric characteristics, in terms of DOE design variables, of these solutions. It is interesting to notice that all the solutions deriving from an optimization with no constraints on the maximum wing span all feature the same, maximum allowable value of wing aspect ratio (14.19), while the constrained wing span solutions feature a constant value of the wing span (equal to 36 m) and different combinations of wing aspect ratio and planform area, depending on the combinations of airframe technologies and on the constraint on the maximum allowable fuel for the design mission.
Tables from 2.36 to 2.38, provide a more detailed description, in terms of numerical values and percentage differences, of the results included in the previous figures. Regarding information on applied optimization constraints included in these tables, a checked box means that the constraint was applied, e.g., checked ACT means that the maximum allowable fuel on-board was strictly constrained and no additional central tank was located in the lower deck.
The abovementioned triplet of possible solutions per combination of constraints were then compared in terms of block fuel, pollutant emissions (CO_2 and NO_x) and total DOC with respect to the ADORNO reference UM configuration, to check the effects of the implemented technologies (airframe and powerplant) on the matching of ambitious targets set by the CS2 program.
Regardless of the set of constraints adopted for the single-objective optimizations on block fuel, it was noticed that the abovementioned triplets of solutions shared the same combinations of advanced airframe technologies. In addition to the more-electric OBS architecture and the advanced powerplant system:

- Advanced materials for both fuselage and landing gears, for all four minimum total DOC solutions;
- HLFC system on the wing, horizontal tail, vertical tail and nacelles, riblets on the fuselage and on all the lifting surfaces of the airplane, variable camber wing,

and advanced composites and alloys for the fuselage and the landing gears, for the minimum block fuel solutions;

- HLFC system on all the lifting surfaces and on the nacelles, along with the use of advanced materials for both the fuselage and the landing gears, for the balanced solutions.

Therefore, the minimum block fuel solutions, were also the ones characterized by the highest increase in terms of total DOC with respect to the reference model. This was strictly related to the impact of advanced airframe technologies on aircraft price and maintenance costs, at least according to the modelling implemented as described in section 2.3.3, and despite the provided reduction in terms of block fuel. Nevertheless, in order to comply with the project objectives in terms of emissions reduction, the minimum block fuel solution obtained from the optimization study with a constraint on the maximum wing span and with an additional central tank (the one described in the first column of table 2.36) was selected as the optimized target UM A/C model. This solution, as reported in table 2.36), guaranteed a 20.12 % reduction in terms of CO_2 emissions, which is beyond the minimum target set by CS2. Although the solution coming from the optimization study with no limitations on the maximum wing span would have allowed even higher reductions (an additional -1.42 % for CO_2 emissions), it was concluded that, for a planned EIS of the target A/C in the 2030-2035 timeframe, a modification to the limitation in terms of maximum allowable wing span for category C airplanes (due to the current size of taxi-ways and hangars) would have been excessively unrealistic.
It is important to notice, from the results included in the tables from 2.36 to 2.38, that the estimated NO_x emissions percentage reductions were always higher than the CO_2 reductions. This phenomenon was explained by performing a detailed analysis of the output data provided by the JPAD mission performance analysis module. It was observed that the target A/C engine always worked at lower cruise throttle settings than those of the reference baseline model. Although the reference and the advanced engines shared rather similar values of NO_x EI at maximum cruise setting, lower throttle settings for the target A/C models implied lower NO_x EI values, that, once combined with the fuel burn reduction, allowed for increased NO_x emissions reductions.
Finally, as it can be deduced from figure 2.33, the selected minimum block fuel solution, among all the solutions with constrained maximum wing span, was the one characterized by the lowest wing planform surface combined with the highest allowable aspect ratio.

Target UM A/C multidisciplinary analysis

In preparation of the work for the fourth work package of ADORNO, dealing with the design of a set of reference aircraft models based on a parametric studies on engine BPR performed by MTU, the optimized target UM aircraft model was subjected to an extensive review. Minor flaws were identified in the modelling of the effect of additional power off-takes (with respect to those required by the OBS only) and of the weight increment due to some of the advanced airframe technologies. Moreover, an incorrect value had been used to model the nacelle fan cowl length, with respect to the one reported in table 2.33. All these minor issues led to the necessity to reassess results for this model, and explain why some of the outcomes reported in this section and concerning fuel burn and emissions slightly differ from the values already reported in table 2.36.
For the reasons exposed above, an optimization was carried out, but this time just for the

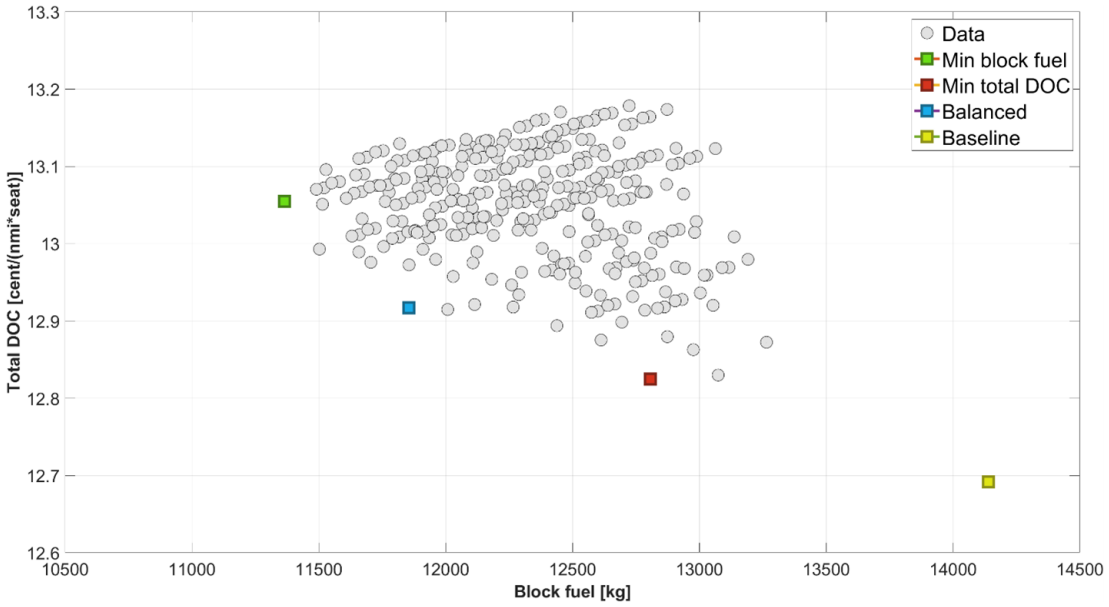

Figure 2.28: Results of the optimizations carried out with constraints on both the maximum wing span and ACT availability. Minimum block fuel, minimum total DOC and balanced solutions are highlighted and compared with the baseline.

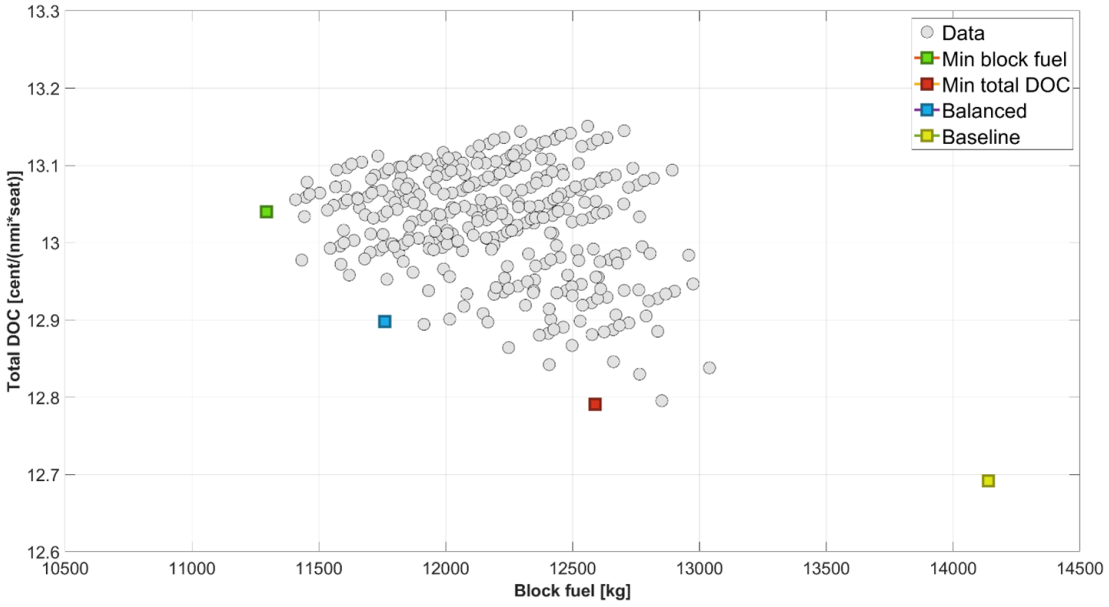

Figure 2.29: Results of the optimizations carried out with a constraint on the maximum wing span, with an ACT housed in the lower deck of the fuselage. Minimum block fuel, minimum total DOC and balanced solutions are highlighted and compared with the baseline.

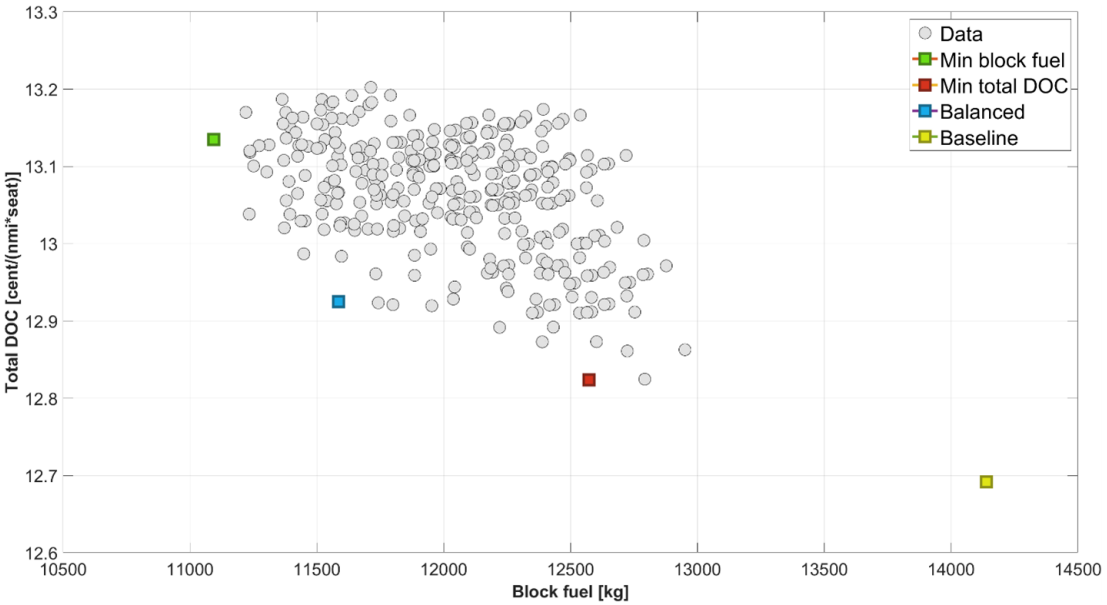

Figure 2.30: Results of the optimizations carried out with no constraint on the maximum allowable wing span, but with no ACT housed in the lower deck of the fuselage. Minimum block fuel, minimum total DOC and balanced solutions are highlighted and compared with the baseline.

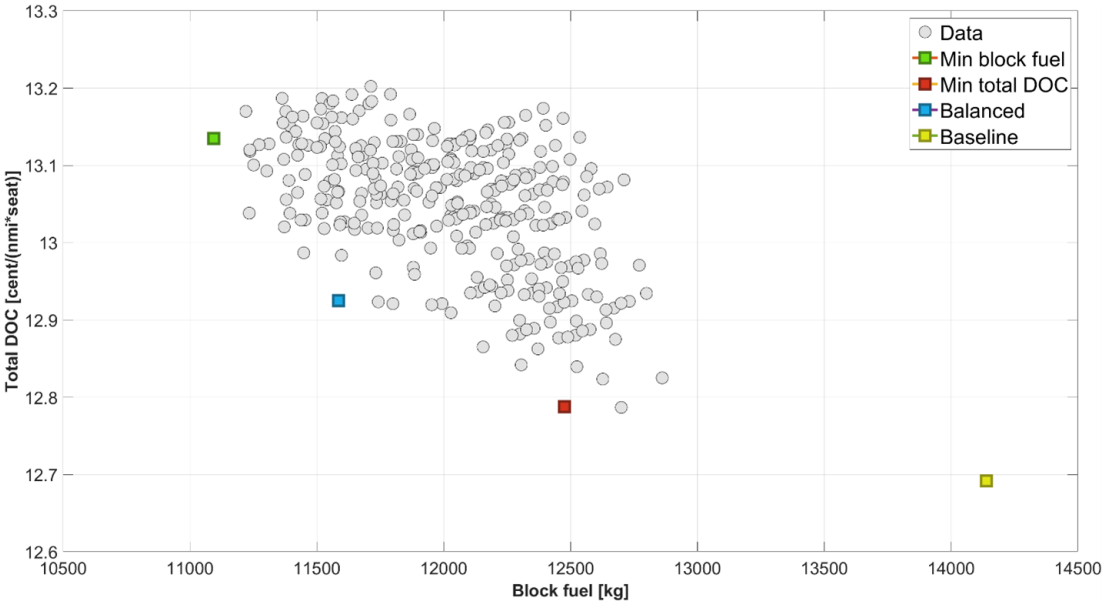

Figure 2.31: Results of the optimizations carried out with no constraint on the maximum allowable wing span and housing an ACT in the lower deck. Minimum block fuel, minimum total DOC and balanced solutions are highlighted and compared with the baseline.

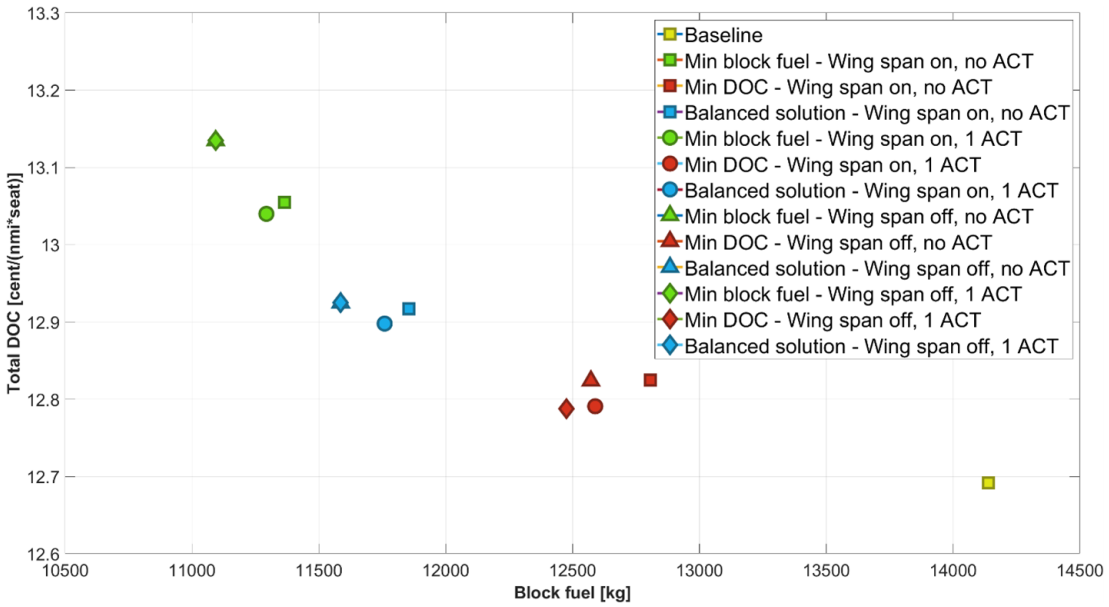

Figure 2.32: Comparison between minimum block fuel, minimum total DOC and balanced solutions per optimization constraints permutation, also compared with respect to the baseline.

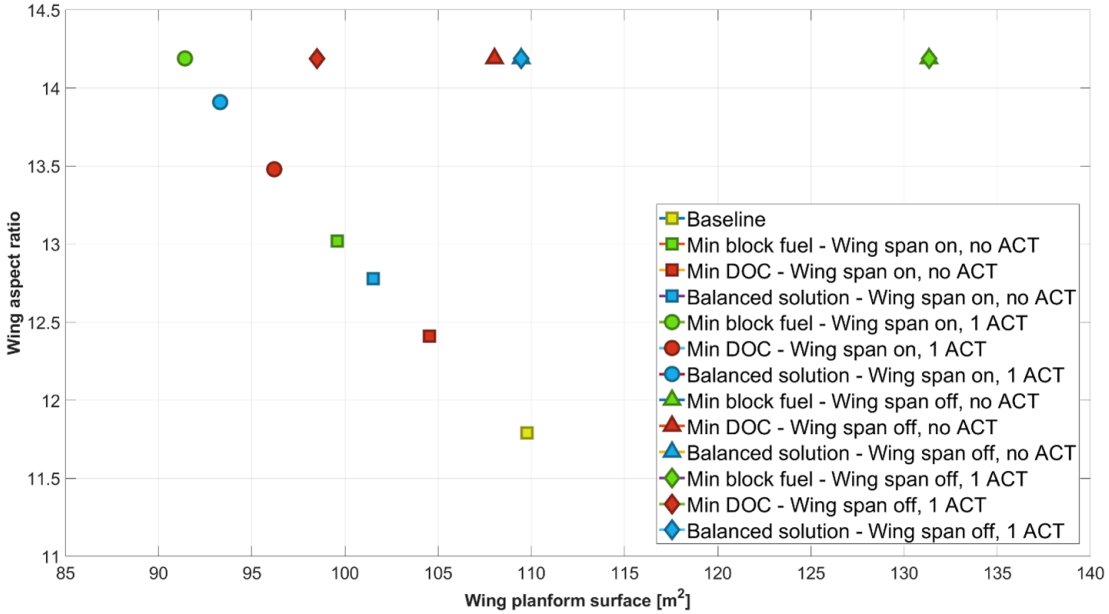

Figure 2.33: Geometric characteristics in terms of fuel burn optimization design variables of the minimum block fuel, minimum total DOC and balanced solutions, considering the four different sets of constraints.

Table 2.36: Minimum block fuel solutions according to the four combinations of optimization constraints.

Minimum block fuel solutions – 3100 nmi, 140 passengers mission				
	Optimization constraints combinations			
	Wing span ☒ ACT ☐	Wing span ☒ ACT ☒	Wing span ☐ ACT ☐	Wing span ☐ ACT ☒
Block fuel, kg	11294	11365	11094	11094
Block fuel Δ% wrt baseline	**−20.12 %**	**−19.62 %**	**−21.54 %**	**−21.54%**
CO_2 emissions, kg	40874	41130	40147	40147
CO_2 Δ% wrt baseline	**−20.12 %**	**−19.62 %**	**−21.54 %**	**−21.54 %**
NO_x emissions, kg	186.57	188.08	184.29	184.29
NO_x Δ% wrt baseline	**−35.09 %**	**−34.56 %**	**−35.88 %**	**−35.88 %**
Total DOC, cent/(nmi*seat)	13.040	13.055	13.135	13.135
Total DOC Δ% wrt baseline	+2.75 %	+2.86 %	+3.49 %	+3.49%

Table 2.37: Minimum total DOC solutions according to the four combinations of optimization constraints.

Minimum block fuel solutions – 3100 nmi, 140 passengers mission				
	Optimization constraints combinations			
	Wing span ☒ ACT ☐	Wing span ☒ ACT ☒	Wing span ☐ ACT ☐	Wing span ☐ ACT ☒
Block fuel, kg	12590	12807	12476	12573
Block fuel Δ% wrt baseline	**−10.95 %**	**−9.42 %**	**−11.76 %**	**−11.07 %**
CO_2 emissions, kg	45566	46349	45152	45505
CO_2 Δ% wrt baseline	**−10.95 %**	**−9.42 %**	**−11.76 %**	**−11.07 %**
NO_x emissions, kg	229.64	236.56	226.24	229.33
NO_x Δ% wrt baseline	**−20.11 %**	**−17.69 %**	**−21.29 %**	**−20.21 %**
Total DOC, cent/(nmi*seat)	12.791	12.825	12.788	12.824
Total DOC Δ% wrt baseline	+0.78 %	+1.05 %	+0.76 %	+1.04 %

Table 2.38: Balanced solutions (i.e., compromise solutions between minimum block fuel and minimum total DOC) according to the four combinations of optimization constraints.

Minimum block fuel solutions – 3100 nmi, 140 passengers mission				
	Optimization constraints combinations			
	Wing span ☒ ACT ☐	Wing span ☒ ACT ☒	Wing span ☐ ACT ☐	Wing span ☐ ACT ☒
Block fuel, kg	11760	11855	11587	11587
Block fuel Δ% wrt baseline	**−16.82 %**	**−16.16 %**	**−18.05 %**	**-18.05 %**
CO_2 emissions, kg	42562	42900	41933	41933
CO_2 Δ% wrt baseline	**−16.82 %**	**−16.16 %**	**−18.05 %**	**-18.05 %**
NO_x emissions, kg	200.50	203.49	196.87	196.87
NO_x Δ% wrt baseline	**−30.24 %**	**−29.20 %**	**−31.51 %**	**-31.51 %**
Total DOC, cent/(nmi*seat)	12.898	12.917	12.925	12.925
Total DOC Δ% wrt baseline	+1.63 %	+1.77 %	+1.84 %	+1.84 %

combination of airframe technologies and constraints of the previously selected optimum target model. It is worth to mention that the correction of the abovementioned issues would have not led to any significant difference in terms of results of the optimization study on technologies and block fuel reported in the previous sub section: it was tested that those corrections would have impacted almost in the same way on each of the examined A/C models. Table 2.39 provides a summary on the main results coming from the multidisciplinary analysis carried out on the optimized target UM model, as well as a comparison in terms of project-related metrics with respect to the reference A/C models, which again provides proof of the matching of the environmental objectives set by the CS2 program, but at the expense of an increase in terms of direct operating costs. It is important to mention that, for both the reference and advanced engines, the same and constant (through the different ratings and throttle settings) value of CO_2 EI was adopted for the analyses on emissions. This is the reason for which the optimized target CO_2 total emissions reduction equals the reduction on total fuel used for the mission.
In addition, figure 2.34 provides a visual representation of the optimum target UM A/C model.
An analysis on the impact of each technology (airframe and powerplant) on the optimized target UM A/C model was carried out. Seven analyses were performed in total, for the following configurations:

- ADORNO reference UM A/C model.
- ADORNO reference UM A/C model, equipped with MTU advanced BPR 13.4 GTF engines and the more-electric on-board systems architecture.
- The previous configuration, but with the addition of a HLFC system on wing, horizontal tail, vertical tail, and nacelles.
- The previous configuration, with riblets applied on all the lifting surfaces and on the fuselage external surface.
- The previous configuration, with the addition of a variable camber system on the trailing edge of the wing.
- The previous configuration, including the use of advanced materials for the fuselage structure (CFRP) and for the landing gears system (advanced Ti-based alloys).
- The previous configuration, including the set of modifications to the A/C geometry (wing planform parameters and derived horizontal and vertical tail parameters) suggested by the optimization study on the target UM A/C. These are the ones reported in table 2.39.

These analyses for progressively improved A/C models allowed to have a clearer picture on the single contributions to the overall reduction in terms of pollutant emissions of the ADORNO target UM model. These results are presented in table 2.40, and in figure 2.35 and 2.36, focusing on the total fuel used and on the total CO_2 and NO_x emissions in particular. These analyses highlighted that the advanced BPR 13.4 engine designed by MTU allowed for a reduction greater than 7 % on the total amount of fuel burn by the aircraft during the design mission with respect to the reference A/C model, meaning more than one-third of the total reduction. The remaining contribution was mostly due to the adoption of advanced airframe technologies, with the HLFC system being responsible of a further 4.7 % of the total fuel consumed, which accounted for a 23 % on the overall fuel

burn, and for a 42 % on the contribution provided by airframe advanced solutions. The advanced engine and the HLFC system were also responsible of most of the reduction of NO_x emissions, each allowing for more than 30 % of the total reduction. In addition to the analysis on the emissions, it is interesting to examine the evolution of the remaining results of the multidisciplinary analyses reported in table 2.40. The aircraft MTOW, up to the application of advanced materials, slightly changed, mostly due to the fact that technologies previously applied had a negligible or even negative impact on the OEW. The take-off field length mostly benefited of the effect of the new advanced powerplant system, capable of producing an higher SL static thrust with respect to the reference engine, and of the advanced materials, which sensibly reduced the aircraft OEW (by more than 2.5 tons) and the total amount of fuel required for the completion of the design mission. The time to climb (n.b., the one reported in table 2.40 is the minimum time to climb, and not the one for a constant climb speed reported in 2.39) increased with the application of the advanced powerplant system despite the higher value of static thrust, due both to a different behaviour of the thrust lapse with respect to the reference engine and to the increased aircraft drag caused by the bigger nacelle. The application of technologies acting on the aerodynamics of the aircraft (n.b., the HLFC system is designed to work only during cruise conditions), of advanced materials leading to a dramatic reduction of the MTOW, and modifications to the wing aspect ratio (from almost 12 up to more than 14), led to a significant reduction of the climb time required by the optimized target A/C model. Finally, speaking of direct operating costs, these continued to grow with the application of new technologies, with just the use of advanced materials and the modifications to the wing geometry (which only impacted on MTOW and mission fuel) allowing to slightly reverse this trend.
It is easy to notice that the estimated values of mission fuel reductions linked to the use of airframe technologies reported in figure 2.35 tend to differ from those reported in table 2.24, which were used for testing and calibration. The HLFC contribution, in particular, is quite different from the reference one. The reason for these differences is mostly linked to the fact that during calibration activities, each single technology was individually tested on the baseline, reference UM aircraft, with no additional technology being simultaneously applied. Moreover, speaking of HLFC system, it was tested that its effect on the aircraft aerodynamics alone did allow for fuel burn reductions included in the interval reported in table 2.24, and that the addition of the effect on SFC due to the additional power off-takes only partially reduced the overall impact. These tests, however, were performed using the UNINA reference engine model, adopting literature-based scale factors [160] for the effect of power off-takes on SFC and not accounting for the impact on powerplant system mass. Not last, the required amount of thrust for the cruise phase, once the aircraft was equipped with the HLFC system, led to substantially lower values of engine throttle, that, coupled with the performance dataset for the new advanced engine, implied a not-negligible effect on the cruise SFC.

Table 2.39: Comparative table of multidisciplinary analysis results of the optimized reference and target UM A/C models of ADORNO.

	Reference UM	**Target UM**	**Δ%**
Geometry			
Wing area, m^2	109.76	91.34	
Wing aspect ratio	11.79	14.19	
Wing leading edge sweep angle, degrees	27	27	

Table 2.39 continued from previous page

Wing apex X position (BRF), m	12.5	12.5	
Wing apex Z position (BRF), m	−1.25	−1.25	
Horizontal tail area, m^2	26.34	18.09	
Horizontal tail span, m	11.58	9.62	
Horizontal tail aspect ratio	5.09	5.12	
Horizontal tail leading edge sweep angle, degrees	32	32	
Horizontal tail apex X position (BRF), m	33	33	
Horizontal tail apex Z position (BRF), m	1.0	1.04	
Vertical tail area, m^2	23.17	19.19	
Vertical tail span, m	6.19	5.63	
Vertical tail aspect ratio	1.65	1.65	
Vertical tail leading edge sweep angle, degrees	45	45	
Vertical tail apex X position (BRF), m	31.0	31.0	
Vertical tail apex Z position (BRF), m	1.52	1.52	
Powerplant			
Single engine SL static thrust (kN)	103.6	116.6	
Weights			
Maximum take-off weight, kg	68177	63926	−6.23 %
Maximum landing weight, kg	57950	54360	
Operating empty weight, kg	36684	35871	−2.22 %
Design payload, kg	14462	14462	
Balance			
Maximum forward X CG, % MAC	10.10	−2.86	
Maximum afterward X CG, % MAC	36.64	31.75	
Operative X CG, % MAC	26.73	22.18	
Aerodynamics and static stability			
Maximum clean lift coefficient	1.52	1.53	
Maximum take-off lift coefficient	2.47	2.40	
Maximum landing lift coefficient	2.96	2.99	
Cruise zero-lift drag coefficient	0.0209	0.0187	
Cruise SSM, at maximum afterward X CG	18.9	19.71	
Maximum cruise aerodynamic efficiency	17.98	21.02	
Performance			
Take-off field length, MTOW, ISA SL, m	1814	1798	
Landing field length, MLW, ISA SL, m	1568	1674	
Time to climb at 270 KCAS, min	18	16	
Absolute OEI ceiling, ft	21,263	30,446	
Service OEI ceiling, ft	20817	29075	
Typical cruise Mach number	0.78	0.78	
Maximum cruise Mach number	0.82	0.82	
Typical cruise altitude, ft	37000	37000	
Block time, min	424	424	
Block fuel, kg	14139	11127	−21.30 %
Total fuel used (no reserves), kg	16199	12912	−20.29 %
Total NO_x emissions, kg	287.43	185.37	−35.51 %
Total CO_2 emissions, kg	51222	40829	−20.29 %
Costs			
Cash DOC, cent/(nmi*seat)	6.774	6.995	+3.26 %
Total DOC, cent/(nmi*seat)	12.703	13.017	+2.47 %

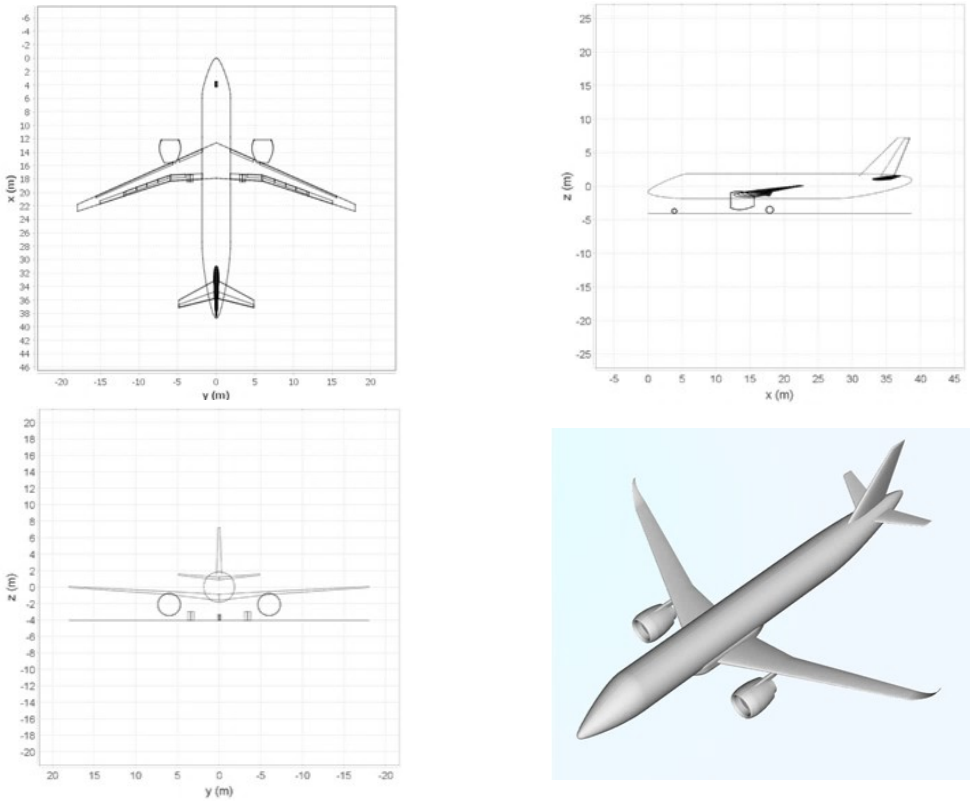

Figure 2.34: Optimum target UM A/C model three-view and 3D model.

Table 2.40: Comparative table of the progressive effect of each technology and update to the geometry on the performance and characteristics of the target UM model.

Parameter	**Reference UM A/C**	**+ Engines & MEA**	**+ HLFC**	**+ Riblets**
MTOW, kg	68177	67305	68283	67846
OEW, kg	36684	37087	38854	38812
TOFL, m	1814	1704	1762	1734
Minimum climb time, min	17	19	19	18
Design fuel mass, kg	17050	15767	14968	14578
Block fuel, kg	14139	13165	12329	11973
Total fuel used, kg	16199	14979	14219	13843
Total NO_x emissions, kg	287.43	255.66	224.33	212.42
Total CO_2 emissions, kg	51222	47364	44959	43772
Total DOC, cent/(nmi*seat)	12.703	12.861	12.978	13.054
Parameter	**+ Variable Camber**	**+ Advanced Materials**	**+ Geometry**	
MTOW, kg	67700	64541	63926	
OEW, kg	38798	36191	35871	
TOFL, m	1717	1577	1798	
Time to climb, min	18	16	15	
Design fuel mass, kg	14448	13892	13598	
Block fuel, kg	11835	11412	11127	
Total fuel used, kg	13718	13194	12912	
Total NO_x emissions, kg	207.84	193.05	185.37	

Table 2.40 continued from previous page

Total CO_2 emissions, kg	43,375	41,718	40,829	
Total DOC, cent/(nmi*seat)	13.117	13.069	13.017	

2.4 ADORNO trade factor analyses (WP4)

The following sections provide information on the work that was carried out for the fourth work package of ADORNO. This work package aims at the definition of an advanced trade factor methodology and of advanced aircraft design methodologies, allowing for a more efficient modelling of the effects related to new HBPR engines installation on a regional jet aircraft platform. The work performed by the time this thesis was completed included:

- the generation of a set of reference aircraft model, to be designed around the characteristics of a set of advanced HBPR turbofan engines, whose dataset is provided by MTU.
- the description and the analysis of this aircraft set with respect to the main topics of ADORNO.

This set of aircraft models will be used later in the project, in order to assess the applicability of linear trade factors on block fuel to predict the effect on the aircraft of changes applied to main engine parameters (such as the SFC, the weight and the overall dimensions)[6]. Moreover, this same set of models will provide the foundation for the definition of the abovementioned advanced trade factors and design methodologies. The first item of the above list is discussed in section 2.4.1, while section 2.4.2 includes information on the second topic.

2.4.1 Generation of the set of reference A/C models

The description of the design process of the reference aircraft models of WP4 is split in two sub sections, each providing information on specific tasks.

Engine datasets

An engine design study in BPR was performed by MTU for an advanced GTF engine, to be equipped on a 140 passengers regional A/C with a 2025+ expected entry into service. A/C fuel burn trade factors for this study were previously provided by UNINA, and are the ones reported in table 2.30 and table 2.31.
Three engines were designed by MTU based on these trade factors and on the set of requirements (in terms of thrust, power off-takes and overboard bleed) provided by UNINA for the target, year 2025+, A/C models of ADORNO. These are advanced HBPR GTF engines, with bypass ratio values ranging from 10 to 13.4. The main characteristics of these engines are summarized in table 2.41. Table 2.42, instead, provides information on the variations of the main parameters of these engines with respect to the characteristics of the BPR 10 engine.
It is important to highlight that the engine with BPR equal to 13.4 is the one that was

[6] At the time this thesis was being written, this task was already almost completed by the author, but it still necessitated to be reviewed by the Topic Manager of the project.

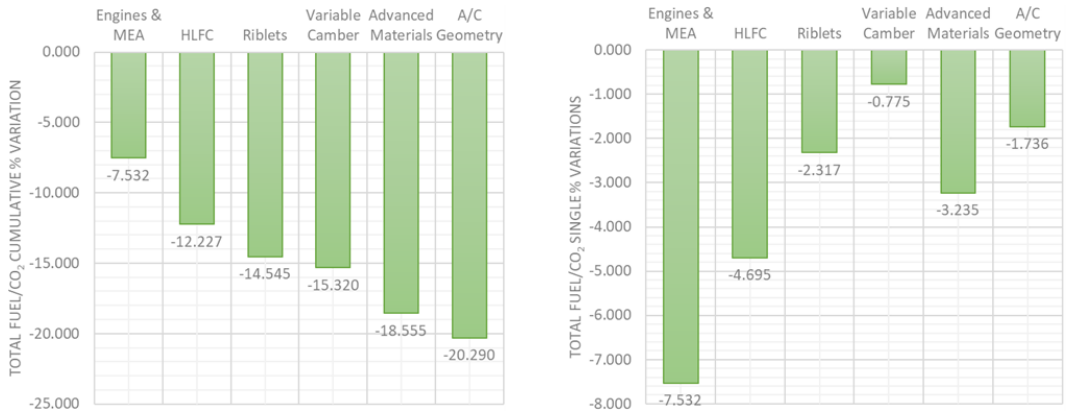

(a) Cumulative effect (b) Individual contributions

Figure 2.35: Cumulative and individual effects of advanced airframe technologies, powerplant system, and geometry modifications on the overall mission fuel burn and CO_2 emissions, based on results summarized in table 2.40

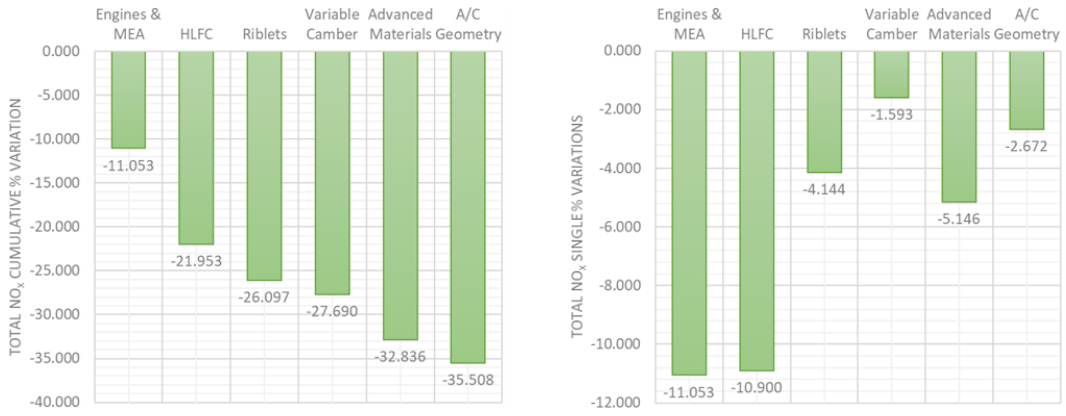

(a) Cumulative effect (b) Individual contributions

Figure 2.36: Cumulative and individual effects of advanced airframe technologies, powerplant system, and geometry modifications on the NO_x emissions, based on results summarized in table 2.40

Table 2.41: Main characteristics of the three engines delivered by MTU for the activities of WP2 and WP4 of the ADORNO project. Percentage variations of SFC and mass are provided with respect to BPR 10 engine characteristics.

Variable	**BPR 10.0 engine**	**BPR 12.0 engine**	**BPR 13.4 engine**
BPR (ADP)	10:1	12:1	13.4:1
OPR (MCL)	52:1	51.7:1	51.5:1
SFC (ADP), lb/(lbf*h)	-	−2.0 %	−3.0 %
PPS mass, kg	-	+2.6 %	+4.9 %
Dry mass, kg	-	+1.2 %	+2.7 %
Max. nacelle diameter, mm	2456	2606	2704
Nacelle cowl length, mm	3420	3560	3650
Fan diameter, mm	1777	1909	1997

Table 2.42: Percentage variations with respect to BPR 10 of main engines characteristics.

Variable	**Δ% variation with respect to BPR 10 engine**	
	BPR 12 engine	**BPR 13.4 engine**
SFC	−2.000 %	−3.000 %
Dry mass	+1.215 %	+2.691 %
PPS mass	+2.632 %	+4.954 %
Max. nacelle diameter	+6.107 %	+10.098 %
Nacelle cowl length	+4.094 %	+6.725 %

used for WP2, for the design of the target UM A/C model. For this specific engine, in addition to the characteristics in terms of ADP SFC, weight and main dimensions, an actual customer deck was also provided. This engine deck included information on engine performance (thrust and SFC) and emission indices (NO_x and CO_2) for different engine ratings, flight Mach numbers, flight altitudes, ISA conditions, and throttle settings (n.b., only for the cruise condition, as required by the JPAD performance module, in order to enable a correct execution of the simulations). In addition, scale factors for the effects of additional power off-takes on the SFC and on the PPS mass were provided. No additional engine decks were produced for the BPR 10 and the BPR 12 engines, but the SFC maps of the original BPR 13.4 deck were scaled according fudge factors equals to percentage variations reported in the first row of table 2.42. Although the three engines were designed with (slightly) different values of the overall pressure ratio, no corrective scaling factors were provided or used for the NO_x EI of the two additional engines. Moreover, the same SFC and PPS mass calibrations for off-takes of the BPR 13.4 engine were assumed for the BPR 10 and BPR 12 models.
With respect to the modelling of masses and main nacelle dimensions, the same considerations included in section 2.3.4 were applied in this case. The same ratios in terms of inlet and outlet nacelle diameter with respect to maximum fan cowl diameter, and maximum nacelle diameter longitudinal position with respect to nacelle fan cowl length were kept for all the examined engines.

Approach to the design of the set of aircraft

The optimized target UM model of WP2 was used as the baseline aircraft model to carry out the MDAO process reported in this sub section. Only minor modifications were applied to the geometric characteristics of this aircraft in order to retrofit the BPR 10 and BPR 12 engines and generate the actual baseline models for MDAO activities. The main landing gear leg length (uncompressed) was lowered, in order to keep the minimum engine ground clearance constant and equal to 550 mm, as for the optimized target aircraft equipped with the BPR 13.4 engine. These modifications were checked by means of the JPAD module for ground manoeuvrability, to ensure that they did not impact negatively on the ground performance of the aeroplanes. The values of these modifications are reported in table 2.43.
In order to generate the optimized aircraft models equipped with the BPR 10 and the BPR 12 engines, a design approach similar to the one described in section 2.3.5 was implemented. With respect to this approach, several modifications were applied, starting from the results achieved during the design activities of the target UM model of WP2. Instead of considering the overall pool of airframe technologies combinations, only the complete set was examined. This was made to keep fair the performance comparison between aircraft models equipped with different engines, given that the only combination of advanced technologies allowing to match both CS2 objectives in terms of pollutant emissions reduction was the one including all the technologies simultaneously, at least according to the outcomes presented in section 2.3.5. The hypothesis of applying different sets of constraints to the optimization was also removed, for the reasons already explained in the same section. A constraint was applied on the maximum allowable wing span (36 m), and an ACT, granting the possibility to transport an additional amount of fuel (2132 kg) with respect to what could be possibly stored in the wing tanks, was included in the modelling of the lower deck of the fuselage.
For the complete set of advanced airframe technologies and for both the BPR 10 and the BPR 12 engines, a full-factorial DOE was carried out, including modifications to the wing planform area and the wing aspect ratio. No variations were directly applied to the geometry of the aircraft: the fuselage, the relative position of the wing with respect to the main body, the relative position of the engines with respect to the wing, and the characteristics of the landing gears system were not modified in the parametric analysis, keeping the same values of the baseline aircraft models.
The wing aspect ratio was made vary from -35 % (9.22) up to the baseline value (14.19, which was already considered an upper limit for the wing aspect ratio during the parametric study for the target UM aircraft with the BPR 13.4 engines), assuming 8 equally spaced values (i.e., 5 % step increments). The wing planform area was changed from -5 % (86.77 m^2) up to +25 % (114.18 m^2) with respect to the baseline value (91.34 m^2), using 7 equally spaced values, leading to a total of 56 permutations. For each permutation, the remaining wing planform parameters (wing panels inner and outer chords, as well as panel spans) were automatically updated: chords were modified by using the ratio between the new and the baseline planform areas; spans were updated to match the target aspect ratio, while keeping the same relative ratio between them.
As already explained in section 2.3.5, modifications to wing planform parameters implied indirect changes to several aircraft main and secondary components, such as the wing fuel tanks, the horizontal tail, the vertical tail, the high-lift devices and the control surfaces. These automatic updates were performed according to the updated strategies outlined in section 2.3.5.

Table 2.43: Main landing gear leg length (uncompressed) values for the three reference A/C models designed for the WP4 of ADORNO.

Main landing gear leg length (uncompressed)	Value
BPR 10 A/C	2.695 m
BPR 12 A/C	2.790 m
BPR 13.4 A/C	2.850 m

For each of the abovementioned permutations of wing parameters, the characteristics of the powerplant system in terms of PPS mass and SFC were consequently updated, to comply with different demands of the HLFC systems.
Each aircraft resulting from the parametric study was analysed according to the multi-disciplinary workflow depicted in figure 2.3. An iterative loop aiming at the matching of the necessary amount of mission fuel mass was preliminarily performed, to set the aircraft maximum take-off weight. Thrust update loops were excluded from the analysis: the performance of the engine was left unchanged during the aircraft fuel mass iterative loop, but the matching of required take-off, climb and cruise performance was assigned by including dedicated constraints in the follow-up optimization process. At the end of the iterative loop on aircraft weight, the set of analyses listed in figure 2.3 was performed. Analyses on noise were excluded from this specific case study, since results on noise emissions are not the main topic of this work package (activities of WP4 are more focused on block fuel analyses), and because no data on noise was provided for the two additional engines too.
The response surfaces produced by means of the parametric study (one for each new engine) were then provided to the JPAD sub-module for optimizations, in order to perform single-objective optimizations on block fuel (one for each response surface). The same set of constraints for the optimizations listed in section 2.3.5 was adopted in this case.
The overall MDAO process described in this section is represented in figure 2.37 and in figure 2.38. The following sub section provides a description of the main results achieved, as well as a direct comparison of the performance of the three aircraft equipped with the set of engines characterized by increasing BPR.

2.4.2 Description and analysis of the aircraft set

Table 2.44, table 2.45 and table 2.46 provide information on the main outcomes of the analyses carried out on the set of three A/C models that were optimized according to the strategy outlined in section 2.3.5 (for the BPR 13.4 engine) and in the previous sub section (for the BPR 10 and the BPR 12 engines). Table 2.44 provides a recap on the main results regarding geometry, weights, performance, emissions, and costs. Results of the reference UM A/C for these disciplines are also included in this table. Table 2.45 and table 2.46 provide comparative analyses both between the reference A/C model and the target ones, and solely between target models.
It is immediate to notice from table 2.44 that the geometry of the three optimized target A/C is practically the same, and that there are just small differences between the BPR 10 A/C and the remaining two models. This can be further highlighted by means of the response surfaces reported in figure 2.39, figure 2.40 and figure 2.41. These figures report the contour plots resulting from parametric analyses performed for the optimization of the A/C models for each of the three advanced engines. The one for the aircraft equipped

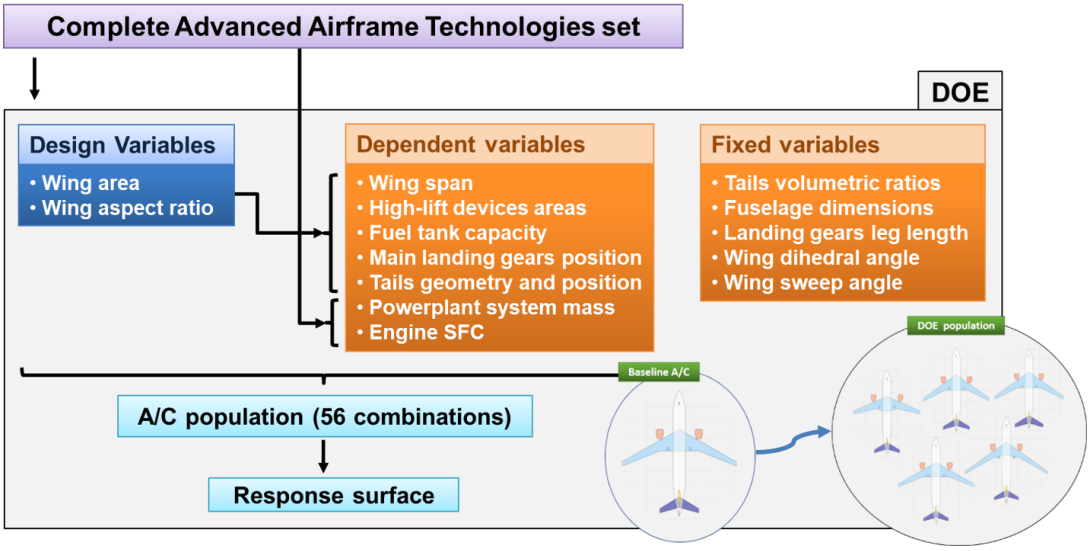

Figure 2.37: Set of steps for the generation of the response surfaces to be used for the optimization of the A/C models equipped with the BPR 10 and BPR 12 engines.

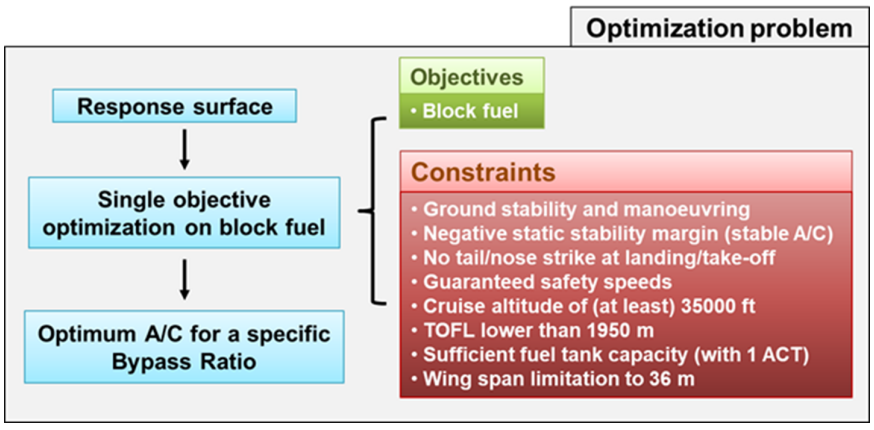

Figure 2.38: Set of steps and assumptions of the optimizations on block fuel for the design of the A/C models equipped with the BPR 10 and BPR 12 engines.

with the BPR 13.4 engine resulted from the MDAO process carried out after that minor flaws were identified in the modelling of airframe technologies, as already mentioned in section 2.3.5. In these contour plots, black lines identify block fuel contours, while red and green lines help to highlight limitations in terms of wing span and allowable on-board fuel (i.e., below zero values mean that there is no more available room for fuel, both in the wing fuel tanks and in the additional central tank), respectively. These limitations restrict the available design space to the area on the left of the plot. It is clear to see that these plots are quite similar for the three A/C models, and that they lead, in order to obtain the lowest possible block fuel value, to similar (if not identical) combinations of wing planform parameters.
All three target A/C models have a maximum take-off weight noticeably lower than the one for the reference model, which is linked directly to the lower design fuel mass and the lower operating empty weight. It is important to notice that, due to the increasing weight of the powerplant, the A/C models equipped with the higher BPR engines, despite a lower design fuel mass, have higher OEW and higher MTOW, which for sure has a negative impact on the A/C performance.
The aircraft model equipped with the BPR 13.4 advanced engines is still the one enabling the greatest reduction in terms of fuel used for the accomplishment of the design mission with respect to the year 2014 reference A/C. It allows to reduce the total amount of fuel burn and the total CO_2 emissions by more than 20 % and the block fuel by more than 21 %. Nevertheless, the differences with respect to the remaining two aircraft models are quite small. In fact, the BPR 13.4 A/C model has an advantage with respect to the BPR 10.0 one in terms of total fuel mass used equal to 1.16 %. This advantage reduces even more with respect to the BPR 12.0 A/C model: in this case the difference on total fuel burn reduces to just 23 kg, equal to a further 0.17 % decrease. This happens despite the data on SFC reported in table 2.42 would suggest quite differently. According to this table, the BPR 13.4 engine has an advantage on SFC equal to 3 % with respect to the BPR 10 one, and to 1 % with respect to the BPR 12 one. The reason behind these differences is easily explained by the significant increase in PPS and overall dimensions (nacelle fan cowl maximum diameter and length) for higher values of engine BPR. This growth gives way to a snowball effect on the A/C, which significantly reduces the advantage given by the SFC reduction alone. Figure 2.42, for example, shows how the nacelle zero-lift drag coefficient, C_{D0}, grows with the engine BPR and the overall size of the nacelle, due to the increase in base drag (i.e., the drag due to the separation at the termination of the nacelle) and the skin friction drag. This growth, together with the increase in PPS mass, negatively impacts on the performance of the aircraft in all the phases of the design mission, counteracting the benefit in SFC.
In terms of total NO_x emissions, the three advanced aircraft perform quite similarly, all showing an advantage with respect to the reference A/C model greater than 35 %. It is interesting to analyse why the BPR 13.4 A/C in this case performs slightly worse than the BPR 12 model, and almost the same as the BPR 10 one. Table 2.47 provides a breakdown of the single contributions per design mission phase for the three target A/C models. From this table it is easy to notice that the A/C models produce quite the same amount of NO_x emissions in each phase. For the take-off, first descent and second descent phases, the reduction in fuel consumed wins over any other additional factor. For the first climb, second climb, approach and landing phases, a slight increase in the duration of each phase causes a minor growth in the NO_x total emission for the BPR 13.4 A/C. This increase, at least for the climb phases, is linked to the rise in aircraft MTOW. Regarding the cruise, the alternate and the holding phases, the effect of a bigger

and heavier engine weighs more than the SFC reduction: the increase in nacelle drag and powerplant mass requires higher values of engine throttle for those phases. This causes an increase in the average NO_x EI values during the simulation, which, especially for the aircraft equipped with the BPR 13.4 engines, counteracts and even exceeds the reduction in fuel burn. This is quite the same effect explained in section 2.3.5, which caused a reduction of total NO_x emissions greater than the one of total fuel used or CO_2.
Regarding the costs, there are no remarkable differences between the three advanced aircraft models. They show almost the same increment in total DOC with respect to the reference A/C model. But it is important to remark that the only contribution to the total DOC variation between the three advanced A/C is the one due to the fuel, and that the total DOC of the BPR 12 and BPR 13.4 equipped A/C models takes only advantage of the lower value of total fuel required to complete the design mission. The same assumptions on prices and the same assumptions on maintenance costs were performed for the three A/C models, since no data was included in the engine dataset that could be included in the analyses of the aircraft.
In conclusion, the following results can be deduced from this comparative analysis:

- The target A/C equipped with the BPR 13.4 engine (i.e., the optimized target UM aircraft of section 2.3.5) is still the aircraft model granting the biggest reduction in terms of total fuel needed for the accomplishment of the design mission, while the BPR 12 A/C allows to further decrease, though by a quite small amount, the total NO_x emissions.

- Only the A/C models equipped with the BPR 12 and BPR 13.4 engines match both the Clean Sky 2 objectives in terms of CO_2 and NO_x emissions. The BPR 10 A/C model, in fact, fails to match, though by less than 1 %, the goal on CO_2 reduction.

- This analysis has again highlighted the need of an interaction between aircraft and engine designers, in order to be able to predict the snowball effect due to modifications applied to the powerplant, and allowing to select the most suitable combination of engine design parameters for a specific A/C platform. This is clearly shown in figure 2.43. The increment in engine mass and size due to a higher BPR value may actually cause an increase in A/C weight and total drag, capable of drastically reducing any advantage in terms of SFC.

Table 2.44: Main results of the optimization study for the design of the A/C models equipped with the set of advanced engines provided by MTU.

Parameter	Reference A/C	Target A/C BPR 10	Target A/C BPR 12	Target A/C BPR 13.4
Wing area, m^2	109.76	91.68	91.34	91.34
Wing AR	11.79	14.14	14.19	14.19
MTOW, kg	68177	63610	63712	63,926
OEW, kg	36684	35372	35634	35,871
Design fuel mass, kg	17050	13780	13621	13,598
TOFL, m	1814	1762	1769	1798
Time to climb, min	17	15	15	15
Cruise altitude, ft	37000	37000	37000	37,000
LFL, m	1568	1674	1700	1674
Block time, min	424	424	424	424
Block fuel mass, kg	14139	11257	11147	11,127
Total fuel mass, kg	16199	13086	12935	12912
Total NO_x emissions, kg	287.43	185.36	184.45	185.37
Total CO_2 emissions, kg	51,222	41,379	40,899	40,829
Total DOC, cent/(nmi*seat)	12.703	13.03	13.017	13.017
Cash DOC, cent/(nmi*seat)	6.774	7.007	6.994	6.994

Table 2.45: Percentage variations of main analysis output of the three optimized target A/C models equipped with the set of advanced turbofan engines with respect to the ADORNO reference UM A/C.

	% Variations with respect to UM reference A/C		
Parameter	Target A/C BPR 10	Target A/C BPR 12	Target A/C BPR 13.4
MTOW	−6.699	−6.549	−6.235
OEW	−3.576	−2.862	−2.216
Design fuel mass	−19.179	−20.111	−20.246
Block fuel mass	−20.383	−21.161	−21.303
Total fuel mass	−19.216	−20.153	−20.290
Total NO_x emissions	−35.511	−35.828	−35.508
Total CO_2 emissions	−19.216	−20.153	−20.290
Total DOC	+2.574	+2.472	+2.472

Table 2.46: Percentage variations of main analysis output with respect to the ADORNO target UM A/C equipped with BPR 10 engines.

	% Variations with respect to BPR 10 target A/C model	
Parameter	Target A/C BPR 12	Target A/C BPR 13.4
MTOW	+0.160	+0.497
OEW	+0.741	+1.411
Design fuel mass	−1.154	−1.321
Block fuel mass	−0.977	−1.155
Total fuel mass	−1.160	−1.329
Total NO_x emissions	−0.491	+0.005
Total CO_2 emissions	−1.160	−1.329
Total DOC	−0.100	−0.100

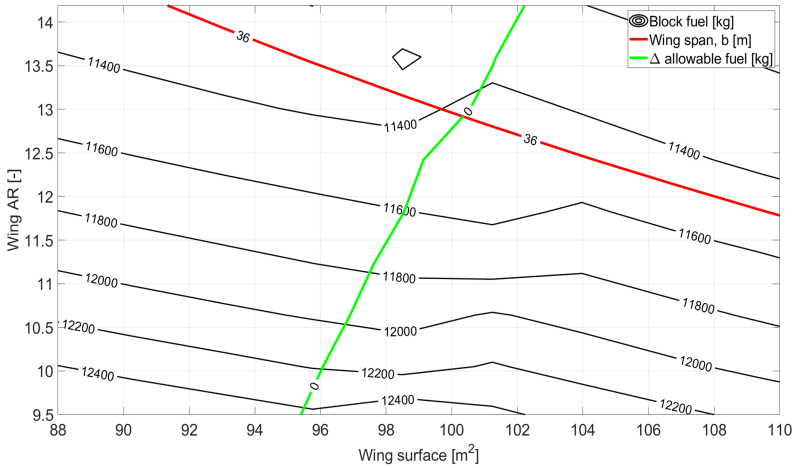

Figure 2.39: Response surface for the optimization of the A/C model equipped with the BPR 10 advanced engine.

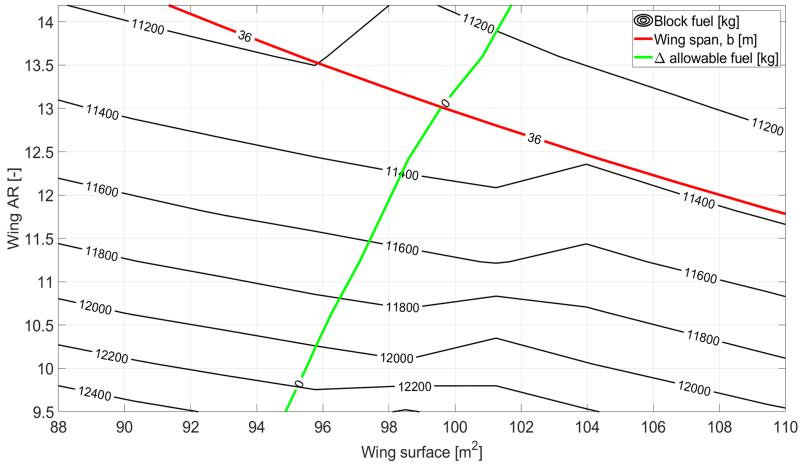

Figure 2.40: Response surface for the optimization of the A/C model equipped with the BPR 12 advanced engine.

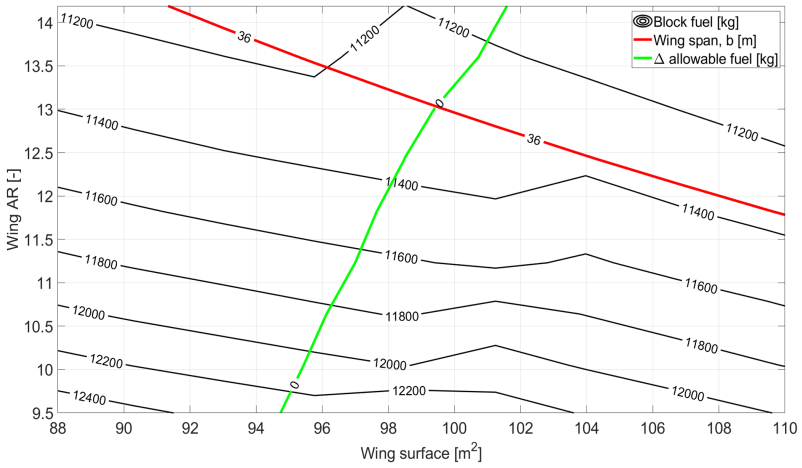

Figure 2.41: Response surface for the optimization of the A/C model equipped with the BPR 13.4 advanced engine.

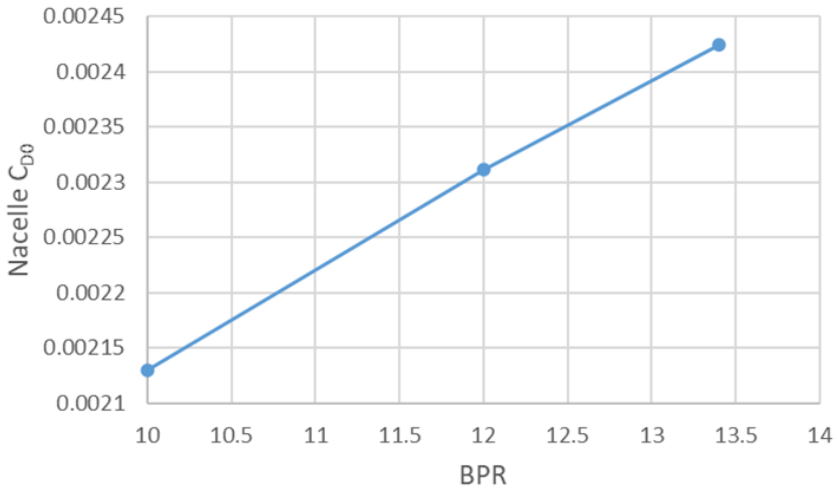

Figure 2.42: Nacelle zero-lift drag coefficient growth with increasing engine BPR, for the MDAO process performed on the set of advanced HBPR engines provided for ADORNO WP4.

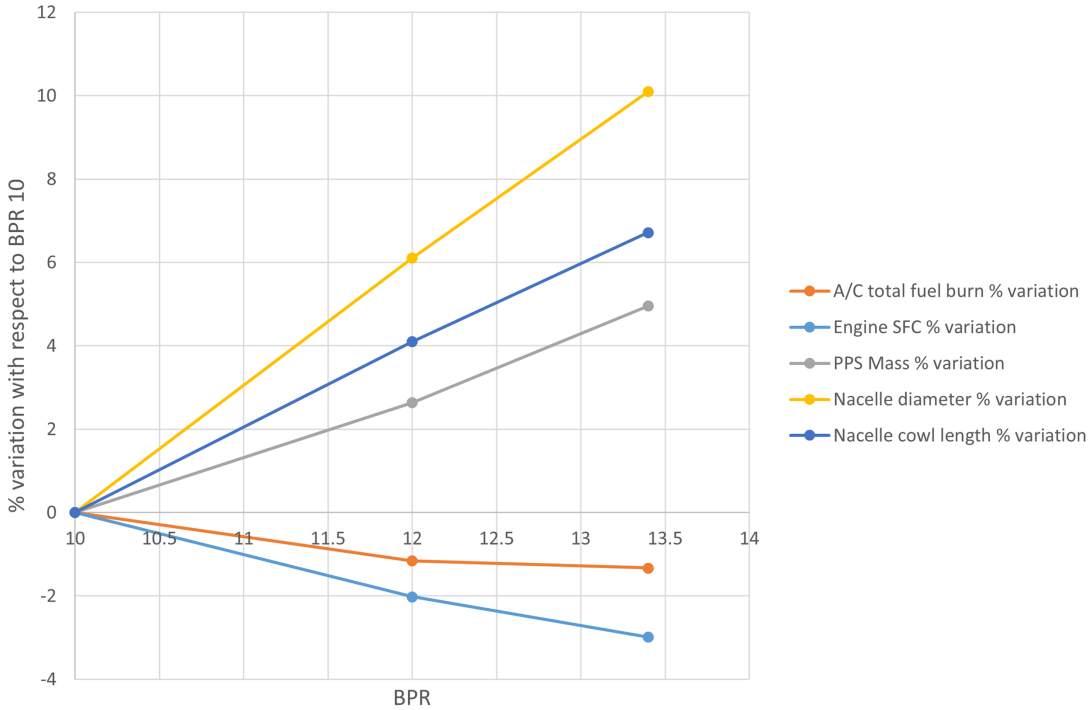

Figure 2.43: Engine main parameters and A/C total fuel burn percentage variations with respect to engine BPR, assuming values for the BPR 10 engine and the related optimized A/C model as the references.

Table 2.47: Breakdown of the NO_x emissions contributions per phase for the three optimized target A/C models.

	NO_x Emissions, kg		
Design Mission Phase	**Target A/C BPR 10**	**Target A/C BPR 12**	**Target A/C BPR 13.4**
Take-Off	2.18	2.15	2.13
First Climb	35.88	35.63	35.72
Cruise	116.98	117.05	117.83
First Descent	2.55	2.51	2.48
Second Climb	13.92	13.79	13.78
Alternate Cruise	5.46	5.43	5.46
Second Descent	1.77	1.75	1.74
Holding	5.58	5.12	5.2
Approach and Landing	1.05	1.02	1.03
TOTAL	**185.37**	**184.45**	**185.37**

2.5 Lessons learnt

The previous sections helped to highlight the main outcomes of the ADORNO project in terms of activities that involved the interaction of both engine and aircraft design specialists. The cooperation between such different expertise was undoubtedly supported by the following aspects:

- A continuous search for the confrontation between the two parties, obtained thanks to the frequent organization of web meetings, used to solve issues and to smooth over difficulties raising from the necessity to include in each others tools and methodologies unfamiliar information and input data coming from external research activities. In addition, face-to-face workshops were organized on topics such as turbofan engine competitive assessment and aircraft noise modelling, in order to:
  - ease the mutual understanding of the activities carried out by each of the different parties involved in the project, by providing the necessary set of information on the methodologies and tools adopted for the accomplishment of technical tasks;
  - speed-up part of the technical work required by the action plan of the project, such as the definition of the requirements to the aircraft noise tool, and the validation of the customer engine deck adopted for the performance analyses on the reference aircraft model.
- The framework of analysis tools provided by JPAD, which allowed an efficient and effective implementation of the different engine models adopted for the analyses of ADORNO. Though by requiring a limited amount of information on the engine model (which is a fundamental and appreciated aspect for an aircraft tool to be used to perform conceptual and preliminary aircraft design studies), in addition to an engine performance file (which could be also conveniently adapted by using one of the default decks provided by the tool), it allowed to perform comparative analyses between aircraft models equipped with different powerplant systems, in which the effect on aircraft characteristics and performance of different assumptions regarding the engine specific fuel consumption, weight and main dimensions were

well reflected by the results. Moreover, the addition of a new module on airframe technologies, specifically designed on the needs of the project, made possible to model in a plausible (literature-based) way the effect of different requirements in terms of power off-takes on the engine model. In terms of this aspect too, the interaction with engine design experts was essential, since it allowed to define a simple (based on fudge factors for powerplant system mass and specific fuel consumption) but functional implementing strategy.

From the experience matured during ADORNO, and from the set of information on tools and methodologies for the preliminary engine design and competitive assessment acquired during the involvement in project-related activities, the idea for a further improvement to the general approach adopted for the modelling of the main characteristics (overall dimensions, weights, performance, gaseous emissions, costs, and, possibly, environmental noise) of aeronautical engines, still suitable for a preliminary aircraft design tool such as JPAD, was developed.
The main concept revolved around the idea of removing, or at least limiting, the necessity to provide a detailed engine performance file, which, for a preliminary aircraft design tool, might imply the necessity to generate (or even assume) a significant amount of data: information should be provided for all the main engine ratings, in terms of available thrust, specific fuel consumption, pollutant species emission indexes (at least for CO_2 and NO_x), for different flight conditions (i.e., Mach number, altitude and ISA condition) and, for the cruise rating, for different throttle settings. As already explained in the previous sections, JPAD allows to perform reasonable scaling of reference engine decks in terms of specific fuel consumption based on information provided in terms of actual bypass ratio, but of course this scaling can only be applied to turbofan engines, and the implemented methodology is based on indications provided by aircraft design textbooks rather than a physics-based approach. Giving the possibility to automatically generate a reasonable engine deck, based on a user-defined set of input data including engine design parameters, would for sure ease a deeper integration of engine-related aspects in a typical preliminary aircraft design workflow.
Moreover, ADORNO demonstrated that, even during a project in partnership with an engine manufacturer, some data may still be difficult to be shared. As highlighted in the previous sections, none of the engine datasets provided by MTU included information on engine noise spectra, that could be used in combination with ATTILA++ to perform trade-off analyses including noise. And regarding the direct operating costs of the aircraft, neither engine production costs, nor maintenance charges were provided, which would have allowed to better characterize the differences between different engine models. The implementation of a simple yet effective methodology, requiring a limited number of input parameters and eventually based on a semi-empirical approach, would definitely be a significant added value to an engine model.
A workshop on engine competitive assessment and, primarily, a three-month internship at MTU (conducted remotely, due to the COVID-19 pandemic) done by the author, helped to lay the foundations for a general approach, allowing to include, in a generic framework for preliminary aircraft design, a rubberized gas turbine model, allowing to perform fast estimations of engine-related parameters, enabling trade-off studies and optimization processes. The next chapter provides information on how such an approach was adopted in GENESIS, an European, CS2-funded project aiming at providing, for different time perspectives, the best combinations of powertrain technologies (including conventional gas turbine engines, batteries and fuel cells) for a regional, hybrid-electric,

turboprop aircraft. This project, for which UNINA and the author were firsthand involved in the task related to the technological analysis (over the 2025-2055 time period) of the gas turbine engine, provided the perfect proving ground for the abovementioned approach. With just indicative values on the amount of power required from each propulsive technology per time perspective, and considering the necessity to include aspects related to the effect of different technology level assumptions (related to the different time perspectives analyzed during the project), which imply the possibility to perform different assumptions on the maximum allowable temperatures for the materials, for example, the idea of implementing a rubberized gas turbine model in the hybrid-electric aircraft design chain seemed to be the most appropriate approach. Dealing with a scalable engine model, which could be conveniently updated based on different power splits between the propulsive technologies and different time perspectives, it would have been possible for the aircraft designers to perform significant trade-off analyses, allowing to select the best suitable combination of technologies for each time horizon.
The same approach was extended to turbofan engines and implemented in JPAD. This activity is described in chapter 4, in which additional information on the methodology are provided for those assumptions strictly related to turbofan engine configurations, and that could not be anticipated in chapter 3. Information on the actual implementation of a detailed engine module in JPAD are also given in this chapter, including a description of the main input file, of the interconnection of this module with the remaining modules of JPAD, and on the output file produced. Moreover, this chapter provides several test-cases, allowing to validate the methodology and its implementations, as well as to check its capability to actually enable significant trade-off analyses on engine design variables.

Chapter 3

The experience in GENESIS

GENESIS (**G**auging the **EN**vironm**E**ntal **S**ustainability of electr**I**c aircraft **S**ystems) is a European, CS2-funded project (call H2020-CS2-CFP11-2020-01, project number 101007968) aiming at determining the environmental sustainability of hybrid-electric and all-electric aircraft platforms, by means of life-cycle analyses and propulsive technologies foresight. The reference configuration for the aircraft design activities is a regional, 50-seat A/C, similar in terms of general layout to the ATR 42. The main focus of the project is on the identification, for three different time horizons (2025-2035, 2035-2045, 2045-2050+), of the most promising combinations of powertrain technologies (including gas turbine engines, batteries and fuel cells), supported by a design and analysis framework for hybrid and all-electric aircraft platform developed by UNINA DAF research group (named HEAD and standing for Hybrid-Electric Aircraft Design [142]).
The project comprises three technical work packages:

- WP1, dealing with aircraft design activities focused on the generation of hybrid-electric and all-electric A/C concepts for the abovelisted time perspectives.
- WP2, focused on the performing of technology foresight analyses on conventional (gas turbines) and innovative (electric motors, batteries, fuel cells) powertrain elements, for the same time horizons, supporting the aircraft design activities of WP1.
- WP3, developing life-cycle inventories for all the technologies involved in GENESIS (airframe and powertrain) and their production processes, to be used to perform life-cycle assessments for future aircraft configurations developed within WP1.

The following sections provide a detailed explanation of the work that was carried out by the author, as UNINA contributor, on the generation of technology perspective analyses for conventional gas turbine engines for the short-term (2025-2035, with 2030 selected as the reference year) scenario, and, mainly, on the methodology that was elaborated and applied in order to allow an easy (i.e., requiring a limited amount of input variables) yet effective (i.e., validated according to available public data) preliminary modelling and rubberization of a generic gas turbine engine for a turboprop application.

Author contribution

The author of this thesis work was firsthand involved in the WP2 task related to the development of perspective technology analyses on conventional gas turbine engines, for which he was the main contributor. For this task, he applied

the methodology based on gas turbine rubberization mentioned in the previous chapters, which is the main focus of this thesis. Moreover, he was involved, for WP3, in the definition of the life-cycle inventory for a conventional powerplant system (comprising gas turbine engines, propellers, reduction gearboxes, and fuel system), by collecting data on production processes, typical materials, buy-to-fly ratios, and end-of-life management information.
These tasks could only be accomplished thanks to knowledge and the experience collected during the ADORNO project, and thanks to the supervision of Prof. Giovanni Torella, expert of aeronautical engines and Professor at the University of Ferrara.

List of publications related to GENESIS and involving the author

Conference papers

- (*Extended abstract sent*) V. Marciello, M. Ruocco, **M. Di Stasio**, and F. Nicolosi. Market analysis, TLARs selection and preliminary design investigations for a regional hybrid-electric aircraft. In *33rd Congress of the International Council of the Aeronautical Sciences*, 4-9 September 2022, Stockholm, Sweden.

  The candidate contributed by suggesting the topic and the structure of the extended abstract and of the final manuscript. He moreover contributed to the extended abstract by writing the sections summarizing the aspects related to the design of a regional hybrid electric plane.

Journal papers

- (*In preparation*) **M. Di Stasio**, M. Ruocco, V. Marciello, and F. Nicolosi. Performance modelling and perspective analyses on a three-spool, free turbine turboprop engine for regional hybrid-electric aircraft application.

  A paper collecting the main achievements linked to the second WP of GENESIS and dealing with the scientific outcomes presented in this chapter will be submitted during the first half of 2022 to a an internationally respected journal, such as Aerospace by MDPI.

3.1 Introduction

Several types of engines are used nowadays on civil and military aircraft to produce the necessary power and thrust. For a commuter or a small regional aircraft, turboprop engines are generally preferred over reciprocating engines or turbofans. This results from trade-off analyses including considerations on reliability, costs, ground performance, and fuel consumption. A turboprop engine comprises three main components: a gas turbine core (pretty similar to the one for a turbojet/turbofan engine), a reduction gearbox, and a propeller. The gearbox helps to transfer the power from the core engine to the propeller, reducing the rotational speed. The gas turbine includes one or more compressors (axial or radial ones), a combustion chamber, and one or more turbines. There are several available options concerning the core engine configuration. These mainly differ in how

the power is transferred to the gearbox and to the propeller. In some designs, the turbine powering the gearbox is directly linked to one of the compressors. A different solution is to link the gearbox to a turbine that is not on the same shaft of any of the compressors extracting work from the gas, leading to what is usually called a free turbine turboprop engine. Just as the turbojet engine, the turboprop adopts a gas turbine core to generate power. What really distinguishes one solution from the other is how this power is used. In turboprop engines, most of the available power is extracted by the turbine linked to the propeller, thus noticeably reducing the kinetic energy of the air expelled through the exhaust and the amount of jet thrust produced by the engine.
This chapter provides an overview on the approach adopted to model a gas turbine engine for the short-term scenario (2025-2035) in terms of performance (basically power-specific fuel consumption), emissions, weight, main dimensions, and costs. It is important to highlight that this approach is independent of the selected timeframe and can be easily adapted to different time horizons by simply modifying those assumptions that depend on technological factors or the expected entry into service.
The main objective was to build a rubber engine model that could be easily integrated into an aircraft design chain and used to perform trade factor analyses on fuel burn concerning engine dry mass, engine maximum diameter, and production costs, enabling aircraft designers to carry out single and multi-objective optimizations. By including specific aircraft requirements among the set of available input variables, such as the shaft power delivered (SPD), the power off-takes, and the overboard bleed, the engine model was made sensitive to variations applied to the aircraft model, since those are reflected in the fuel consumption, in the engine dry mass, and in the main gas turbine dimensions. At the same time, this rubber engine model can provide valuable information to engine design experts in terms of main gas turbine design parameters, such as the burner exit temperature T_4, the overall pressure ratio, and the entry mass flow rate W_2, since those were also included in the sets of input/output variables of the model.
The effect of advanced technologies and production processes was included in the rubber engine model as well. The selected EIS has a direct impact on the performance of the main components of the engine (i.e., compressors, turbines and combustion chamber). An additional technology factor was also introduced in the model, to account for more/less conservative designs. This factor impacts, again, on the performance of the compressors, on the materials for the turbines, on the cooling air technology, on the pressure losses in the main ducts of the engine, and on the mechanical efficiencies. The value selected for this additional technology factor also directly impacts the final production cost of the engine. As discussed in section 3.4, the dataset produced for the rubber engine model of the short-term scenario also includes variations to this input variable, allowing to perform for the same timeframe different analyses based on distinct assumptions on the technology level.
The impact of alternative fuels on the engine design was included in the rubber engine model too. Biofuels in the form of synthetic paraffinic kerosene (SPK) were modelled to consider their impact on fuel consumption and emissions. A basic strategy based on fuel lower heating value (LHV) of different blends of SPK with conventional jet fuel (namely Jet A-1) was adopted, with calibration factors on emission indexes accounting for differences in terms of emissions with respect to traditional kerosene.
Table 3.1 provides a recap on the list of input variables managed in the adopted approach. Section 3.2 provides information on the assumptions and the methodology adopted to generate a rubber engine model representative of the gas turbine of a generic turboprop engine. Details are also provided on the tools that were used to generate this model.

Table 3.1: List of input variables of the rubber engine model generated for GENESIS project.

Number	Input Variable
1	Shaft power delivered
2	Burner exit temperature
3	Overall pressure ratio
4	Power off-takes
5	Overboard bleed
6	Biofuel blending ratio
7	Entry into service
8	Technology level

Section 3.3 provides proof of validation of the adopted methodology for a representative engine (i.e., the Pratt & Whitney PW127E engine model, equipped on the ATR 42 aircraft), while section 3.4 gives an overview on the results produced by the analyses on the short-term scenario, carried out by means of the rubber engine model. Finally, section 3.5 focuses on the approach and on the tools used to generate a surrogate rubber engine, to be actually implemented in the hybrid-electric aircraft design framework of GENESIS.

3.2 Methodology

Since the ATR 42 aircraft was the reference aircraft model selected for the performance comparisons concerning hybrid-electric and all-electric aircraft platforms, its Pratt & Whitney PW127 engine was selected as the reference gas turbine engine model for the analyses. The PW127 model is part of the PW100 family, a series of 1300 to 3700 kW turboprop engines manufactured by Pratt & Whitney Canada [37]. The first engine of the 127 series was certified in 1992, with the PW127E, the actual reference model used for validation and the analyses, certified in 1994. Except for the PW150 engine model, all the engine of this family feature a three-shaft configuration, with a low-pressure (LP) radial compressor, driven by a single-stage low-pressure turbine, supercharging a high-pressure (HP) radial compressor, driven by a single-stage high-pressure turbine. A third, two-stage, free/power turbine (PT) finally powers the propeller through a reduction gearbox. A scheme of this engine configuration is reported in figure 3.1.
The main characteristics of the PW127E model are summarized in table 3.2. Ratings are provided at sea-level, with information on the temperatures provided in terms of variation with respect to the ISA model. Most of the values included in this table were used to validate the rubber engine model, as reported in section 3.3. The actual rubber engine model was developed using GasTurb[1], version 11. GasTurb is a gas turbine cycle program that simulates the most important gas turbine configurations used for propulsion or power generation. GasTurb allows performing gas turbine cycle simulations both for design and off-design conditions. For the off-design simulations, GasTurb requires compressors and turbines maps to simulate the performance of the engine. The program also provides default maps, but they need to be appropriately scaled to produce reasonable results. The program can automatically perform this operation.

[1] https://www.gasturb.de/

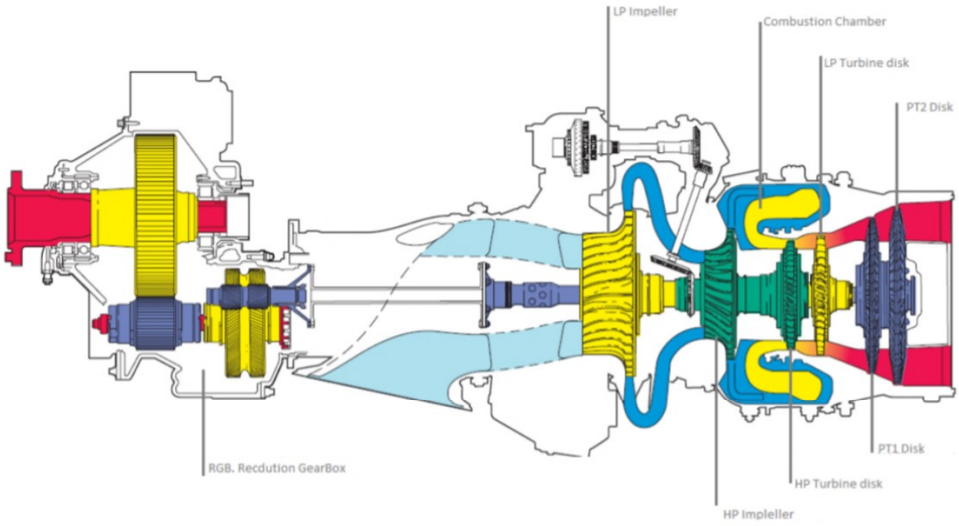

Figure 3.1: Pratt & Whitney PW127 engine configuration. Image taken and adapted from [54].

Table 3.2: Pratt & Whitney PW127E engine data.

Description	Value	Source
Ratings		
Take-off, SL ISA +30	2160 SHP – 1611 kW	[51][4][12]
Take-off (one engine), SL ISA +30	2400 SHP – 1790 kW	[51][4][12]
Max. continuous, SL ISA +30	2400 SHP – 1790 kW	[51][4][12]
Max. climb, SL	2160 SHP – 1611 kW	[51][4][12]
Max. cruise, SL ISA +10	2132 SHP – 1590 kW	[51][4][12]
Fuel consumption		
Max. take-off, ISA SL	0.474 lb/(hp*h) – 0.288 kg/(kW*h)	[51]
Mass		
Dry mass	1060 lb – 481 kg	[51][12]
Dimensions		
Length	81 in – 2.134 m	[51][12]
Width	26 in – 0.660 m	[51][12]
Height	33 in – 0.838 m	[51][12]
Cycle values		
Entry mass flow rate	18.72 lb/s – 8.49 kg/s	[85]
Overall pressure ratio	14.7	[51]

In order to produce a parametric model of a gas turbine engine, similar in terms of configuration to the PW127 model, a set of engine design laws and automatic update strategies were implemented in the GasTurb design calculation mode, starting from the GasTurb template model for a three-spool turboprop engine. For each generic template model, GasTurb provides a set of default values, which need to be appropriately adjusted for the model to reflect the actual characteristics of the engine at the design point. These input quantities include:

- Burner exit temperature, T_4;
- Overall pressure ratio, OPR;
- Entry mass flow rate, $\dot{m}_2$;
- Polytropic efficiencies of the compressors and turbines, η_{pol};
- Pressure ratios of the low and high-pressure impellers;
- Relative amount of cooling air for the nozzle guide vane and rotor blades of the high-pressure turbine;
- Pressure losses for the inter-compressor and inter-turbine ducts;
- Burner efficiency and pressure loss;
- Inlet duct pressure loss and nozzle pressure ratio.

Since the first three quantities in the above list were selected, along with technological factors, as the main input variables of the GasTurb parametric model, strategies needed to be picked and implemented to automatically updated the remaining input quantities. GasTurb supports the implementation of these strategies through the definition of additional input variables, the possibility to define custom composed values, and by enabling the setting of specific iterative loops, aiming at the matching between model input values and calculated composed values. The following sub sections provide more information on the assumptions performed for each of the input variables listed above.
It is necessary to remark that GasTurb (at least version 11) does not provide an engine template for a three-spool turboprop with the same characteristics in terms of compressors group of the PW100 series. The adopted engine template supposes a compressor unit consisting of two distinct (mounted on different shafts) axial compressors. However, it was concluded that, for the GENESIS objectives on gas turbine related tasks, and for the elaborated approach on the integration of a scalable engine model in the aircraft design chain, this approximation would have not impacted on the results. In fact, information on the type of the compressors are not relevant in GasTurb for design point cycle analyses, as long as detail calculations for geometry (not the basic ones performed for the estimation of efficiencies, as explained in the following) and disc stresses are not involved. On the opposite, these information are fundamental to off-design calculations, for which appropriate components maps are necessary. However, the scalable engine model in the making makes use only of results coming from design point cycle calculations, thus allowing to avoid any risk linked to the use of unsuitable compressor maps.
Maximum take-off was assumed as the design point condition, which is typical for a gas turbine engine for a turboprop application such as the one examined in GENESIS. The design point, in fact, should either reflect a condition in which the engine will spend most

Table 3.3: Set of operating conditions assumed for the rubber engine design point.

	Rating	**Altitude**	**Mach number**	**ISA**
Design point condition	Max. take-off	0 m	0.17	+30

of its operational life, or a highly demanding (in terms of power, for example) condition [181][104]. The set of assumptions for the design point are summarized in table 3.3. Assumptions on the flat rating derive from the characteristics of the reference engine, while the Mach number reported is the typical Mach number at take-off end-of-rotation (EoR) condition for an aircraft like the ATR 42, as indicated in [4]. These assumptions on the design point conditions were made for the rubber engine model implemented in GasTurb, therefore these were assumed also for all the engine models generated by its usage.
It is also important to remark that the parametric model that was implemented in GasTurb is valid for a three-spool turboprop engine configuration similar to the one of the reference engine model: centrifugal compressors on separate shafts, single-stage high-pressure and low-pressure turbines, and a two-stage free turbine. As with the reference gas turbine engine, only the high-pressure turbine was supposed to be cooled, for this reason no relative cooling air for the low-pressure turbine was included in the parametric engine model. Unfeasible engine designs, generated from the assumption of a fixed engine configuration are typically discarded, either because they are not competitive (e.g., too high specific fuel consumption) or because they do not comply with thermal and/or mechanical limitations, as reported in the following sub sections.

3.2.1 Pressure ratios

Since the engine OPR was set, through the definition of a dedicated custom input quantity) as one of the main input parameters of the rubber engine model implemented in GasTurb, the pressure ratios of the LP and HP impellers needed to be consequently set. Suggestions on a plausible pressure split between the two impellers were taken from [78], in which statistical data are provided for the pressure ratio, mean stage loading, inducer and exducer diameters, and rotational speed of single and double-stage radial compressors. It was assumed that the LP impeller provided a total pressure rise equal to 2.0 times the one provided by the HP radial compressor. Due to the lack of additional and more refined statistical data, variations of this pressure split with respect to input engine OPR were not assumed. Instead, it was deemed constant in the GasTurb-implemented parametric model. However, during the validation phase of the rubber engine, it was tested that this pressure split allowed to match the target rotational speeds of the LP and HP spools, which were calculated using the approach and the set of equations reported in the next sub section.

3.2.2 Polytropic efficiencies and basic gas path modelling

Two distinct approaches were adopted to calculate polytropic efficiencies of the radial compressors and axial turbines of the rubber engine.
For the centrifugal compressors, an approach based on the set of assumptions and equations suggested in [181] was implemented. Polytropic efficiency values are assumed in the GasTurb parametric model starting from the related chart of [181], hereby adapted and reported in figure 3.2. According to [181], the polytropic efficiency of a radial com-

pressor is a function of the technology level (f_{tech}) and of the non-dimensional specific speed (NS), defined as:

$$NS = \frac{N * VW^{0.5}}{\Delta T_{ideal}^{0.75}}, \tag{3.1}$$

where N is the (dimensional) rotational speed of the compressor (expressed in rpm), VW is the volumetric inlet flow, and ΔT_{ideal} is the ideal temperature rise across the radial compressor stage. For a fixed technology level, the polytropic efficiency is at its peak for a distinct value of the non-dimensional specific speed, as can be seen from the chart of figure 3.2. This value is assumed by the rubber engine model as the polytropic efficiency of the radial compressors, once corrected for the EIS, according to the statistical data provided in [78], and hereby adapted and reported in figure 3.3. For this correction, the suggested tendency line in [78] for two-stage radial compressors was considered.
Starting from the values for the pressure ratios, the non-dimensional specific speeds, and the polytropic efficiencies (corrected for EIS), the rotational speeds and the exit speeds can be consequently calculated, by inverting the equation for the specific speed and the equation for the pressure ratio of the impeller (P_3/P_2), also provided in [181]:

$$P_3/P_2 = \left(\frac{1 + (\eta_2 F_{P\ input} F_{slip} U_{ex}^2)}{c_p T_2} \right)^{\frac{\gamma}{(\gamma-1)}}, \tag{3.2}$$

in which $\eta_{is,2}$ is the isentropic efficiency of the radial compressor, $F_{P\ input}$ is the power input factor (whose value typically ranges between 1.02 and 1.05, according to [181]), F_{slip} is the slip factor (which, according to [181], can assume values from 0.9 to 0.935), U_{ex} is the exducer tip speed, T_2 is the total temperature at the inlet section of the radial compressor, c_p is the specific heat capacity of the gas at constant pressure, and γ is the heat capacity ratio of the fluid. At this point, the exducer diameter of the radial compressor can be easily calculated, having both the rotational speed and the exducer tip speed. This diameter is quite important, especially for the LP radial compressor (i.e., the one positioned at the front of the gas turbine), because, for particularly high values of the OPR, it may drive the general dimensions of the engine and, consequently, those of the nacelle.
For the turbines, the general approach suggested in [78] was adopted. This method was not implemented for the radial compressors too, for the already mentioned lack in [78] of sufficient data on this type of compressors, preventing to link polytropic efficiency to remaining design parameters. The polytropic efficiency of a generic component (fans, compressors and turbines), according to [78] is a function of different contributions, which can be listed as follows.

- For cooled components:

$$\eta_{pol} = \eta_{pol}^{***} + \Delta\eta_{EIS} + \Delta\eta_{RNI} + \Delta\eta_{size} + \Delta\eta_{cool} \tag{3.3}$$

- For uncooled components:

$$\eta_{pol} = \eta_{pol}^{***} + \Delta\eta_{EIS} + \Delta\eta_{RNI} + \Delta\eta_{size} \tag{3.4}$$

In these equations:

- η_{pol}^{***} is the normalized polytropic efficiency, for which [78] provides several charts, one (or more than one) for each engine component. These charts of normalized

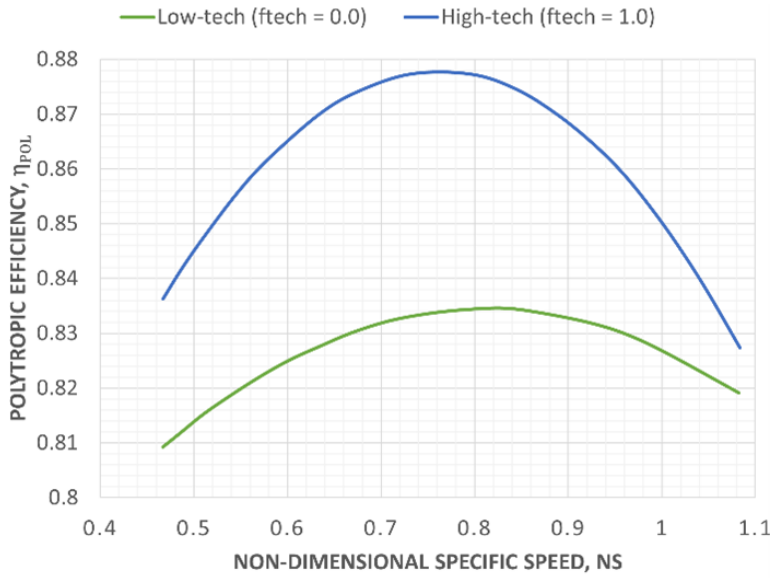

Figure 3.2: Radial compressors polytropic efficiency versus non-dimensional specific speed and technology level. Chart taken and adapted from [181].

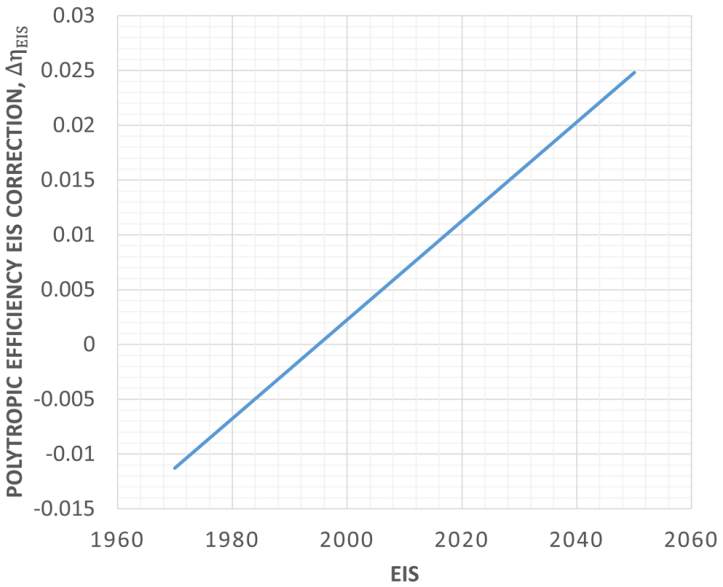

Figure 3.3: Radial compressors polytropic efficiency EIS correction. Chart taken and adapted from [78].

polytropic efficiency are based on statistical data, collected by the author of [78] during years of working in the aircraft engine industry. These data were normalized with respect to reference values of corrected entry mass flow rate (70 kg/s), Reynolds number Index RNI (1.0), and entry into service (1995). For most of the engine components, the normalized polytropic efficiency is reported in these charts as a function of the mean stage loading, $\overline{\Psi}$:

$$\overline{\Psi} = \frac{2\Delta H}{n_{stg}\overline{U}^2}, \tag{3.5}$$

where ΔH is the specific work of the component, n_{stg} is the number of stages, and $\overline{U}$ is the circumferential speed at the mean diameter of the component.

- $\Delta\eta_{EIS}$ is the correction for EIS, which is also provided in [78] by means of dedicated charts per engine component. Corrections are all provided in terms of differences to be applied with respect to 1995 normalized data.

- $\Delta\eta_{RNI}$ is the RNI corrections. As specified in [105], in gas turbine performance simulations is much more convenient to work with the RNI instead of the true Reynolds number. RNI is the actual Reynolds number divided by a reference Reynolds number, and allows to compare conditions at the same Mach number. In the general approach for a first estimation of the efficiencies provided in [78], the RNI correction is calculated according to the following equation:

$$\Delta\eta_{RNI} = \eta_{pol}^{***} - 1 + (1 - \eta_{pol}^{***}) * RNI^{-n}, \tag{3.6}$$

in which n is a parameter depending on the modelled component, and equal to 0.14 for fans, 0.12 for boosters, 0.10 for high-pressure compressors (HPC) and intermediate-pressure compressors, and 0.18 for turbines.

- $\Delta\eta_{size}$ is the size correction, and accounts for the actual corrected mass flow rate at the entry of compressors and turbines stages. According to the approach described in [78], this correction can be calculated with the following equation:

$$\Delta\eta_{size} = \eta_{pol}^{***} - 1 + (1 - \eta_{pol}^{***}) * (\dot{m}_{corr}/\dot{m}_{corr}^{*})^{-m}, \tag{3.7}$$

where $\dot{m}_{corr}$ is the actual corrected entry mass flow rate, $\dot{m}_{corr}^{*}$ is the reference corrected mass flow rate (equal to 70 kg/s), and n is a parameter depending on the type of the component, and equal to 0.063 for compressors, 0.236 for turbines.

- $\Delta\eta_{cool}$ is the correction for cooling air. Its calculation relies on the related chart, also derived from statistical data, included in [78]. In this chart, the efficiency loss due to total cooling air is reported as a function of the relative cooling air, $\dot{m}_{cool}/\dot{m}_{25}$, which is the ratio between the total amount of cooling air (i.e., including demands from both stators and rotors) and the mass flow rate at the entry of the HPC (supposing that cooling air is taken from intermediate stages of this compressor). This ratio depends on the burner exit temperature, on the supposed cooling technology, and on the materials adopted for the manufacturing of the different components of a turbine. More details are provided in the following sub sections on the assumptions that were performed for the calculation of this quantity.

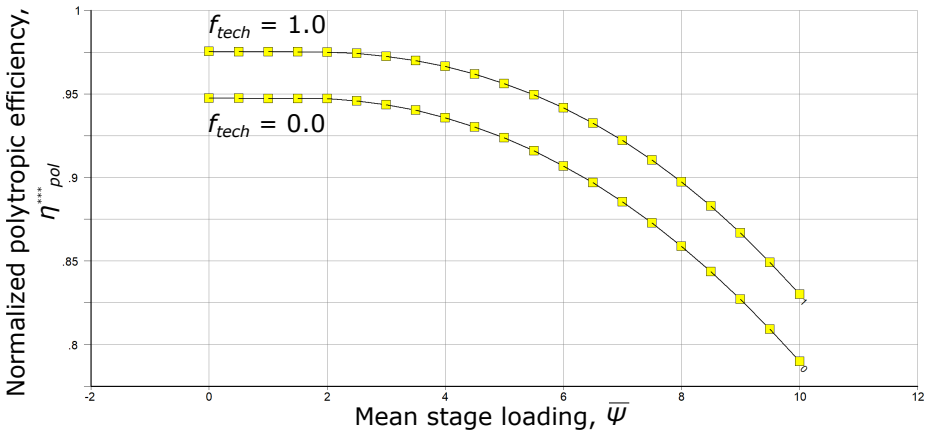

Figure 3.4: HP turbine normalized polytropic efficiency versus mean stage loading and technology level. Adapted from [78].

The calculation of normalized polytropic efficiencies was implemented in the GasTurb rubber engine model taking advantage of the possibility to define lookup tables, and by digitizing the abovementioned charts included in [78]. These digitized charts are reported in figure 3.4 for the HP turbine, and in figure 3.5 for the LP and for the free turbine. The adoption of the same chart for these turbines was suggested by the presence, in the related dataset, of both LP and free turbines data. It is worth to observe that [78] does not provide, for any of the charts for normalized polytropic efficiency, a unique trend-line. Instead, statistical data coming from components of different gas turbine engines are enclosed within two tendency lines, thus suggesting that higher normalized polytropic efficiency values, for the same amount of mean stage loading and assuming the same EIS, may be linked more technologically advanced and/or less conservative design choices. For this reason, the model input variable accounting for the technology level and independent of the EIS, f_{tech}, was included in the calculation process for the polytropic efficiencies of the turbines. In particular, a value equal to 0.0 of the f_{tech} input variable was linked to the lower curves, implying lower efficiency values. A value equal to 1.0, instead, was associated with the upper curves.
Polytropic efficiency EIS correction were included as well in the GasTurb-implemented parametric engine model, by adopting the same approach of the normalized polytropic efficiencies. Lookup tables obtained from digitizing charts included in [78] were adopted for the calculation of these corrections. Figure 3.6 and figure 3.7 report, respectively, the corrective chart for the HP turbine, and for the LP and free turbines. The same motivation expressed above guided the selection of the same chart for the modelling of EIS corrective deltas for efficiencies.
Similar to the previous ones, the chart included in [78] for cooling air correction was adapted to the use within the parametric gas turbine model of GasTurb. The related digitized chart is provided in figure 3.8. It is worth to mention again that this correction was applied only to the single-stage HP turbine, since it was supposed to keep the same general architecture of the PW127E engine.
As mentioned above, the strategy implemented for the estimation of the efficiencies of the turbines is based on the preliminary calculation of the mean stage loading. This step requires to perform a basic modelling of the gas path, in order to allow the calculation of annulus areas at the entry and at the exit of engine components, determining entry and

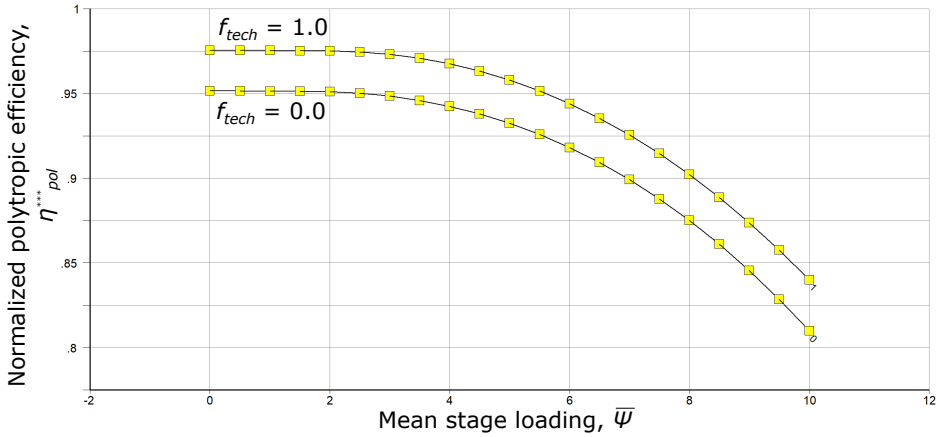

Figure 3.5: LP and free turbine normalized polytropic efficiency versus mean stage loading and technology level. Adapted from [78].

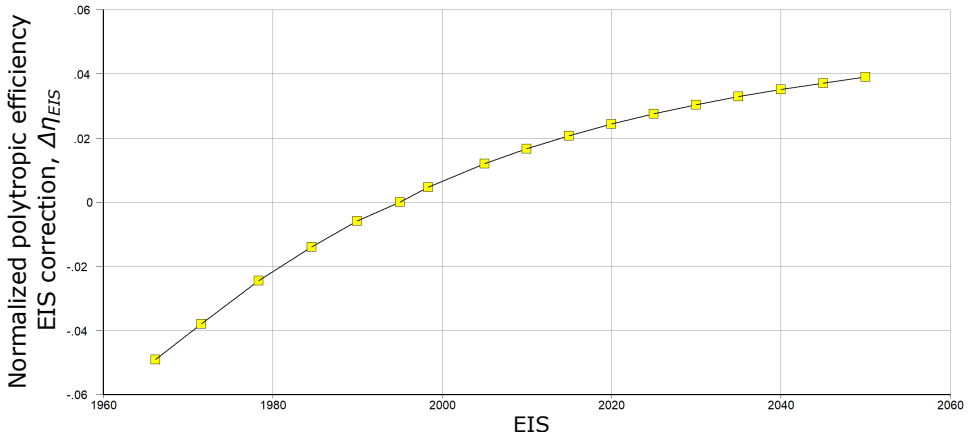

Figure 3.6: HP turbine EIS correction for the calculation of the polytropic efficiency. Adapted from [78].

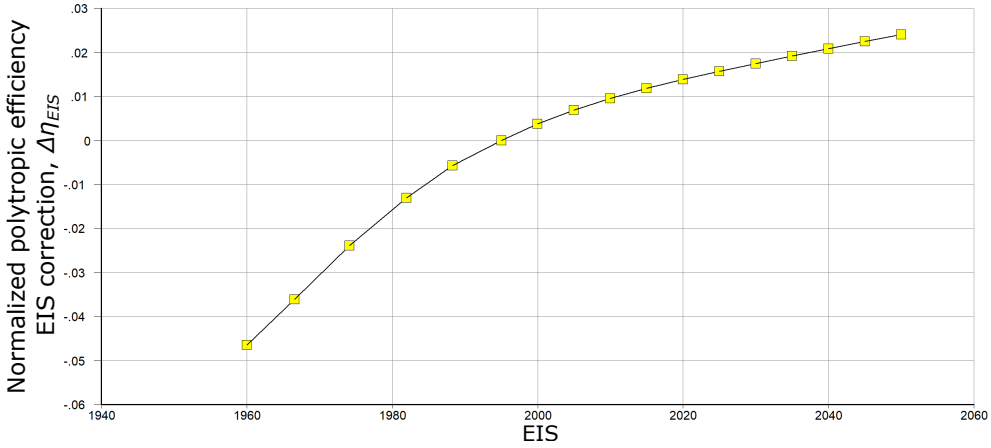

Figure 3.7: LP and free turbine EIS correction for the calculation of the polytropic efficiency. Adapted from [78].

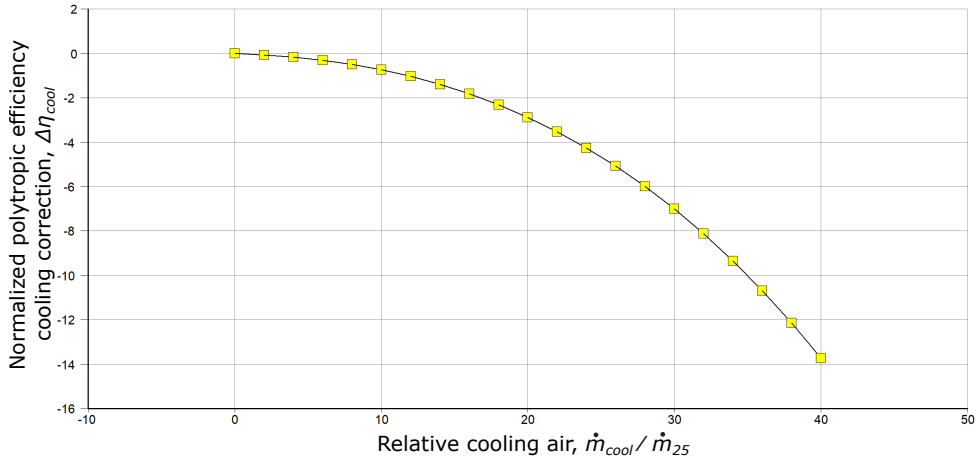

Figure 3.8: HP turbine relative cooling air correction for the calculation of the polytropic efficiency. Adapted from [78].

Table 3.4: Assumptions on Mach number and hub-to-tip ratio values at the inlet and outlet sections of the turbines for the scalable engine model of GENESIS.

Location	**Mach number**	**Hub-to-tip ratio**
HPT entry	0.24	0.826
HPT exit	0.25	0.826
LPT entry	0.25	0.740
LPT exit	0.26	0.740
PT entry	0.26	0.705
PT exit	0.36	0.583

exit tip and hub diameters, as well as entry and exit mean diameters. For this purpose, assumptions are necessary on the hub to tip ratios of the components, in addition to suppositions for the entry and exit Mach numbers of the gas. For the GENESIS implementation, just those for the turbines were required, but more generally speaking, in order to apply the same approach on efficiencies to all the components, these type of data should be assumed both for compressors and turbines. Information on the typical values for these quantities can be retrieved from [78][181][106]. The ones that were adopted for the scalable engine model of GENESIS are reported in table 3.4. Hub-to-tip ratio values were assumed starting from the cutaway of the PW127E engine reported in figure 3.1. It is important to remark that these parameters were not assumed as dependent or independent variables of the GasTurb-implemented scalable engine model, but were deemed constant.
The calculation of annulus areas at turbines inlet and oulet sections was implemented by means of the option for the definition of additional variables provided by GasTurb. The following equation, based on isentropic flow considerations, and taking advantage of the output from cycle design point calculations, was implemented:

$$A_i = \frac{\dot{m}_i \sqrt{T_i} \left(1 + \frac{\gamma-1}{2} M_i^2\right)^{\frac{\gamma+1}{2(\gamma-1)}}}{M_i P_i \sqrt{\frac{\gamma}{R}}}, \tag{3.8}$$

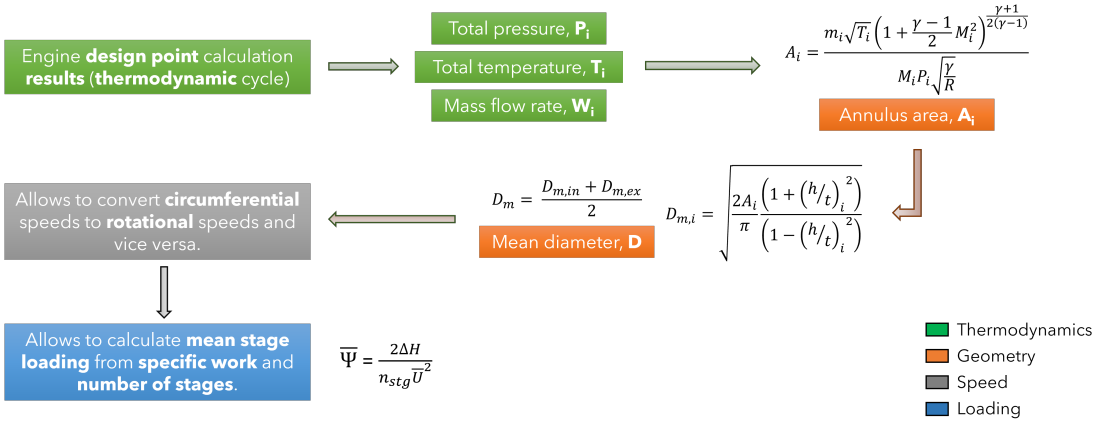

Figure 3.9: Series of steps implemented in the GasTurb rubber engine model allowing to perform a basic modelling of the flow path (from the combustion chamber onward).

in which A_i, $\dot{m}_i$, T_i, P_i, and M_i are respectively the annulus area, the mass flow rate, the total temperature, the total pressure, and the Mach number at a non-specific location (i.e., comprised between the entry and the outlet ones) of a generic single or multi-stage component. Using calculated annulus area and information on assumed hub-to-tip ratio, the average component diameter at the i^{th} stage can be calculated with the following equation:

$$D_{m,i} = \sqrt{\frac{2A_i}{\pi}\frac{\left[1+\left(\frac{h}{t}\right)_i^2\right]}{\left[1-\left(\frac{h}{t}\right)_i^2\right]}}, \tag{3.9}$$

where $(h/t)_i$ is the hub-to-tip ratio at the generic i^{th} location, estimated by linearly interpolating assumed values at inlet and outlet sections. At this point, the average diameter of a generic component can be easily calculated with the following operation:

$$D_m = \frac{D_{m,in}+D_{m,ex}}{2}, \tag{3.10}$$

in which $D_{m,in}$ and $D_{m,ex}$ are, respectively, the average component diameters at entry and exit sections.
With information on the rotational speeds, coming for the HP and LP shafts from the calculations performed for the pressure ratios and the polytropic efficiencies of the HP and LP impellers, and for the free turbine shaft from having assumed a constant ratio with respect to the rotational speed of the LP shaft (equal to the one assessed for the reference engine during validation activities), and with the addition of the data on average diameters, the mean circumferential speeds $\overline{U}$ can be easily calculated. As well as the mean stage loading, since it was assumed that the number of stages per component was neither an input variable of the GasTurb-implemented engine model, nor a parameter depending on other input or cycle-calculated terms, but a value to be kept constant and equal to the one of the reference engine. Figure 3.9 provides a recap on the steps implemented in order to perform a basic modelling of the flow path for the turbines, allowing to have a direct estimate of the mean stage loadings. Figure 3.10, instead, provides a visual representation of some of the geometrical variables mentioned in this sub section.

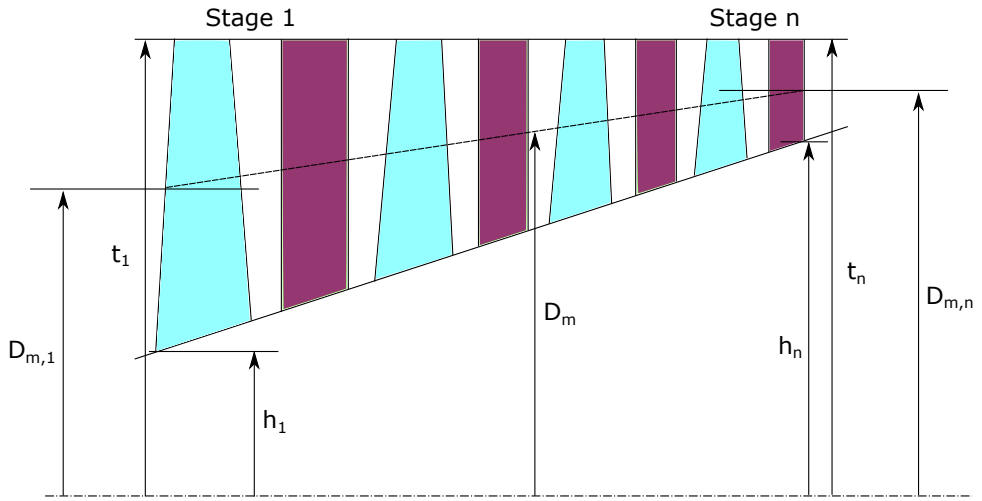

Figure 3.10: Visual representation of the set of geometrical parameters required for the basic modelling of the gas turbine flow path.

3.2.3 Cooling air requirements

The amount of required cooling air should always be estimated for the most demanding condition in terms of engine temperatures, which is usually take-off. Since the design point selected for the gas turbine engines to be designed for GENESIS matches this condition, the amount of cooling air required by the engine, in particular, by the nozzle guide vanes and by the rotor of its single-stage high-pressure turbine, can be directly estimated at the design point, thus allowing to avoid any iteration involving off-design simulations. Its correct estimation is quite important, since it allows to determine the actual amount of air used by the engine in order to generate power and thrust.
There are several semi-empirical methods described in literature for the estimation of the amount of necessary cooling air. One of the most popular approaches is reported in [181], and allows to estimate the amount of cooling air required by the rotor and by the stator of each turbine stage starting from information on the stator outlet temperature (SOT) and on an assumed technology level for the engine. This method is provided in the form of a chart, with four distinct straight lines (two for the stators and two for the rotors) giving upper and lower boundaries (linked to lower and higher technology levels, respectively) of required cooling air percentage with respect to engine inlet flow, in relation to the air temperature at the stator outlet. Though this approach is the one of the most used when it comes to perform a first-order estimate of the total amount of cooling air for an aeronautical engine, the data on which the abovementioned chart is based come from cruise condition, which, in terms of engine temperatures, is quite different from the one adopted for the design of the gas turbine engines of GENESIS.
A different approach is described in [78]. A chart is provided, based on data from single-stage and multi-stage HP and LP turbines of different engine applications (civil turbofan, military turbofan, turboprop and propfan), allowing to have an estimate of the total amount (stator plus rotor) of percentage cooling air required by each stage of a cooled turbine from the calculation of the following intermediate temperature:

$$T_m = \frac{T_{4.n} + T_3}{2}, \tag{3.11}$$

in which $T_{4.n}$ is the SOT of a generic stage of the turbine, and T_3 is the temperature of the air spilled from the HP compressor and used to cool the turbine stages. The data on which this chart is based, according to [78], come from engines operating at ISA SL take-off condition.
For the gas turbine engines modelled for GENESIS, another approach was preferred. The method proposed in [75] allows to determine the relative cooling air mass flow required by each grid of a cooled turbine starting from the calculation of the following quantity:

$$\eta_{cool} = \frac{T_{HG} - T_M}{T_{HG} - T_{CA}}, \tag{3.12}$$

which is basically the definition of the cooling effectiveness of heat exchangers, in which:

- T_{HG} is the hot gas temperature, i.e., the temperature of the air-fuel mixture at the entry of the turbine grid, which needs to be appropriately incremented, according to [75], in order to include the following effects:
  - hotspot profiles, by multiplying the hot gas temperature by so-called *pattern factors*, depending on the grid location, and for which typical values are provided;
  - upstream cooling air dilution, by performing a calculation of mass averaged enthalpy;
  - relative velocity, by multiplying the hot gas temperature by a constant factor, equal to 0.92;
  - work extraction, by adequately decreasing the hot gas temperature for the downstream rows of vanes and blades;
  - safety factor, by first increasing T_{HG} by 150° R (83.3 K).
- T_M is the allowable bulk metal temperature, and depends upon the year of material technology of the turbine components, and on the desired life and duty cycle.
- T_{CA} is the cooling air temperature, which reflect the stage of the HP compressor from which the cooling air flow is extracted.

Regarding the maximum allowable material temperature, [75] suggests two simple semi-empirical equations (one for the vanes of the stator and the other for the blades of the rotor) to perform a first-order estimation. These equations are the following:

$$T_{M,vanes} = (10 * Year - 17640) - (100 * \log(Life) - 400), \tag{3.13}$$

$$T_{M,blades} = (10 * Year - 17740) - (100 * \log(Life) - 400), \tag{3.14}$$

providing results expressed in R degrees, and in which Year is the year of material technology and Life is the desired life of the stator/rotor airfoil, expressed in hours. It can be noticed from these equations that [75] suggests to use a maximum allowable material temperature for the rotor blades 100° R (55.6 K) lower than that of the stator vanes, all else being equal. The application of these equations was preliminarily tested and it was assessed that their usage would have led to excessively optimistic values of bulk metal temperatures, especially for future engine applications of the long-term scenario.
For this reason a new semi-empirical regression was elaborated and adopted, starting

Table 3.5: Maximum limiting temperature assumptions for the calculation of the required amount of cooling air and for the setting of design boundaries, assumed from data reported in [107][189].

	Max. T_M	**Max. T_M (cooled)**	**Technology factor f_{tech}**
Inconel 713C	1200 K	1450 K	0.0
Inconel 792	1250 K	1550 K	0.2
PWA 1480	1300 K	1750 K	0.4
PWA 1492	1350 K	1950 K	0.6
CMC	1400 K	2050 K	0.8
CMC (advanced thermal coating)	1450 K	2100 K	1.0

from suggestions included in [107][189]. From these sources, allowable maximum temperature values for turbine materials were collected and linked to the input technology factor f_{tech} (not the EIS) of the rubber gas turbine engine in the making. These values are reported in table 3.5, which also provides information on the assumptions that were performed, starting from the same references, on the maximum allowable temperatures for cooled turbine materials (second column of table 3.5). These information are not used by the implemented model for relative cooling air calculation but, as it is shown in one of the upcoming sub sections, they are adopted to set a limit on the maximum reachable temperatures, thus restricting the available design space.
For the calculation of the actual allowable material temperature, a desired 20000 hours life for the turbine airfoils was accounted, thus reducing the T_M values reported in the first column of table 3.5 by 30 K, according to equations 3.13 and 3.14. This value was kept constant for all the gas turbine related analyses performed for GENESIS.
By using the above definition for cooling effectiveness, the required amount of cooling air mass flow relative to the HP compressor entry mass flow for a generic turbine grid (i.e., stator or rotor of a turbine stage) can be derived from the following correlation, still provided by [75]:

$$\frac{\dot{m}_{cool}}{\dot{m}_{25}} = 0.022 c_{cool} \left(\frac{\eta_{cool}}{1 - \eta_{cool}} \right)^{1.25}, \tag{3.15}$$

in which c_{cool} is the cooling factor, depending on the characteristics of the cooling air system and its related technology level. Typical values of this factor are provided in [75], which were used to determine a relationship with respect to the input f_{tech} parameter. The assumptions performed concerning this relationship are summarized in table 3.6. More information on the cooling technology concepts included in this table can be found in [75] and in [78]. It is worth to mention too that the link between different cooling technology concepts and values of the f_{tech} input variable was set in accordance with the design point calculations performed for the reference engine (the PW127E model), for which [85] provides basic information on the cooling air system of the HPT.
As suggested in [75], implementation of equation 3.15 should account for additional effects (such as endwall, shroud cooling, disk cooling, and leakage), which tend to lower the effectiveness of the cooling system. In order to account for all these items, [75] suggests to multiply the value resulting from the application of equation 3.15 by a factor equal to 4/3, for all the turbine grids.
All the equations and the assumptions presented above were implemented in the GasTurb

Table 3.6: Cooling factor typical values, according to [75], adopted for the definition of a technological trend inside the GasTurb rubber engine model.

Cooling technology	**Cooling factor c_{cool}**	**Technology factor f_{tech}**
Advanced convection (100 % trailing edge ejection)	1.4	0.00
Film with convection (75 % trailing edge ejection)	1.3	0.17
Film with convection (50 % trailing edge ejection)	1.2	0.33
Film with convection (25 % trailing edge ejection)	1.1	0.50
Full cover film	1.0	0.66
Transpiration with convection	0.9	0.83
Transpiration	0.8	1.00

rubber engine model, by means of the definition of additional composed values for cycle design point calculations.

3.2.4 Miscellaneous input variables

In order to complete the definition of the set of input variables required by the GasTurb template for a three-spool turboprop, a complete search was performed in the available literature on the topic of gas turbine engine modelling.
Pressure losses for compressor and turbine inter-ducts were assumed starting from typical values reported in [181], and were linked to the input factor accounting for the level of technology. In fact, [181] provides typical boundaries for these losses. A linear trend with respect to the f_{tech} input term was supposed, assuming lower boundary values for f_{tech} equal to 0.0, and upper boundaries for f_{tech} equal to 1.0.
A pretty much similar approach was adopted for the setting of the mechanical efficiencies of the high-pressure, low-pressure and free turbine spools, and for the burner and the turbine exit duct pressure losses. Suggested values of the mechanical efficiencies were also taken from [181], as well as the ones for the turbine exit duct. Information included in [78], instead, were used to set lower and upper boundaries of the pressure loss at the combustion chamber.
Table 3.7 provides boundary values adopted for all the abovementioned quantities, along with the reference from the literature source from which they were taken.
With regards to burner efficiency, a lookup table was elaborated and implemented in the GasTurb rubber engine model by mainly using suggestions from [117] and by extrapolating for future tendencies, assuming a flat behaviour. A graphical representation of the data used for this lookup table is provided in figure 3.11, while the related dataset is presented in table 3.8. As it is possible to see from them, the input EIS parameter of the engine model was selected as the independent variable in this case, rather than the technology factor.
For the intake and nozzle pressure ratios, constant values (i.e., independent of the technology level and EIS) were assumed, reflecting the selected design point condition. In particular, the nozzle pressure ratio was fixed by performing validation of the rubber

Table 3.7: Lower and upper boundaries adopted for the modelling of pressure losses and spool mechanical efficiencies of the GasTurb-implemented rubber engine model of GENESIS.

	Lower bound	Upper bound	Reference
Compressor duct pressure ratio	0.980	0.990	[181]
Turbine duct pressure ratio	0.975	0.995	[181]
Turbine exit duct pressure ratio	0.985	0.995	[181]
Burner pressure ratio	0.945	0.970	[78]
Spool mechanical efficiency	0.990	0.999	[181]

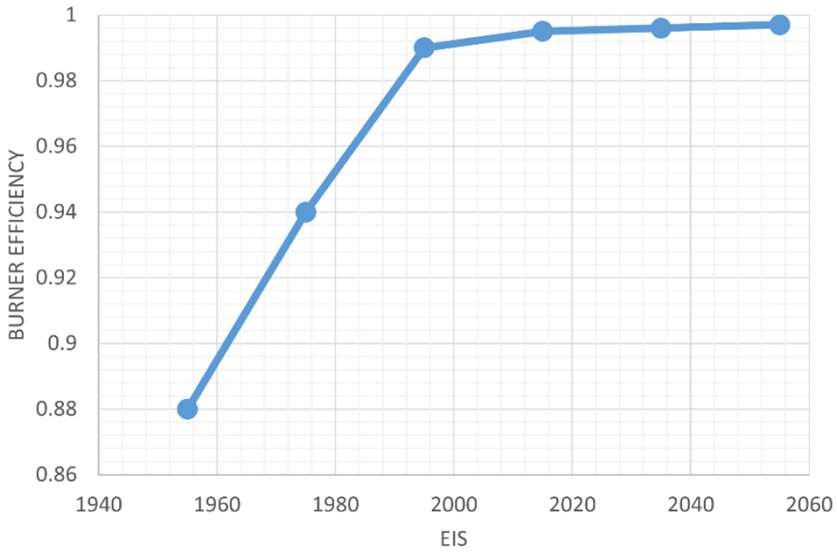

Figure 3.11: Burner efficiency versus entry into service, according to [117] and to the elaborated extrapolation.

Table 3.8: Collected data for the modelling of the burner efficiency.

EIS	Burner efficiency	Reference
1955	0.880	[117]
1975	0.940	[117]
1995	0.990	[117]
2015	0.995	[117]
2035	0.996	extrapolated
2055	0.997	extrapolated

Table 3.9: Dataset used for the generation of the linear regression model for the engine dry mass. Engines data taken from [121].

Manufacturer	Model	Year	T/O W_2, kg/s	Weight, kg
Pratt & Whitney	PW120	1979	6.7	417
Pratt & Whitney	PW127	1990	8.49	481
Pratt & Whitney	PW150	1995	14.44	690
Walter Aircraft Engines	M602B	1986	7.33	490
Klimov	TV7-117S	1993	7.95	530
Rolls-Royce	AE-2100J	1990	16.33	702
Europrop	TP400-D6	2005	26.3	1938
GE BGA Turboprops	H85	2009	3.8	180
Allison Engine Company	C20R	1960	1.73	78
Allison Engine Company	C40B	1960	2.77	127
Garrett AiResearch	TPE331-10U	1960	3.49	175

engine model against data for the PW127E engine: the correct value was estimated iteratively, matching the amount of equivalent shaft power (i.e., the sum of the shaft power and the power derived from the jet thrust) of the reference engine.

3.2.5 Dry mass calculation

There is plenty of semi-empirical methods in literature for the estimation of the engine dry mass of a turboprop engine. Most of these methods are based on single-input equations in which the shaft power of the engine (usually for maximum take-off condition) is the independent variable. Remarkable examples of this type of regression laws can be found in [167] and in [79].
Within the context of GENESIS, in order to link the engine dry mass to one of the driving design parameters of the engine and to highlight the effect of different design choices on the dry mass for a selected target shaft power, the entry mass flow was adopted as the input parameter for a novel semi-empirical law. For this purpose, engines were selected from an online database [121], discarding derated variants of the same engine in order to increase the reliability of the final regression. The list of engines that were used to generate this new regression law is reported in table 3.9. Figure 3.12, instead, provides a visual representation of this model, along with its single-input equation. It must be noted that the proposed linear regression seems to fit quite well the dataset, especially for entry mass flow rate values below 10 kg/s, which are the quite typical for a turboprop engine application for a small regional jet, such as the one examined in GENESIS. It is also important to remark that the reference engine dry mass values listed in 3.9 and used for the generation of the linear regression include the contribution of both the gas turbine and the gearbox.

3.2.6 Main dimensions estimation

Unlike the dry engine mass, there are not so many semiemprirical methods available in literature allowing to perform a first-order estimation of the main dimensions of the engine. There are some methods, like the ones reported in [158] and in [182], which allow to perform, even at preliminary design stage, a fast estimation of the main dimensions of the main components of an aeronautical engine. However, they still require more refined

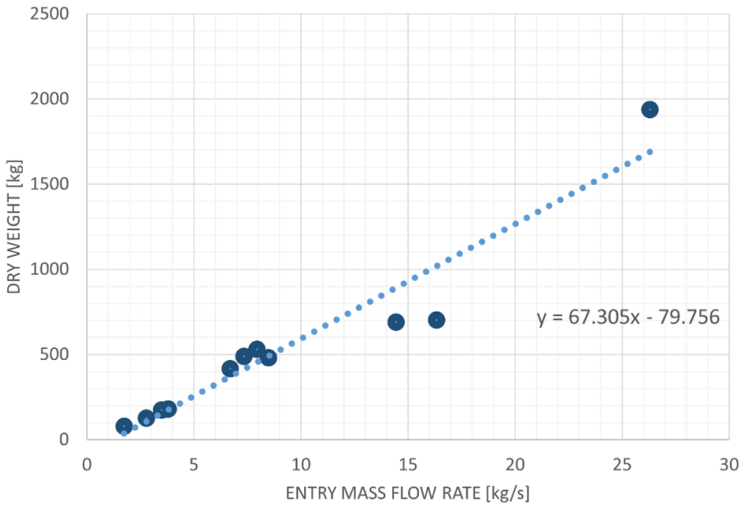

Figure 3.12: Engine dry mass linear regression law with respect to entry mass flow rate.

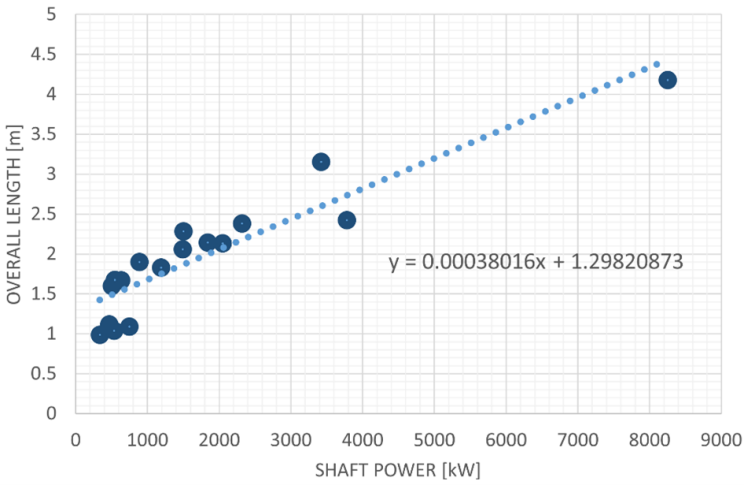

Figure 3.13: Engine overall length linear regression with respect to take-off shaft power.

information and assumptions on the characteristics of the engine than those produced by the rubber engine model implemented with GasTurb. Moreover, these methods rely on outdated datasets (the abovementioned reports are from the 1970s), and were designed for turbofan or for VTOL applications. For these reasons, it was preferred to generate for the overall engine length, height and width simple single-input semiempririca relationships, like the one for the engine dry mass.
To estimate the overall length (including the gearbox), an approach similar to the one reported in the previous sub section was adopted. The overall length was linked to the take-off shaft power of the engine by means of a linear regression law, which is shown in figure 3.13. The dataset of [121] was again used for this task, still discarding derated engine models from the overall data.
In order to assess the maximum width and height of the gas turbine, an *almost* component-based approach was adopted. What typically drives the size of a gas turbine for a turboprop configuration such as the reference one, excluding the contribution of the reduction gearbox, is the outer diameter of the exducer of the low-pressure impeller (i.e.,

Table 3.10: Ratios for engine dimensions with respect to LP impeller and power turbine last stage diameter.

	Ratio	**Driving diameter**
Maximum width	1.5	Max. between LP impeller and free turbine
Maximum height	2.0	LP impeller

the foremost one) and the tip diameter of the last stage of the free turbine. These two quantities are actually estimated by the rubber engine model implemented in GasTurb. The first one derives from the calculations related to the LP impeller pressure ratio and polytropic efficiency. The second one is one of the results of the basic flow path modelling for the turbines group. By setting constant multipliers for these diameters, based on ratios estimated starting from the cutaway of the reference engine, it was possible to link some of the external dimensions of the gas turbine to the outcomes of design point thermodynamic cycle calculation. These ratios are reported in table 3.10. In the implemented modelling for GENESIS, the width of the engine is driven by the bigger of the two previously cited diameters. The diameter of the low-pressure impeller, instead, always drives the overall height of the engine.

3.2.7 Costs-related estimations

As with the overall dimensions of the engine, there is lack of first-order, semi-empirical methods allowing to estimate the costs and the development time of a gas turbine engine. In [191] provides several basic single and multi-input formulas to estimate development costs, development time, and production costs for turbofan military engines. These cost-estimating relationships were developed through a series of least-square regressions, based on turbofan cost data available as of publication time in 2002. Although these formulas were developed from historical data for quite different engines application with respect to the ones examined in GENESIS, these cna be still useful in the early conceptual design stages of a new/derivative engine, in order to perform significant trade-off analyses, as exemplified in [36].
For the estimation of development costs, [191] suggests the use of the following equation for a new centerline development engine:

$$C_{dev} = e^{-24.429+4.027\ln(T_{4.1}-460)}, \tag{3.16}$$

in which $T_{4.1}$ is the HP turbine rotor inlet temperature, expressed in Rankine degrees. For a derivative engine, instead, a different equation is suggested:

$$C_{dev} = e^{-39.422+5.066\ln(T_{4.1}-460)-1.299\ln(S)+0.582\ln(FSTH)}, \tag{3.17}$$

where S is the cruise specific fuel consumption (expressed as lb/(lbf*h)) and FSTH is the number of test hours for a full-scale model. As it can be seen, the development costs are essentially driven, according to this approach, by the design temperature at the HPT rotor inlet, which sets the technology level of a new or derivative engine.
For the production costs, [191] suggests two different equations:

- For the first production engine:

$$C^1_{prod} = e^{-10.40-8.550\ln(slope)+1.162\ln(T_{4.1}-460)+0.261\ln(W_{dry})}. \tag{3.18}$$

- For the production of the 375$^{\text{th}}$ engine:

$$C_{prod}^{375} = e^{-10.40+1.162\ln(T_{4.1}-460)+0.262\ln(W_{dry})}. \tag{3.19}$$

In these equations, *slope* is the cost improvement and can be assumed equal to 0.9 for new engines and equal to 0.95 for derivative engines, while W_{dry} is the engine dry mass expressed in pounds. It is interesting to notice the production cost reduction given by the second equation, due to an overall lower cost of the production process. According to these equations, heavier engines, as well as engines designed to work at higher temperatures, have higher production costs, linked to the necessity to use more materials to build the engine, and due to the requirements for more expensive solutions for the manufacture of the hot sections.
A semi-empirical equation for the estimation of the development time is also provided in [191]:

$$T_{dev} = e^{-0.243+0.425new+1.151\ln(OPR)}, \tag{3.20}$$

in which *new* should be set equal to 1.0 for new centerline engines. The value returned by this equation is expressed in months and it is higher for compressor units characterized by an higher number of compressor stages. In order to better fit the abovementioned methodology to the engine applications of GENESIS, the equations for production costs were adequately calibrated, to match the price data of the reference engine, as explained in section 3.3. This calibration was performed by introducing a fudge factor for costs, f_{cost}, which was also conveniently linked to the input technology factor as reported in the following equation:

$$f_{cost} = 0.775 f_{tech} + 0.225. \tag{3.21}$$

With the performed assumption on the technology level of the reference engine and by multiplying the result coming from equation 3.19 by the calibration for costs, the estimated engine price was adjusted to better fit the actual data.
It is also important to mention that the costs calculated with equations 3.16, 3.17, 3.18, and 3.19 are expressed in 2001 M$ and that they need to be adequately converted by using calculated or predicted (depending on the supposed EIS) cumulative inflation rates. For the applications regarding GENESIS, new centerline engines were always supposed, leading to the use of those dedicated equations.

3.2.8 Engine limitations

Mechanical and thermal limitations can be assumed to restrict the design space only to those combinations of input parameters leading to feasible engine configurations.
Useful information on the maximum circumferential speed that can be sustained by compressor and turbine blades can be retrieved from [78] and [181]. In [78], in particular, several charts are provided for average circumferential speeds of compressor and turbines, covering different engine types and different number of stages per component. These charts rely on actual engine data collected by the author of [78] through the years, thus providing remarkably useful information for these assumptions. Despite these charts are provided with respect to engine EIS, for most of the turbomachineries it is quite hard to determine an actual correlation with the year of introduction. For this reason, constant values were assumed. Important indications are reported in [180] also regarding the maximum allowable value for AN^2, which is the product of the annulus area at a generic turbine station and the square of the turbine rotational speed. For the last stage

Table 3.11: Set of mechanical limitations assumed for the analyses of GENESIS.

	Upper limit	**Reference**
Radial compressor exducer tip speed, U_{RC}	625 m/s	[181]
HP turbine average circumferential speed, $\overline{U}_{HPT}$	550 m/s	[78]
LP turbine average circumferential speed, $\overline{U}_{LPT}$	470 m/s	[78]
Power turbine average circumferential speed, $\overline{U}_{PT}$	400 m/s	[78]
AN^2	$50*10^6$ m^2rpm^2	[181]

of the power turbine, its value should be kept below certain limits, in order to avoid too high disc stress. All these limiting values are summarized in table 3.11.
Concerning temperature limitations, these were already collected in table 3.5, in the previous section dealing with relative cooling air calculations for the HPT. These limitations apply to the HP turbine rotor inlet temperature $T_{4.1}$ and to the LP turbine inlet temperature $T_{4.3}$. For the HPT (cooled) limitations reported in the second column of table 3.5 apply, while the ones included in the first column of the same table are used for the LP turbine. Improvements in the maximum allowable temperature of turbine materials mainly derive from the adoption of more advanced materials, better cooling technology, and from the use of improved thermal coatings.
The last set of limitations was derived from information contained in [181], and comprises upper boundary values concerning the usage of radial compressors. According to [181], in fact:

- Despite single-stage radial compressors can achieve pressure ratios as high as 9, higher values are not typically suitable, due to a remarkable sudden decrease in the efficiency. Since the implemented approach for the calculation of the polytropic efficiencies of the LP and HP impellers is not capable of modelling this decrease, an upper limit equal to 10 was set on the maximum reachable pressure ratio of a single-stage radial compressor.
- For entry mass flow rate values higher than 10 kg/s, radial compressor units are no longer competitive with respect to axial compressors, due to the much higher frontal area and weight, which overturn the benefit of lower costs.
- The diameter of the centrifugal impeller should not exceed 0.8 m. This upper boundary is linked to manufacturing limitations, which make the construction of bigger radial compressor pretty unpractical. As a consequence, this limits the maximum pressure ratio and entry mass flow rate reachable by a this type of turbomachinery.

3.2.9 Emissions

Pollutant emissions cannot be directly estimated with GasTurb (version 11). The only related information provided directly by the tool for cycle calculations is the NO_x severity index, which is calculated according to the following equation:

$$S_{NO_x} = \left(\frac{P_3}{2965}\right)^{0.4} e^{\left(\frac{T_3-826}{194}+\frac{6.29-100*war}{53.2}\right)}, \tag{3.22}$$

in which P_3 and T_3 are, respectively, the total pressure and temperature of the gas at the combustion chamber entry, and *war* is the water-to-air ratio. From this equation it

Table 3.12: EI for CO_2, H_2O, and SO_2 according to [62].

	EI (g/kg)
CO_2	3149.0
H_2O	1230.0
SO_2	0.84

is immediate to notice that the higher the total pressure achieved at the burner entry (i.e., the higher the OPR), the higher the NO_x severity index. According to [105], the NO_x emission index increases linearly with the NO_x severity index. The linear relationship between these two quantities depends on the technology level of the combustion chamber. For conventional combustors the NO_x severity index should be multiplied by a value equal to 32 to obtain NO_x EI. This factor should be assumed equal to 23 for dual annular combustors, instead.
There are several methodologies for the estimation of aircraft engine emissions. However, most of these are particularly suited for turbofan engines. In [69], a simple methodology for fast and reasonable predictions of pollutant species emissions for turbofan and turboprop engines is provided. This methodology is based on emissions data collected in the ICAO emissions databank [8] (which includes only information on the emissions of turbofan-powered aircraft), which were conveniently adapted by the authors of [69] to fit the emissions for a turboprop engine. In fact, two different sets of polynomial coefficients, used to fit the following generic surface:

$$z(x_1, x_2) = a + bx_1 + cx_1^2 + dx_1 + ex_2^2 + fx_1x_2, \tag{3.23}$$

to the data included in the ICAO databank, are provided in [69] for turbofan and turboprop/turboshaft engines, respectively. In equation 3.23, x_1 represents the engine overall pressure ratio, while x_2 is the fuel flow. The variable z represents the reference emission index for a certain pollutant, which must be then adjusted using the corrections for atmospheric conditions reported in [29]. Since the ICAO emissions databank does not include information on the emissions of turboprop/turboshaft engine, correlations for these engines were based by the authors of [69] on a rather limited amount of public available information.
This methodology allows the estimation of emission indices of NO_x, CO, and HC. To enable the use of this simplified model, input must be provided in terms of fuel flow and design OPR, which are information that can be easily derived from GasTurb cycle calculations. Moreover, for the GENESIS case, the engine OPR is one of the input variables of the GasTurb-implemented rubber engine.
Regarding the EI for CO_2, H_2O, and SO_2, it is reasonable to assume constant values, not specifically related to the characteristics of the engine. Constant values suggested in [62] and here reported in table 3.12 were assumed for these species.

3.2.10 Alternative fuels

GasTurb allows to choose between different fuels for the cycle simulations. Conventional jet fuel for civil aircraft applications, Jet A-1, named *generic fuel* in GasTurb, was selected as the standard kerosene fuel for the GENESIS analyses and for the GasTurb rubber engine model. GasTurb provides for this fuel a LHV equal to 43.124 MJ/kg at ISA SL static temperature [105]. This value was adjusted for the analyses on gas turbine

Table 3.13: Input values for the LHV and CO_2 EI of the fuels examined for GENESIS.

Fuel	**LHV, MJ/kg**	**CO_2 EI, g/kg**
Jet A-1	43.26	3149.0
SPK 50 %	43.65	3124.5
SPK 100 %	44.04	3100.0

engines of GENESIS to consider information provided in [187] on the average LHV for Jet A-1 fuel, which should be around 43.26 MJ/kg.
In order to consider the effects related to the use of alternative fuels on the engine thermodynamic cycle, a simplified approach, similar to the one presented in [30], was selected. Different blends of biofuel were considered by varying the GasTurb input defining fuel LHV. The LHV for these blends was estimated starting from pure kerosene and pure biofuel LHV values, interpolating linearly for different blends depending on the percent by mass of the mixture. This is a simplified approach, since the fuel properties file used by GasTurb for the analyses was not updated accordingly with the different assumptions on the fuel. A more accurate approach would have required the generation of fuel performance data by using an additional tool, as explained in [187], possibly in the same format required by GasTurb for the input file of fuel properties.
However, gas turbine engine cycle simulations including the effect on LHV should still account for the impact of biofuel blends on the performance of the engine, as exemplified in [30].
Hydro-processed esters and fatty acids synthetic paraffinic kerosene (HEFA-SPK) and synthetic paraffinic kerosene derived from the Fischer-Tropsch process (FT-SPK) were chosen among the set of biofuels certified for civil aviation use [147]. For both these biofuels, blending ratios up to 50 % with conventional jet fuel are already approved, with this value being destined to grow in the coming years, since several tests and demonstrations on civil aircraft engines with 100 % SAF fuel are already taking place [119]. Moreover, among all the available biofuels, the two typologies selected for GENESIS have the highest TRL for commercialization, according to [147].
Speaking of the rubber engine model of GENESIS, three fuels were taken into consideration:

- Conventional kerosene (Jet A-1),
- Conventional kerosene 50 % blend with SPK,
- 100 % SPK biofuel.

Distinction between the two typologies of biofuel identified above were not performed at this level, since it was assumed they provided almost the same LHV. Information on this quantity for the abovementioned biofuel blends were collected from [187] and are presented in table 3.13. This same reference also provides indications on CO_2 EI, which were conveniently adapted and are here reported in table 3.13 too. No additional reliable information was retrieved from the available literature on the impact that biofuel blends may have on the EI of the remaining species. For this reason, no assumptions were performed.

3.3 Validation

In order to validate the rubber engine model implemented in GasTurb, this was tested using input for the reference engine, the PW127E gas turbine model. Reference data for this engine was mainly collected from [85][51][94][12][37], and reasonable assumptions were performed for those values for which direct information were not included in these references. The design point calculation was performed under the same conditions listed in table 3.3. Table 3.14 summarizes the selected values for the most important model input variables, whereas table 3.15 lists information on the cycle output and the set of derived output variables.
Assumptions on the power off-takes and on the overboard bleed were performed starting from semi-empirical methodologies provided in [95] and [181], respectively. These approaches base the estimation of these quantities on aircraft characteristics in terms of maximum take-off weight on one hand, and on the number of persons typically carried on-board (passengers and flight crew) on the other, for which information were taken from [4]. Coefficients based on linear regressions of available data are provided:

- 0.001 kW of power off-takes per kg of maximum take-off weight, to be divided by the number of equipped engines;
- 0.01 kg/s of overboard bleed per passenger on-board, to be divided among the engines.

It is important to highlight that the coefficient of the power off-takes was adjusted, at a later stage, in order to make it compliant with the reference data on off-takes gathered for ADORNO, and reported in section 2.3.3. A factor equal to 0.0015 was finally selected for the analyses of GENESIS. It is also worth to mention that the bleed air extraction estimated with the approach described above allows to take into account only the requirement related to the environmental control system of the aircraft, and not the one linked to the ice protection system. Finally, both the extractions were assumed to be performed from the HP compressor. This assumption applies in general to all the gas turbine engines modelled for GENESIS.
The value of the technology factor f_{tech} was selected based on information included in [94] and [85] regarding the turbine materials and the cooling air technology, respectively:

- Mar M-200 nickel-based superalloy for the high-pressure turbine blades, Inconel 792/100 nickel-chromium-based superalloy for the remaining components of the HPT, both with a maximum allowable metal temperature around 1250 K, according to [107].
- Film with convection and trailing edge ejection for the cooling air system of the HPT.

Regarding the last item of the above list, a high value of trailing edge ejection was assumed for the reference engine, due to information also included in [85] on the cooling concept adopted for the PW150 engine variant. According to this reference, the PW150 model should be able to achieve much higher turbine inlet temperature, requiring a more sophisticated cooling system. Since the PW127 and the PW150 adopt basically the same cooling air system concept, a higher trailing edge ejection value was assumed for the reference engine of GENESIS, in order to make a distinction. It is important to remark that, according to the information included in [75] and [78], higher airfoil

Table 3.14: Set of input data to the rubber engine model for the validation against known performance of the PW127E engine model.

Input variable	Value	Source	Notes
Shaft power delivered	1790 kW	[51][12][37]	Maximum take-off power
Inlet mass flow	8.49 kg/s	[85]	-
Burner exit temperature	-	-	Iterated to match target shaft power
Overall pressure ratio	14.7:1	[51]	-
Technology factor	0.2	-	Set to match available information
EIS	1990	[85]	PW127 program start
Power off-takes	14 kW	-	Estimated starting from [95]
Overboard bleed	0.25 kg/s	-	Estimated starting from [181]
Fuel LHV	43.26 MJ/kg	-	Conventional kerosene (Jet A-1)

trailing edge ejection values for the film with convection cooling concept imply higher c_{cool} values, thus lower cooling effectiveness, according to the modelling of cooling air requirements described in section 3.2 and implemented in the GasTurb rubber engine model.
Table 3.15 gives evidence of the good matching between the output data of the GasTurb-implemented rubber engine model and the expected values for the reference engine. The differences in terms of specific fuel consumption are quite negligible: lower than 1 % at ISA SL static take-off condition. The remaining two values of SFC were also tested against data coming from a customer deck for an engine almost identical to the reference one. These tests returned differences of the same order of magnitude. For parameters such as the dry mass and the dimensions, the model tested quite well too, with larger differences with respect to the reference data than those achieved for the SFC, but still below 10 %. Moreover, the model passed the tests concerning assumed limitations too, with the cycle output being compliant with both thermal and mechanical limitations.
It is important to mention that for the calculations involving equivalent shaft power and equivalent SFC, assumption were performed on the characteristics of the propeller in terms of diameter, rotational speed and efficiency starting from the ones available in the abovementioned reference customer deck for a PW127E-like engine.
It is necessary to remark too that the burner exit temperature value was not assumed (since no precise information is available for the reference engine), but its value was calculated with GasTurb, after setting up an iterative loop, aiming at the matching of the target shaft power delivered. As it is shown in table 3.15, the estimated value falls exactly in the expected interval provided by [85], which applies for all the engines of the PW100/150 family.
Regarding the costs, equation 3.19 was used to test against price data of the reference engine reported in [94], applicable for 2010. This equation, with input from the results of the cycle simulation reported in table 3.15, provided a $1,376,200 production cost for 2001 which, once converted to 2010 US dollars by using a 23.2 % cumulative rate of inflation (calculated from public available data on US dollar annual inflation rate) gave a production cost for 2010 equal to $1,695,500, quite distant from the $920,000 price tag suggested in [94] for the reference engine model. Supposing a 30 % profit margin per engine sold, assuming a value equal to 0.38 for the cost correction factor f_{cost} (deriving from the previous assumption on the technology factor f_{tech}), and by applying equation 3.19 calibrated, a price pretty much identical to the one reported in the reference was obtained.

Table 3.15: Design point cycle direct output and derived variables for the PW127E engine, using the GasTurb-implemented rubber engine model.

Output variable	Value	Expected value	Source	Difference
Equivalent shaft power	1877 kW	1876 kW	[51]	+0.05 %
Burner exit temp.	1442 K	1420 – 1530 K	[85][94]	-
LP turbine inlet temp.	1219 K	< 1220 K	-	-
LP impeller exit speed	564 m/s	< 625 m/s	-	-
HP turbine mean speed	469 m/s	< 550 m/s	-	-
LP turbine mean speed	438 m/s	< 470 m/s	-	-
Free turbine mean speed	372 m/s	< 400 m/s	-	-
Free turbine AN^2	$39*10^6$ m^2rpm^2	$< 50*10^6$ m^2rpm^2	-	-
Cooling relative air	5 %	-	-	-
Engine dry mass	492 kg	481 kg	[51][12]	+2.29 %
Engine width	652 mm	660 mm	[51]	−1.21 %
Engine height	770 mm	838 mm	[51]	−8.11 %
Engine overall length	1979 mm	2134 mm	[51]	−7.26 %
SFC @ design point	0.3080 kg/(kW*h) 0.5063 lb/(hp*h)	-	-	
Equivalent SFC @ design point	0.2937 kg/(ekW*h) 0.4828 lb/(ehp*h)	-	-	
Equivalent SFC @ SLS ISA T/O	0.2900 kg/(ekW*h) 0.4768 lb/(ehp*h)	0.4740 lb/(ehp*h)	[51]	+0.59 %

3.4 Short-term scenario analysis

The rubber engine model implemented in GasTurb was tested for the short-term scenario of GENESIS, corresponding to the 2025-2035 timeframe. For these analyses, 2030 was selected as the representative year. The results of these tests were used as a benchmark of the methodology for gas turbine modelling adopted for GENESIS, and were included in a related deliverable of the project, focusing on the short-term analysis of all the propulsive technologies involved.
In order to carry out these preliminary analyses, several parametric studies were performed, involving most of the input variables of the model listed at the beginning of section 3.2. More specifically:

- The burner exit temperature T_4 was selected this time as a direct input variable, and was not adjusted iteratively to match any specific target. For this variable, values were made to vary between 1300 and 1900 K.

- The engine OPR was varying between 13 and 22. The pressure ratios of the LP and HP impellers were automatically updated according to the approach on pressure ratios described in section 3.2.

- A constant value was selected for the shaft power delivered, equal to 1790 kW. This is the same value of the reference engine. With the burner exit temperature selected as one of the driving variables of the parametric study, the (corrected) entry mass flow rate of the engine was iteratively tuned in order to allow the matching of the target shaft power.

- Studies were performed for two distinct values of the technology factor f_{tech}, equal

to 0.4 and 0.6. As in-depth discussed in section 3.2, this variable, according to the adopted approach, has a direct impact on:

  - the polytropic efficiencies of radial compressors and turbines;
  - the cooling air system technology and, as a consequence, the cooling factor c_{cool};
  - the material of the turbines group and, consequently, the relative cooling air requirement of the HPT and the thermal limitations of the engine;
  - the inter-duct, the turbine exit duct, and the burner pressure losses;
  - the mechanical efficiencies of the HP, LP, and PT spools;
  - the production costs.

  Moreover, this input quantity has an indirect, noticeable impact on several output variables of the model, such as the engine dry mass and the engine maximum diameter, since it acts on those parameters on which the calculation of these output quantities is based, like the entry mass flow.

- With respect to the fuel, blending ratio up to 50 % with HEFA- and FT-SPK biofuels were considered reasonable for this short-term analysis, due to their high TRL and depending on the fact that they are already approved for aeronautical use. Since tests are already ongoing for higher blending ratios and certification should be reasonably expected within the next ten years, blending ratio up to 100 % were included too in this preliminary analysis.

- Finally, for the power off-takes and the overboard bleed, the same values reported in table 3.14 for the reference engine were used for all the analyses.

Results are presented in this section for SFC, dry mass, maximum diameter (i.e., the highest value between maximum height and width), and production costs (using equation 3.19) in terms of contour plots and tables, assuming different combinations of fuel blending ratio and technology level. For each combination, a plausible design point was selected, thus fixing the characteristics of the engine in terms of performance, dimensions and weight. Different limitations were included, in addition to the ones already listed in the dedicated sub section, in order to restrict the available design space even further, just to provide examples of which motivations could drive the selection of a new engine for an aeronautical application, in addition to considerations on the specific fuel consumption. An upper limit, for example, was introduced on the NO_x severity index, in order to have NO_x EI values lower than 20 g/kg, assuming to adopt for the new engines of the parametric study a dual annular combustor, thus leading to a calibration factor for NO_x EI equal to 23. Limitations like this could be set in order to match specific objectives in terms of aircraft emissions.
Moreover, an upper bound to the relative cooling air flow, equal to 5 % (the same value estimated for the reference engine), was added to the set of limitations. Such a limitation could be introduced to restrain the complexity of the cooling air system, avoiding to select design points featuring too high cooling air requirements, which might be difficult to be designed and/or manufactured. As a note, the NO_x severity index values of the following analyses were calculated using the approach implemented by GasTurb, rather than the approach suggested in [69], which was in general preferred for the remaining pollutant species.

For the estimation of the production costs, the scaling procedure for turboprop engines, technology level and US dollar inflation rate outlined in section 3.2 and in section 3.3 was adopted. For the 2021-2030 time span, a cumulative inflation rate equal to the one for the 2011-2020 decade (obtained from public data on US dollar annual inflation rate) was assumed.
Figures from 3.14 to 3.16 provide contour plots of SFC with respect to engine OPR and burner exit temperature, for f_{tech} equal to 0.4 and for different types of fuel. It is possible to deduce from these plots that the temperature at the inlet of the LP turbine, $T_{4.3}$, together with the limitation on the maximum achievable NO_x severity index, S_{NO_x}, and the relative amount of cooling air (reported as $Cool_{\%}$ in these plots), restrict the available design space to the polygon in the lower-left corner. Basing the selection of the design point of the gas turbine on the minimum SFC objective, the point at the intersection of the boundary lines for NO_x and relative cooling air (i.e., the purple and the cyan dashed lines of figure 3.14) should be picked. This selection leads to the values reported in table 3.16. With respect to the reference engine, the one designed for conventional jet fuel allows for a reduction of specific fuel consumption greater than 20 %. This value is line with expected benefits in terms of fuel burn reductions with respect to current engines of recent new turboprop development programs, such as the GE Catalyst [27]. Dealing with the effect of biofuel blendings, these would allow to go even further with SFC reduction. Engines designed for 50 % biofuel blend and 100 % biofuel would allow for additional 0.7 % and 1.4 % reductions with respect to the fuel consumption of the reference engine, respectively. These values are pretty much in line with those reported in [187], for a similar analysis on turbofan engines.
Figures from 3.17 to 3.19 provide instead, for f_{tech} equal to 0.4 and for conventional kerosene, contour plots for engine dry mass, maximum engine diameter, and production costs. Table 3.17 collects data from these plots, assuming the previous choice in terms of design point targeting the minimum fuel consumption. According to the implemented modelling and to the previously mentioned assumptions on the level of technology, a 28.5 % weight reduction and a 15.9 % smaller maximum diameter should be expected for a gas turbine engine of the short-term scenario. These reductions are mainly driven by the general improvement in terms of turbomachinery efficiencies. The same contour plots were also produced for the remaining fuels examined for the project. Unlike the one for SFC, no remarkable differences could be highlighted with respect to the results obtained for a gas turbine designed for conventional jet fuel. It is also quite interesting to analyse the effect of turbine entry temperature T_4 and OPR on the output quantities plotted in these figures. For a fixed T_4 value, the SFC tends to decrease with increasing OPR. This applies, at least according to the investigated intervals, for T_4 values higher than 1500 K. For lower values, there is a breakpoint from which the SFC stops to reduce and it starts to slightly increase. This breakpoint is for higher OPR values as T_4 increases. The engine dry mass shows a much more simple behaviour:

- it tends to decrease with increasing operating temperatures, which is quite predictable, since lower entry mass flow rate values are required to generate the same amount of power, implying smaller engine components which require less material to be manufactured;
- it increases with engine OPR, which is also expected, since bigger impellers are required to generate higher pressure ratios.

As regards the maximum diameter, pretty much the same considerations made for the

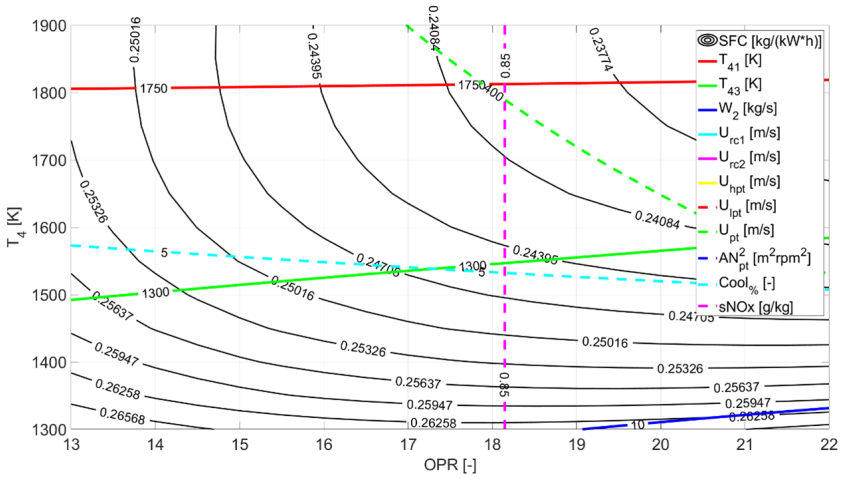

Figure 3.14: SFC contour plot for f_{tech} equal to 0.4 and conventional kerosene, resulting from the example parametric analysis carried out for the short-term scenario.

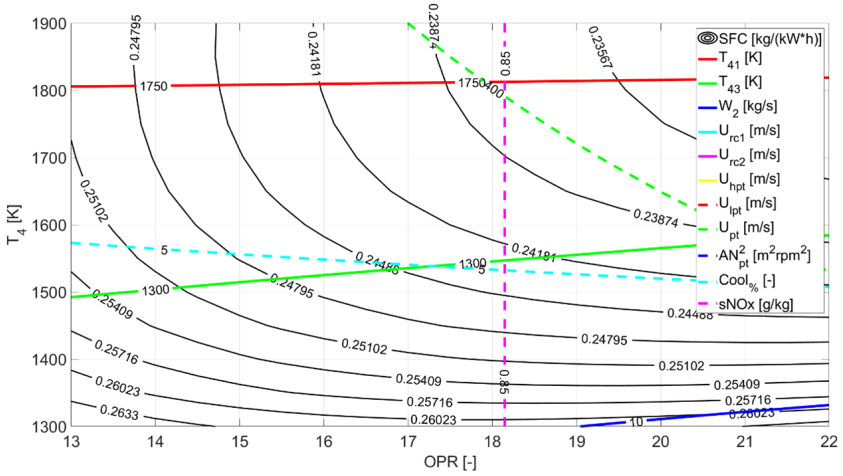

Figure 3.15: SFC contour plot for f_{tech} equal to 0.4 and 50 % biofuel blending ratio, resulting from the example parametric analysis carried out for the short-term scenario.

dry mass apply. Whereas for the production costs, they tend to increase with the operating temperatures, as expected by equation 3.19. Moreover, they also increase with the overall pressure ratio, due to the effect of increasing engine dry mass.
As mentioned above, the same analyses were performed assuming a higher value for the technology factor, equal to 0.6. Figure 3.20 provides the contour plot for the specific fuel consumption. As can be seen from this figure, the higher technology level moves upward the limitations provided by the low-pressure turbine entry temperature and by the relative cooling air flow. Moreover, the amount of cooling air required by the high-pressure turbine is no longer a limitation to the available design space. On the other hand, the limitation provided by the NO_x severity index still restricts the maximum achievable OPR to a value a little higher than 18. Differently from the previously examined case, the selection of a less restrictive value for NO_x would have granted an additional margin for SFC reduction. In fact, the SFC contour lines of figure 3.14 are much more flat (i.e., little margin for improvement for increasing OPR) next to the NO_x limitation than those of figure 3.20. The selection of a different limitation on allowable emissions,

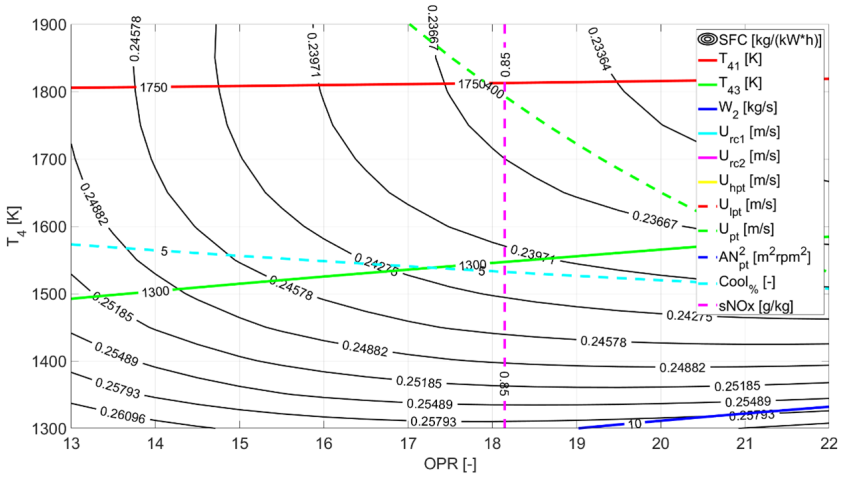

Figure 3.16: SFC contour plot for f_{tech} equal to 0.4 and 100 % biofuel blending ratio, resulting from the example parametric analysis carried out for the short-term scenario.

Table 3.16: Effect of alternative fuels on the fuel consumption for f_{tech} equal to 0.4, resulting from the example parametric analysis carried out for the short-term scenario.

SFC, kg/(kW*h)	**Value**	**Difference wrt 0 % biofuel blending**	**Difference wrt reference engine**
Conventional kerosene (0 % blending)	0.2455	-	−20.3 %
SPK 50 % (HEFA-SPK / FT-SPK)	0.2433	−0.89 %	−21.0 %
SPK 100 % (HEFA-SPK / FT-SPK)	0.2412	−1.75 %	−21.7 %

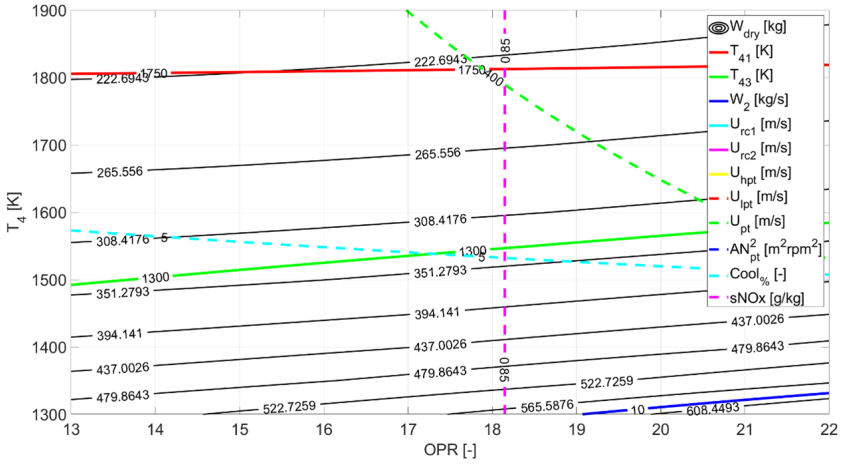

Figure 3.17: Dry mass contour plot for f_{tech} equal to 0.4 and conventional kerosene, resulting from the example parametric analysis carried out for the short-term scenario.

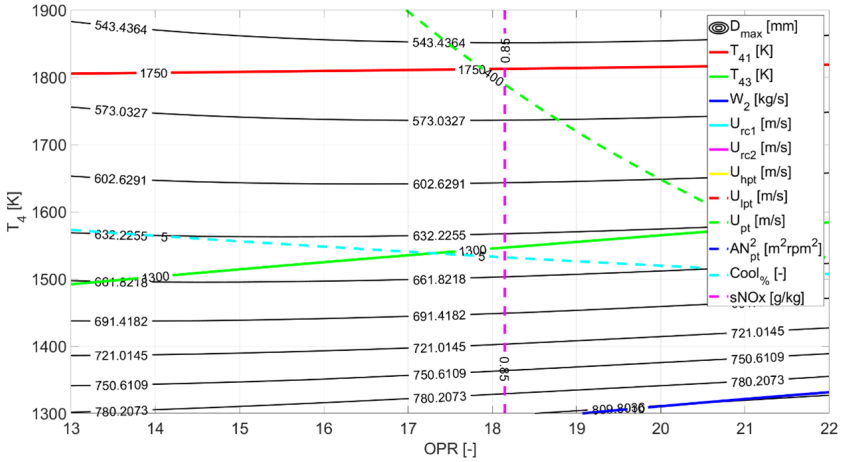

Figure 3.18: Engine maximum diameter contour plot for f_{tech} equal to 0.4 and conventional kerosene, resulting from the example parametric analysis carried out for the short-term scenario.

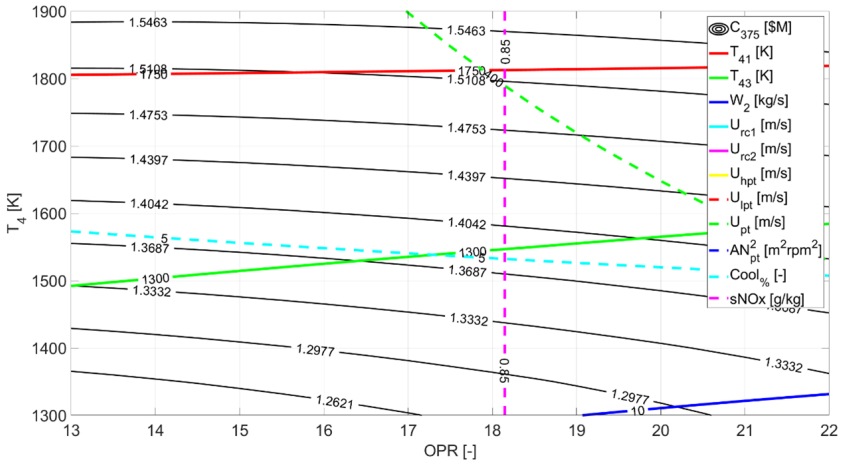

Figure 3.19: Production costs contour plot for f_{tech} equal to 0.4 and conventional kerosene, resulting from the example parametric analysis carried out for the short-term scenario.

Table 3.17: Obtained values for the main output variables of a gas turbine engine designed for the short-term scenario, assuming a value for the technology factor equal to 0.4 and conventional jet fuel.

Variable	Value	Reference engine	Difference
SFC, kg/(kW*h)	0.2455	0.3080	−20.3 %
Dry mass, kg	351	481	−28.5 %
Max. diameter, mm	647	770	−15.9 %
Production cost, M$	1.37	-	-

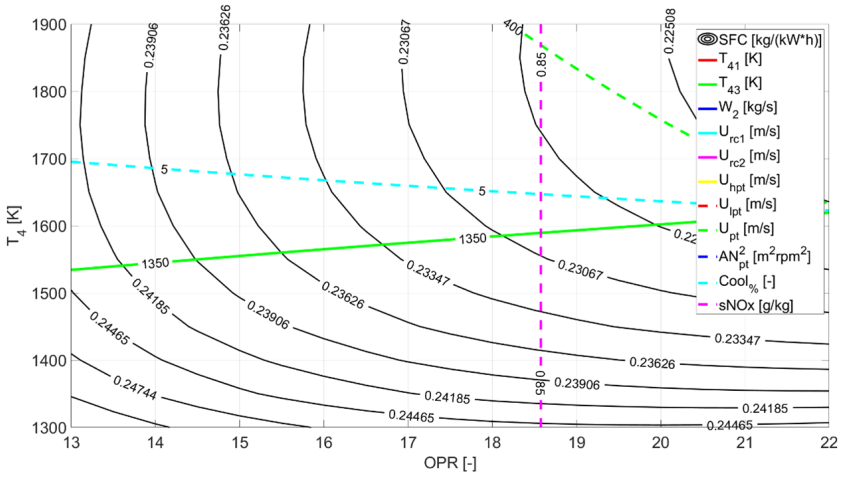

Figure 3.20: SFC contour plot for f_{tech} equal to 0.6 and conventional kerosene, resulting from the example parametric analysis carried out for the short-term scenario.

thus the choice of a different design point for the gas turbine, is pretty much a matter of judgment of the aircraft designer in this case. The same, of course, applies to the previously examined contour plots: depending on the aircraft design task and on the set of requirements for the aeroplane, the designer might have decided to pick a different design point than that guaranteeing the lowest possible SFC, depending on the trade-off for dry mass, dimensions, and costs.
Nevertheless, the intersection between the LP turbine entry temperature limitation and the NO_x severity index upper boundary (i.e., the green solid line and the purple dashed line) was selected as the design point for this analysis. Table 3.18 provides the main results for this design point selection assuming conventional jet kerosene, comparing them with respect to both the reference engine and the advanced engine designed for a different assumption on f_{tech}. This new engine shows, for SFC, dry mass and maximum size, significant improvements both with respect to the reference engine and the more conservative advanced gas turbine model. However, according to the implemented methodology, its production cost is more than 30 % higher than the previously examined engine, which could represent a significant downside when it comes to select between these two different designs. Table 3.19, instead, provides an overview on the effect of alternative fuels on the fuel consumption, for f_{tech} equal to 0.6. These results are pretty much the same obtained with the previous assumption on the technology level.

Table 3.18: Obtained values for the main output variables of a gas turbine engine designed for the short-term scenario, assuming a value for the technology factor equal to 0.6 and conventional jet fuel.

Variable	**Value**	**ftech 0.4**	**Reference engine**	**Difference wrt f_{tech} 0.4**	**Difference wrt reference**
SFC, kg/(kW*h)	0.2296	0.2455	0.3080	−6.5 %	−25.4 %
Dry mass, kg	285	351	481	−18.8 %	−40.7 %
Max. diameter, mm	608	647	770	−6.0 %	−21.0 %
Production cost, M$	1.79	1.37	-	+30.6 %	-

Table 3.19: Effect of alternative fuels on the fuel consumption for f_{tech} equal to 0.6, resulting from the example parametric analysis carried out for the short-term scenario.

SFC, kg/(kW*h)	**Value**	**Difference wrt 0 % biofuel blending**	**Difference wrt reference engine**
Conventional kerosene (0 % blending)	0.2296	-	−25.4 %
SPK 50 % (HEFA-SPK / FT-SPK)	0.2277	−0.83 %	−26.1 %
SPK 100 % (HEFA-SPK / FT-SPK)	0.2257	−1.70 %	−26.7 %

3.5 Surrogate model and implementation

In order to enable the use of this rubber engine model in the aircraft design framework of GENESIS, some additional steps were required. GasTurb allows the possibility to build elaborate workflows involving gas turbine design and off-design cycle calculations by means of several dynamic-link libraries (DLL), each dedicated to a specific engine configuration. Unfortunately, these DLLs are not included in the base package of GasTurb 11, thus were not in the set of available instruments to perform the implementation of the abovementioned model in the hybrid-electric aircraft design work chain of UNINA. To overcome this issue, a strategy based on the definition of a surrogate model, based on the results produced by the GasTurb-implemented scalable engine, was adopted. For this purpose, several parametric analyses at design point were performed, involving the following input variables of the model:

- Shaft power delivered,
- Burner exit temperature,
- Overall pressure ratio,
- Power off-takes,
- Overboard bleed,
- Biofuel blending ratio with conventional jet kerosene, and
- Technology factor.

As for the analyses presented in section 3.4, the engine entry mass flow rate was not selected as an input variable, but was iterated in GasTurb to automatically match the

Table 3.20: Set of input variables of the parametric study carried out for the generation of the surrogate engine model for the short-term scenario of GENESIS.

Input variable	Lower boundary	Upper boundary	Step size
Shaft power delivered	1000 kW	2000 kW	100 kW
Burner exit temperature	1300 K	1700 K	50 K
Overall pressure ratio	13:1	22:1	1
Power off-takes	0.0 kW	50 kW	50 kW
Overboard bleed	0.0 kg/s	0.50 kg/s	0.25 kg/s
Biofuel blending ratio	0.0 %	100 %	50 %
Entry into service	2030	2030	-
Technology level factor	0.4	0.6	0.2

required amount of shaft power, for each combination of the remaining input parameters. Since the project objective in the near-term was the definition of the gas turbine technology set for the first, closest in time scenario (2025-2035 timeframe), these parametric analyses were focused on a specific entry into service (2030, the representative year selected by the project coordinator for the short-term scenario) and for the same values of the technology factor examined in the previous section. For these reasons, these preliminary parametric analyses performed were an extension on the work illustrated in the previous section, which was carried out to provide proof of the capability of the designed rubber gas turbine model.
Table 3.20 provides an overview on this parametric study. Information are provided regarding lower and upper boundaries adopted for each input variable, as well as the step size of each parameter variation. A total of 35640 design point cycle simulations were performed, helped by the GasTurb dedicated operating mode for parametric analyses, which allowed to speed-up the process and to perform automatically those analyses concerning different combinations of burner exit temperature and overall pressure ratio.
The dataset produced with these parametric analyses, including information on the results of cycle simulations in terms of total temperatures, total pressures, mass flow rates, rotational speeds, gas path dimensions, cooling air requirements, specific fuel consumption, and nitrogen oxides emissions, was used to train separate linear regression models for each of the cycle output variables of interest. This allowed the generation of a mathematical model, used in place of the original GasTurb-implemented rubber engine, that could be easily exported and included in an external tool, in order to perform trade-off analyses and optimizations at aircraft level.
The Regression Learner App provided by MATLAB [116] was used for this purpose. This application uses machine learning to train regression models on the provided dataset. Generally speaking, it provides much more sophisticated and flexible to the dataset models than the simple linear ones. The advantage of using linear models stems from the fact that:

- they are much more easy to be interpreted, since simple linear equations are used to perform data regression;
- they can be easily exported to applications outside the MATLAB environment, due to their abovementioned easy interpretabilty.

This application provides for linear models several options, especially concerning the terms of the linear model. It allows, in fact, to choose between four typologies of terms:

- Linear, which includes one constant term and linear terms, as exemplified in the following equation:

$$F = c_0 + c_1 P_1 + c_2 P_2 + \cdots c_i P_i + \cdots c_n P_n, \tag{3.24}$$

  in which F is the variable to be modelled, c_i are the coefficients of the prediction, and P_i are the predictors (i.e., the input variables of the regression model).

- Interactions, which comprises a constant term, linear terms, and interaction terms, as follows:

$$F = c_0 + \sum_{i}^{n} c_i P_i + \sum_{i,j}^{n} c_{i,j} P_i P_j, \tag{3.25}$$

  in which $c_{i,j}$ is the generic coefficient of interaction terms.

- Pure quadratic, including a constant term, linear terms, and purely quadratic terms, according to the following general equation:

$$F = c_0 + \sum_{i}^{n} c_i P_i + \sum_{i}^{n} q_i P_i^2, \tag{3.26}$$

  in which q_i are the coefficients of the purely quadratic terms.

- Quadratic, which includes one constant term, linear terms, interaction terms, and purely quadratic terms:

$$F = c_0 + \sum_{i}^{n} c_i P_i + \sum_{i,j}^{n} c_{i,j} P_i P_j + \sum_{i}^{n} q_i P_i^2. \tag{3.27}$$

For each cycle output variable of interest within the context of GENESIS, it was tested which of the abovementioned linear models fitted the best the dataset. For all the examined variables, the linear models to provide the best result in terms of minimum root-mean-square error (RMSE) was the quadratic model. The results of these trainings are summarized in table 3.21, including information on the terms of the model and the residual errors. As it can be seen from this table, the results obtained for each training in terms of RMSE are quite good, especially for the specific fuel consumption and emissions, if compared with reference values of these quantities for the examined engine applications reported in section 3.3 and in section 3.4.
Once the surrogate model was defined, it was ready to be coupled with a reference customer deck (i.e., the one already mentioned in sub section 3.3) for a PW127E-like gas turbine engine, similar in terms of general formatting to the engine deck file used by JPAD and described in section 2.1:

- several sheets, each corresponding to a specific engine rating (e.g., MTO, MCL, MCN, etc.);

- for each engine rating, information in terms of shaft power delivered, specific fuel consumption, and pollutant species emission indices are provided, for different combinations of flight altitude, flight speed, ISA condition, and throttle rate.

Similarly to JPAD, the UNINA-developed preliminary aircraft design tool of GENESIS, HEAD, makes use of such a file in order to carry out aircraft performance and emissions

Table 3.21: Results of the training for the surrogate engine model of the short-term scenario.

Output variable	Regression model	Terms	RMSE
SFC, kg/(kW*h)	Linear	Quadratic	0.0017
S_{NO_x}, g/kg	Linear	Quadratic	0.0014
$\dot{m}_2$, kg/s	Linear	Quadratic	0.1562
LP exducer diameter, m	Linear	Quadratic	0.0024
PT exit diameter, m	Linear	Quadratic	0.0024
$T_{4.1}$, K	Linear	Quadratic	1.0753
$T_{4.3}$, K	Linear	Quadratic	1.7495
LP exducer tip speed, m/s	Linear	Quadratic	0.3739
HP exducer tip speed, m/s	Linear	Quadratic	0.6861
HP turbine averaged speed, m/s	Linear	Quadratic	1.0946
LP turbine averaged speed, m/s	Linear	Quadratic	0.9385
PT averaged speed, m/s	Linear	Quadratic	0.7281
PT AN^2, $m^2rpm^2/10^6$	Linear	Quadratic	0.1682
HPT stator relative cooling	Linear	Quadratic	$3.8668*10^{-4}$
HPT rotor relative cooling	Linear	Quadratic	$2.3492*10^{-4}$

assessments. Based on the output from the surrogate engine model, the reference customer deck would be scaled adopting the following approach: all the data on shaft power delivered, specific fuel consumption, and pollutant species emission indices included in the deck would be multiplied, independently from the rating and the operating conditions, by the ratio between the target MTO shaft power (i.e., one of the input variables of the surrogate engine model) and the reference deck shaft power at the same condition, and by the ratio between output design SFC and NO_x EI with respect to data for those variables included in the engine deck at the design point conditions (i.e., those listed in table 3.3), respectively. This is a simplified but rather effective approach, since it allows to reflect the effect of different design choices on the engine, without the need to produce a detailed engine deck for each new combination of design variables, which, as already said in section 3.2, would have been too much problematic for GENESIS applications.
With respect to the remaining output variables not covered in table 3.21, these can be estimated by the aircraft design tool by using the set of methodologies and equations outlined in sub section 3.2.5, 3.2.6, 3.2.7, 3.2.9, by using as input the results coming from the application of the surrogate engine model.
Finally, in order to provide to the aircraft design tool the required information on the thrust available per each flight phase, the scaled engine deck would be combined with a UNINA in-house built design tool for aircraft propellers, based on XROTOR[2].

3.6 Conclusions

The previous sections presented the approach that was adopted to model a gas turbine engine for the perspective technology analyses of GENESIS. This approach is summarized in figure 3.21.
A rubber engine model was first implemented in GasTurb, by assuming the configuration

[2]https://web.mit.edu/drela/Public/web/xrotor/

of the PW127 engine model as a reference. This scalable model included considerations on pressure ratios of the radial compressors, on the polytropic efficiencies of the turbomachineries, on the materials, technology and relative cooling air requirements for the high-pressure turbine, on the pressure losses along the main ducts of the engine, and on the pressure losses and efficiency of the combustion chamber. The setting and the update of these quantities were automated and linked to the values of several major input variables at design point, such as the required shaft power, the overall pressure ratio, and the burner exit temperature, along as well with the values of the presumed entry into service and of a specifically elaborated for GENESIS technology factor. The implementation of these update rules, based on the methodologies, suggestions and best practices of renown authors of articles and textbooks on the topic, enabled to keep the design of gas turbine for current and future scenarios consistent.
Moreover, additional approaches were retrieved from the literature, or eventually specifically elaborated for GENESIS, in order to allow the estimation, for this rubber engine, of those much valuable variables when it comes to perform trade-off analyses on engine-aircraft integration: dry mass, main external dimensions, emissions, and costs.
This GasTurb-implemented scalable engine model was tested and calibrated against available data on the PW127E engine variant, the actual reference gas turbine model of GENESIS. Furthermore, it was used to carry out representative analyses for a short-term scenario (2025-2035), assuming reference values for aircraft requirements in terms of shaft power, power off-takes, and overboard bleed. These analyses helped to provide an overview on the capability of the developed methodology and tool to perform reasonable predictions of potential benefits in terms of fuel burn reduction, as well as to provide meaningful results for the effect of cycle simulations output variables on engine dry mass, main dimensions, and costs.
In order to allow the implementation of this model in the aircraft design chain provided by UNINA for GENESIS, a surrogate, mathematical model was developed, starting from the results of several parametric studies performed with the GasTurb scalable engine. Machine learning trained linear regression models were developed, with the help of a dedicated software. Moreover, a strategy was elaborated concerning the usage of the information deriving from this surrogate model to updated an already existing engine performance deck, for an engine similar to the PW127E.
Unfortunately, due to the schedule of the project (the elaboration of the technology set for the short-term scenario was concluded in late November 2021), it was not possible to perform tests including the elaborated engine model in the aircraft design framework, since the integration process in HEAD of all the propulsive technologies developed for GENESIS is still ongoing. However, the activities performed for the project were extremely helpful in the sense of the objectives of this thesis work, since they promoted the development of a new tool for a more precise modelling of the effect of different design choices on the characteristics of the engine, thus enabling meaningful engine trade-off analyses since conceptual and preliminary aircraft design stage. The present work, more in general, inspired the elaboration of a strategy, like to the one reported in figure 3.21, applicable to the development of similar tools for different engine applications (e.g., turbofan engines). Chapter 4 will provide more information in this regard.

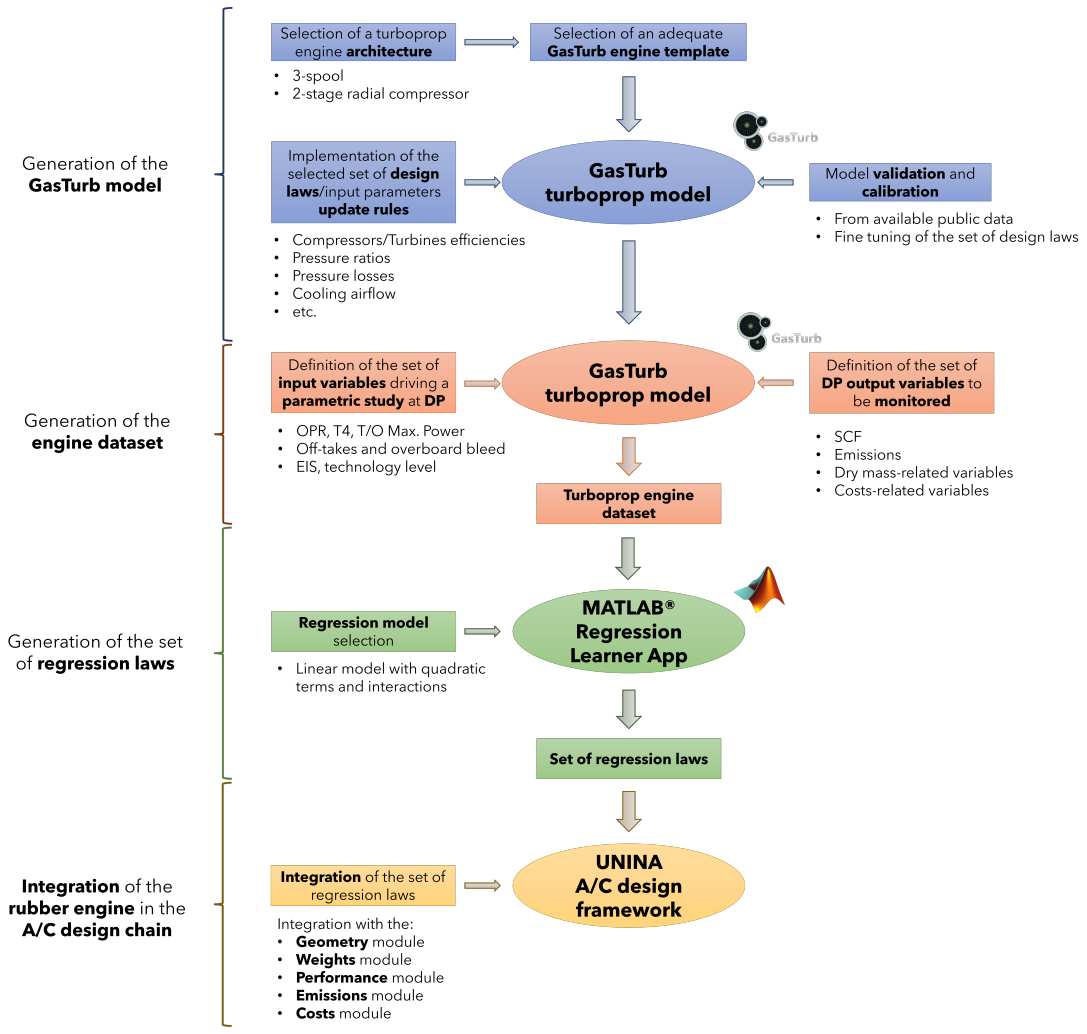

Figure 3.21: Set of steps elaborated for the development of a new tool for the rubberization of gas turbine engines for turboprop applications.

Chapter 4

Turbofan engine rubberization

This chapter provides an overview on the work that was performed to apply the methodology for gas turbine modelling reported in chapter 3 for a specific turbofan engine configuration: two-spool, direct-drive, unmixed flow, high-bypass ratio turbofan. The objective is to demonstrate that the approach described in the previous chapter for an effective modelling of turboprop engines in conceptual and preliminary aircraft design workflows can be generalized and implemented even for quite different propulsive solutions, as reported in 4.1. Moreover, this chapter aims at providing a description of the actions undertaken in order to actually implement a tool for a simplified engine modelling, generated with the abovementioned approach, in an preliminary aircraft design tool, which, in this specific case, is JPAD.
Section 4.1 includes a detailed description of the set of assumptions and methodologies that were applied for this case study. Most of these correspond to those already reported in section 3.2, but since there are some differences in the adopted approach, it was preferred to provide some additional details. These deviations are mainly linked to:

- Differences between the two engine typologies (gas turbines for turboprop applications and turbofan engines are designed with distinct requirements, and operate quite differently in order to produce the required amount of power/thrust).
- Differences in terms of when these two sets of methodologies were elaborated and applied. The development of the approach adopted for GENESIS was actually conducted in a (slightly) later stage with respect to the one described here, thus taking also advantage of a more mature knowledge of some aspects, especially concerning engine limitations and the selection of turbine materials for different time perspectives/technology levels.

Differently from GENESIS, the effect of alternative fuels was not taken into account, but a basic modelling of fan noise was included in the set of implemented methodologies.
Section 4.2 provides proof of validation of the elaborated turbofan engine model, by comparing results with respect to available data for a reference engine. Moreover, this section includes an analysis on the effect of the input parameters selected for this model on the most important engine parameters, such as specific fuel consumption, emissions, dry mass, and size.
Section 4.3 includes a description of the implementation process of such a model in a preliminary aircraft design tool such as JPAD, leading to the creation of a dedicated calculation tool. This section also provides details on the established interactions between

this module for preliminary engine design and the remaining geometry and analysis packages of JPAD. Finally, section 4.4 delivers several examples of usage of this tool within the aircraft design and analysis framework offered by JPAD. Examples of applications are provided for an aircraft similar to the Airbus A320neo, and for an evolved version of this model, featuring advanced airframe technologies included in the list reported in section 2.3.3. The effect of different design choices for the engine on the aircraft performance is analyzed, aiming at providing proof of the applicability and effectiveness of such a simplified engine design tool to perform meaningful trade-off analyses for preliminary aircraft design workflows.

Author contribution

The author of this thesis work was the main and only contributor to the activities reported in this chapter.
Once again, the scientific activities reported in the following could be performed thanks to knowledge and the experience matured during the ADORNO project, and thanks to the constant supervision of Prof. Giovanni Torella, expert of aeronautical engines.

List of related publications

Conference papers

- (*Extended abstract sent and accepted*) **M. Di Stasio**, V. Trifari, F. Nicolosi, and A. De Marco. Bypass ratio parametric analyses and optimization for a short-haul narrow-body aircraft.

  The candidate contributed by implementing in JPAD a module for automatic turbofan engine sizing, described in this chapter. In addition, he contributed to the extended abstract by setting the topic and the final manuscript structure, and by providing a first draft of the paper. For the final manuscript, he will be responsible for running the analyses and the optimizations, as well as to provide a summary of the main outcomes.

4.1 Methodology

Turbofan engines are an evolution of turbojet engines, specifically designed to more efficiently fly at subsonic speeds. At these speeds, in fact, turbojet engines generate thrust by strongly accelerating exhaust flow, which implies a great amount of wasted fuel. A better approach for subsonic flight is to use part of the energy produced by the combustion of fuel to drive an additional compressor, more specifically a ducted fan, which accelerates part of the air flowing through the engine but not passing through the combustion chamber and the turbines group. The amount of this air, compared with the air actually flowing through the engine core, determines the bypass ratio of the engine. Nowadays, also military supersonic aircraft adopt turbofan engines, though with small bypass ratios (less than 1). On the other hand, civil jet aircraft are equipped with high-bypass ratio engines, characterized by BPR values even higher than 10, such as the LEAP-1A model developed by CFM International [92] or the engines of the Pratt & Whitney PW1000 series [185]. These high BPR values allow to further improve fuel

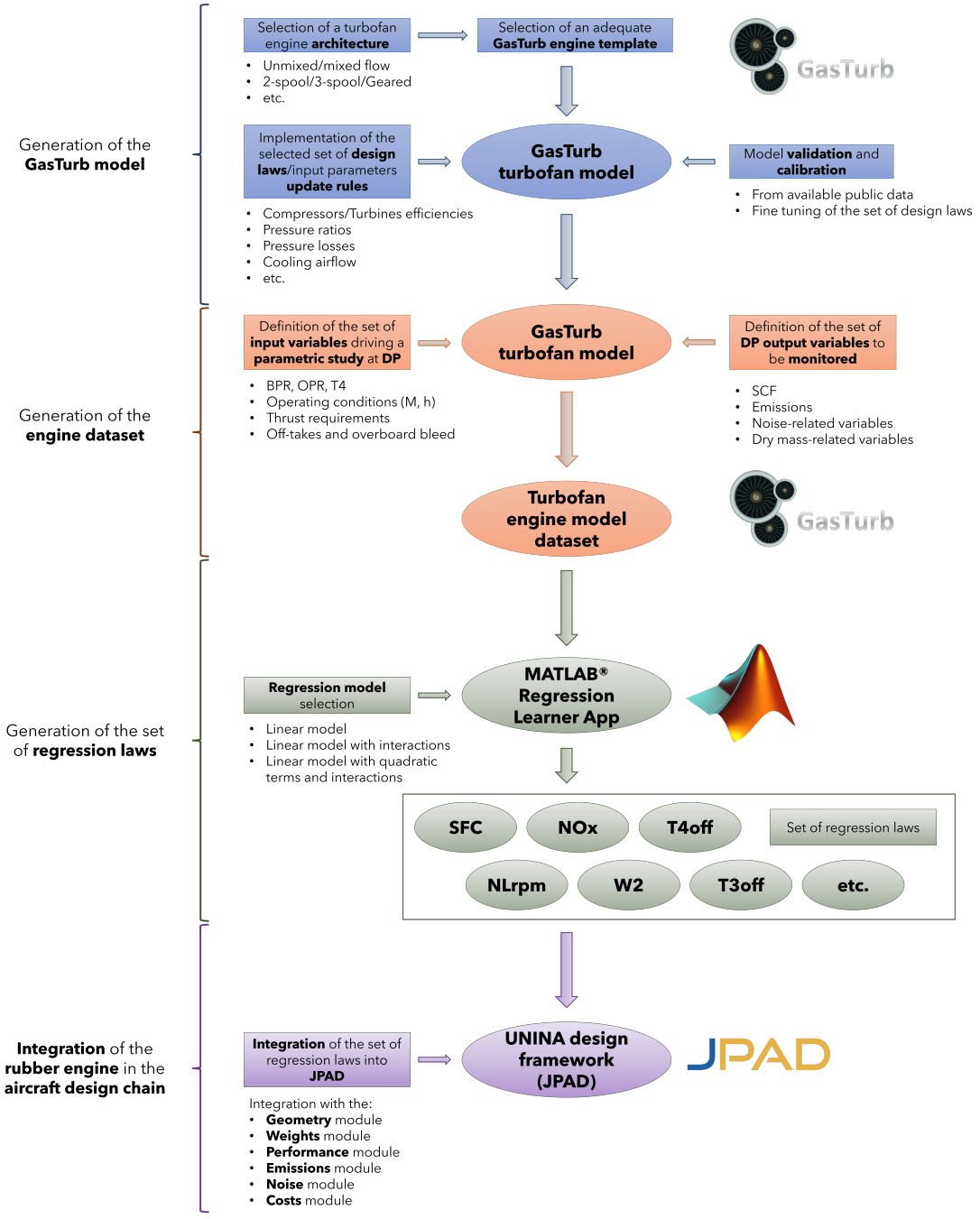

Figure 4.1: Set of steps elaborated for the development of a new tool for the rubberization of specific turbofan configurations.

economy and decrease engine noise.
Distinctions can be made between turbofan engine configurations depending on:

- The number of spools. Most of the turbofan engines equipped nowadays on civil aircraft feature two spools, with the fan and the high-pressure compressor driven by separate low-pressure and high-pressure turbines, respectively. In many modern two-spool engines, an additional compressor named booster, positioned in the core section of the engine between the fan and the high-pressure compressor, and rotating on the same shaft of the fan and the LP turbine, supercharges the HPC, allowing to obtain higher values of overall pressure ratio, thus higher efficiency. Some powerful engines (especially those produced by Rolls-Royce), instead, feature a three-spool architecture, in which an additional shaft links an intermediate-pressure turbine to an intermediate-pressure compressor.

- The adoption of a reduction gearbox. The engines of the PW1000 series, along with some older models produced by Garrett and Honeywell, feature a reduction gearbox on the low-pressure spool, which allows to reduce the rotational speed of the fan with respect to that of the low-pressure turbine, thus generating a lower load on the LPT (which, as a consequence, can be designed to feature a reduced number of stages, impacting on the overall weight of the engine) and reducing the noise generated by the fan.

- Whether the flow coming from the fan duct and the core are mixed before leaving the engine. Some turbofan engines are designed to allow the mixing of fan duct air and exhaust gas in a dedicated section of the engine called mixing chamber. This choice allows, especially for those engines characterized by a lower BPR, to increase the specific thrust and decrease the fuel consumption, as well as to reduce jet noise. On the other hand, the length of the nacelle fan cowl increases, determining a rise in terms of nacelle skin friction drag.

For the specific case here examined, the following turbofan architecture was selected:

- two-spool configuration, with a booster on the LP spool;

- direct-drive, with both the fan and the low-pressure turbine rotating at the same speed, with no reduction gearbox;

- unmixed flow.

In light of these choices on the general layout of the engine, the CFM International (a joint venture between GE Aviation and Safran Aircraft Engines) LEAP-1A model was selected as the principal reference for all the following assumptions. This model is part of the LEAP family of HBPR turbofan engines, where LEAP stands for *Leading Edge Aviation Propulsion*. It features maximum take-off thrust ranging from 106.8 kN (24000 lbf) up to 143.05 kN (32160 lbf), depending on the specific variant, allowing it to power short/medium-haul, narrow-body commercial aircraft such as the Airbus A320/A321neo. Bypass ratio in cruise can reach up to 11, while its 10-stage high-pressure compressor, capable alone to produce a 22:1 pressure rise, combined with a 3-stage booster and a single-stage, 1.98 m diameter fan, allows to reach overall pressure ratio as high as 50:1 at top-of-climb (ToC) condition, and 40:1 at take-off. The fan and the booster are driven by a 2-stage, cooled high-pressure turbine, followed by a 7-stage low-pressure turbine.

Table 4.1: LEAP-1A engine model reference data.

Data	Value	Source
Architecture	1-stg Fan + 3-stg booster + 10-stg HPC 2-stg HPT + 7-stg LPT	[10][93]
Max. take-off thrust, kN	106.8 - 143.05	[10]
Bypass ratio (cruise)	11.0:1	[93]
Overall pressure ratio (ToC)	50.0:1	[93]
Fan diameter, mm	1980	[93]
Weight, kg	2990 - 3153	[10]
Max. rotational speeds, rpm	LP spool - 3894 HP spool - 19391	[10]

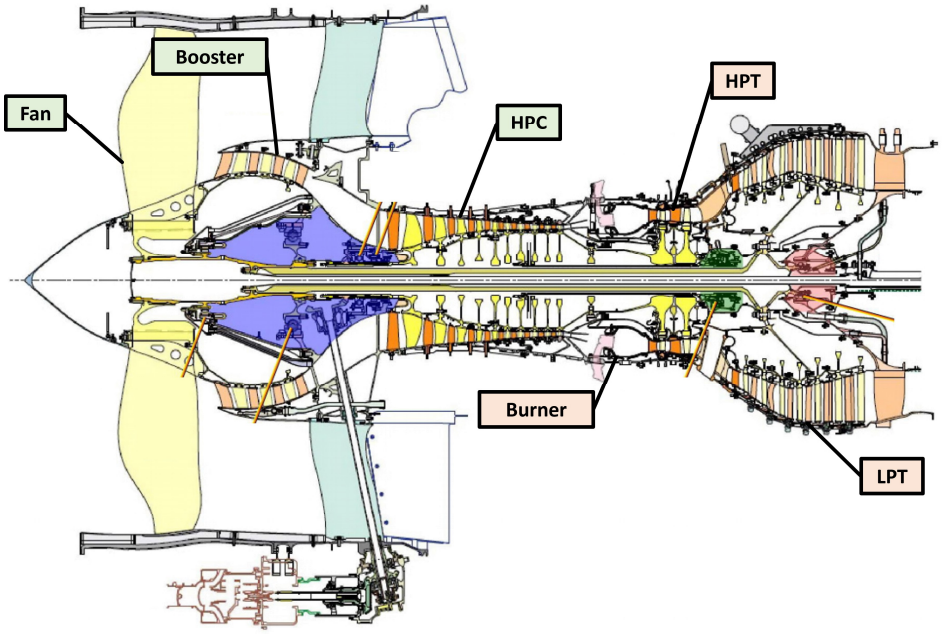

Figure 4.2: Schematic cross section of the CFM International LEAP-1A turbofan model.

These and further main characteristics are summarized in table 4.1 along with information on the sources adopted for these data. Whereas figure 4.2 provides a schematic of the general, internal architecture of this model. Of all the LEAP-1A engine variants, the 1A-26 equipped on the Airbus A320-251N aircraft model [16] was selected as the actual reference for assumptions, test calculations and validations, as shown in section 4.2. This selection allowed to better specify the reference thrust class of the rubber engine model in the making. Moreover, its assumed characteristics in terms of net thrust were used to set boundaries in terms of thrust input variables for the subsequent parametric analyses. These reference thrust values are reported in table 4.2, as well as information on the operating conditions. It must be highlighted that only the T/O SL static thrust was assumed starting from actual information on this engine variant. The remaining values were assessed by the author, or assumed starting from data for engines for similar aircraft applications (i.e., the CFM56-5B4 engine equipped on the Airbus A320-214). The abovementioned engine architecture drove the selection of the most suitable Gas-

Table 4.2: Thrust values for different operating conditions assumed for the reference engine variant.

Condition	Net thrust	Source
T/O, M = 0.0, h = 0 ft, ISA +15	120.6 kN	[10]
T/O EoR, M = 0.20, h = 0 ft, ISA +15	93.85 kN	Estimated with GasTurb
ToC, M = 0.78, h = 35,000 ft, ISA +10	25 kN	Value for the CFM56-5B4, equipped on the A320-214 [51]
Cruise, M = 0.78, h = 35000 ft, ISA	22.3 kN	Value for the CFM56-5B4, equipped on the A320-214 [51]

Turb template to be adopted to implement a scalable turbofan model, following the steps outlined in figure 4.1. Among all the templates offered by the tool, the one for a geared, unmixed flow turbofan was selected. Differently from the one for a two-spool, unmixed flow turbofan, in fact, this template features a booster on the LP spool, just as the reference model. This template can be then easily adapted to the one for a direct-drive turbofan by selecting a value of the gear ratio of the reduction gearbox equal to 1.
As with the template model for a three-spool turboprop of chapter 3, in order to perform design point cycle simulations it is necessary to provide to GasTurb several input quantities, starting from the definition of the operating conditions. Differently from the turboprop case, for a civil turbofan engine the top-of-climb condition is quite commonly the one used to set the dimensions of the engine. This condition, in fact, is the most demanding in terms of speeds and flow [181], and usually drives the size of the fan. Similar choices can be observed in [80][58][31]. Two off-design conditions were also defined, which were used to perform calibrations and to build ad hoc models, to be implemented at design point calculations level, by taking advantage of the possibility provided by GasTurb in terms of custom composed values and iterative cycles definitions. More about this is reported in the next sub sections. All these conditions are summarized in table 4.3, along with the design point one. As it is possible to infer from this table, the operating conditions, at least those of the design and of the cruise off-design point, were included in the set of input variables of the rubber engine model, and they were made to vary in the parametric study described in sub section 4.3.1 for the generation of the surrogate model.
Generally speaking, the quantities reported in 4.4 were selected as the independent variables of the GasTurb-implemented scalable turbofan engine. These variables include both standard input parameters of the GasTurb template, and custom input variables, which were conveniently defined. In this case, only the EIS was considered as a technology factor. In order to set the remaining input quantities required by the GasTurb model, several design laws and equations, including the variables listed in 4.4 and the output provided by cycle simulations as dependent variables, were defined and implemented. In order to ensure the matching between the results provided by these equations and the values of specific GasTurb variables, the already mentioned possibility to define iteration targets was exploited.
The following sub sections provide an overview on the complete set of assumptions, formulas, and iterative processes that were implemented in GasTurb to generate a rubberized turbofan model. Some of these have been already reported in section 3.2.

Table 4.3: List of design and off-design conditions considered for the definition of the turbofan rubber engine model.

Condition	Altitude	Mach number	ISA deviation
Top-of-climb (design point)	33000 - 37000 ft	0.76 - 0.80	+10 K
Cruise	33000 - 37000 ft	0.76 - 0.80	+0 K
Take-off EoR	0 ft	0.20	+15 K
Take-off	0 ft	0.0	+15 K

Table 4.4: List of input variables selected for the turbofan rubber engine model.

Number	Input Variable
1	Bypass ratio
2	Overall pressure ratio
3	Burner exit temperature
4	Flight altitude
5	Mach number
6	Net thrust
7	Take-off EoR net thrust
8	Overboard bleed
9	Power off-takes
10	Entry into service

4.1.1 Pressure ratios

For a turbofan engine configuration such as the one examined, the overall pressure ratio is given by:

$$OPR = PR_{inner\,fan} * PR_{booster} * PR_{HPC} * PL_{comp\,id}, \tag{4.1}$$

where $PR_{\text{inner fan}}$ is the pressure ratio generated by the root of the fan (i.e., the lower portion compressing air for the core of the engine), PR_{booster} is the booster pressure ratio, PR_{HPC} is the high-pressure compressor pressure ratio, and $PL_{\text{comp id}}$ are the pressure losses in the inter-ducts of the compressors group. As reported at the beginning of this section, the engine OPR was selected as one of the main input variables of the model, thus its value has to be considered set.
The HPC pressure ratio is given by the number of stages and by the selected EIS, which sets the single-stage pressure ratio according to the modelling reported in figure 4.3, which was produced starting from a chart included in [78]. This chart, including actual engine data, was adapted by the author in order to include additional data for more recent engines. A quadratic regression was performed on these data, supposing a flat behaviour for future designs. Regarding the number of stages, this was supposed constant and equal to the one of the reference engine. Regarding the inner fan pressure ratio, this may be set according to [181] as a function of the outer fan pressure ratio (i.e., the pressure ratio generated by the portion of the fan compressing air for the fan duct), $PR_{\text{outer fan}}$, by implementing the following formula:

$$PR_{inner\,fan} = 1 + 0.8(PR_{outer fan} - 1). \tag{4.2}$$

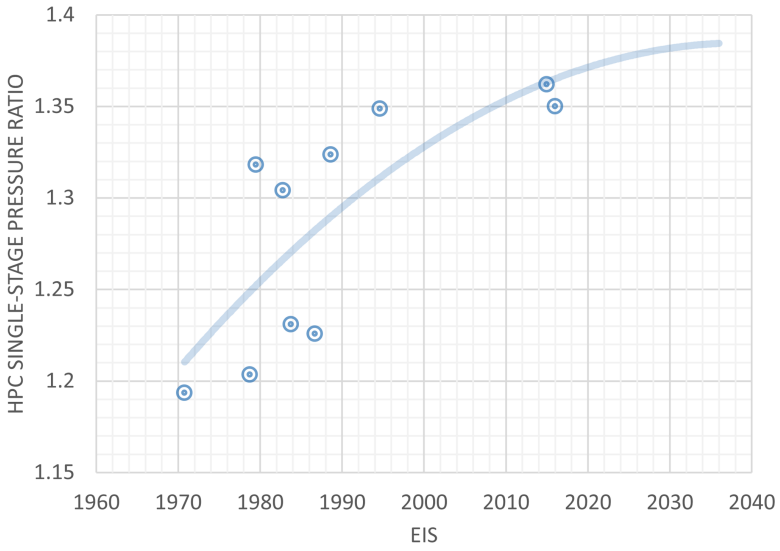

Figure 4.3: HPC single-stage pressure ratio as a function of EIS, adapted from data included in [78].

This equation applies especially for high-bypass ratio turbofan. For low BPR values, the fan root pressure ratio can be assumed equal to the fan tip.
The outer fan pressure ratio was set as an iteration variable in the GasTurb model, in order to match the following target:

$$\left(\frac{V_{18}}{V_8}\right)_{ideal} = \eta_{is,Fan}\ \eta_{is,LPT}, \tag{4.3}$$

in which:

- $(V_{18}/V_8)_{ideal}$ is the ratio between fan and low-pressure turbine speeds for ideal conditions (i.e., they are calculated from a full expansion to ambient pressure);
- $\eta_{is,Fan}$ and $\eta_{is,LPT}$ are the isentropic efficiency of the fan and of the low-pressure turbine, respectively.

In fact, according to [74], in order to get the optimum fan pressure ratio, the ratio between the ideal exhaust velocities must be equal to the product between the isentropic efficiencies of the fan and of the LPT. A similar suggestion is provided in [106] too. The booster pressure ratio was set as an iteration variable in GasTurb in order to match the target overall pressure ratio, assuming that the remaining pressure ratios and pressure losses (for which more details are provided in sub section 4.1.4) were calculated according to the abovementioned equations/assumptions. Differently from the HPC, the number of stages of the booster was not defined as a constant quantity of the model. But instead, it was set as a derived variable, depending on the booster mean stage loading, defined according to the general definition given by equation 3.5. For this quantity a constant value was rather selected, equal to 1.19. Such a value is in line with those reported by [78] for similar engine applications, and was selected after several calibrations performed to match the characteristics of the reference engine in terms of number of stages per component.

4.1.2 Polytropic efficiencies and basic gas path modelling

For the estimation of the polytropic efficiencies of the turbo components of the engine, the approach provided by [78] and reported in section 3.2.2 was adopted.
Equation 3.4 was implemented for the estimation of the polytropic efficiencies of the inner and outer fan (the same value was assumed for both the efficiencies, without the contribution of the size correction, as suggested in [78]), of the booster, of the high-pressure compressor, and of the low-pressure turbine, while equation 3.3 was used for the estimations related to the high-pressure turbine.
With regards to η_{pol}^{***} terms, they were estimated for the high-pressure and for the low-pressure turbines using the lookup tables represented by the charts reported in figure 3.4 and in figure 3.5, respectively. For the elements of the compressors group, similar charts, supported by lookup tables derived by turbomachineries data reported in [78], were implemented in the GasTurb model. These charts are reported in figure 4.4 for the fan, in figure 4.5 for the booster, and in figure 4.6 for the HPC. It must be noted that the one for the fan does not use the component mean stage loading $\overline{\Psi}$ as independent variable but the pressure ratio, more specifically the outer fan pressure ratio. Moreover, it is important to remark that for this implementation, only the EIS was considered as a model input for engine technology level. All the lookup tables for η_{pol}^{***} terms were used assuming a value for f_{tech} equal to 0.5, thus leading to normalized polytropic efficiency values halfway between the boundaries suggested by [78].
Regarding the corrections for RNI, size, and EIS, the same set of equations, assumptions, reference values, and lookup tables reported in section 3.2.2 were adopted also for this implementation. Figure 4.7, figure 4.8, and figure 4.9 provide the representative charts of the lookup tables implemented for the EIS correction of fan, booster, and HPC polytropic efficiencies, respectively.
As already highlighted in section 3.2.2 and summarized in figure 3.9, the application of such a strategy for efficiency estimation requires a basic modelling of the gas path and assumptions on the rotational speeds of the low- and high-pressure spools.
With regards to the first, an approach similar to the one for GENESIS and the turboprop engine model was adopted. Values for Mach number at the entry and at the exit of turbo components were assumed starting from reference data from the literature [78][181][106]. Whereas hub-to-tip ratios were assumed equal to the ones of the reference engine, using cutaway and cross-section images, like the one reported in 4.2, to perform reasonable estimations. As with the turboprop model, all these values were assigned as constant in the GasTurb rubber engine and were not set to be automatically updated in any way. Table 4.5 provides an insight into these values. Since the estimation of the fan normalized polytropic efficiency was based on fan outer pressure ratio rather than mean stage loading, assumptions in this sense were not required here for this component. These were used later instead, for the calculation of the fan diameter and for the estimation of the overall size of the engine nacelle. The fan entry Mach number might seem quite high, with respect to typical values reported in [181] (comprised between 0.55 and 0.65). However, since ToC was selected as the design point condition (which, as already reported before, is the most demanding condition in terms of flow speeds for a turbofan engine), and since [78] provides similar information to those of [181] but for a MCR condition, a value comprised between the maximum suggested for MCR and the upper boundary (0.70) provided by GasTurb was selected. Moreover, several tests were performed in this regard based on public available data for different engines, and these tests provided that only this high Mach number entry values allowed to match both the

expected engine performance and the fan geometry, assuming ToC as design condition. For the estimation of rotational speeds, assumptions based on actual engines data provided by [78] were performed in this case too. A chart relating fan corrected tip speed (i.e., the actual fan tip speed divided by the square root of the fan total entry temperature) and fan outer pressure ratio at MCR condition is given by [78]. Data were taken from this chart and used to build a lookup table, represented in figure 4.10, similarly to what was performed for the normalized polytropic efficiencies. Three plausible quadratic regression curves were assumed from these data, as suggested by [78]. Since the original data were provided for a lower load condition (MCR) than the selected design one (ToC), the curve in the middle of those reported in figure 4.10 was selected as the quadratic regression curve setting the relationship between fan tip speed and pressure ratio. For the rotational speed of the HP spool, instead, information on the average mean diameter circumferential speed, $\overline{U}$, of HPC were taken into consideration in order to set a constant value to be used for all the cycle simulations. This values was set equal to 393 m/s, once it was tested that allowed to match the performance of the reference engine. It must be noted that data on the circumferential speed of components of the compressor group were used to set the rotational speeds of the spools, rather than those of the turbines, for which [78] also provides information. This choice was driven by the consideration that, in a real engine, the rotational speeds of the compressors (booster and HPC) are the ones to be monitored in order to ensure sufficient surge margin and to avoid the stall of the compressors.
Different assumptions were performed in this specific case on the number of stages per component. The approaches for the booster and the HPC have been already outlined in section 4.1.1. Regarding the HPT, a constant value equal to 2 (as for the reference LEAP engine) was assumed. For the low-pressure turbine, instead, an approach similar to the one for the booster and to the one explained in [31] was adopted. A constant value of 5.0 was assumed for the mean stage loading of the LPT, which is in accordance with reference values reported in [78]. Then, the number of stages is calculated starting from equation 3.5, assuming the results coming from the basic sizing of the gas path in terms of mean component diameter, and from the estimation of the rotational speed of the LP spool. Such an approach enables to keep track of the number of stages required by these turbomachineries to match a target mean stage loading, thus a target normalized polytropic efficiency, allowing to eventually discard those configurations requiring a high number of stages, implying both manufacturing issues and an increased impact on the final weight of the engine.
It is relevant to mention that an additional correction was applied to the calculated efficiencies, taking into consideration the fact that the methodology proposed by [78] is based on efficiency estimations performed at typical MCR conditions. In order to apply these corrections, several iterations involving off-design cycle simulations at MCR (performed according to the operating conditions listed in table 4.3) and turbomachineries maps (the default ones provided by GasTurb were assumed) adjustments were performed, in order to match in off-design the polytropic efficiencies returned by the method. These corrective actions were conducted for a specific combination of ToC and MCR thrusts, as well as operating conditions:

- design point thrust equal to 25.0 kN, at Mach 0.78 and 35000 ft flight altitude, ISA deviation +10 K;
- off-design (MCR) thrust equal to 22.3 kN, at Mach 0.78 and 35000 ft flight altitude, ISA deviation +0 K.

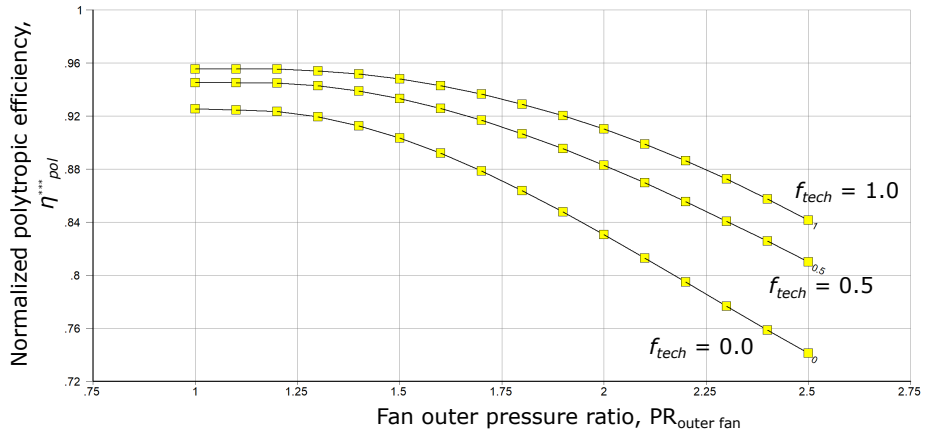

Figure 4.4: Fan normalized polytropic efficiency as a function of the outer fan pressure ratio and technology level, adapted from data included in [78].

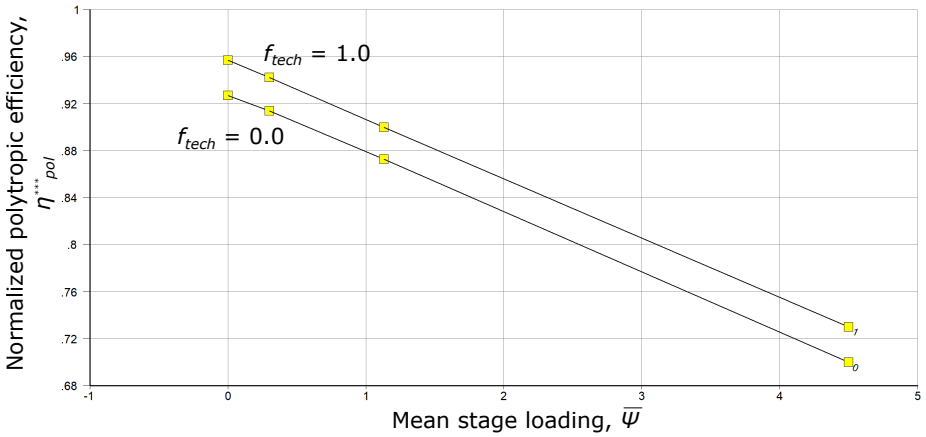

Figure 4.5: Booster normalized polytropic efficiency as a function of the mean stage loading and technology level, adapted from data included in [78].

Despite a more precise approach would have required to determine different corrections for different combinations of net thrust and operating conditions, it was concluded that for the present work such a level of approximation would have been sufficient. Moreover, that combination of thrust requirements and conditions is the same assumed for the reference engine and it is just midway between the upper and lower boundaries selected for the parametric analyses carried out for the generation of the surrogate engine model, thus limiting the impact of this approximation. It is also worth to mention that this corrective strategy could not be applied for the gas turbine engine modelling of GENESIS, due to the limitations on off-design analyses already mentioned in section 3.2.

4.1.3 Cooling air requirements

For the estimation of the required amount of relative cooling air by the two-stage high-pressure turbine (the LPT was not supposed to be cooled, as for the reference engine), the methodology proposed by [75] and already illustrated in section 3.2.3 was selected. However, additional steps were required in this case in order to efficiently implement this approach:

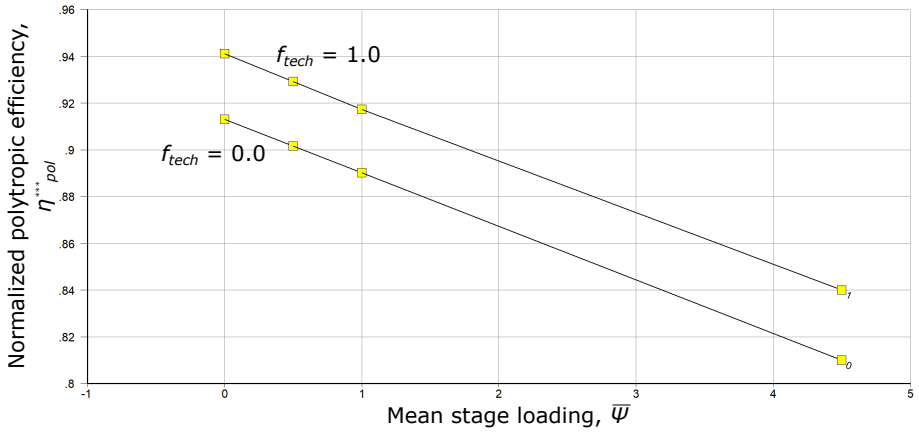

Figure 4.6: HPC normalized polytropic efficiency as a function of the mean stage loading and technology level, adapted from data included in [78].

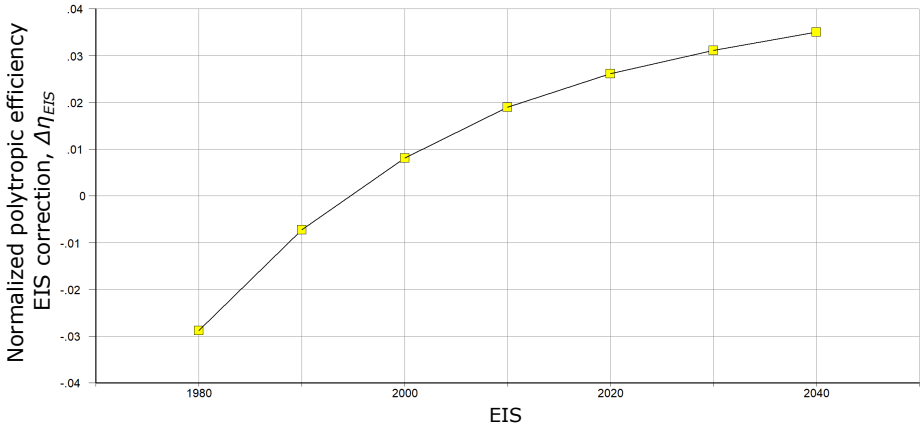

Figure 4.7: Fan normalized polytropic efficiency correction for entry into service, adapted from data included in [78].

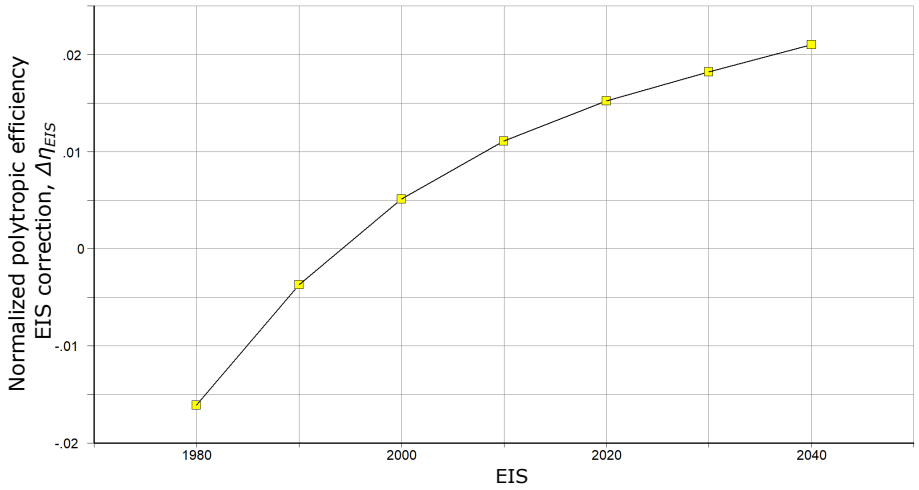

Figure 4.8: Booster normalized polytropic efficiency correction for entry into service, adapted from data included in [78].

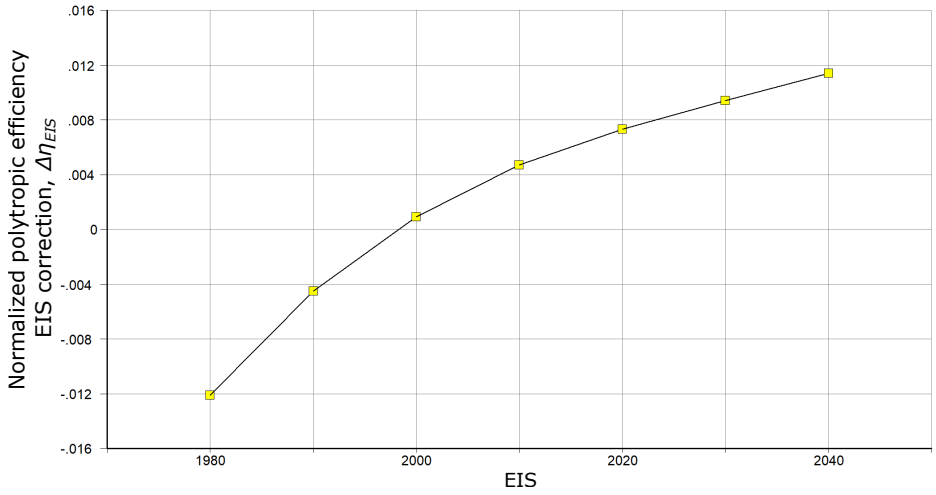

Figure 4.9: HPC normalized polytropic efficiency correction for entry into service, adapted from data included in [78].

Table 4.5: Mach number and hub-to-tip ratio assumptions for the turbomachineries of the GasTurb-implemented rubber engine model.

Location	Mach number	Hub-to-tip ratio
Fan entry	0.68	0.268
Booster entry	0.50	0.843
Booster exit	0.45	0.860
HPC entry	0.45	0.450
HPC exit	0.30	0.908
HPT entry	0.20	0.807
HPT exit	0.30	0.800
LPT entry	0.30	0.865
LPT exit	0.40	0.650

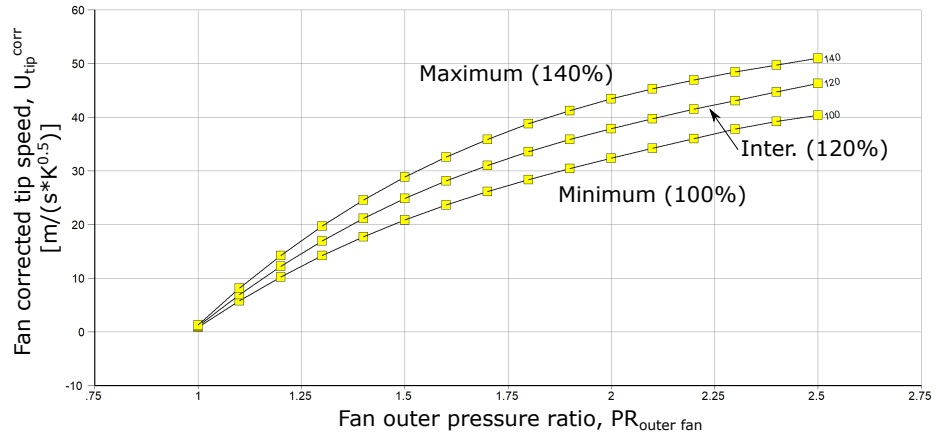

Figure 4.10: Fan corrected tip speed as a function of fan outer pressure ratio, adapted from data included in [78]. The intermediate curve (120 %) was selected for the turbofan rubber engine model.

- The design point selected for the turbofan application was ToC, which is not the typical condition at which the highest temperatures are reached by the engine. Most usually, MTO is the most demanding operating condition in this sense, at least for not extremely high BPR values (below 14/15:1). This particular result was tested by performing design point analyses with GasTurb, using the implemented scalable turbofan model and by including specific off-design calculations at design point (which is a possibility provided by this tool, even if only for graphical output).
- GasTurb implements an *equivalent* single-stage model of the HPT, while it was supposed that the reference engine and all the engine design points produced by the GasTurb-implemented rubber turbofan featured a two-stage high-pressure turbine.

In order to overcome the first issue, several calculations involving iterations between design point and off-design were performed, assuming for the latter the operating conditions for take-off EoR (the most demanding condition in terms of engine temperatures) listed in table 4.3. For different combinations of the variables listed in table 4.4 at design point, an initial assumption was performed on the relative cooling air requirement of the stator and of the rotor for the equivalent single-stage HPT model implemented by GasTurb. Then off-design calculations were performed (using the calibrated maps adjusted for polytropic efficiencies, as illustrated in section 4.1.2) and actual relative cooling air requirements were calculated in an Excel sheet, using the methodology proposed by [75] and the output data provided by GasTurb in terms of:

- T_3, which is the temperature of the cooling air;
- T_4, the burner exit temperature;
- $T_{4.1}$, the stator outlet temperature of the equivalent single-stage model;
- $T_{4.4}$, the high-pressure turbine exit temperature;
- $\dot{m}_{25}$, the mass flow rate at the entry of the high-pressure compressor;
- $\dot{m}_4$, the mass flow rate at the entry of the high-pressure turbine.

To solve the second issue, an *actual* $T_{4.1}$ was calculated in the Excel file, by using the following equation suggested by [102]:

$$h(T_{4.1}^{actual}) = \frac{\dot{m}_4 h(T_4) + \dot{m}_{s1}^{cool} h(T_3)}{\dot{m}_4 + \dot{m}_{s1}^{cool}}, \tag{4.4}$$

in which h is the enthalpy, and takes into account the mixing of the *actual* first HPT stage stator cooling air, $\dot{m}_{s1}^{cool}$, with the turbine entry mass flow, $\dot{m}_4$. The correct estimation of this *actual* stator cooling air was one the main objectives of this iterative process involving design point and off-design calculations, as well as the estimation of the remaining three contributions to the total cooling air:

- $\dot{m}_{r1}^{cool}$, first HPT stage rotor cooling air;
- $\dot{m}_{s2}^{cool}$, second HPT stage stator cooling air;
- $\dot{m}_{r2}^{cool}$, second HPT stage rotor cooling air.

For these quantities, first try values were provided in terms of their ratio with respect to HPC entry mass flow rate, which where then successively updated as iterations went on. For the estimation of the hot gas temperature at the entry of the second stage of the HPT, a simplified approach based on the calculation of an intermediate temperature was used:

$$T_{4.2} = \frac{T_{4.1}^{actual} + T_{4.4}}{2}. \tag{4.5}$$

Then equation 4.4 was applied again, this time for the calculation of the entry temperature to the rotor of the second stage of the HPT, $T_{4.21}$:

$$h(T_{4.21}) = \frac{\dot{m}_{4.2} h(T_{42}) + \dot{m}_{s2}^{cool} h(T_3)}{\dot{m}_{4.2} + \dot{m}_{s2}^{cool}}, \tag{4.6}$$

in which $\dot{m}_{4.2}$ is given by:

$$\dot{m}_{4.2} = \dot{m}_4 + \dot{m}_{cool}^{s1} + \dot{m}_{cool}^{r1}. \tag{4.7}$$

In order to convert the multi-stage cooling air calculated with the process described above to the single-stage model implemented by GasTurb, the approach suggested in [161] and derived from [102] was adopted. This conversion is based on the concept of work potential per turbine grid. These work potentials are provided for three different turbine layouts in table 4.6. For the case here examined, the values reported in the second column were used and the equivalent stator and rotor cooling air were calculated as follows:

$$\dot{m}_{cool}^{s,eq} = \dot{m}_{cool}^{s1} + 0.5\dot{m}_{cool}^{r1} + 0.5\dot{m}_{cool}^{s2}, \tag{4.8}$$

$$\dot{m}_{cool}^{r,eq} = 0.5\dot{m}_{cool}^{r1} + 0.5\dot{m}_{cool}^{s2} + \dot{m}_{cool}^{r2}. \tag{4.9}$$

A total of 576 calculations involving design point and off-design T/O EoR simulations were performed, by carrying out a full-factorial parametric study based on the set of variables listed in table 4.7. This contains all variables set at design point condition, with the exception of the T/O EoR thrust requirement, which was used to set the target thrust for the off-design simulations. Nevertheless, this quantity was later adopted as an additional input variable of the rubber engine model, by setting up a dedicated custom input parameter, allowing to estimate the required amount of cooling air starting from design point conditions. The variables of table 4.7 were carefully selected after a sensitivity analysis, which was performed in order to detect which input parameters of table 4.4 were the most impacting ones in terms of T/O EoR off-design results.
The information provided by this parametric study in terms of:

- equivalent HPT stator cooling air $\dot{m}_{cool}^{s,eq}$,
- equivalent HPT rotor cooling air $\dot{m}_{cool}^{r,eq}$,
- T/O EoR HPC total exit temperature T_3^{EoR},
- T/O EoR burner exit temperature T_4^{EoR},
- and T/O EoR LPT turbine entry temperature T_{45}^{EoR},

were used to train five linear regression models, by using the same tool described in section 3.5. Of these five models, the ones for cooling air were directly implemented in

Table 4.6: Coefficients applied for the conversion of cooling air from multi-stage to the equivalent single-stage model of GasTurb. Table adapted from [161].

Cooling air share	**1-stage**	**2-stage**	**3-stage**
Stator 1	100 %	100 %	100 %
Rotor 1	0 %	50 %	66 %
Stator 2	-	50 %	66 %
Rotor 2	-	0 %	33 %
Stator 3	-	-	33 %
Rotor 3	-	-	0 %

Table 4.7: Set of rubber model input variables involved in the parametric study for the estimation of cooling air requirements.

Variable	**Range**	**Values**
Entry into service	2015 - 2040	3
Bypass ratio	10.0:1 - 14.0:1	3
Overall pressure ratio	45.0:1 - 60.0:1	4
Burner exit temperature, K	1700 - 1900	3
Overboard bleed, kg/s	0.0 - 0.85	2
Design point net thrust, kN	22.0 - 25.0	2
T/O EoR net thrust, kN	93.85 - 100.0	2
Total	-	**864**

the GasTurb rubber turbofan model, in order to perform prediction on off-design cooling requirements based on input parameters provided at design point. The remaining three models on off-design temperatures were instead saved for later, to be added to the set of linear equations of the surrogate engine model, in order to allow checks on engine feasibility based on assumed thermal limitations per component and EIS. Table 4.8 provides more information on the results of this training. The adopted nomenclature for these models is the same of section 3.5.
With regards to the assumptions on materials and cooling air technology for the application of equations 3.12 and 3.15, a simpler approach with respect to the one presented in section 3.2.3 was adopted in this case. Table 4.9 provides reference values for maximum allowable material temperatures and c_{cool} for three representative EIS. These values were selected based on the same reference data reported in 3.2.3. Differently from the model for the turboprop gas turbine, no mapping between temperatures and specific turbine materials was performed. Moreover, a higher allowable metal temperature was supposed

Table 4.8: Results of the training for the models for T/O EoR relative cooling air and maximum temperatures.

Output variable	**Regression model**	**Terms**	**RMSE**
$\dot{m}_{cool}^{s,eq}/\dot{m}_{25}$	Linear	Interaction	$4.779*10^{-3}$
$\dot{m}_{cool}^{r,eq}/\dot{m}_{25}$	Linear	Interaction	$2.734*10^{-3}$
T_3^{EoR}, K	Linear	Interaction	0.6973
T_4^{EoR}, K	Linear	Interaction	3.4059
T_{45}^{EoR}, K	Linear	Quadratic	3.5181

Table 4.9: Input for maximum allowable material temperature and cooling factor of equation 3.12, adopted for the modelling of cooling air requirements.

Variable	EIS 2015	EIS 2030	EIS 2040
T_M stator	1260	1320	1350
T_M rotor	1200	1260	1290
c_{cool}	1.050	1.000	0.975

for the stator with respect to the rotor blades, as suggested in [75]. Regarding the cooling factor, an improvement with respect to EIS was supposed, based on reference data for typical cooling concepts provided in [75].

4.1.4 Miscellaneous input variables

In order to set duct pressure losses, typical values suggested in [181] were mainly used. Differently from the model described in chapter 3, these losses were not linked to any input variable or technology factor. Instead, constant values were assumed, not depending on the EIS. These values are summarized in table 4.10. The only exception in this sense is represented by the pressure loss in the bypass duct. In this case, typical boundary values suggested by [181] for this quantity were used to generate a relationship with respect to the outer fan pressure ratio. According to [80], in fact, it is reasonable to assume that engine with higher outer fan pressure ratios show higher bypass duct pressure losses, since the air flows with much higher speed thorough the duct. Values of 1.6 and 2.2 were selected as lower and upper boundary, respectively, of the fan outer pressure ratio at ToC, starting from data of real engines reported in [78]. By linking these values to the lower and upper boundary of bypass duct pressure losses provided by [181] and by reasonably assuming null losses for fan pressure ratio equal to 1.0, the following quadratic relationship was derived:

$$PL_{bypass\ duct} = -0.0139 PR_{outer\ fan} + 0.0778 PR_{outer\ fan} - 0.0639. \tag{4.10}$$

The burner efficiency was modelled according to the same approach presented in section 3.2.4, while the values presented in table 4.11 were adopted to model the burner pressure ratio with respect to the EIS. These values were suggested by a related chart reported in [78], which allows to assume a trend for slight improvements over the years. Differently from the turboprop model of chapter 3, more optimistic values reported in the above-mentioned chart of [78] were taken as reference to perform assumptions on this quantity, which explains differences in this sense.
With regards to spools mechanical efficiencies, a constant value of 0.999, suggested by [181] for ball and roller bearings, was assumed for all EIS.
Concerning nozzle characteristics, a model based on the fitting of real engine data provided by [78] was preferred over the automatic calculation provided by GasTurb. This model, elaborated by [161], allows the estimation of the nozzle thrust coefficients, C_F, and discharge coefficients, C_{Dis}, starting from nozzle pressure ratio values. As explained in [161], these thrust and discharge coefficients allow to, respectively:

- take into account effective jet velocity at the exit of a nozzle with respect to ideal jet velocity;
- consider the reduction of the nozzle exit area due to flow separation.

Table 4.10: Constant values of pressure losses adopted for the modelling of the rubber turbofan engine.

Losses	Value
Intake pressure loss	0.5 %
Compressor duct pressure loss	1.0 %
Turbine duct pressure loss	0.5 %
Turbine exit duct pressure loss	0.5 %

Table 4.11: Burner pressure ratios of the rubber turbofan model selected for representative EIS.

	EIS 2015	EIS 2030	EIS 2040
Burner pressure ratio	0.970	0.975	0.980

From the fitting curves provided by [161] for both cold (bypass) and hot (core) nozzles, four models were extracted and implemented in the turbofan rubber engine. The equations of these models, together with the adapted fitting curves of [161], are given in figure 4.11 and figure 4.12.

4.1.5 Dry mass calculation

The weight of the propulsive system is a crucial parameter when it comes to compare similar engine designs in terms of fuel consumption and overall size, due to the snowball effect it generates at aircraft level. For a turbofan configuration such as the one examined in this chapter, the parameters most influencing the final weight of the engine, for a given target thrust, are the bypass ratio, the overall pressure ratio, and the turbine entry temperature. Rising the bypass ratio while keeping the remaining parameters constant implies increased engine overall size, thus increased engine weight. Higher overall pressure ratios require more booster/HPC stages, which in turn increases the mass of these components. Higher turbine entry temperatures deliver a beneficial effect on the size of the core of the engine, and on the overall mass of the propulsive system, as a consequence.
The literature on this topic does not provide too many semi-empirical formulations allowing to take into account all the previously listed parameters for a preliminary estimation of the weight of the engine. The method presented by [154], based on a modification of the formulation provided by [167], actually allows to take into account all these quantities, but, as highlighted by [150], provides contradicting results for high-bypass ratio engines. In fact, according to this method, for constant turbine entry temperature, OPR, and thrust requirement, increasing the bypass ratio leads to lighter engines, which is inconsistent with information provided by [181].
Component-based approaches, such as the one proposed by [111], would allow to take into account several engine design parameters for a preliminary weight estimation of the gas turbine. However, they also require a much more detailed definition of the geometry of the turbomachineries, and additional assumptions on the characteristics of compressors/turbines blades, vanes, disks, etc., which goes too far with respect to the basic gas path modelling implemented by the GasTurb model, as described in sections 3.2.2 and 4.1.2.
As suggested by [150], a good compromise between semi-empirical, single- and multi-

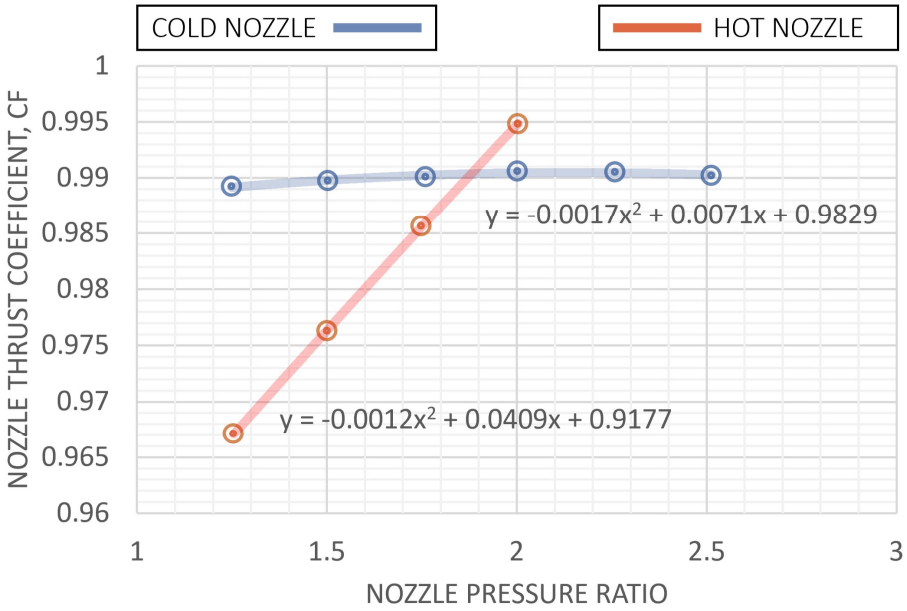

Figure 4.11: Implemented models for hot and cold nozzle thrust coefficients with respect to nozzle pressure ratio, adapted from [161].

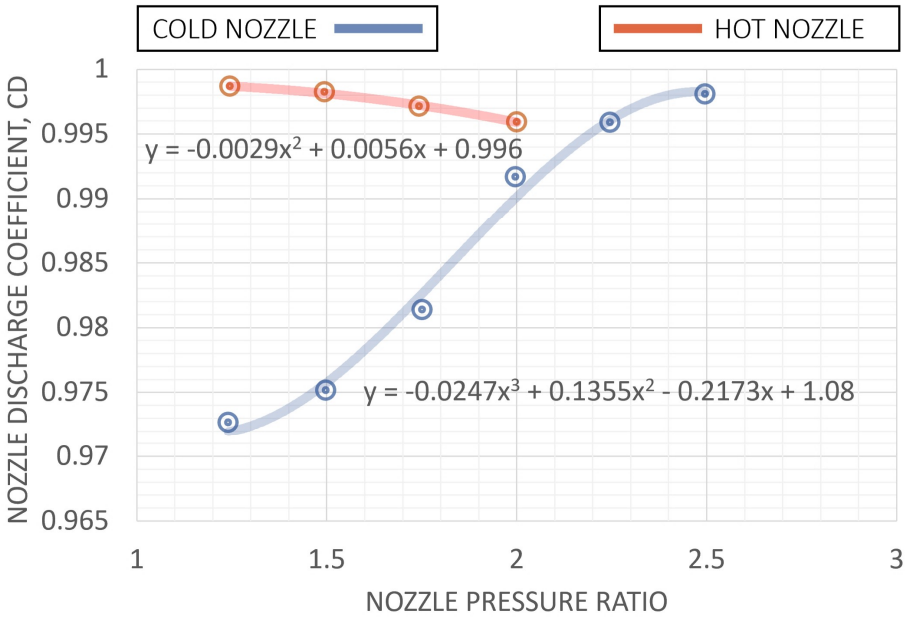

Figure 4.12: Implemented models for hot and cold nozzle discharge coefficients with respect to nozzle pressure ratio, adapted from [161].

input equations and component-based approaches could be represented by the set of equations provided by [141]. These equations provide the possibility to perform engine weight predictions based on characteristics at SL static take-off in terms of bypass ratio, overall pressure ratio, and core entry mass flow rate, for both direct-drive and geared turbofan engines and for different assumptions on the technology level. These equations were prepared by first performing hundreds of cycle simulations (performed with NPSS[1], an advanced tool for the modelling of propulsive systems) matched by gas turbine weight estimations (carried out with WATE++[2], a tool for component-based engine weight predictions developed by Boeing for NASA). The results of these simulations in terms of engine weight were used to perform a regression, in order to generate a fast and easy-to-use parametric model, similar in this sense to the ones provided by well-known aircraft design textbooks, but based on simulations rather than only empirical data. For a direct-drive configuration, the engine dry weight, expressed in lb, can be calculated as follows:

$$W_{dry} = a \left(\frac{\dot{m}_{core}}{100} \right)^{b} \left(\frac{OPR}{40} \right)^{c}, \tag{4.11}$$

in which $\dot{m}_{core}$ is the core entry mass flow rate, in lb/s, and the coefficients a, b, and c are given by:

- For a low technology level (as suggested by [141], EIS up to 2005):

$$a = 1.809 * 10^{1} BPR^{2} + 4.769 * 10^{2} BPR + 701.3, \tag{4.12}$$

$$b = 1.077 * 10^{-3} BPR^{2} - 3.716 * 10^{-2} BPR + 1.190, \tag{4.13}$$

$$c = -1.058 * 10^{-2} BPR + 0.326; \tag{4.14}$$

- For assumption on improved/lighter materials usage (EIS from 2005 onwards):

$$a = 1.538 * 10^{1} BPR^{2} + 4.011 * 10^{2} BPR + 631.5, \tag{4.15}$$

$$b = 1.057 * 10^{-3} BPR^{2} - 3.693 * 10^{-2} BPR + 1.171, \tag{4.16}$$

$$c = -1.022 * 10^{-2} BPR + 0.232, \tag{4.17}$$

Before being adopted, it was tested that these equations provided reasonable results in terms of engine weight changes dictated by modifications to the abovementioned parameters. All the expected effect were observed, as exemplified in figure 4.13.
In order to enable the use of these equations for the modelling of the dry mass of the rubber turbofan engine, an additional step was required. As already mentioned above, the application of these formulas requires that input parameters are provided at SL static take-off condition, which is different from the design point condition selected for the rubber engine and from which cycle output data are derived. For this purpose, a preliminary parametric study, like the one for the cooling air requirements, was carried out. This parametric study involved off-design cycle simulations at the abovementioned

[1] https://www.swri.org/consortia/numerical-propulsion-system-simulation-npss
[2] https://software.nasa.gov/software/LEW-19687-1

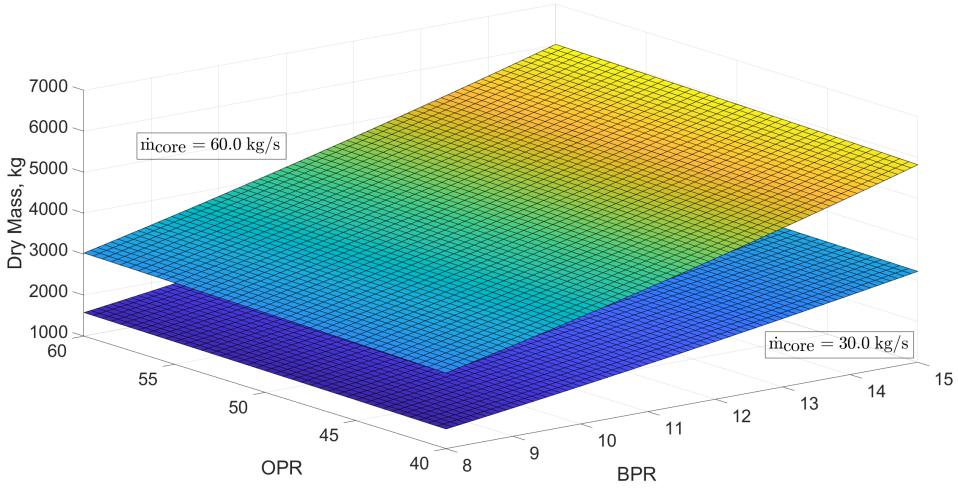

Figure 4.13: Results obtained from the application of equation 4.11 assuming the usage of advanced materials and two different values of core entry mass flow rate.

Table 4.12: Set of input variables of the rubber engine involved in the creation of the regression models for weight-related off-design parameters.

Variable	**Range**	**Values**
Entry into service	2015 - 2040	3
Bypass ratio	8.0:1 - 14.0:1	7
Overall pressure ratio	45.0:1 - 60.0:1	4
Burner exit temperature, K	1550 - 1900	6
Overboard bleed, kg/s	0.0 - 0.85	2
Power off-takes, kW	0.0 - 120.0	2
Design point net thrust, kN	22.0 - 28.0	2
T/O EoR net thrust, kN	88.0 - 100.0	2
Total	-	**8064**

take-off condition for different combinations of input parameters at design point. The complete list of input parameters adopted for this analysis is provided in table 4.12, along with information on the range of variation and on the number of values used for each variable. These off-design analyses took advantage of both the maps scaling for efficiencies, reported in section 4.1.2, and the implemented model for a more precise estimation of the cooling air demand, described in section 4.1.3.
After that results were collected from these parametric analyses, they were used to train three separate linear regression models, by using the dedicated tool of MATLAB. The results of this training are reported in table 4.13. It is important to remark that, as with the off-design temperatures of section 4.1.3, these linear regression models were not implemented in GasTurb, but were kept for later, to be included in the surrogate engine model of JPAD.
Dealing with the estimation of the weight of the propulsion system and of the nacelles, no further assumptions were performed or additional methodologies were researched with respect to those reported in section 2.1 and already implemented by JPAD.

Table 4.13: Results of the training for the models of BPR, OPR and core entry mass rate at SLS condition, for the application of the selected weight prediction method.

Output variable	Regression model	Terms	RMSE
BPR SLS	Linear	Interactions	0.0867
OPR SLS	Linear	Interactions	0.1702
$\dot{m}_{core}$ SLS, kg/s	Linear	Interactions	1.4538

4.1.6 Main dimensions estimation

The following three main parameters were taken into account in order to determine the overall size of the engine and of the nacelle:

- the fan diameter,
- the maximum nacelle fan cowl diameter,
- and the nacelle fan cowl length.

The estimation of the first was carried out with the help of GasTurb at design point calculation level. GasTurb, in fact, allows to perform the design of the fan if the following information are provided:

- Fan tip speed, whose estimation was already implemented by the rubber engine model thanks to the chart reported in figure 4.10.
- Fan inlet Mach number, which was kept constant in the present modelling and equal to 0.68, following the assumptions reported in section 4.1.2 regarding the gas path sizing.
- Fan inlet hub-to-tip ratio, for which a value of 0.268, equal to the one of the LEAP-1A, was assumed and kept for all the analyses.

With these information set, the fan tip diameter is an output of the thermodynamic cycle simulation at design point.
For the estimation of the nacelle maximum diameter, an approach similar to the one suggested in [150] was adopted. It is reasonable to assume that this diameter is strictly related to the fan dimensions through a linear relationship. In [97], for example, the following equation is suggested:

$$D_{max,nac} = 1.21 D_{fan}, \tag{4.18}$$

where $D_{max,nac}$ is the maximum transverse dimension of the nacelle, and D_{fan} is the fan tip diameter. However, it was tested already by [150] that this equation tends to return slightly underestimated values, and for this reason a dedicated study was performed, which provided the results reported in table 4.14. In light of these data, a calibration equal to 1.30 was adopted for this diameter with respect to fan size. For the calculation of the fan cowl length, the following equation provided by [161] was considered in the first place:

$$\frac{L_{nac}}{D_{max,nac}} = 0.95 PR_{outer\ fan} - 0.09, \tag{4.19}$$

in which $L_{nac}/D_{max,nac}$ is the ratio between the nacelle cowl length and the maximum nacelle diameter. However, it was observed that this equation provided quite similar

Table 4.14: Reference ratios between maximum nacelle fan cowl diameter and fan size, adapted from [150].

Engine	$\mathbf{D_{max\ nac}/D_{fan}}$
GE Aviation CF6-50	1.33
CFM International CFM56-3	1.34
GE Aviation CF34-10	1.51
GE Aviation GE90	1.29

Table 4.15: Set of assumptions for the remaining geometric parameters of the nacelle.

Variable	**Value**
D_{in}	1.0*D_{fan}
D_{out}	0.8*D_{fan}
$X_{max,nac}$	0.3*L_{nac}
Z_{out}	0.0

values of L_{nac} for different combinations of design point input parameters. Moreover, the results were quite distant from expected values when tested against known data. For this reason, the equation provided by [97] was preferred:

$$L_{nac} = 2.36 D_{fan} - 0.01 (D_{fan} M_{MO})^2, \tag{4.20}$$

in which M_{MO} is the maximum operating Mach number, that in the actual implementation of the surrogate rubber turbofan engine in JPAD was supposed to be related to the cruise Mach number through a constant scale factor, equal to 1.05. All lengths in the previous equation are expressed in inches.
Dealing with the remaining geometric parameters of a typical nacelle reported in figure 2.4, constant fraction with respect to the main parameters listed above were selected, reflecting usual turbofan nacelle characteristics. These values are reported in table 4.15.

4.1.7 Costs-related estimations

The set of equations already described in section 3.2.7 was used in order to estimate development costs, production costs, and development time of turbofan engines designed with the GasTurb-implemented rubber engine model. No adjustments were applied to the methodology of [191] in this case in order to obtain more reasonable results: it was tested that the values produced by the equations for costs were fairly close to those expected for reference engines. Neither corrections were applied for technology level, but just calibrations for cumulative inflation rate were accounted. For the estimation of engine price starting from engine production costs, a reasonable 30 % profit margin per engine sold was assumed.

4.1.8 Engine limitations

In order to further ensure the feasibility of the engines designed by means of GasTurb (and later by the surrogate engine model), a set of thermal and mechanical limitations was defined, to be used as boundary values for the related quantities provided by the application of the rubber engine model, allowing to eventually discard borderline/extreme

Table 4.16: Speed limitations assumed for the turbo components of the turbofan engine model.

Component	Variable	Upper boundary
Fan	U_{hub}	180 m/s
Fan	U_{tip}	500 m/s
Compressors	U_{hub}	400 m/s
Compressors	U_{tip}	500 m/s
High-pressure turbine	U_{hub}	400 m/s
High-pressure turbine	AN^2	$30*10^6$ rpm^2m^2
Low-pressure turbine	U_{hub}	350 m/s
Low-pressure turbine	AN^2	$50*10^6$ rpm^2m^2

Table 4.17: Maximum allowable temperatures assumed for the modelling of the turbofan engine.

Temperature	EIS 2015	EIS 2030	EIS 2040
T_3, K	950	1000	1020
T_4, K	2000	2050	2070
$T_{4.5}$, K	1260	1320	1350

solutions.
Table 4.16 provides limitations in terms of maximum allowable circumferential speeds at the hub and at the tip of turbo components. Moreover, upper boundaries are also provided in terms of AN^2 at the last stage of the high-pressure and low-pressure turbines. These reference values were mainly gathered from [78] (using analogous charts to those already mentioned in section 3.2.8) and from [181]. As with the ones for the gas turbine of the turboprop model, no correlation with respect to EIS was supposed.
Upper boundary values for the total temperatures at the exit of the HPC, T_3, at the exit of the combustion chamber, T_4, and at the entry of the low-pressure turbine, $T_{4.5}$, were collected too, using information from [117],[161], and [75]. These values are reported in table 4.17. It should be noted that:

- These maximum allowable temperatures were supposed functions of the EIS, due to the greater (at a lower cost) availability of high-performance materials and to the evolution of cooling air concepts.
- Limitation to the maximum temperature reachable by the last stages of the HPC was supposed in this case, due to the much higher (more than three times with respect to the reference turboprop engine of chapter 3) overall pressure ratios supposed for the turbofan engine model.
- The values assumed as upper boundaries over EIS of the LPT entry total temperature correspond, as it should be, to the maximum allowable metal temperature values of the first-stage stator of the HPT, reported in the first row of table 4.9.

4.1.9 Emissions

Implementation of emissions estimation for the species listed in section 2.1.1 was carried out in this way:

- NO_x EI estimation is performed using results provided by GasTurb at design point in terms of S_{NO_x}, calculated according to equation 3.22. This value is then multiplied by a scaling factor (depending on the combustion chamber technology, as explained in section 3.2.9) to obtain the emission index of NO_x.
- The calculation of emission indices for pollutant species such as CO and HC is carried out according to the methodology developed by [69] and already illustrated in section 3.2.9, using this time fitting equations specific to turbofan engines. This methodology requires just data in terms of engine SLS OPR and fuel flow rate at different operating settings to be applied, which are all information available from the scaling of a reference engine deck according to the output coming from a surrogate engine model, as it will be shown in section 4.3.
- Finally, constant values (i.e., independent of the characteristics of the engine and of the ambient conditions) are assumed for the EIs of CO_2, H_2O, and SO_2, which are reported in table 3.12.

4.1.10 Noise

The methodology proposed in [177] and already described in section 2.2 (in the paragraph dedicated to the modelling of engine noise for ATTILA++) was adopted in order to carry out a preliminary estimation of the environmental noise produced by the fan. Although it is not the only contribution to the overall noise produced by the engine (which also includes the contribution of jet noise, LPT, and combustor), it is still the most significant one, as highlighted by the noise simulations for certification reported in [68].
The list of input parameters required by this method to be effectively applied is reported in table 2.5. In addition to geometric parameters, which might be assumed equal to the ones for a reference engine (this is the strategy adopted, for example, for the analyses of section 4.4), several thermodynamic input variables are also required. These can be easily estimated with GasTurb, since are all included in the set of output quantities provided at the end of cycle calculations. However, the operating point selected for the design condition, ToC, substantially differs from the operating conditions of the engine during aircraft noise certification, which for civil jet applications such as the ones examined are approach/landing and take-off. In order to overcome this issue, two different approaches could be adopted:

- Perform several off-design analyses at operating conditions similar to those typical during aircraft noise certification, involving different combinations of input variables at design point, in order to generate surrogate models (one for each off-design condition representative of noise certification) of those thermo-fluid dynamic parameters required by the fan noise method of [177]. This is the same strategy adopted, for example, for the calculation of cooling air, and for the modelling of off-design variables required by the equations selected for the estimation of engine dry mass.
- Adopt a simplified strategy, based on scale factors for fan temperature rise, fan rotational speed, and engine entry mass flow rate, allowing to reasonably calibrate these parameters for an operating condition different from ToC and closer to noise certification.

In this case, in order to save time for testing, the second approach was adopted.
SL T/O, Mach 0.2, ISA +10 was selected as the representative off-design condition for

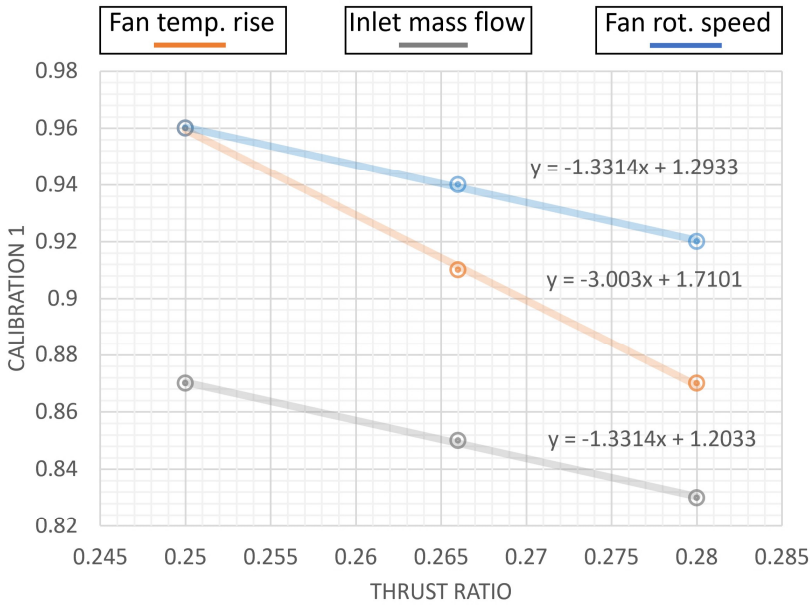

Figure 4.14: Set of calibration laws with respect to design/off-design thrust ratio for fan temperature rise, fan rotational speed, and engine entry mass flow rate, for a simplified estimation of fan noise at certification conditions.

noise certification to be used to perform the necessary analyses for the definition of the abovementioned scale factors. An engine with characteristics in terms of design BPR, OPR, and T_4 similar to those of the reference turbofan model and generated through the GasTurb-implemented rubber engine was adopted for these analyses. Three different values of thrust ratio (i.e., the ratio between the design net thrust requirement and the thrust required for the previously mentioned off-design point) were initially investigated: 0.250, 0.266, and 0.280. With these three values, three different linear regressions, one for each of the abovementioned variables to be scaled, were derived. These are reported in figure 4.14, and are meant to be applied for full-throttle settings.
In order to allow also the simulation of lower load conditions, which might be used for approach and flyover cutback noise simulations, three additional laws for linear scaling were derived, by using the possibility provided by GasTurb for the off-design mode to perform operating line calculations, simulating different throttle settings. These are reported in figure 4.15, and are supposed to be used together with the scaling factors provided by the previous equations, in order to define the actual calibrations.
These calibrations can then be conveniently used in order to generate, together with the application of the methodology of [177], and the output coming from GasTurb design point simulations for the rubber turbofan model, a noise engine deck like the one required by ATTILA++ for aircraft noise analyses including the contribution of the propulsive system, which was described in section 2.2.1.
It is important to remark that this approach, as well as those for the calculation of engine weight, engine and nacelle size, costs, and emission indices (excluded S_{NO_x}), were not implemented in the GasTurb rubber engine model, but the cycle output variables required by these methods were adequately mapped, as it will be shown in section 4.3.1.

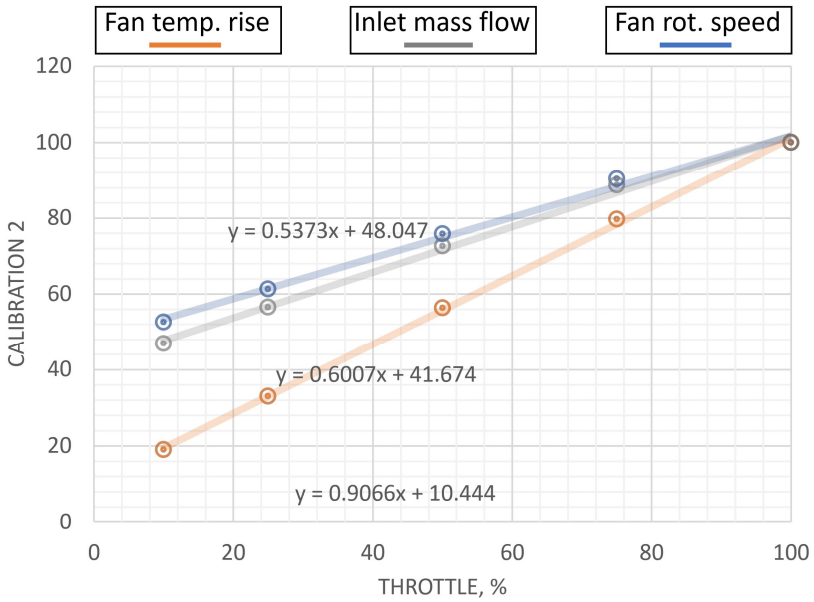

Figure 4.15: Set of calibration laws with respect to off-design throttle setting for fan temperature rise, fan rotational speed, and engine entry mass flow rate, for a simplified estimation of fan noise at certification conditions.

4.2 Validation and testing

4.2.1 Validation against existing engines data

In order to validate the rubber turbofan engine model, once implemented in GasTurb by means of the set of equations reported in the previous sections, it was tested against available information on the reference model, the LEAP-1A. The main characteristics of this engine in terms of performance, weight and dimensions were retrieved from sources already cited in section 4.1. Table 4.1 and 4.3 provided an insight on these numbers. In addition, the analysis performed by [65] was considered in order to have a check on those parameters of the engine for which it was not possible to retrieve any direct information from the manufacturer or from certification documents.
Table 4.18 provides the values that were adopted for the main input parameters of the rubber turbofan model. Top-of-climb, with Mach number equal to 0.78, flight altitude equal to 35000 ft, and ISA +10, was selected as the design point condition. In order to match the characteristics of the reference engine in terms of fan diameter, the burner exit temperature was set as an iteration variable. For the thrusts (ToC, cruise, and T/O EoR) the reference values reported in table 4.2 were selected. These were used to perform off-design analyses in GasTurb. With regards to power off-takes and overboard bleed, assumptions based on the results provided by the approaches illustrated in section 3.3 and in section 2.3.3, respectively, and essentially based on the design passengers number of the reference aircraft, were adopted.
Table 4.19 collects main results of this analysis. Unless otherwise specified, the results reported in this table refer to the design point condition. The first thing to notice is that the cruise SFC falls exactly in the range provided by [65]. As reported in this reference, this value may seem slightly higher than expected, especially if compared with information provided by other sources [99]. However, these references usually do not

Table 4.18: Set of selected main input values of the rubber engine model for the validation against known data and performance of the LEAP-1A engine model.

Input variable	**Value**	**Source**	**Notes**
Entry into service	2016	[42]	Introduced on the A320neo
Bypass ratio	11.0:1	[93]	Assumed equal to the cruise value
Overall pressure ratio	50.0:1	[93]	-
Burner exit temperature	-	-	Iterated to match target fan diameter
Net thrust	25.0 kN	[51]	Set according to the assumption reported in table 4.2
T/O EoR net thrust	93.85 kN	[51]	Set according to the assumption reported in table 4.2
Overboard bleed	0.85 kg/s	-	Calculated according to the approach reported in section 3.3
Power off-takes	59 kW	-	Calculated according to the approach reported in section 2.3.3

take into account the contribution to higher fuel consumption given by power off-takes and overboard bleed. This estimated value is in line with declaration of the engine manufacturer in terms of fuel consumption advantage with respect to previous generation engines: -15 % SFC with respect to CFM56 series [93], for which a cruise SFC between 0.60 and 0.65 lb/(lbf*h) can be assumed [65]. Moreover, this SFC estimation was also checked with preliminary engine design experts of MTU, during activities related to the author's internship, who considered such a result reasonable for this engine.
The design burner exit temperature was not arbitrarily assumed, but was a result of the calculation. The value returned by the DP simulation is in line with the technology trend provided by [150] (which in turn adapts data taken from [81]) for this parameter. Moreover, the design T_4 was included in the set of input and output variables that were checked with MTU experts for this validation activity. In this case too, the result was considered reasonable.
The cooling air regression model allowed to correctly predict the amount of relative air required by the HPT at T/O EoR condition: a 24 % value was obtained for this quantity, matching the estimation of [65].
All the speed limitations listed in section 4.1.8 were sufficiently satisfied, and the same goes for the maximum temperatures. With regards to the T/O EoR T_4, [65] also provides an estimated value, which is not too distant from the one calculated with the GasTurb model. It must be noted that the off-design temperatures of table 3.15 were not predicted by means of the regression models of section 4.1.3, but were directly checked by performing an off-design calculation. However it was later tested that the surrogate models did return quite the same values.
With regards to main engine dimensions, the equations and the assumptions of section 4.1.6 produced results reasonably close to the actual values. While for the dry mass, which was estimated using equation 4.11 and the surrogate models for SLS T/O BPR, OPR, and core mass flow, the number obtained is close to the upper boundary of the assumed interval provided in [10].
The last row of table 3.15 provides a comparison in terms of engine price. According to available information, the engine list price should be comprised between 7.3 (loss indicated by GE Aviation for each canceled order of 2020 [82]) and 14.5 (derived from [43], by dividing the total fleet value by the number of engines) US M$. The two estimated engine prices reported in this table were calculated:

Table 4.19: Design point cycle direct output, off-design variables and derived variables for the LEAP-1A engine, using the GasTurb-implemented rubber engine model.

Output variable	**Value**	**Expected value**	**Source/Note**
SFC (cruise), g/(kN*s)	15.52	15.01 - 15.86	[65]
T_4, K	1800	-	Iterated to match D_{fan}
$PR_{outer\ fan}$	1.51	≈ 1.5	[65]
$PR_{booster}$	1.64	≈ 1.5	[65]
$\dot{m}_{cool}/\dot{m}_{25}$, %	24 %	> 20 %	[65]
Booster stages	3	3	[10][93]
LPT stages	7	7	[10][93]
Fan tip speed (EoR), m/s	400	< 500	Limit from table 4.16
LPT AN^2 (EoR), rpm^2m^2	$14*10^6$	$< 50*10^6$	Limit from table 4.16
LP spool speed (EoR), rpm	3865	3894	[10]
HP spool speed (EoR), rpm	19340	19391	[10]
T_3 (EoR), K	930	< 950	Limit from table 4.17
T_4 (EoR), K	1865	< 2000; ≈ 1820	Limit from table 4.17; [65]
$T_{4.5}$ (EoR), K	1180	< 1260	Limit from table 4.17
D_{fan}, m	1.98	1.98	[93]
$D_{max,nac}$, m	2.58	2.60	[20]
L_{nac}, m	3.64	3.55	[20]
W_{dry}, kg	3148	2990 - 3153	[93]
Engine list price, M$ US	6.4 - 15.5	7.3 - 14.5	[82][43]

- Using equation 3.19 (with input coming from regression models for off-design burner exit temperature and dry mass), assuming a 2.11 % inflation rate (average US dollar inflation rate during the last two decades), 2016 EIS, and 30 % profit margin.
- Using equation 3.18, with the same assumptions reported above.

It can be seen that these values well suits the interval assumed from the previously cited references.
It is clear from the previous validation that, for most of the characteristics of the engine, experts' analyses were considered in order to assess the correctness of the results, to overcome the lack of real engine data available in the open literature. This is a remarkable problem, especially for newer engines. Sometimes actual engine data may be available from testbed analyses [104][28][115], but even in this case the amount of information would not be sufficient to perform the validation of a simulated engine for the whole flight envelope. What would be actually required in this case is an engine deck software, as described in [183]. But this is proprietary information from the engine manufacturer, which is rarely or never shared with the public. Even if this thesis was, at least in part, carried out under the supervision of engine experts from MTU, no actual engine data could be disclosed. However, as already mentioned before, the results of the previous validation activity were shared and checked with industry specialists, who assessed that the main results in terms of specific fuel consumption, operating temperatures, and cooling air requirements were aligned with their expectations.
To further validate the rubber engine model implemented in GasTurb, three additional analyses were performed, based on the known characteristics of the following engine models: the CFM56-5B4 produced by CFM International, the GE90-94B produced by GE Aviation, and the CF34-10E, also produced by GE. The first engine is in the same

thrust class (27000 lbf/120 kN) of the engine used for the previous validation. The other two are in different thrust classes: the GE90-94B model produces 97000 lbf/430 kN in SLS T/O conditions, while the CF34-10E engine 20000 lbf/90 kN. In this case too, information about the characteristics of the engines were collected from sources such as TCDS, manufacturer's brochure, aero engines encyclopedias, literature and internet databases. For some variables, reasonable assumptions were performed starting from the data available for engines with similar characteristics or installed on similar aircraft. Off-takes, overboard bleed, nacelle main dimensions, weight, and costs were all estimated using the methodologies described in the previous sections.
The results of these additional validations are provided in tables 4.20, 4.21, and 4.22. Unless specified otherwise, input and output values of the cycle refer to the ToC, i.e., design, condition. The plot reported in [81] was used in order to reasonably determine the highest turbine entry temperature of the engines and the design T_4, as a consequence. Main assumptions regarding the geometry (hub-to-tip ratios, essentially) were updated by using cutaways and drawings, thus taking into account actual characteristics of the abovementioned engines. For the engine list price, intervals were produced by using equations 3.18 and 3.19, and corrections for inflation rate and for profit margin (30 %) were applied as well.
For the CFM56-5B4 engine model (table 4.20), much of the data (both input and reference values for checks) was assumed starting from [51]. For climb and cruise conditions, a Mach number equal to 0.8 and a flight altitude equal to 35000 ft were considered. In addition, a deviation from ISA temperature equal to 10 K was assumed for climb. Overall, the results produced by the rubber engine model are pretty much in agreement with the data collected from the available literature. The highest difference can be detected in terms of engine dry mass, even though the result is not too far off (less than 10 %). The cruise specific fuel consumption lies in the interval suggested in [65], and it is also pretty close to the value reported in [51]. The method selected for costs also provides predictions which are in line with expectations.
Table 4.21 provides results for the CF34-10E engine. In this case, it was not possible to retrieve from the available literature direct information on the thrust values for the three selected conditions. However, reasonable values were assumed starting from those for engines for similar aircraft applications (in terms of MTOW) reported in [96]. The ambient conditions reported in [25], Mach number equal to 0.8 and flight altitude equal to 35000 ft, were adopted for cruise and climb. An ISA +10 K deviation was also assumed in this case for the design point condition. It can be observed that the cruise SFC value is perfectly in agreement with the one reported by the reference. The value obtained for the entry mass flow rate is not in line with the reference values, but it must be observed that the interval included in table 4.21 was determined starting from data reported in [51] for engines of the same family. Noticeable differences can be observed in terms of maximum nacelle diameter and engine dry mass. The first one can be easily linked to having assumed a constant scale factor with respect to the fan diameter, which does not take into account additional variables that may have an impact on the external shape of the nacelle. While the second one can be attributed to limitations of the adopted methodology.
The results of the analysis for the GE90-94B engine are reported in table 4.22. For the cruise and climb thrusts, similar considerations to the ones reported above for the CFM engine apply. In this case, in particular, reasonable assumptions were performed starting from the information included in [51] for engines of the same family. With regards to the ambient conditions, a flight altitude equal to 35000 ft and a Mach number of 0.84

Table 4.20: Main input variables, design point cycle direct output, off-design variables and derived variables for the CFM56-5B4 engine, using the GasTurb-implemented rubber engine model.

Input variable	**Value**	-	**Source/Note**
EIS	1994	-	[51]
ToC net thrust, kN	25.04	-	[51]
Cruise net thrust, kN	22.33	-	[51]
T/O net thrust, kN	120.1	-	[51]
BPR	5.7	-	[51]
OPR	32.6	-	[51]
Output variable	**Value**	**Expected value**	**Source/Note**
SFC (cruise), g/(kN*s)	17.27	16.99 - 18.41; 16.98	[65]; [51]
$\dot{m}_2$ (SLS T/O), kg/s	408.6	408.2	[51]
Fuel flow (SLS T/O), kg/s	1.057	1.142	[8]
Booster stages	4	4	[9]
LPT stages	5	5	[9]
Fan tip speed (EoR), m/s	444	< 500	Limit from table 4.16
LPT AN^2 (EoR), rpm^2m^2	$1.7*10^6$	$< 50*10^6$	Limit from table 4.16
LP spool speed (EoR), rpm	4903	5200	[9]
HP spool speed (EoR), rpm	15633	15183	[9]
T_4 (EoR), K	1677	1660 - 1670	[81]
D_{fan}, m	1.73	1.73	[51]
$D_{max,nac}$, m	2.25	2.30	Assumed from [20]
L_{nac}, m	3.30	3.33	Assumed from [20]
W_{dry}, kg	2251	2456	[9]
Engine list price, M$ US	4.1 - 6.33	5.83 - 6.25	Assumed from [51]

Table 4.21: Main input variables, design point cycle direct output, off-design variables and derived variables for the CF34-10E engine, using the GasTurb-implemented rubber engine model.

Input variable	**Value**	-	**Source/Note**
EIS	2005	-	[25]
ToC net thrust, kN	22.01	-	Assumed from [96]
Cruise net thrust, kN	20.56	-	Assumed from [96]
T/O net thrust, kN	90.57	-	[15]
BPR	5.4	-	[25]
OPR	29	-	[25]
Output variable	**Value**	**Expected value**	**Source/Note**
SFC (cruise), g/(kN*s)	18.32	18.13	[25]
$\dot{m}_2$ (SLS T/O), kg/s	255	278 - 335	Assumed from [96]
Fuel flow (SLS T/O), kg/s	0.96	0.87	[8]
Booster stages	3	3	[15]
LPT stages	4	4	[15]
Fan tip speed (EoR), m/s	431	< 500	Limit from table 4.16
LPT AN^2 (EoR), rpm^2m^2	$1.9*10^6$	$< 50*10^6$	Limit from table 4.16
LP spool speed (EoR), rpm	6123	6325	[15]
HP spool speed (EoR), rpm	17887	18018	[15]
T_4 (EoR), K	1733	1750	[81]
D_{fan}, m	1.35	1.35	[25]
$D_{max,nac}$, m	1.76	2.03	Assumed from [60]
L_{nac}, m	2.70	2.72	Assumed from [60]
W_{dry}, kg	1338	1700	[25]
Engine list price, M$ US	5.05 - 7.81	6.84	Assumed from [26]

Table 4.22: Main input variables, design point cycle direct output, off-design variables and derived variables for the GE90-94B engine, using the GasTurb-implemented rubber engine model.

Input variable	**Value**	**-**	**Source/Note**
EIS	2000	-	[51]
ToC net thrust, kN	86	-	Assumed from [51]
Cruise net thrust, kN	82.56	-	Assumed from [51]
T/O net thrust, kN	432.8	-	[14]
BPR	5.4	-	[164]
OPR	29	-	[164]
Output variable	**Value**	**Expected value**	**Source/Note**
SFC (cruise), g/(kN*s)	15.79	15.6	[38]
$\dot{m}_2$ (SLS T/O), kg/s	1484	1361 - 1483	Assumed from [51]
Fuel flow (SLS T/O), kg/s	3.351	3.513	[8]
Booster stages	3	3	[14]
LPT stages	6	6	[14]
Fan tip speed (EoR), m/s	390	< 500	Limit from table 4.16
LPT AN^2 (EoR), rpm^2m^2	$9.8*10^6$	$< 50*10^6$	Limit from table 4.16
LP spool speed (EoR), rpm	2258	2456	[14]
HP spool speed (EoR), rpm	9835	10918	[14]
T_4 (EoR), K	1785	1770	[81]
D_{fan}, m	3.12	3.12	[164]
$D_{max,nac}$, m	4.07	3.96	Assumed from [33]
L_{nac}, m	4.39	5.03	Assumed from [33]
W_{dry}, kg	7989	7893	[14]
Engine list price, M$ US	6 - 9.31	15 - 16	Assumed from [51]

were assumed for these operating point, as suggested by [164]. Like above, an ISA deviation of +10 K was considered for the ToC point. The results reported in table 4.22 show an overall agreement in terms of all the meaningful variables. The only exceptions are represented by the nacelle cowl length and by the engine price. The difference in terms in nacelle cowl maximum length may be linked to inaccuracies in the estimation of the actual value: this, in fact, was roughly estimated starting from aircraft drawings reported in [33]. With respect to the engine price, this is probably due to limitations of the implemented methodology for production costs, which is essentially based on statistical data for military engines, and does not cover aero engines characterized by such high values of dry mass.
The previous analyses have demonstrated that the rubber engine model does not only produce reasonable results for the LEAP-1A reference engine, but it can be actually used to perform competitive assessment of existing engines, once provided with the required set of input information.

4.2.2 In-depth analysis of effects

In order to perform a further check on the results produced by the rubber engine model implemented in GasTurb, and by the set of surrogate models and equations adopted to define quantities not directly provided by this tool, several analyses were performed by assuming different combinations of values for the input parameters of table 4.4, allowing to ensure that the engine behaviour with respect to these changes was in accordance with what expected. The results of these analyses, mainly in terms of contour plots, are

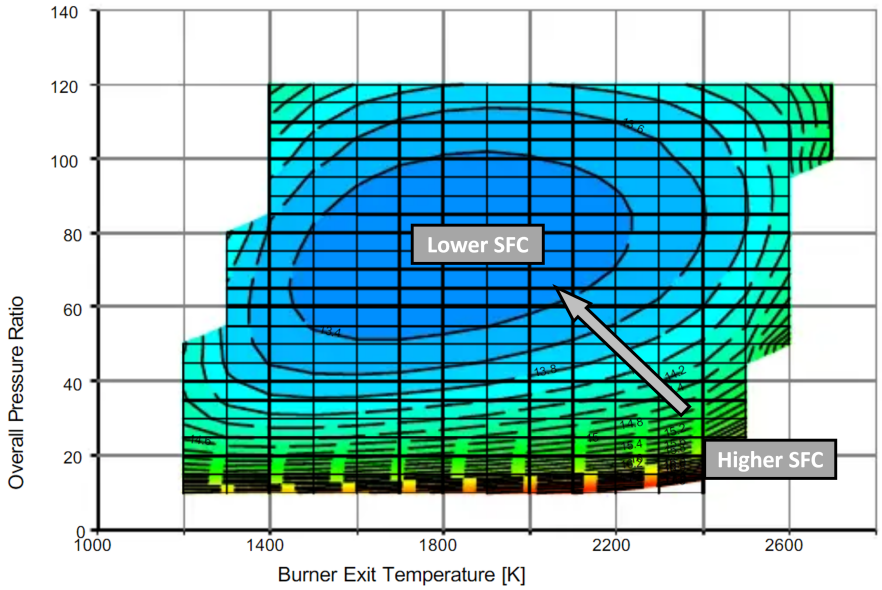

Figure 4.16: Specific fuel consumption of a turbofan engine at cruise condition for constant propulsive efficiency. Adapted from [103].

reported in section 6, in order to ease their commenting in this sub section.
Figures 6.1, 6.2, and 6.3 provide an overview on the effect of design BPR and T_4 on the ToC SFC, fan diameter, and engine dry mass, respectively. As it can be deduced from the first contour plot, the BPR has always (i.e., independently of the T_4 value) a beneficial effect on the specific fuel consumption. On the opposite, increasing the design burner exit temperature for a selected BPR value always determines an increment of the SFC. This is not so surprising considering the analyses reported in [103] and whose results are reproduced in figure 4.16, which suggest that increasing T_4 with constant OPR does not necessarily lead to lower fuel consumption. On the other hand, 6.2 and 6.3 tell that for a fixed bypass ratio value, increasing the design burner exit temperature leads to lower dry mass and lower fan diameter, which would require to carry out dedicated trade-off analyses in order to assess, at aircraft level, which design choices are the best. Moreover, possible restrictions to the available design space dictated by thermal, mechanical, and manufacturing limitations, as the ones reported in section 4.1.8, should be always considered.
Figure 6.4 provides a contour plot similar to the one of figure 6.1, but assuming a design OPR value equal to 50:1, rather than 45:1. From the comparison of these two figures it is possible to deduce, as expected, the beneficial effect of greater OPR values on the fuel consumption. However, at least for the examined EIS, this effect is quite small, also due to the negative effect of greater HPC exit total temperature on the total amount of cooling air required by the HPT at T/O EoR condition. Figures 6.5 and 6.4, on the other hand, provide example of the effect of the OPR on the NO_x emissions. For the second plot, an increased OPR (50:1 instead of 45:1) is assumed. An average 20 % increase can be estimated from their comparison.
Figure 6.7 and figure 6.8 allow to show the effect of different assumptions in terms of engine EIS on specific fuel consumption and engine dry mass. As expected, the improvement in terms of polytropic efficiencies and HPT cooling technology and materials allows to progressively improve the performance of the engine in terms of fuel consump-

tion. These improvements also allow to reduce the core entry mass flow rate, thus the dimensions of the core, and the weight of the engine, once assumed the remaining characteristics of the engine.
Figures from 6.9 to 6.12 allow to highlight the effect of different assumptions regarding the power off-takes on the engine fuel consumption and on the dry mass. As expected, the request of additional off-takes has a detrimental effect on the SFC. For 100.0 kW of additional off-takes, an average 2.0 % increment can be deduced from the contour plots of figure 6.9 and figure 6.10, which is not far distant from the 1.57 % calibration suggested by MTU for the activities related to ADORNO. With regards to the engine dry mass, a slight increment can be observed, which is expected from a physical point of view: with all the remaining parameters constant, the core mass flow must increase in order to compensate the additional request of power. However, the observed increment from these plots is quite constant, for different combinations of design BPR and T_4 at least, and far from the calibration (the same cited above) used for ADORNO. But it is necessary to remark that calibration was intended for the powerplant system weight, rather than for the dry weight of the engine, which might explain this difference.
A similar analysis is reported in figures from 6.13 to 6.18, in which the effect of overboard bleed is highlighted. As expected, the increase of overboard bleed determines a significant raise of consumed fuel: +4 to +7 % per 1.0 kg/s, depending on the values of the remaining design variables. The increase in terms of core entry mass flow determined by a request for overboard bleed, assuming all the remaining input design variables constant, has a detrimental effect on the dry weight of the engine too, as highlighted by figure 6.15 and figure 6.16. The same effect also explains the growth of the fan diameter illustrated by figure 6.17 and figure 6.18. Finally, figures 6.19, 6.20, 6.21, and 6.22 allow to show the impact of different choices in terms of design point net thrust on the weight and size of the engine. In order to minimize the effect of the T/O EoR net thrust on the results provided by the implemented surrogate model for the relative cooling air demand, variations in terms of DP net thrust were tightly linked to those of the abovementioned off-design thrust: a constant ratio between the two, equal to 0.255, was selected for this comparative analysis. As expected, both the dry mass and the fan diameter grow for increasing thrust demand. And for both of them, this increase does not depend on the specific combination of DP BPR and T_4.

4.3 Implementation

The next sub sections provide an insight into the actions that were performed in order to generate, from the rubber engine model for a turbofan implemented in GasTurb, a surrogate, mathematical model that could be actually implemented in a preliminary aircraft design framework. Moreover, information are provided on the integration process in this framework.

4.3.1 Surrogate model generation

To generate the surrogate engine model, the same steps and tools described in section 3.5 were adopted. The motivations that led to the decision of such an approach are the ones already mentioned in the same section.
The dataset to be used for the training of linear regression models was generated with a full-factorial parametric study, involving the input quantities of the rubber engine model previously implemented in GasTurb listed in table 4.23. All the input variables

Table 4.23: Set of input variables, with related lower and upper boundary values, adopted for the full-factorial parametric study for the generation of a surrogate model of the rubber engine.

Input variable	Lower boundary	Upper boundary	Values
Bypass ratio	8.0:1	14.0:1	7
Overall pressure ratio	45.0:1	60.0:1	4
Burner exit temperature, K	1550	1900	8
Flight altitude, ft	33000	37000	3
Mach number	0.76	0.80	3
Net thrust, kN	22.0	28.0	3
T/O EoR net thrust, kN	88.0	100.0	3
Overboard bleed, kg/s	0.0	0.85	3
Power off-takes, kW	0	120	3
Entry into service	2015	2040	3
Total	-	-	**489,888**

in this table are to be intended at design point (ToC) condition, with the exception of the T/O EoR net thrust, which was used by the regression model for cooling air demand implemented in GasTurb in order to correctly estimate the actual operating temperatures of the engine in off-design conditions and the relative cooling air flow. In order to match the target design point net thrust, the engine corrected entry mass flow rate was set as an iteration variable, and for this reason it was an output of the analyses. Different assumptions on EIS impacted on the estimated values of efficiencies of the turbo components, on the efficiency of the burner, and on the assumptions regarding the maximum allowable metal temperatures of turbine materials (therefore on the total amount of relative cooling air and on the HPT polytropic efficiency).
With regards to output variables (at design point) provided directly by the GasTurb analyses, the following were monitored and included in the final dataset for the training of linear regression models of the surrogate engine:

- For the estimation of performance and emissions, the values of SFC and S_{NO_x} provided by different combinations of input variables of table 4.23 were tracked;
- In order to allow the evaluation of the overall size of the engine/nacelle, values of fan diameter were included in the training dataset;
- Fan temperature rise, entry mass flow rate, and tip Mach number values were collected as well, in order to allow an initial assessment of fan/engine noise, according to the simplified approach explained in section 4.1.10;
- To enable the possibility to perform checks on the feasibility of engines produced with the illustrated approach, the number of stages required by the booster and by the LPT (in order to match target mean stage loading values), the hub and tip circumferential speeds of turbines and compressors, as well as AN^2 values for HPT and LPT last stages, were monitored too and incorporated in the training dataset.

For each of the abovementioned quantities, a different linear regression model was trained, using the dedicated MATLAB tool. Table 4.24 provides information on the actual model adopted for each variable, and on the performance in terms of RMSE.

Table 4.24: Results of the training for the surrogate turbofan engine model to be implemented in JPAD. Performance and characteristics of regression models for maximum temperatures and weight estimations have been already reported in table 4.8 and in table 4.13, respectively.

Output variable	Regression model	Terms	RMSE
SFC, g/(kN*s)	Linear	Quadratic	0.1207
S_{NO_x}, g/kg	Linear	Quadratic	0.0023
Fan diameter, m	Linear	Quadratic	0.0098
Outer fan exit temperature, K	Linear	Quadratic	0.3827
Fan entry mass flow rate, kg/s	Linear	Quadratic	2.4283
Fan tip Mach number	Linear	Quadratic	0.0104
Fan hub circumferential speed, m/s	Linear	Quadratic	0.5634
Fan tip circumferential speed, m/s	Linear	Quadratic	0.7890
Booster hub circumferential speed, m/s	Linear	Quadratic	0.7765
Booster tip circumferential speed, m/s	Linear	Quadratic	0.8921
HPC hub circumferential speed, m/s	Linear	Quadratic	0.6570
HPC tip circumferential speed, m/s	Linear	Quadratic	0.9299
HPT hub circumferential speed, m/s	Linear	Quadratic	1.0234
HPT AN^2, $rpm^2m^2/10^6$	Linear	Quadratic	0.2156
LPT hub circumferential speed, m/s	Linear	Quadratic	0.6619
LPT AN^2, $rpm^2m^2/10^6$	Linear	Quadratic	0.1567

To the previous list of output variables it is necessary to add two more sets, for which values were not actually derived from GasTurb cycle simulation output at design point. Instead, these variables are returned by the previously elaborated regression models, which were not included in the set of equations of the rubber engine of GasTurb in order to save space for the definition of other necessary composed values[3], since their calculation would have not added any significant information to the GasTurb cycle simulations. These quantities are:

- The maximum temperatures T_3^{EoR}, T_4^{EoR}, and T_{45}^{EoR} at off-design condition, which add to the set of output variables monitored to check engine feasibility;
- The values of BPR, OPR and core mass flow rate at T/O SLS condition, which allow to perform engine dry mass calculation according to the set of equations included in section 4.1.5.

Information on these regression models have been already provided in table 4.8, for the temperatures, and in table 4.13, for the weight-related parameters.

4.3.2 Integration in JPAD

The integration of the surrogate engine model illustrated in the previous section in the UNINA preliminary aircraft design framework of JPAD, described in section 2.1, was performed by coding and including an additional calculation tool, specifically dedicated to preliminary turbofan engine sizing.

[3]GasTurb 11 allows the definition of a limited amount of composed values (up to 99) and iteration targets (not more than 20).

The main objective was to allow the users of JPAD to define the characteristics of the engine in terms of performance, emissions, weight, dimensions, noise, and costs by providing a limited amount of information, mostly related to the desired characteristics of the engine at design point (which was supposed to be always ToC) and to the expected EIS. For this reason, an additional attribute was included in the input XML file of JPAD dedicated to the engine (*engine.xml*) allowing to select whether the information on the engine and on the nacelle had to be retrieved directly from their dedicated input XML files, or had to be assumed starting from estimations performed with the surrogate engine model. In this last case, the data on the engine and on the nacelle included in the input files would have been completely bypassed.
Table 4.25 provides an overview on the complete set of input variables that can be provided to define the characteristics of a turbofan engine starting from the surrogate rubber model, as implemented by JPAD. In this table, input variables are distinguished based on their field of action, and information are provided in terms of interaction with the other modules of JPAD.
For input parameters setting engine operating conditions at design point (ToC), the possibility to automatically set them to conditions provided in the aircraft analysis input files of JPAD in terms of target cruise Mach number and flight altitude (supposing a flat cruise) is provided.
A similar option is given for the setting of engine overboard bleed and power off-takes at design point. With regards to the first, it can be automatically set using information included in the JPAD input file of the cabin in terms of design passengers number (by following the same basic approach described in section 3.3), and in the input file of airframe technologies for the OBS architecture (e.g., in case of bleed-less system architecture, the overboard bleed is automatically set to null). The same goes for the power off-takes, with base on-board system requirements estimated with the approach described in section 2.3.3 and based on passengers number and OBS architecture, and with additional off-takes for advanced systems, such as hybrid laminar flow control, used to determine a calibration to be applied on engine dry mass as well as on SFC, but only for those flight phases for which these advanced systems are supposed to be operative (i.e., cruise).
In order to allow JPAD to carry out aircraft performance and emissions analyses using results coming from the surrogate engine model, a simple strategy based on the scaling of a reference engine deck, based on the same formatting illustrated in section 2.1.1, was implemented.
This reference engine deck was produced with GasTurb, starting from the design point for an engine model similar to the one described in section 4.2, characterized by main design input parameters (e.g., BPR, OPR, T_4, and ToC net thrust) with intermediate values with respect to the lower and upper boundaries adopted for the full-factorial parametric analysis of the surrogate model, in order to make this engine deck the most representative possible of the behaviour, especially in off-design condition, of all the engines produced by the surrogate model. Off-design analyses were performed adopting the scaled components maps of section 4.1.2, and using the values reported in table 4.2 as target net thrusts for the main engine ratings. Only for the cruise setting, operating line simulations were performed, allowing to include the effect of different throttle settings in addition to those of Mach number, flight altitude and ISA deviation. For the calculations related to the idle rating, since no reference thrust values could be assumed, the approach suggested by [183], and based on the definition of a limiter for the rotational speed of the HPC, was adopted.
Then a simplified approach for the scaling of this reference engine deck was implemented

by the new calculation tool of JPAD for engine preliminary design. In particular:

- **Climb rating** - All the thrust values (i.e., for each combination of Mach number, flight altitude, and ISA deviation) are scaled based on the ratio between the design point net thrust request and the engine deck net thrust value, for the same ambient conditions of the design point. This allows to have, at design point condition, the value of engine net thrust specified in the surrogate model input file. The same applies to SFC and S_{NO_x}, which makes sure that the output values of the surrogate model in terms of specific fuel consumption and NO_x emissions are set in the reference engine deck, for the assumed set of design point ambient conditions.

- **Cruise rating** - The same scale factors of climb for thrust, fuel consumption, and emissions are applied to the cruise rating. Moreover, in case the user has requested to automatically estimate engine power off-takes and the aircraft is equipped with advanced airframe systems such as HLFC, an additional scaling is applied to the SFC, which takes into account the effect of additional off-takes. This effect is estimated directly through the surrogate engine model, by assuming the same input parameters but applying two different values of off-takes.

- **Take-off rating** - Engine thrust is scaled based on the ratio between the T/O EoR request and the value provided by the reference engine deck for the same ambient conditions. For SFC and S_{NO_x}, instead, the same scale factors of climb are used.

With regards to the remaining emission indices that can be managed through the JPAD engine deck, no scaling is performed, but values are eventually (i.e., if the user has requested it) calculated with the methodology of [69] or assumed according to the reference values of [62]. Fuel flow can be estimated from the scaled engine deck for different flight conditions, using information on the specific fuel consumption and on the net thrust. Then the correlations of [69], together with the information on the engine SLS OPR, can be used to determine EIs for CO and HC.
An approach based on an engine dataset was implemented for noise estimations too. As already mentioned in section 4.1.10, the methodology proposed in [177] was implemented by the new engine pre-design module of JPAD. By making use of the simplified approach reported in section 4.1.10, an engine noise deck with the same formatting reported in figure 2.13 can be produced and provided to ATTILA++, in order to perform aircraft noise analyses at certification conditions including reasonable contribution of the engine.
With regards to the remaining characteristics of the engine, all the equations presented in the previous sections for the estimation of weight, main dimensions, and costs were implemented by the JPAD engine pre-design module. The results provided by these equations were linked to the other modules of JPAD, dealing with the geometry, the weight, and the analysis on costs of the aircraft.
Last but not least, checks on limitations (speeds and temperatures) were included as well in this new module. At the end of each aircraft analysis involving the use of this engine surrogate model, an output Excel file is produced, providing both a recap on the main results coming from the engine preliminary design, and a list of warnings, dealing with output control parameters potentially exceeding the abovementioned limitations. Moreover, these warnings are collected by the Java classes of JPAD implementing the surrogate engine, and can be used by the analysis modules to exclude unfeasible engine designs during aircraft iterative design loops.
The next section will provide several test cases, in which this module was used in com-

bination with the other modules of JPAD dealing with the characteristics and the performance of the aircraft.

Table 4.25: List of input parameters required by the surrogate turbofan engine model implemented by JPAD.

Field	Input	Type	Description
Cycle	BPR	Double	The bypass ratio at design point (ToC) condition.
	OPR	Double	The overall pressure ratio at design point (ToC) condition.
	T4	Double	The burner exit temperature at design point (ToC) condition.
	Mach number	Double	The Mach number at design point (ToC) condition. An additional boolean attribute is provided, allowing to assume this quantity from information included in the input file of operating conditions of JPAD in terms of (flat) cruise target Mach number.
	Flight altitude	Double	The flight altitude at design point (ToC) condition. An additional boolean attribute is provided, allowing to assume this quantity from information included in the input file of operating conditions of JPAD in terms of (flat) cruise target flight altitude.
	ToC net thrust	Double	The design (ToC) net thrust
	T/O EoR net thrust	Double	The target net thrust for off-design T/O EoR condition
	Overboard bleed	Double	The overboard bleed of the engine. An additional boolean attribute is provided, allowing to assume this quantity starting from information included in the input cabin file in terms of design passengers number, and in the input file of airframe technologies in terms of OBS architecture (e.g., bleedless or not).
	Power off-takes	Double	The engine power off-takes. An additional boolean attribute is provided, allowing to assume this quantity starting from information included in the input cabin file in terms of design passengers number, and in the input file of airframe technologies in terms of OBS architecture.
Technology	EIS	Integer	The supposed entry into service of the engine.
	S_{NO_x} scaling	Double	The supposed NO_x severity index scaling, based on assumptions on combustion chamber technology.
Emissions	NO_x	Boolean	Boolean variable allowing to select whether NO_x EI, estimated with GasTurb, have to be included in the set of data of the scaled engine deck used by JPAD for aircraft performance and emissions assessment.
	CO	Boolean	Boolean variable allowing to select whether CO EI, estimated with the approach of [69], have to be included in the set of data of the scaled engine deck used by JPAD for aircraft performance and emissions assessment.
	HC	Boolean	Boolean variable allowing to select whether HC EI, estimated with the approach of [69], have to be included in the set of data of the scaled engine deck used by JPAD for aircraft performance and emissions assessment.
	CO_2	Boolean	Boolean variable allowing to select whether CO_2 EI, assumed according to average values included in [62], have to be included in the set of data of the scaled engine deck used by JPAD for aircraft performance and emissions assessment.
	SO_2	Boolean	Boolean variable allowing to select whether SO_2 EI, assumed according to average values included in [62], have to be included in the set of data of the scaled engine deck used by JPAD for aircraft performance and emissions assessment.

Table 4.25 continued from previous page

Field	Input	Type	Description
	H_2O	Boolean	Boolean variable allowing to select whether H_2O EI, assumed according to average values included in [62], have to be included in the set of data of the scaled engine deck used by JPAD for aircraft performance and emissions assessment.
Costs	Annual inflation rate	Double	The average annual inflation rate value to be eventually used to scale the results provided by equations 3.16, 3.17, 3.18, and 3.19 (which are based on 2001 data).
	Derivative engine	Boolean	Sets whether the designed engine is a derivative engine or a new centerline engine, allowing a correct estimation of the costs based on the equations provided by [191].
	Full scale test hours	Double	Sets the number of full scale test hours, eventually required for the application of equation 3.17.
Noise	Num. of stator blades	Integer	Sets the number of blades of the fan stator, in order to apply the fan noise method of [177].
	Num. of rotor blades	Integer	Sets the number of blades of the fan, in order to apply the fan noise method of [177].
	Rotor-stator spacing	Double	Sets the fan minimum stator-rotor spacing, according to the definition given in [177].
	Forward attenuation	Double	Sets the noise attenuation due to blade row in the forward arc of the engine, in order to apply the fan noise method of [177].
	Rear attenuation	Double	Sets the noise attenuation due to blade row in the rear arc of the engine, in order to apply the fan noise method of [177].
	Inlet guide vanes	Boolean	Allows to select whether inlet guide vanes are used, in order to apply the fan noise method of [177].

4.4 Aircraft-integrated tests

This section provides several applications of the surrogate turbofan engine model implemented in JPAD. Sub section 4.4.1 provides further validation of this model, by comparing results from its usage for the competitive assessment of the characteristics of the LEAP-1A engine equipped on the A320neo with respect to public available data on the performance of this aircraft. Sub section 4.4.2, instead, deals with the analyses of a hypothetical advanced A320, equipped with both advanced airframe technologies and direct-drive turbofan engines. The objective of these analyses is to highlight the capability of this surrogate engine model to allow both competitive assessment analyses of existing engines and significant trade factor analyses on engine BPR and other key engine design parameters for meaningful aircraft metrics, including emissions, costs, and noise.

4.4.1 A320neo-like aircraft model application

In order to carry out this first analysis, an aircraft similar to the Airbus A320neo was modelled in JPAD. In particular, the -251N variant, equipped with LEAP-1A26 engines (the one for which the surrogate model was validated in section 4.2) was considered in this study. Main information regarding the geometry were retrieved from [20], using charts and plots digitization in order to estimate those quantities not directly provided by this document. These characteristics are reported in table 4.26, whereas figure 4.17 provides both the three-view and the 3D model of this aircraft produced with JPAD.

Table 4.26: Main geometric parameters of the A320neo-like aircraft modelled in JPAD in order to perform test analyses of the surrogate engine model. Data related to the powerplant geometry already included in table 4.19.

Description	Value	Unit
Fuselage		
Overall length	37.570	m
Height	4.141	m
Width	3.950	m
Cabin width	3.490	m
Accommodation (typical)	165	pax
Wing		
Planform area	123.920	m^2
Aspect ratio	10.343	-
Total span	35.800	m
MAC	4.032	m
Leading edge sweep angle	28.0	deg
Dihedral angle	6.0	deg
Horizontal tail		
Planform area	32.621	m^2
Aspect ratio	4.829	-
Total span	12.552	m
MAC	2.839	m
Leading edge sweep angle	31.0	deg
Dihedral angle	9.0	deg
Vertical tail		
Planform area	22.806	m^2
Aspect ratio	1.579	-
Total span	6.0	m
MAC	4.160	m
Leading edge sweep angle	41.6	deg
Landing gears		
Main groups	2	-
Number of total main wheels	4	-
Main strut length	2.835	m
Wheeltrack	7.590	m
Number of nose wheels	2	-

Instead of providing engine and nacelle data through the dedicated input XML files of JPAD, the option to model the characteristics of the powerplant using the surrogate model for turbofan engines was activated. In order to enable this model to carry out this task, input was provided for all the variables (26) listed in table 4.25. With regards to the engine cycle variables, the same values already reported in table 4.18 were used, assuming a design flight altitude equal to 35000 ft and a Mach number equal to 0.78. For S_{NO_x}, a scaling factor equal to 23 was adopted, according to the available information on the combustion chamber technology: twin-annular pre-mixing swirler combustor [10]. The estimation of the EIs of the main gaseous emissions was carried out according to the results of the GasTurb model for NO_x, according to the model provided by [69] for

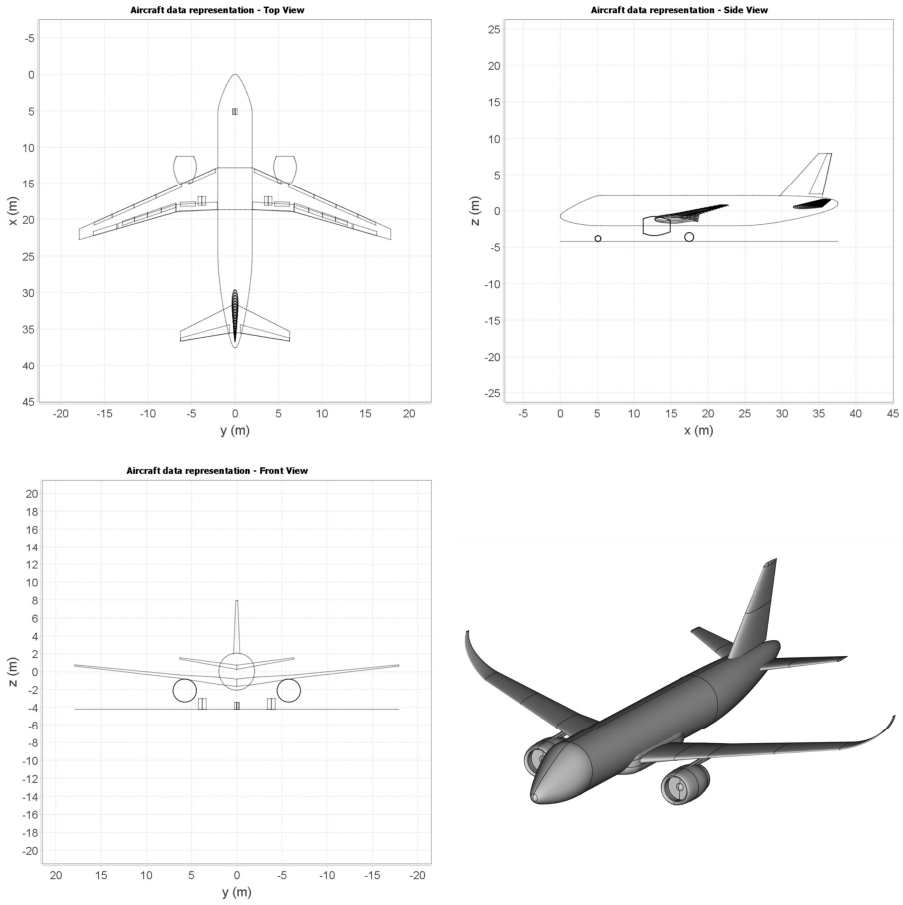

Figure 4.17: Three-view and 3D model of the A320neo-like aircraft modelled with JPAD for the test analyses of the surrogate engine model.

CO and HC, and based on suggestions given by [62] for the remaining species. The same average inflation rate already adopted for the estimations of section 4.2 was assumed, whereas the derivative engine option was set to false, since the design of a new centerline engine was supposed. For this reason, no value was provided for the full scale test hours input variable. Dealing with the input for noise estimations, the number of rotor and stator blades of the fan was inferred from online available pictures of the engines and of its components, whereas the spacing between these two was estimated starting from engine cutaways, like the one reported in figure 4.2. The option for the presence of inlet guide vanes was set to false, and null values were provided for both forward and rear fan blade row attenuations.
Once provided with this set of input variables, the surrogate turbofan model automatically carried out the sizing of the engine, estimating all the design point cycle output variables listed in table 4.24, the off-design point cycle variables of table 4.13, and all the derived variables accounting for weight, size, emissions, noise, and costs of the powerplant. Moreover, two engine decks were produced:

- one for the assessment of the performance of the aircraft, generated according to the scaling procedure described in section 4.3.2;
- one for the noise calculations, generated according to the formatting required by ATTILA++ and based on the theoretical backgrounds reported in sections 2.2.1 and 4.1.10.

Then a complete multidisciplinary analysis cycle was launched in JPAD, aiming at the determination of the following characteristics of the aircraft:

- weights,
- balance and ground stability,
- aerodynamics and static stability,
- performance (including take-off and landing simulations, and the complete mission profile analysis of the aircraft),
- emissions (including LTO cycle calculations),
- environmental noise (for the three certification conditions prescribed by regulations for FAR/CS 25 aircraft),
- and direct operating costs.

Table 4.27 provides the set of assumptions performed regarding the design mission. With regards to payload and range information, these were retrieved from [19] and checked using the payload-range diagram for the A320neo model with one additional central tank reported in [16]. Dealing with the remaining quantities, these were reasonably assumed starting from available information for similar aircraft.
In order to estimate the design mission fuel mass, the iterative cycle described in section 2.1.1 and reported in figure 2.3 was adopted. No iterations were performed instead in order to match precise mission requirements in terms of climb and cruise performance: the net thrust provided by the engine was not updated in this loop. With regards to aircraft performance, a flat cruise was simulated, for the conditions reported in table 4.27. Dealing with the calculation of aircraft direct operating costs, the method provided by

Table 4.27: Set of assumptions for the design mission of the A320neo-like aircraft model.

Description	Value	Unit
Design passengers	165	-
Design mission range	3500	nmi
Design cruise altitude	35000	ft
Design cruise Mach number	0.78	-
Alternate cruise range	200	nmi
Alternate cruise altitude	20000	ft
Holding duration	30	min
Holding altitude	1500	ft
Fuel reserves	5	%

[162] and based on the estimated aircraft OEW was adopted for the calculation of the aircraft list price. Engine price was estimated starting from the engine production cost provided by equation 3.18, and assuming a constant profit margin of the manufacturer equal to 30 %. Table 4.28 provides all the remaining assumptions performed for the assessment of aircraft DOC.

Table 4.29 provides the main results deriving from this multidisciplinary analysis. Wherever possible, a direct comparison between estimated values and reference values is given. As shown by this table, the estimated operating empty mass is reasonably close to the reference value. The design mission fuel obtained at the end of the iterative cycle allows to obtain a maximum take off weight that is just 320 kg lower than the certification one. Moreover, the estimated design mission fuel (including also the reserves) is below the threshold value provided by the maximum allowable fuel mass, which includes both the contributions of the wing tanks and of an additional central tank. Also this latter matches the reference one from [20].

Dealing with the performance, both the take-off field length and the landing field length are reasonably close to the values provided in [61], with the first exceeding the reference value by 50 m. The minimum climb time differs from the target value (which was estimated starting from performance data reported in [61]) by slightly more than 1 minute and the AEO service ceiling at 100 % maximum take-off weight is perfectly in line with the expected value.

With regards to the emissions and to the values estimated for the LTO cycle, it is clearly evident that they are all quite distant from the reference values provided in [8], except for the CO emissions, which still differ by more than 1 kg. The reason for these inconsistencies was investigated, by going through the detailed output provided by the simulation of the mission profile. These differences were linked to two phases of the LTO cycle calculation in particular: the approach phase for NO_x and the taxiing segment for HC. Since JPAD performs an interpolation of the engine performance deck between cruise and flight idle ratings to carry out the simulation of the last phase of the descent, the NO_x emissions might be influenced by the use of higher, interpolated values of NO_x EIs, which bring to higher emissions than those expected. With regards to the HC emissions, instead, differences may be caused by inaccuracies of the reference engine deck (i.e., the one scaled by the surrogate engine model) at low part load, which may bring to higher fuel flow values than the actual ones, to which CO EIs estimated with the approach of [69] may be quite sensitive. However, the values obtained are not completely off, and they are still useful to perform comparative analyses between different designs.

Table 4.28: Set of assumptions for the estimation of the DOC of the A320neo-like aircraft model analyzed with JPAD.

Description	Value	Unit	Notes
Capital (estimated using the method of [138])			
Life span	16	years	
Residual value	10	%	EoL value with respect to initial value
Airframe relative spares costs	10	%	With respect to airframe cost
Engines relative spares costs	30	%	With respect to engines cost
Interest	5.4	%	Percentage of the total investment
Insurance	0.5	%	Percentage of airframe plus engines cost
Crew (estimated using the method of [138])			
Cabin labour rate	90	US$/h	For each flight attendant
Cockpit labour rate	360	US$/h	For each pilot
Fuel			
Price	92.17	US$/barrel	
Landing charges (estimated using the method of [138])			
Navigation charges (estimated using the method of [138])			
Ground handling charges (estimated using the method of [138])			
Noise charges (estimated using the method of [46][47])			
Noise charge constant	4.12	US$	
Departure threshold	91.0	dB	
Arrival threshold	86.0	dB	
Emissions charges (estimated using the method of [144])			
Emissions charge constant	3.7	US$	Applied for LTO CO, HC and NO_x
Maintenance (estimated using the method of [136])			
Airframe labour rate	40	US$/h	
Engines labour rate	40	US$/h	

Environmental noise calculations were carried out using the noise trajectories simulated by JPAD combined with ATTILA++. As is evident from table 4.29, the results of the noise simulations are particularly good for the approach and for the sideline test cases, whereas the result for the flyover is more than 3 dB higher than the reference value provided by [59]. The reason for this difference may be linked to three main factors:

- Since the flyover (cutback) trajectory is simulated by JPAD according to the constraints provided by the regulations, there might be some differences with respect to actual flight trajectories.
- Moreover, the result of this type of simulation is highly affected by the choice on the time instants for the retraction of the landing gears and of the high-lift devices, as exemplified in [68].
- There might be inaccuracies in the adopted scaling procedure for noise reported in section 4.1.10.

However, the same reasoning expressed for the LTO cycle emissions applies in this case too.

Table 4.29: Results of the multidisciplinary analysis on the A320neo-like aircraft model equipped with the set of engines sized by the surrogate turbofan model and comparison with data from the real aircraft.

Description	Estimated value	Reference value	Source
Weights			
MTOW, kg	78679	79000	[16][20][19]
OEW, kg	43796	44300	[19]
Design payload, kg	14206	-	-
Maximum fuel mass, kg	21028	21005	[20]
Design mission fuel mass, kg	20676	-	-
Balance			
Maximum forward X CG, % MAC	4.23	-	-
Maximum afterward X CG, % MAC	18.72	-	-
Operative X CG, % MAC	14.04	-	-
Aerodynamics and static stability			
Maximum clean lift coefficient at operative X CG	1.50	-	-
Maximum take-off lift coefficient at operative X CG	2.16	-	-
Maximum landing lift coefficient at operative X CG	2.72	-	-
Cruise zero-lift drag coefficient	0.0175	-	-
Cruise SSM at maximum afterward X CG	28.96	-	-
Maximum cruise aerodynamic efficiency	18.64	-	-
Performance			
FAR 25 take-off field length, m	2001	1951	[61]
FAR 25 landing field length, m	1629	1650	[61]
Minimum time to climb, min	26	25	[61]
Service ceiling AEO at 100 % MTOW, ft	39493	39100 - 39800	[16]
Service ceiling OEI at 97 % MTOW, ft	18711	-	-
Block time, min	475	-	-
Block fuel, kg	17478	-	-
Total fuel used, kg	19571	-	-
Emissions			
Total CO2 emissions, kg	61629	-	-
Total NOx emissions, kg	319.76	-	-
LTO total NOx emissions, kg	11.88	3.53	[8]
LTO total CO emissions, kg	2.04	3.26	[8]
LTO total HC emissions, kg	0.76	0.05	[8]
Noise			
Approach, dB	93.07	92.7	[59]
Sideline, dB	86.55	86.2	[59]
Flyover, dB	84.73	81.6	[59]
Costs			
Cash DOC, cent/(nmi*seat)	6.470	-	-
Total DOC, cent/nmi*seat)	12.942	-	-

In order to further highlight the capabilities of the surrogate turbofan model, a parametric analysis on engine BPR was carried out. Five additional engine models, differing with respect to the previous one only in terms of bypass ratio, were equipped on the same reference aircraft. Then a multidisciplinary analysis cycle like the one described above was carried out for each of this five aircraft models, assuming the same design mission and performing a preliminary iteration on MTOW in order to match the design mission fuel. No thrust updates were performed for any of the engines, in order to compensate for changes to the maximum take-off weight.
The results of this parametric analysis are reported in table 4.30, from which it is possible to deduce that the aircraft model equipped with the engine with BPR equal to 11 (i.e.,

the one previously analyzed) is the one granting the lowest block fuel and the lowest total CO_2 emissions (figure 4.18), suggesting that, for an aircraft like the A320neo, an engine with such a BPR could be the best compromise in terms of fuel consumption, size (thus installation issues too), penalty weight, and environmental noise.
With regards to the latter, table 4.30 provides a comparison between the aircraft in terms of approach EPNL. The reason for which the cumulative EPNL is not reported is linked to the previously mentioned dependency of the flyover EPNL on the simulation of the noise trajectory. Since this analysis wants to focus the attention on the effects related to changes to the engine characteristics, the approach EPNL was selected as the metric for noise. It is possible to deduce from table 4.30 that the higher the BPR, the lower the approach EPNL, which is expected. In fact, according to the set of methodologies implemented by the surrogate turbofan model, higher BPR values imply lower fan outer pressure ratio values, thus lower fan tip speeds and tip Mach numbers, in accordance with the plot reported in figure 4.10.
Table 4.30 also provides results in terms of LTO cycle emissions for NO_x, which show that higher BPRs imply lower total emissions. This is linked both to a slight reduction of the NO_x EI with increasing BPR (as reported in table 4.31), and to the lower SFC of course. The other relevant pollutant species for the LTO cycle are not reported in table NO_x, but the same behaviour of NO_x emissions was observed.
Dealing with the total DOC, table 4.30 shows that it constantly increases with higher BPR, regardless of the lower fuel burn or the lower fuel charges for noise and emissions. This is linked to:

- the increase in engine price, due to the increase in engine dry mass, provoked by higher BPR values;
- the increase in aircraft price due to the increase in OEW.

Table 4.31 provides an overview on the characteristics of the different engines modelled for this application example. The first thing that can be noticed is that all the engines comply with thermal limitations assumed and reported in table 4.17. The second thing that is important to highlight is the weight increase generated by the increase in BPR. This is much higher than the one, for example, observed for the applications of section 2.4, but can be explained in multiple ways:

- The engines designed for the ADORNO project were GTF engines, for which also the weight estimation method of [141] predicts lower dry mass values, for the same combination of input parameters, with respect to a two-spool direct-drive engine. Moreover, also the predicted weight penalty when passing to a higher BPR value is significantly lower.
- No information were provided by MTU for the engines of table 2.41 regarding specific characteristics of the core technology (such as the turbine entry temperature). Different assumptions of this kind might explain small dry mass differences between different BPRs.
- On the other hand, the increment in terms of number of required booster and LPT stages reported in table 4.31 when passing from one BPR value to a higher one justifies this weight boost. For a two-spool GTF engine, since the rotational speed of the fan is decoupled from the one of the LPT, it is possible to retain high turbine efficiency values without the need to increase the number of stages too much.

Table 4.30: Results of the parametric study on engine BPR performed on the A320neo-like aircraft model.

Description	**BPR 8 A/C**	**BPR 9 A/C**	**BPR 10 A/C**
MTOW, kg	76393	77115	77878
OEW, kg	41284	42123	42693
Design fuel mass, kg	20902	20784	20708
TOFL, m	1822	1882	1942
Minimum time to climb, min	23	24	25
LFL, m	1576	1576	1598
Block fuel mass, kg	17694	17583	17511
Total fuel used mass, kg	19804	19684	19606
Total CO_2 emissions, kg	62364	61985	61739
LTO total NO_x emissions, kg	12.317	12.118	12.022
Approach EPNL, dB	93.52	93.38	93.16
Total DOC, cent/(nmi*seat)	12.491	12.641	12.791
Description	**BPR 11 A/C**	**BPR 12 A/C**	**BPR 13 A/C**
MTOW, kg	78679	79521	80403
OEW, kg	43796	44624	45442
Design fuel mass, kg	20676	20690	20755
TOFL, m	2001	1982	2038
Minimum time to climb, min	26	27	29
LFL, m	1629	1624	1625
Block fuel mass, kg	17478	17491	17552
Total fuel used mass, kg	19571	19586	19653
Total CO_2 emissions, kg	61629	61676	61886
LTO total NO_x emissions, kg	11.879	11.817	11.748
Approach EPNL, dB	93.07	92.97	92.95
Total DOC, cent/(nmi*seat)	12.942	13.094	13.245

With regards to manufacturing limitations, the engine with BPR equal to 13 might represent an issue, at least according to indications provided by [106] in terms of maximum number of stages per turbo component. Figure 4.19 provides a clearer picture of the differences between the engines.

4.4.2 Advanced A320-like aircraft model applications

In order to stress even more the capabilities of the surrogate turbofan model, additional parametric analyses on engine BPR were performed for two future scenarios:

- a short/medium term scenario, assuming 2030 as reference year,
- and a medium/long term scenario, with 2040 as the reference year for a presumable EIS.

For these analyses the same aircraft model described in the previous section was adopted, but equipped with advanced airframe technologies and with advanced turbofan engines, modelled with the surrogate model and using input values for EIS according to the abovementioned assumptions. The same set of airframe technologies described in section 2.3.3 was adopted and is here recapped:

- hybrid laminar flow control system on wing, horizontal tail, vertical tail, and nacelle cowl;

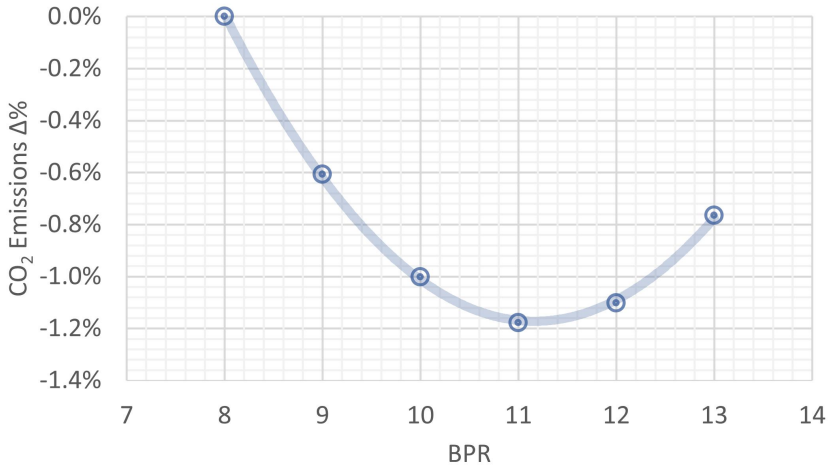

Figure 4.18: Total CO_2 emissions percentage variations for the application example on the A320neo-like model. Percentage variations refer to aircraft models equipped with engines with different BPRs, assuming the BPR 8 A/C model as the reference.

Table 4.31: Characteristics of the engines automatically generated with the surrogate turbofan model implemented in JPAD for the application example on the A320neo-like aircraft.

Description	**BPR 8 engine**	**BPR 9 engine**	**BPR 10 engine**
MCR SFC, g/(kN*s)	16.34	16.03	15.76
DP S_{NO_x}, g/kg	1.1191	1.1182	1.1177
Nacelle max. diameter, m	2.314	2.407	2.496
Nacelle cowl length, m	3.364	3.464	3.557
Engine dry mass, kg	2469	2697	2923
Engine production cost, US M$	10.130	10.318	10.486
Number booster stages	1	2	2
Number LPT stages	4	5	6
T/O EoR T_3, K	937	934	932
T/O EoR T_4, K	1885	1879	1872
T/O EoR $T_{4.5}$, K	1170	1172	1174
Description	**BPR 11 engine**	**BPR 12 engine**	**BPR 13 engine**
MCR SFC, g/(kN*s)	15.52	15.33	15.16
DP S_{NO_x}, g/kg	1.1175	1.1177	1.1183
Nacelle max. diameter, m	2.581	2.661	2.738
Nacelle cowl length, m	3.644	3.725	3.799
Engine dry mass, kg	3148	3369	3585
Engine production cost, US M$	10.638	10.774	10.897
Number booster stages	3	4	4
Number LPT stages	7	9	10
T/O EoR T_3, K	929	927	924
T/O EoR T_4, K	1865	1858	1851
T/O EoR $T_{4.5}$, K	1175	1176	1176

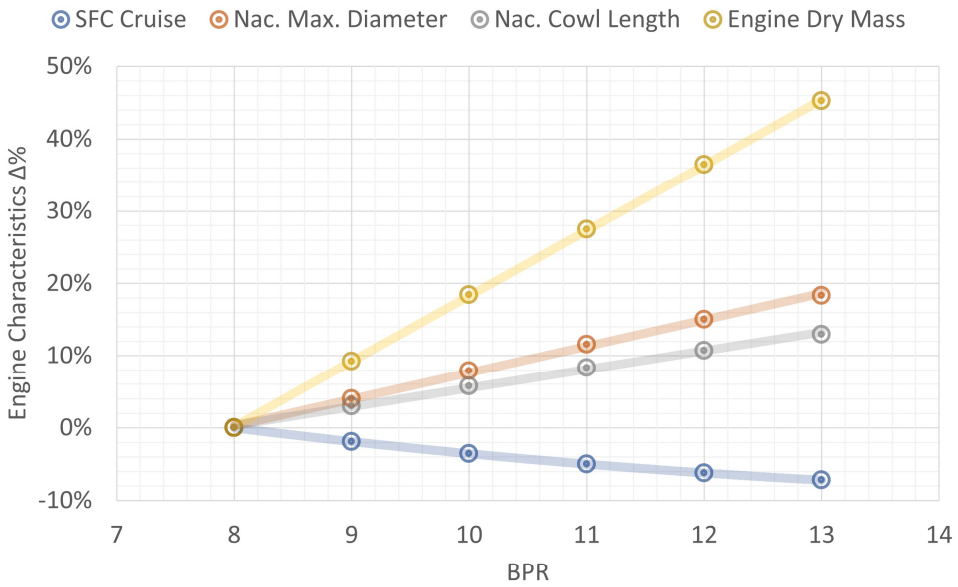

Figure 4.19: Comparison of the main characteristics of the engines used in the parametric study on BPR performed on the A320neo-like A/C model. Percentage variations are evaluated with respect to the characteristics of the engine with BPR equal to 8.

- riblets on wing, horizontal tail, vertical tail, and fuselage;
- variable camber wing with high-lift devices;
- bleed-less MEA architecture (the MEA2 architecture of section 2.3.3);
- advanced composites (CFRP) for the wing and the fuselage structures, advanced Ti-based alloys for the landing gear system.

Regarding the usage of advanced composites for the structures of the aircraft, reasonable calibrations were adopted with respect to the percentage weight reductions reported in section 2.3.3 in order to account for those parts of the aircraft that are already made with advanced light materials in the A320neo. For this reason, a 0.75 scale factor was adopted for the weight calibration of the wing (thus bringing the original -20 % of table 2.23 to -15 %), whereas for the fuselage a final reduction for CFRP usage equal to -21.25 % of the original weight was assumed.
For both the scenarios, the same assumption on airframe technologies implementations was adopted, leading to that the only differences between the results for the two perspectives depended solely on the powerplant. For the engines, a higher OPR, equal to 55, was assumed, while the same value of burner exit temperature, 1800 K, was retained for all the analyses, due to the reasons already explained in section 4.2. The net thrust requirement for ToC was reduced in order to adapt it to the effect of the advanced airframe technologies on the aircraft weight and aerodynamics. A value equal to 22 kN was selected, instead on 25 kN, which allowed to obtain a minimum time to climb under 25 minutes and an AEO service ceiling at 100 % MTOW above 40000 ft for almost all the aircraft, independently of the engine BPR. Then the thrust requirement for T/O EoR

was also adjusted, in order to keep the same original ratio with respect to DP net thrust. For the analyses, the same set of disciplines and the same set of assumptions (including those regarding the design mission) reported in section 4.4.1 were adopted, including the iterative cycle on design mission fuel mass.
The main objective of these investigations was to understand whether and how much the surrogate model was sensitive to changes in terms of airframe and engines technologies and to determine if the best BPR in terms of minimum fuel burn and emissions was influenced by these. The A320neo-like aircraft equipped with BPR 11 engines of section 4.4.1 was assumed as the reference aircraft for performance comparisons.

Advanced A320 EIS 2030

Table 4.32 and table 4.33 include the main results in terms of aircraft analyses and engine characteristics, respectively.
The application of advanced light materials, together with the adoption of lighter advanced engines, allows to noticeably reduce the OEW with respect to the reference aircraft. The lower weight, despite the significant reduction in terms of available thrust, helps to obtain better ground and climb performance with respect to the A320neo-like reference. Independently of the engine BPR and of the MCR SFC obtained from the surrogate sizing (which includes also the additional effect due to HLFC systems power off-takes), block fuel reductions greater than 25 % are obtained. Similar reductions are obtained also for total CO_2 and NO_x emissions (despite the increase in terms of engine OPR, from 50 to 55), whereas lower values can be observed for the LTO cycle. Also the approach EPNL benefits from the adoption of advanced technologies: reductions in the range of 1 dB are achieved.
In terms of engine characteristics, all the analyzed models pass the checks on thermal limitations (values reported in the second column of table 4.17 are used for this inspection). The higher polytropic efficiencies of the turbo components allows to substantially improve the performance and, combined with the lower thrust demand, to design smaller and lighter engines. With regards to production costs, the same analysis reported in section 4.4.1 can be applied.
It is interesting to take note of the fact that, in this case, the engine BPR allowing to obtain the best result in terms of fuel and CO_2 emissions is appreciably greater than the one observed in the previous analysis on the A320neo-like model, as highlighted by figure 4.20. This can be linked to the reduced size and weight of the advanced engines, which allow to further take advantage of the beneficial effect of higher propulsive efficiency on SFC when increasing the engine BPR.

Advanced A320 EIS 2040

The same parametric analyses were performed assuming a different input value for the EIS of the engines. The main results of these analyses are reported in tables 4.34 and 4.35.
With respect to the analyses for 2030 EIS, a further OEW reduction can be observed. This reduction this time depends only on the powerplant, for which even lower engine dry mass values are obtained with respect to the ones for EIS 2030. This is linked to the improved overall efficiency of the engines, which requires lower entry mass flow rate to generate the same thrust. Due to this weight decrease, to the additional improvement in terms of SFC, and to the further reduced size of the engines (which is also linked to the

Table 4.32: Results of the parametric study on engine BPR performed on the advanced A320 with EIS in 2030.

Description	**BPR 9 A/C**	**BPR 10 A/C**	**BPR 11 A/C**
MTOW, kg	66119	66808	67513
OEW, kg	36609	37364	38110
Design fuel mass, kg	15303	15238	15197
TOFL, m	1620	1604	1590
Minimum time to climb, min	20	21	22
LFL, m	1417	1432	1430
Block fuel mass, kg	12757	12700	12664
Total fuel mass used, kg	14498	14437	14398
Total CO_2 emissions, kg	45656	45462	45340
LTO NO_x emissions, kg	11.779	11.645	11.504
Approach EPNL, dB	92.45	92.33	92.20
Total DOC, cent/(nmi*seat)	12.656	12.820	12.979
Description	**BPR 12 A/C**	**BPR 13 A/C**	**BPR 14 A/C**
MTOW, kg	68236	68971	69713
OEW, kg	38848	39571	40276
Design fuel mass, kg	15182	15193	15231
TOFL, m	1718	1701	1685
Minimum time to climb, min	22	23	24
LFL, m	1445	1457	1467
Block fuel mass, kg	12650	12658	12688
Total fuel mass used, kg	14383	14395	14430
Total CO_2 emissions, kg	45292	45328	45439
LTO NO_x emissions, kg	11.469	11.350	11.330
Approach EPNL, dB	91.98	91.91	91.88
Total DOC, cent/(nmi*seat)	13.134	13.284	13.428

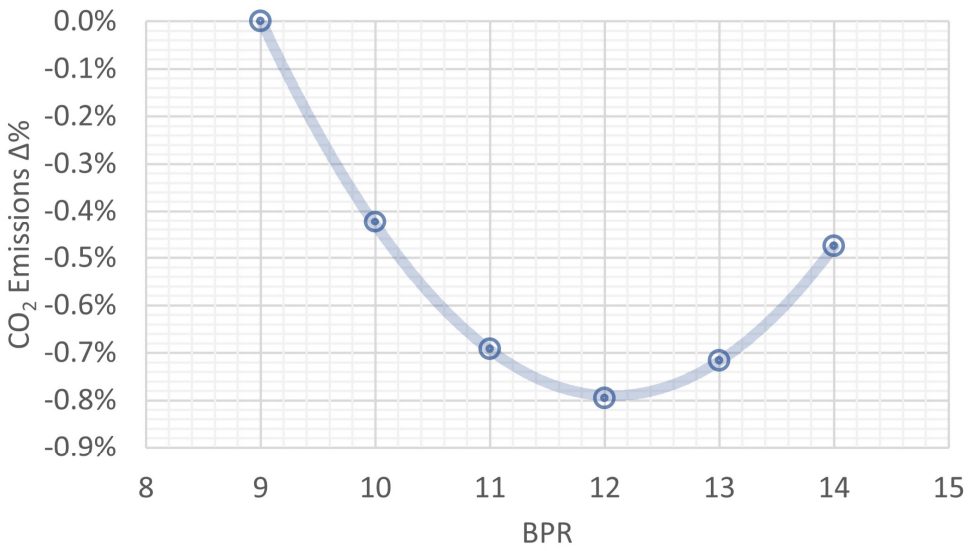

Figure 4.20: Total CO_2 emissions percentage variations for the application example on the advanced A320 (EIS 2030). Percentage variations refer to aircraft models equipped with engines with different BPRs, assuming the BPR 9 A/C model as the reference.

Table 4.33: Characteristics of the engines automatically generated with the surrogate turbofan model implemented in JPAD for the application example on the advanced A320 aircraft with 2030 EIS.

Description	**BPR 9 engine**	**BPR 10 engine**	**BPR 11 engine**
MCR SFC, g/(kN*s)	15.55	15.29	15.06
DP S_{NO_x}, g/kg	1.3223	1.3227	1.3234
Nacelle max. diameter, m	2.164	2.242	2.318
Nacelle cowl length, m	3.197	3.285	3.368
Engine dry mass, kg	2240	2434	2626
Engine production cost, US M$	14.039	14.271	14.480
Number booster stages	1	1	2
Number LPT stages	4	5	6
T/O EoR T_3, K	964	961	958
T/O EoR T_4, K	1940	1932	1925
T/O EoR $T_{4.5}$, K	1278	1280	1281
Description	**BPR 12 engine**	**BPR 13 engine**	**BPR 14 engine**
MCR SFC, g/(kN*s)	14.87	14.70	14.56
DP S_{NO_x}, g/kg	1.3244	1.3256	1.3271
Nacelle max. diameter, m	2.389	2.458	2.523
Nacelle cowl length, m	3.445	3.518	3.585
Engine dry mass, kg	2814	2999	3178
Engine production cost, US M$	14.667	14.833	14.979
Number booster stages	3	3	4
Number LPT stages	7	9	10
T/O EoR T_3, K	954	951	948
T/O EoR T_4, K	1917	1910	1902
T/O EoR $T_{4.5}$, K	1282	1283	1284

Table 4.34: Results of the parametric study on engine BPR performed on the advanced A320 with EIS in 2040.

Description	**BPR 9 A/C**	**BPR 10 A/C**	**BPR 11 A/C**
MTOW, kg	64493	65590	66261
OEW, kg	35892	36622	37350
Design fuel mass, kg	14844	14762	14705
TOFL, m	1503	1559	1545
Minimum time to climb, min	20	20	21
LFL, m	1392	1405	1414
Block fuel mass, kg	12371	12299	12249
Total fuel mass used, kg	14062	13983	13929
Total CO_2 emissions, kg	44281	44034	43864
LTO NO_x emissions, kg	11.481	11.302	11.172
Approach EPNL, dB	92.66	92.46	92.32
Total DOC, cent/(nmi*seat)	13.299	13.476	13.647

Description	**BPR 12 A/C**	**BPR 13 A/C**	**BPR 14 A/C**
MTOW, kg	66953	67667	68393
OEW, kg	38072	38786	39483
Design fuel mass, kg	14675	14675	14703
TOFL, m	1674	1586	1642
Minimum time to climb, min	21	22	23
LFL, m	1422	1437	1457
Block fuel mass, kg	12222	12221	12244
Total fuel mass used, kg	13902	13900	13928
Total CO_2 emissions, kg	43776	43771	43859
LTO NO_x emissions, kg	11.080	10.999	10.961
Approach EPNL, dB	92.28	92.14	91.90
Total DOC, cent/(nmi*seat)	13.813	13.974	14.128

overall efficiency improvement, that allows to reduce the fan tip diameter), the design mission fuel and the MTOW result to be even lower than the previous ones, for each examined BPR. The fuel burn reduction, of course, allows to obtain an additional cut on the emissions, both with respect to the reference A320-like aircraft and the aircraft models with 2030 EIS. With regards to the environmental noise, instead, no additional beneficial effect can be observed. The strong reduction obtained for the aircraft models of the previous parametric analysis was substantially linked only to the noticeable decrease applied on the required net thrust.
Figure 4.21 provides percentage differences of CO_2 emissions for the aircraft models of this parametric analysis with respect to the CO_2 emissions of the aircraft equipped with the BPR 9 engine. It appears clear from this figure that the optimum BPR in terms of minimum fuel burn and minimum CO_2 emissions is between 12 and 13, a value which is higher with respect to the one obtained from the same study performed on the reference aircraft (equal to 11), and also higher than the one achieved during the previous analysis (equal to 12). These results would suggest that the level of technology of the engine has for sure an influence on the optimum BPR for minimum fuel and emissions.

Comparisons

This sub section provides a recap and additional observations on the main results achieved during the previous analyses.
Figure 4.22 shows the advantage in terms of CO_2 emissions of the advanced aircraft

Table 4.35: Characteristics of the engines automatically generated with the surrogate turbofan model implemented in JPAD for the application example on the advanced A320 aircraft with 2040 EIS.

Description	**BPR 9 engine**	**BPR 10 engine**	**BPR 11 engine**
MCR SFC, g/(kN*s)	15.32	15.06	14.82
DP S_{NO_x}, g/kg	1.3144	1.3131	1.3124
Nacelle max. diameter, m	2.077	2.153	2.226
Nacelle cowl length, m	3.097	3.184	3.266
Engine dry mass, kg	2069	2257	2444
Engine production cost, US M$	16.945	17.242	17.510
Number booster stages	1	1	2
Number LPT stages	4	5	6
T/O EoR T_3, K	965	962	958
T/O EoR T_4, K	1940	1932	1925
T/O EoR $T_{4.5}$, K	1319	1319	1320
Description	**BPR 12 engine**	**BPR 13 engine**	**BPR 14 engine**
MCR SFC, g/(kN*s)	14.62	14.45	14.31
DP S_{NO_x}, g/kg	1.3124	1.3130	1.3142
Nacelle max. diameter, m	2.295	2.362	2.426
Nacelle cowl length, m	3.344	3.416	3.484
Engine dry mass, kg	2630	2812	2990
Engine production cost, US M$	17.751	17.966	18.157
Number booster stages	2	2	3
Number LPT stages	7	9	10
T/O EoR T_3, K	954	951	947
T/O EoR T_4, K	1917	1909	1901
T/O EoR $T_{4.5}$, K	1319	1319	1318

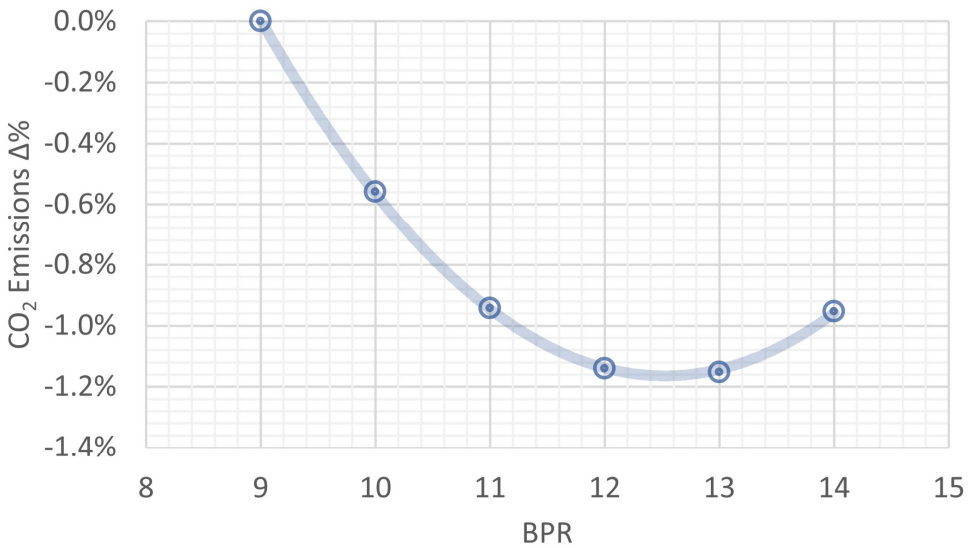

Figure 4.21: Total CO_2 emissions percentage variations for the application example on the advanced A320 (EIS 2040). Percentage variations refer to aircraft models equipped with engines with different BPRs, assuming the BPR 9 A/C model as the reference.

of the short/medium and medium/long-term scenarios with respect to the best aircraft (i.e., the one equipped with engines with BPR equal to 11) of the current scenario. It is evident from this comparative plot that the level of technology has an impact on the best choice, in terms of minimum CO_2 emissions, of engine BPR. For the first time perspective (2030 EIS) the BPR allowing the maximum decrease with respect to the reference is equal to 12. This value grows for the second scenario (2040 EIS), for which the minimum fuel burn and the minimum CO_2 emissions are obtained for a BPR equal to 12.5, approximately. This growth is substantially driven by the increase in engine technology, which allows to design smaller and lighter engines for the same BPR value (as can be deduced by comparing engine characteristics reported in tables 4.33 and 4.35). At the same time, the application of advanced airframe technologies contributed to this shift, since it allowed to design engines with reduced thrust requirements, thus reduced size and overall weight. Moreover, the effect of the application of airframe technologies on the selection of the characteristics of the powerplant system was investigated within the context of ADORNO, by means of two dedicated trade factor analyses aiming at determining individual impacts of variations to engine parameters (such as SFC, maximum nacelle diameter, and dry mass) on the fuel consumed by the aircraft during the mission. One study was carried out on a reference aircraft model (with 2014 EIS) with current technology level engines equipped, the other one on an advanced aircraft mounting the same technologies listed in section 4.4.2 and with advanced GTF turbofans. These studies returned limited but noteworthy differences between the two sets of trade factors, which indicates that the adoption of innovative solutions to reduce the weight and the drag of the airframe may have an impact on the selection of the best BPR possible to reduce the emissions.
In light of the results summarized by figure 4.22, comparative analyses between the performance of the aircraft and engines combinations, allowing, for each time perspective, to achieve the lowest possible fuel consumed for the design mission, can be performed. For this purpose, an additional aircraft, equipped with a 2040 EIS engine with BPR equal to 12.5 was analyzed. The following tables include results descending from the multidisciplinary analysis of this aircraft model.

Table 4.36 and table 4.37 compare the characteristics and the performance of the best aircraft, both in terms of absolute values and percentage differences. No costs comparisons are included in these tables, due to discrepancies between different time perspectives on the assumptions regarding the application of cumulative inflation rates on the different items composing the total DOC analysis.
It is possible to observe from these tables that the 2030 EIS aircraft allows to match both the Clean Sky 2 targets on gaseous emissions cited in chapter 1 and chapter 2: -26.5 % of CO_2, -25.2 % of total NO_x, with respect to the reference aircraft. The 2040 EIS aircraft allows to go even further, granting -28.9 % of CO_2 and -29.3 % of NO_x. With regards to the LTO cycle emissions, lower reductions can be observed in general. For the NO_x, the 2030 and 2040 EIS aircraft allow to achieve 3.45 and 6.87 % reductions, respectively. Higher values are obtained for the HC emissions (-7.89 and -10.39 %) and CO (-8.41 and -10.52 %). This dissimilarity could be attributed to the bond between NO_x EI and engine OPR, which, for the advanced engines with OPR equal to 55 instead of 50, determines lower emissions reductions with respect to the reference aircraft, whereas the remaining emissions depend almost solely on fuel flow.
Dealing with environmental noise, both the advanced aircraft show an overall improvement with respect to the reference. As reported in the previous section, the thrust

demand reduction allowed to noticeably decrease the noise footprint of the advanced engines[4]. The 2030 and 2040 EIS aircraft perform quite similarly, with a relatively high difference (0.74 dB) only between the flyover analyses, but that could be linked to simulation errors. Cumulative EPNL reductions ranging from 2.0 to 3.0 dB can be attributed to modifications to the engines in these perspective analyses, which demonstrates that in order to achieve noise abatement levels hoped for the fulfillment of environmental objectives it is necessary to adopt dedicated engineering solutions.

Table 4.38 and table 4.38 allow to have a more detailed picture on the characteristics of the propulsive systems adopted for the examined time perspectives. For the same reason reported above, no information or comparisons regarding engine production costs are included in these tables.
Both the advanced engines show a significant reduction in terms of SFC with respect to the reference aircraft, despite the huge demand in terms of additional power off-takes provided by the HLFC systems mounted by the 2030 and 2040 EIS A/C models. These, combined with the reduced design thrust, have a strong impact on the fuel consumed by the aircraft.
With regards to the NO_x severity index, the considerable increase reported in these tables is due to the adoption of higher OPR values for the design of the advanced engines. Nevertheless, the significant reduction in terms of fuel burn achieved by the advanced aircraft allowed to obtain NO_x emissions values in line with expectations for the fulfillment of environmental objectives. It is also necessary to account the secondary effect linked to engine throttle and already mentioned in section 2.3.5. Especially during the last stages of the simulation of the cruise phase, the advanced engines may work at sub-optimal engine throttle values, which on one side do not allow to achieve the expected SFC, on the other determine a reduction in the actual NO_x EIs value used for the simulation[5] (lower throttle settings imply lower NO_x EIs). It can be observed from these tables that, despite the higher BPR, both the advanced engines feature reduced size and weight with respect to the reference. This aspect was already clarified in the previous sections and can be attributed to the overall improvement in terms of cycle efficiency of the advanced engine with respect current technology.

[4]For all the analysis, the geometry of the aircraft was kept unchanged, so the only effect impacting on noise analyses of the advanced aircraft is the one due to changes to the propulsive system and, for the flyover analysis, to the simulated aircraft noise trajectory.

[5]These effects could have been limited by adapting the design net thrust to each analyzed combination of aircraft and engine BPR. However this is beyond the scope of the current analysis, which is to provide a first test of the capabilities of this surrogate engine model.

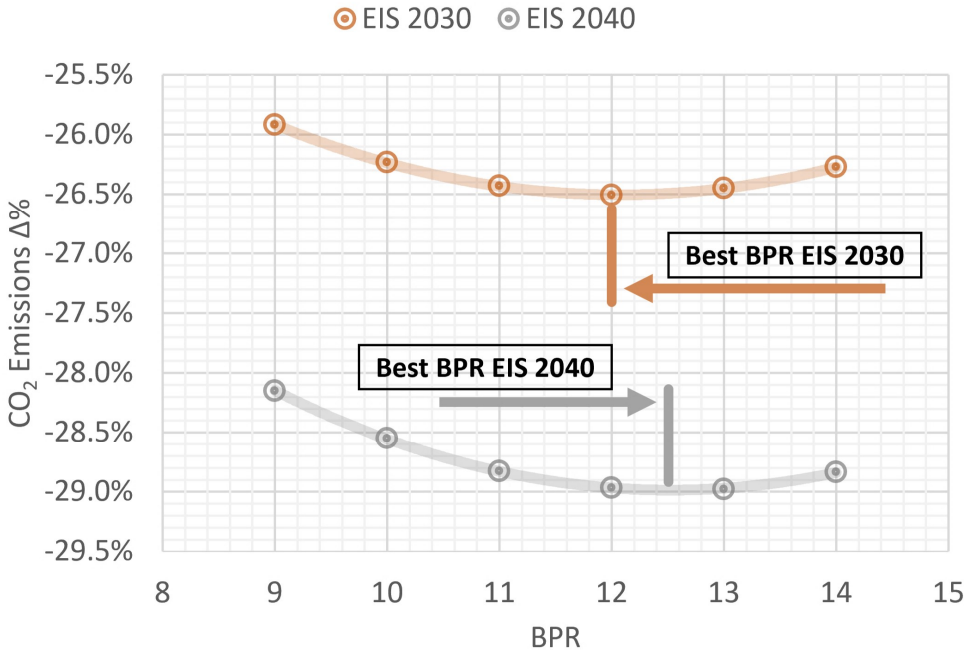

Figure 4.22: CO_2 emissions percentage variations of the advanced aircraft (both scenarios) equipped with engines with increasing BPR, calculated with respect to the performance of the reference A320neo-like aircraft, equipped with the BPR 11 engine.

Table 4.36: Comparative table of the performance of the best (i.e. minimum fuel burn) aircraft for each investigated time perspective: current level of technology, EIS 2030, and EIS 2040.

Description	**A320neo-like A/C BPR 11 engines**	**EIS 2030 A320-like A/C BPR 12 engines**	**EIS 2040 A320-like A/C BPR 12.5 engines**
MTOW, kg	78679	68236	67309
OEW, kg	43796	38848	38431
Design fuel mass, kg	20676	15182	14671
TOFL, m	2001	1718	1594
Minimum time to climb, min	26	22	22
LFL, m	1629	1445	1427
Block fuel mass, kg	17478	12650	12219
Total fuel mass used, kg	19571	14383	13897
Total CO_2 emissions, kg	61629	45292	43761
Total NO_x emissions, kg	319.75	239.31	226.19
LTO NO_x emissions, kg	11.879	11.469	11.063
LTO CO emissions, kg	2.040	1.868	1.825
LTO HC emissions, kg	0.760	0.700	0.681
Approach EPNL, dB	93.07	91.98	92.19
Flyover EPNL, dB	84.73	83.25	83.99
Sideline EPNL, dB	86.55	85.98	86.07
Cumulative EPNL, dB	264.35	261.21	262.25

Table 4.37: Comparative table, in terms of percentage and delta differences, of the performance of the best (i.e. minimum fuel burn) aircraft for each investigated time perspective: current level of technology, EIS 2030, and EIS 2040.

Description	**EIS 2030 A/C BPR 12 engines vs A320neo-like BPR 11 engines**	**EIS 2040 A/C BPR 12.5 engines vs A320neo-like BPR 11 engines**	**EIS 2040 A/C BPR 12.5 engines vs EIS 2030 A/C BPR 12 engines**
MTOW	−13.273 %	−14.451 %	−1.358 %
OEW	−11.298 %	−12.250 %	−1.073 %
Design fuel mass	−26.572 %	−29.043 %	−3.366 %
Block fuel mass	−27.623 %	−30.089 %	−3.407 %
Total fuel mass used	−26.509 %	−28.992 %	−3.379 %
Total CO_2 emissions	−26.509 %	−28.992 %	−3.379 %
Total NO_x emissions	−25.157 %	−29.260 %	−5.482 %
LTO NO_x emissions	−3.451 %	−6.869 %	−3.540 %
LTO CO emissions	−8.412 %	−10.529 %	−2.312 %
LTO HC emissions	−7.895 %	−10.395 %	−2.714 %
Approach EPNL	−1.09 dB	−0.88 dB	+0.21 dB
Flyover EPNL	−1.48 dB	−0.74 dB	+0.74 dB
Sideline EPNL	−0.57 dB	−0.48 dB	+0.09 dB
Cumulative EPNL	−3.14 dB	−2.10 dB	+1.04 dB

Table 4.38: Comparative table of the performance and characteristics of the engines equipped on the best (i.e. minimum fuel burn) aircraft of each investigated time perspective: current level of technology, EIS 2030, and EIS 2040.

Description	**Reference BPR 11 engine**	**EIS 2030 BPR 12 engine**	**EIS 2040 BPR 12.5 engine**
MCR SFC, g/(kN*s)	15.523	14.868	14.532
DP S_{NO_x}, g/kg	1.1175	1.3244	1.3126
Nacelle max. diameter, m	2.581	2.389	2.329
Nacelle cowl length, m	3.644	3.445	3.381
Engine dry mass, kg	3148	2814	2721
Number booster stages	3	3	2
Number LPT stages	7	7	8
T/O EoR T_3, K	929	954	952
T/O EoR T_4, K	1865	1917	1913
T/O EoR $T_{4.5}$, K	1175	1282	1319

Table 4.39: Comparative table, in terms of percentage differences, of the performance and characteristics of the engines equipped on the best (i.e. minimum fuel burn) aircraft of each investigated time perspective: current level of technology, EIS 2030, and EIS 2040.

Description	**EIS 2030 BPR 12 engine vs Reference BPR 11 engine**	**EIS 2040 BPR 12.5 engine vs Reference BPR 11 engine**	**EIS 2040 BPR 12.5 engine vs EIS2030 BPR 12 engine**
MCR SFC	−4.220 %	−6.384 %	−2.260 %
DP S_{NO_x}	+18.514 %	+17.459 %	−0.891 %
Nacelle max. diameter	−7.439 %	−9.764 %	−2.511 %
Nacelle cowl length	−5.461 %	−7.217 %	−1.858 %
Engine dry mass	−10.610 %	−13.564 %	−3.305 %

Chapter 5

Conclusion

5.1 Recap on the work performed

Multidisciplinary frameworks for the design and the analysis of modern aircraft are required to cope with an ever increasing number of variables and requirements, in order to allow consistent and effective studies of evolutionary and/or revolutionary new aircraft concepts. The investigation of such solutions is dictated by the environmental agenda, which has set urgent and ambitious targets in terms of emissions and environmental noise reductions. One of the largest contributors to these reductions may be represented by the propulsion system, but, as evidenced in chapter 1, is often not sufficiently and satisfactorily modelled by well-known conceptual and preliminary aircraft design tools, which usually lack in physics or knowledge-based approaches for the description of the behaviour and characteristics of the powerplant depending on aircraft requirements, generally preferring empirical or semi-empirical approaches provided by renown aircraft design textbooks. These observations brought in chapter 1 to the formulation of the following research question:

How to improve preliminary design workflows focused on the optimization of low-emission aircraft by including detailed effects related to changes to the propulsion system?

This thesis work aimed at providing a feasible solution to the necessity to include even from the earliest design stages of a new aircraft a more reliable and effective modelling of the powerplant system, allowing to perform a preliminary sizing based on a limited but adequate number of input parameters, including aircraft requirements, engine thermodynamic cycle variables, and technology factors.
Chapter 2 provided a description of a typical research context in which aircraft and engine specialists are involved to design both new airframe and engines solutions in order to match environmental targets. The framework of the European Clean Sky 2 funded project ADORNO, in which the author of this thesis was deeply involved during his PhD, was comprehensively described, in order to contextualize part of the observations on modern aircraft conceptual and preliminary design workflows and supporting tools. This chapter also provided the possibility to introduce some of the tools that were later used in order to carry out validation and testing of the proposed methodology and application in response to the research question:

- JPAD, a multidisciplinary framework developed in-house at the University of Naples

supporting conceptual and preliminary aircraft design workflows, and in whose development the author was involved;

- ATTILA++, a tool for preliminary aircraft noise estimations specifically developed for ADORNO, and for which the author collaborated in terms of development, validation, and documentation.

The last section of this chapter helped to perform an analysis on all the aspects of the interaction between aircraft and engine designers that typically occur in a research project like ADORNO, highlighting the limitations and the possibilities to improve this exchange, by making the integration at aircraft level of new engine models run smoother, or by allowing to even perform a preliminary sizing of the engines, based on precise aircraft requirements and input in terms of assumed technology level of the new propulsive system. Basically, the framework of ADORNO provided the necessary knowledge on the topic and the tools in order to carry out the work in response to the research question.
Chapter 3 provided a description of the work carried out by the author for another European Clean Sky 2 funded project, GENESIS, dealing with the design and the analysis of hybrid/full-electric aircraft configurations, supported by technology foresight studies on conventional (gas turbine) and innovative (batteries, fuel cells, electric motors, SAF) solutions for propulsion, performed for three different time perspectives (short, medium, and long-term). The work required by this project in terms of gas turbine modelling fit exactly to the considerations made for ADORNO and allowed to provide a first answer to the research question. In fact, for the second WP of GENESIS, the author worked on the technology foresight analysis on gas turbine engines for turboprop applications, and on the development of a surrogate engine model, allowing to perform a preliminary sizing of the engine based on user's requests in terms of shaft power, off-takes, level of technology, main cycle design parameters (OPR and burner exit temperature), and biofuel blending ratio. This surrogate model was then capable to provide characteristics of the engine in terms of specific fuel consumption, main dimensions, weight, emission indices, and costs. Such a capability was essential for the aircraft design activities to be carried out for the first WP of GENESIS, since, for each time perspective, different levels of aircraft hybridization would have been examined, leading to different levels of gas turbine power and to the necessity to model several gas turbines for each aircraft design loop. A detailed description of the set of assumptions and methodologies adopted for the generation of this surrogate model was provided in this chapter, along with observations on possible strategies in order to ensure the actual feasibility of the engines produced with the surrogate model. Validation and testing of the model were also provided, by first comparing its results against Pratt & Whitney PW127E engine (the reference turboprop engine selected for GENESIS activities) public available information, and by carrying out a technology analysis for the short-term scenario.
The methodology elaborated in chapter 3 for the generation of turboprop engine gas turbine surrogate models was then taken up and conveniently adapted in chapter 4 in order to elaborate a new surrogate engine model, this time for a direct-drive, two-spool, unmixed flow turbofan. Due to inherent differences between these two typologies of gas turbine engines, large part of chapter 4 was dedicated to a detailed description of the updated set of design laws and assumptions implemented for this specific case. Proof of validation of this surrogate engine was also provided, as well as several tests on the consistency of the results returned by this model. Section 4.3.2 illustrated the work performed in order to actually integrate this model in a conceptual/preliminary aircraft design tool, JPAD, allowing to go further, at least for the turbofan category of engines,

with respect to an *almost static* description of the characteristics of the powerplant, as provided in section 2.1, and implement the flexible approach summarized in figure 5.1. The last section of this chapter provided results for several applications. First, the surrogate engine was successfully tested for an aircraft model similar to the A320neo, providing further validation of the performed engine sizing. Then several parametric analyses on engine BPR and for different time scenarios were performed, in order to test the tool capability in an analysis framework similar to the one of ADORNO. The surrogate engine model performed well in this case too, providing consistent results and reasonable predictions in terms of fuel burn, emissions, and environmental noise. These results helped also to highlight how future developments for direct-drive turbofan engines, dictated by improvements in terms of core and propulsive efficiency, will not be sufficient to match the ambitious targets set by the environmental agenda. Even for the mid-term and long-term scenarios, this technology will not be able to provide a drastic cut in terms of carbon emissions, which is fundamental to limit the impact of the aviation on the global warming. A change in terms of engine configuration (i.e., geared turbofan) could lead to slightly higher benefits, allowing for higher propulsive efficiency and lower fuel consumption. But the impact would still be limited. This result is in line with the aviation technology roadmap set in [89], for which net zero carbon aviation can only be matched by transitioning to new propulsive technologies, such as hybrid-electric and full-electric propulsive systems.

5.2 Considerations and outlook

In relation to the research question of this thesis, the main achievement consisted in the definition of a general strategy for the rubberization and the generation of consistent engine surrogate models, that can be easily adapted to the most diverse conventional (and even unconventional) gas turbine architectures, as demonstrated by the applications shown in chapter 3 and in chapter 4. This general approach is provided in figure 5.2, and is a generalization of the ones illustrated in figure 3.21, for a three-spool, free turbine, turboprop engine, and in figure 4.1, for an unmixed-flow, direct-drive, two-spool high-bypass ratio turbofan. It was demonstrated in chapter 4 that a surrogate engine model produced with such an approach can be easily implemented in a typical conceptual/preliminary aircraft design framework, and used to carry out consistent and significant parametric analyses and trade-off studies on engine parameters, in order to determine the actual effect of engine design choices at aircraft level, and to select the best suitable gas turbine engine cycle based on considerations on all the relevant disciplines for this type of downselection: aircraft performance, emissions, environmental noise, and costs. This, for sure, represents an added value for a tool like JPAD and an element of novelty and innovation with respect to the most widely used conceptual/preliminary aircraft tools for research and industrial purposes.
Of course there is room for improvements both in terms of number, type, and level of fidelity of the methodologies applied in order to build a generic surrogate gas turbine model, and number of rubberized engine models implemented and available in JPAD. The list of upcoming tasks in this regard can be summarized as follows:

- Include in the GasTurb rubber model (independently of the gas turbine architecture) considerations on tip clearance effect on turbo components efficiencies, which have been so far ignored and may impact significantly on the performance

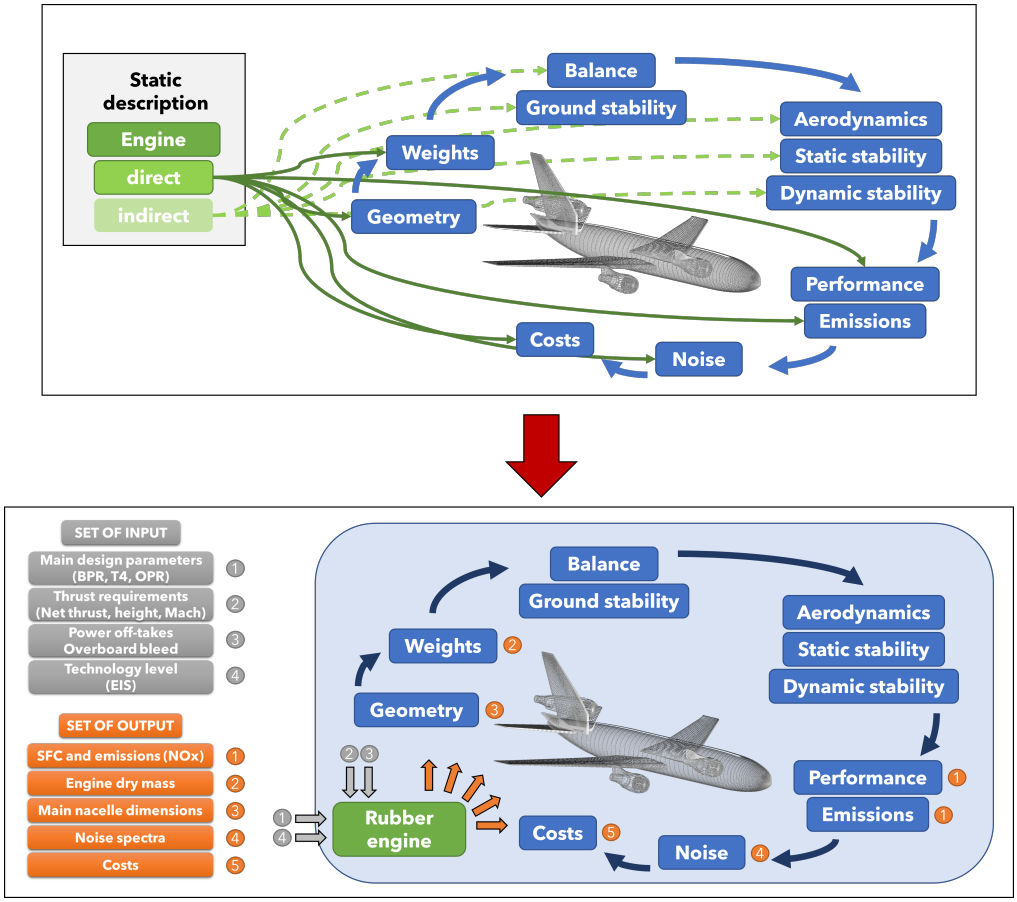

Figure 5.1: Overview on the set of improvements at aircraft analysis level dictated by the integration of a rubberized, surrogate model of a turbofan engine in JPAD.

of small-core engines.

- Already include in the surrogate models of turboprop engines considerations on the design of the propeller, by eventually implementing XROTOR for this purpose.
- Knowing the characteristics of the propeller, the surrogate model of a generic turboprop engine could be further enriched by the possibility to perform noise evaluations, by eventually implementing the approach reported in [176] for propeller noise.
- Expand the set of surrogate engines actually available in JPAD, by generating additional models for different turbofan architectures, such as:
  - three-spool, direct-drive engines;
  - two-spool, geared configurations;
  - mixed-flow turbofans.

  For each of the abovementioned architectures, different models could be elaborated, depending on the selected reference engine for the GasTurb implementation and on its thrust requirements.
- Include in JPAD surrogate engine models representative of turboprop architectures, including the abovelisted improvements.

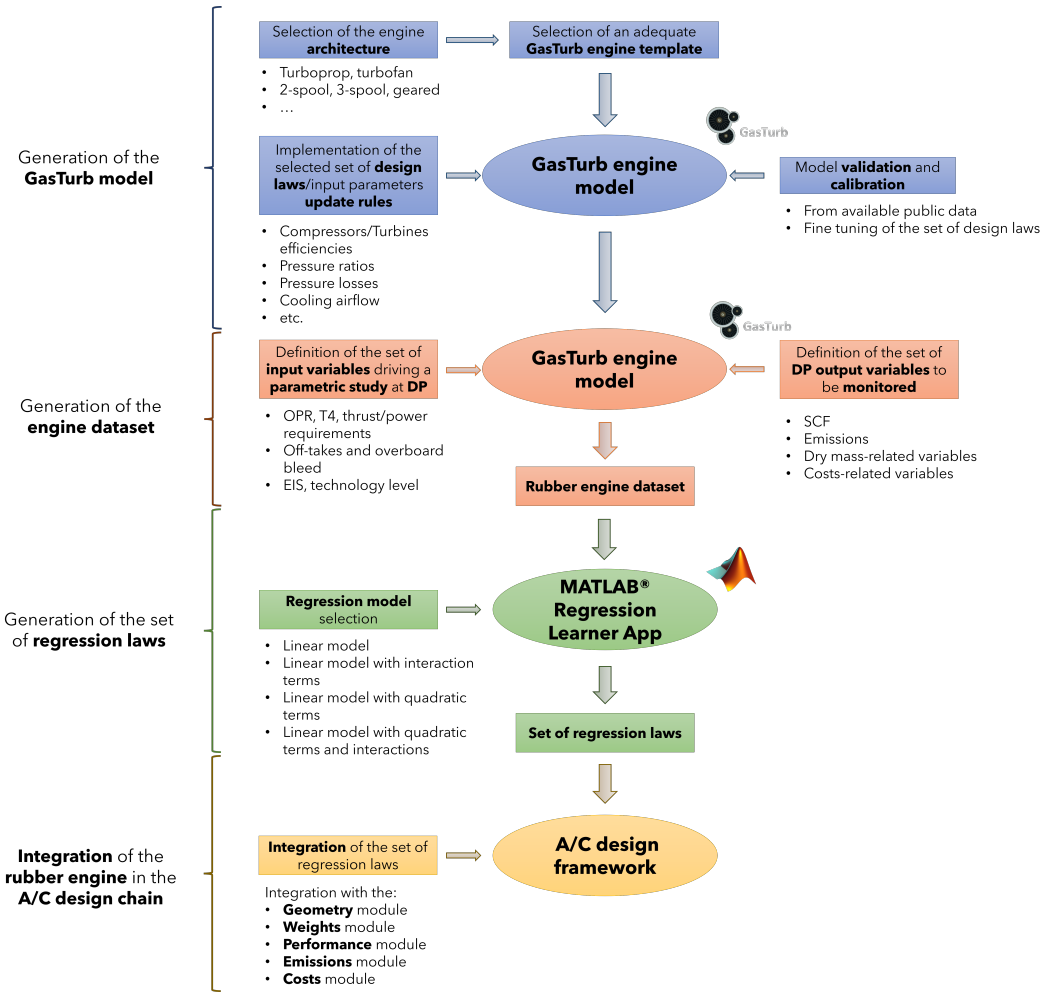

Figure 5.2: Generalized approach for the elaboration and the implementation at aircraft design and analysis level of surrogate model of a gas turbine engine.

Chapter 6

Appendix

6.1 Turbofan rubber model in-depth analysis

This section includes the contour plots derived from the analyses commented in section 4.2.

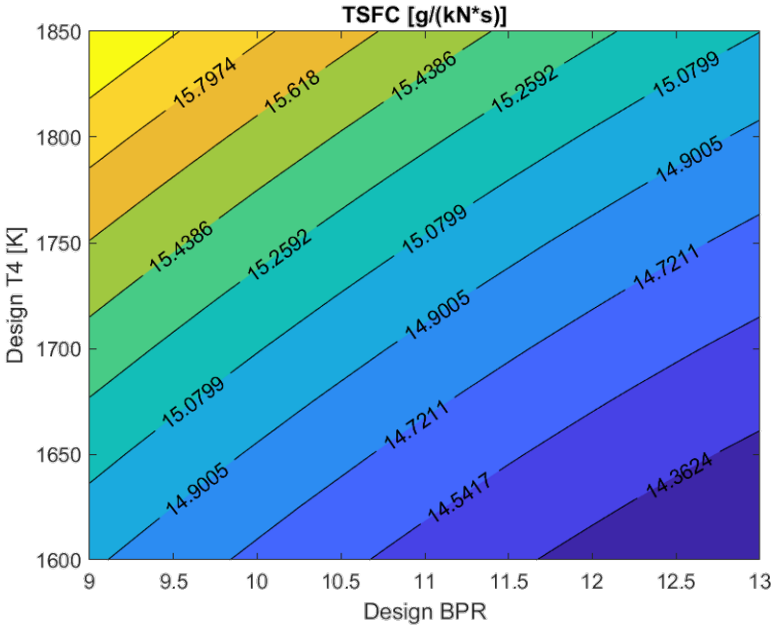

Figure 6.1: Effect of design BPR and T_4 on the ToC SFC. Assumptions on remaining input: EIS 2015, OPR 45:1, Mach 0.78, altitude 35000 ft, ToC net thrust 25 kN, T/O EoR net thrust 94.0 kN, overboard bleed 0.0 kg/s, power off-takes 0.0 kW.

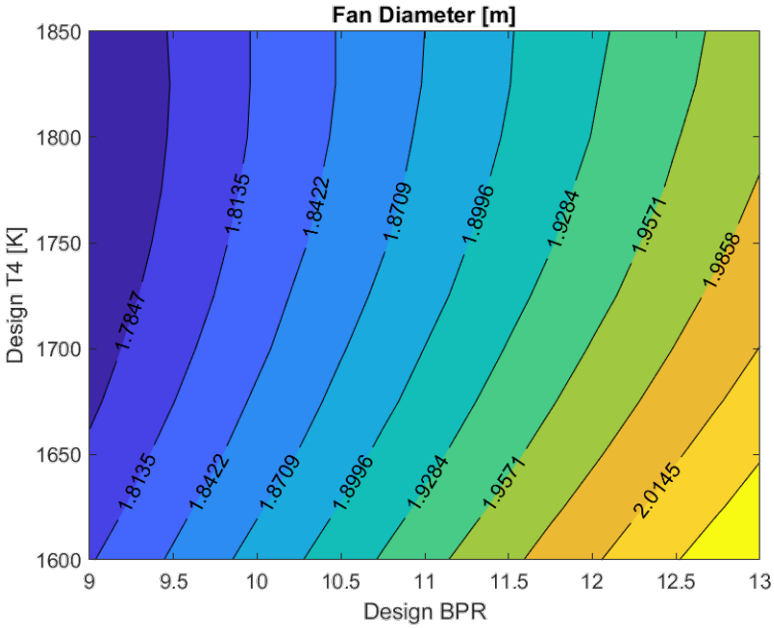

Figure 6.2: Effect of design BPR and T_4 on the fan diameter. Assumptions on remaining input: EIS 2015, OPR 45:1, Mach 0.78, altitude 35000 ft, ToC net thrust 25 kN, T/O EoR net thrust 94.0 kN, overboard bleed 0.0 kg/s, power off-takes 0.0 kW.

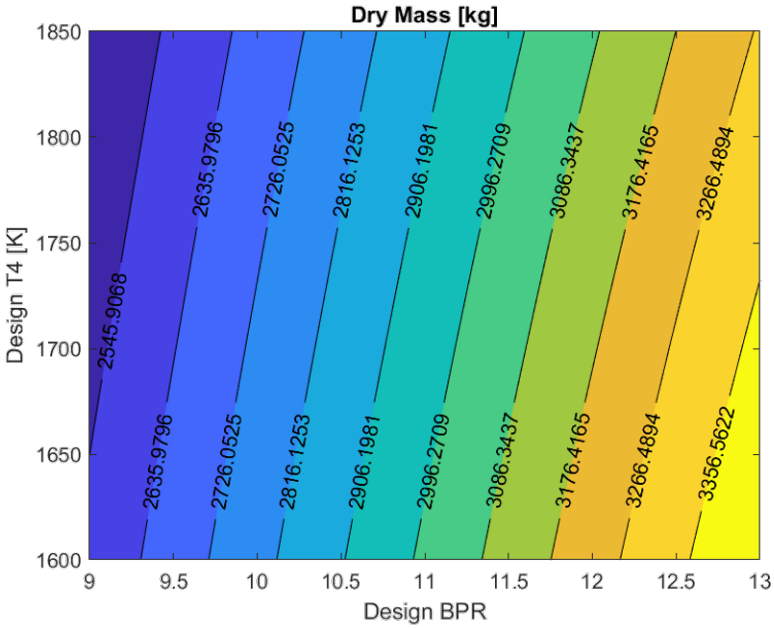

Figure 6.3: Effect of design BPR and T_4 on the engine dry mass. Assumptions on remaining input: EIS 2015, OPR 45:1, Mach 0.78, altitude 35000 ft, ToC net thrust 25 kN, T/O EoR net thrust 94.0 kN, overboard bleed 0.0 kg/s, power off-takes 0.0 kW.

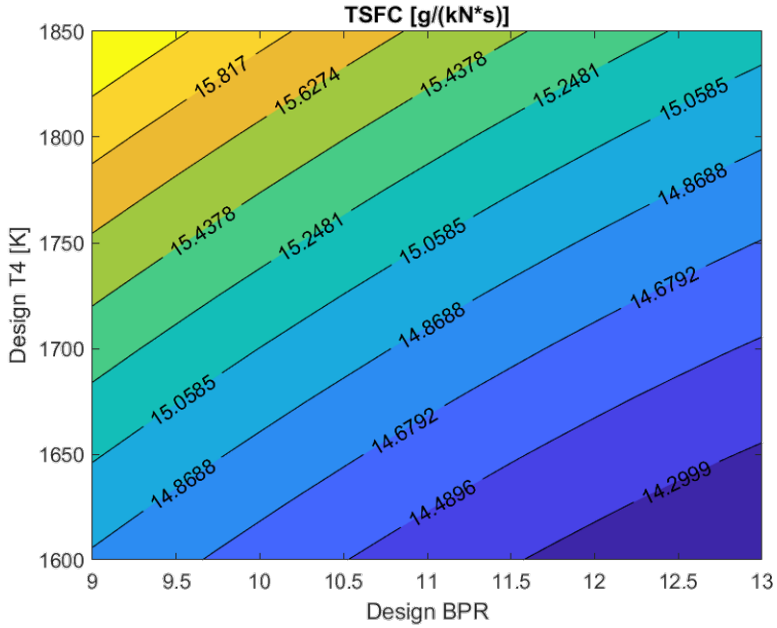

Figure 6.4: ToC SFC contour map with respect to different combinations of design BPR and T_4, and for a design OPR value equal to 50:1. Compared with figure 6.1 allows to check the effect of OPR on fuel consumption. With regards to the remaining input: EIS 2015, Mach 0.78, altitude 35000 ft, ToC net thrust 25 kN, T/O EoR net thrust 94.0 kN, overboard bleed 0.0 kg/s, power off-takes 0.0 kW.

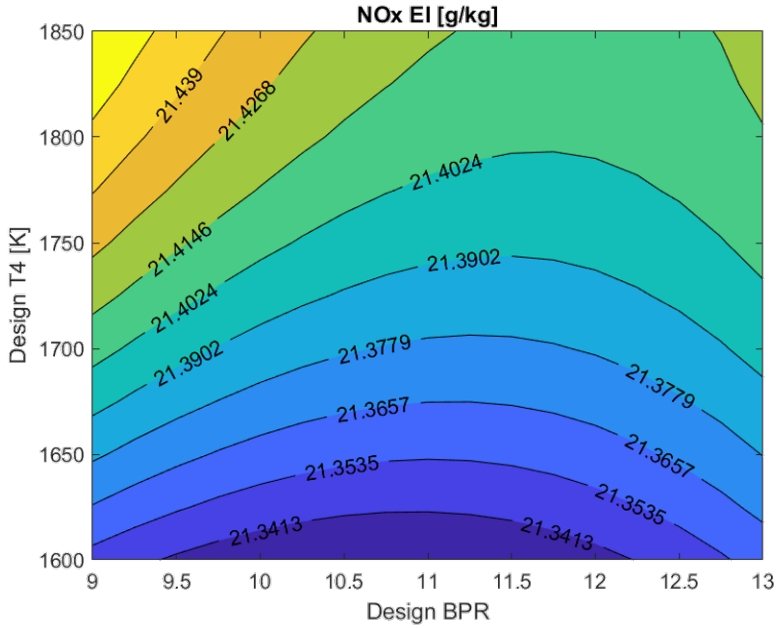

Figure 6.5: NO_x EI at ToC contour map with respect to different combinations of design BPR and T_4, and for a design OPR value equal to 45:1. Assumptions on remaining input: EIS 2015, Mach 0.78, altitude 35000 ft, ToC net thrust 25 kN, T/O EoR net thrust 94.0 kN, overboard bleed 0.0 kg/s, power off-takes 0.0 kW.

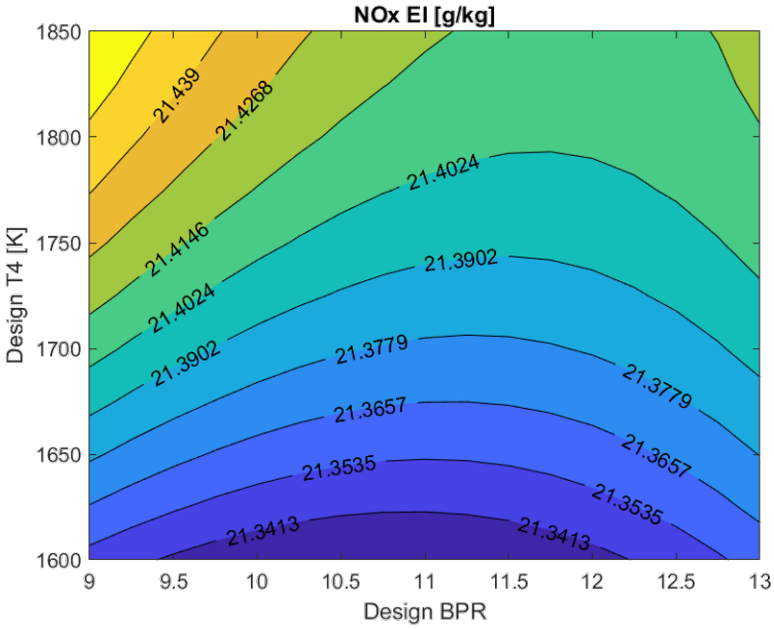

Figure 6.6: NO_x EI at ToC contour map with respect to different combinations of design BPR and T_4, and for a design OPR value equal to 50:1. Compared with figure 6.5 allows to check the effect of OPR on NO_x EI. Assumptions on remaining input: EIS 2015, Mach 0.78, altitude 35000 ft, ToC net thrust 25 kN, T/O EoR net thrust 94.0 kN, overboard bleed 0.0 kg/s, power off-takes 0.0 kW.

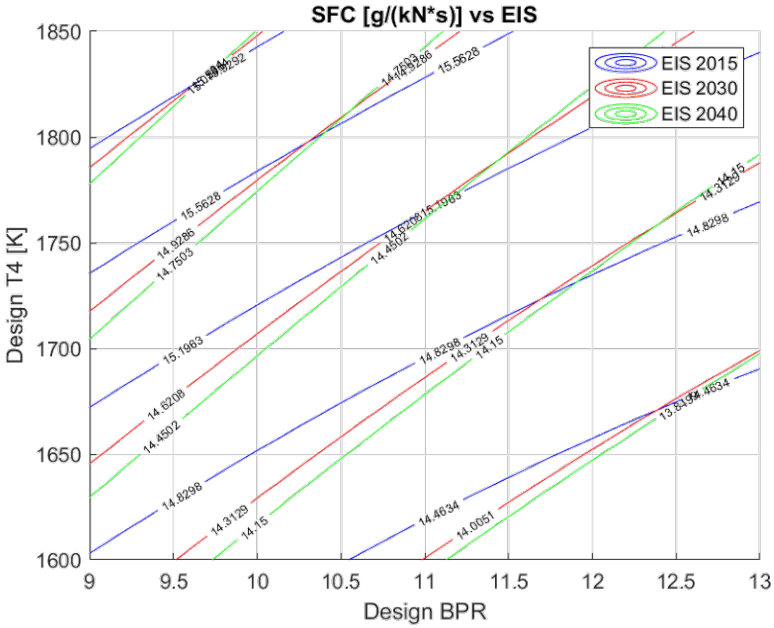

Figure 6.7: ToC SFC contours with respect to different combinations of design BPR and T_4, and for three different assumptions on engine EIS. Assumptions on remaining input: OPR 55:1, Mach 0.78, altitude 35000 ft, ToC net thrust 25 kN, T/O EoR net thrust 94.0 kN, overboard bleed 0.0 kg/s, power off-takes 0.0 kW.

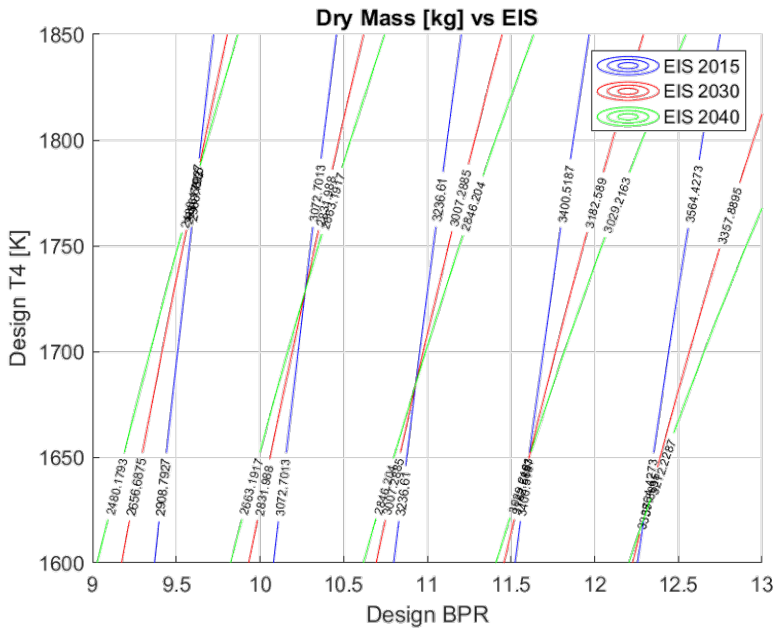

Figure 6.8: Engine dry mass contours with respect to different combinations of design BPR and T_4, and for three different assumptions on engine EIS. Assumptions on remaining input: OPR 55:1, Mach 0.78, altitude 35000 ft, ToC net thrust 25 kN, T/O EoR net thrust 94.0 kN, overboard bleed 0.0 kg/s, power off-takes 0.0 kW.

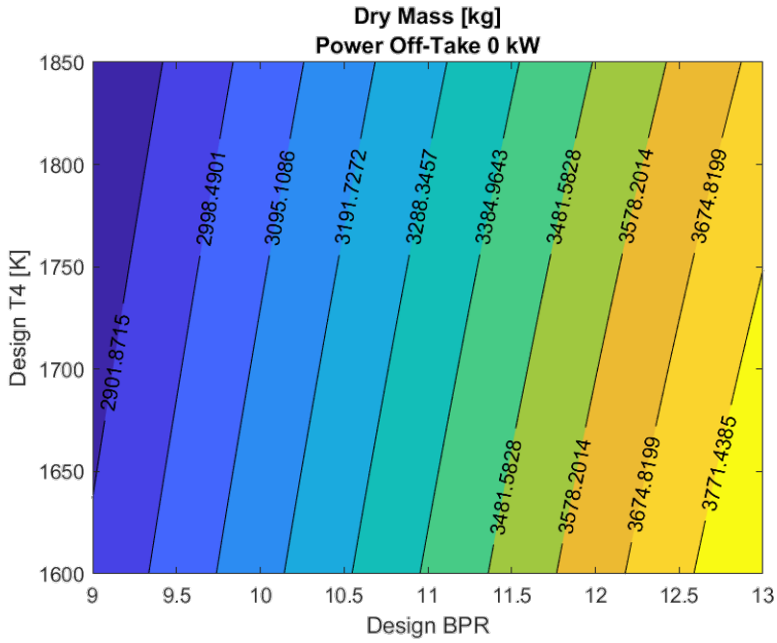

Figure 6.9: ToC SFC contours with respect to different combinations of design BPR and T_4, assuming 0.0 kW power off-takes. With regards to the remaining input: EIS 2015, OPR 55:1, Mach 0.78, altitude 35000 ft, ToC net thrust 25 kN, T/O EoR net thrust 94.0 kN, overboard bleed 0.85 kg/s.

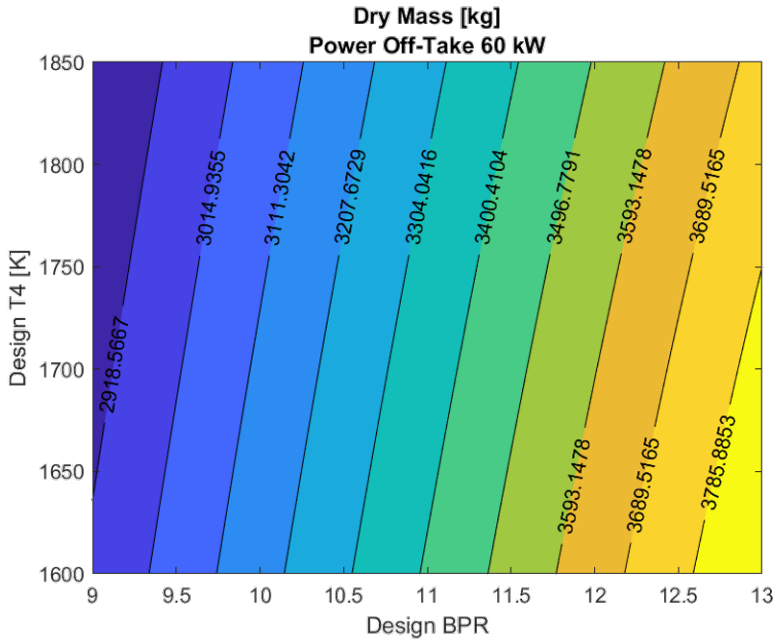

Figure 6.10: ToC SFC contours with respect to different combinations of design BPR and T_4, assuming 60.0 kW power off-takes. With regards to the remaining input: EIS 2015, OPR 55:1, Mach 0.78, altitude 35000 ft, ToC net thrust 25 kN, T/O EoR net thrust 94.0 kN, overboard bleed 0.85 kg/s.

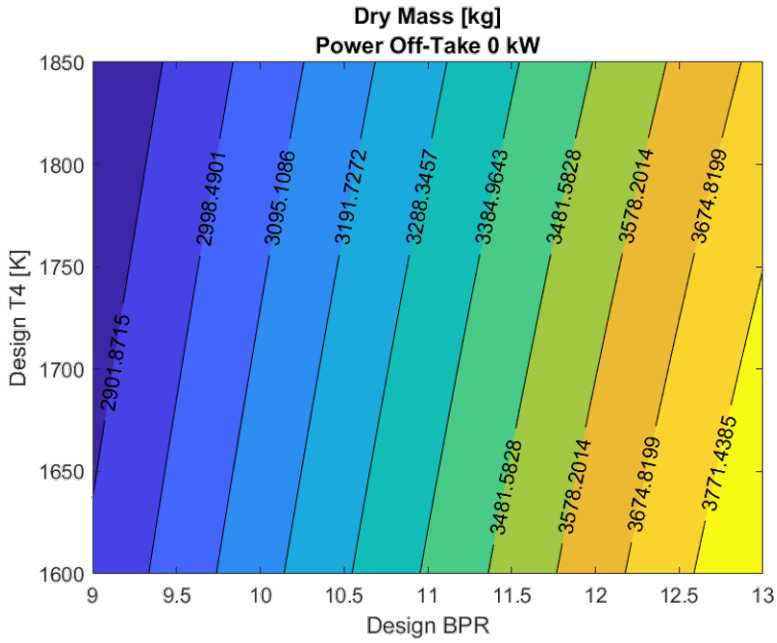

Figure 6.11: Engine dry mass contours with respect to different combinations of design BPR and T_4, assuming 0.0 kW power off-takes. With regards to the remaining input: EIS 2015, OPR 55:1, Mach 0.78, altitude 35000 ft, ToC net thrust 25 kN, T/O EoR net thrust 94.0 kN, overboard bleed 0.85 kg/s.

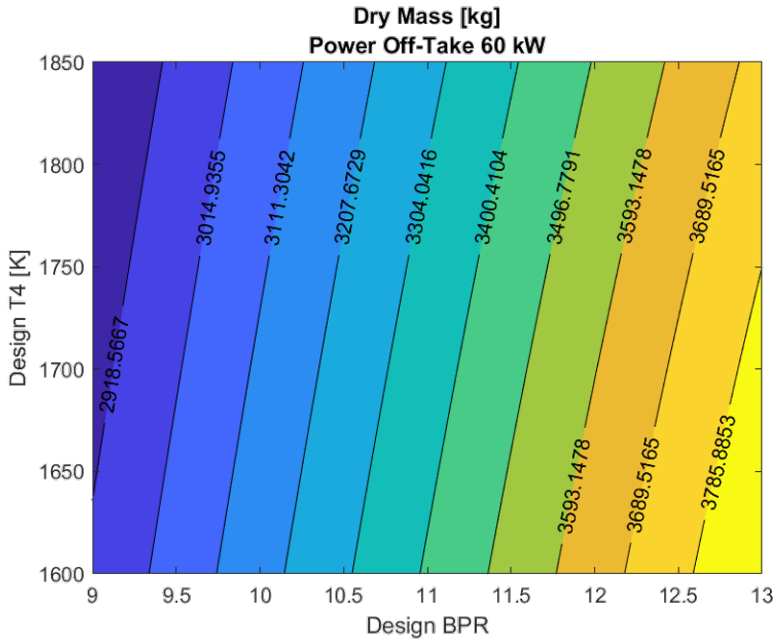

Figure 6.12: Engine dry mass contours with respect to different combinations of design BPR and T_4, assuming 60.0 kW power off-takes. With regards to the remaining input: EIS 2015, OPR 55:1, Mach 0.78, altitude 35000 ft, ToC net thrust 25 kN, T/O EoR net thrust 94.0 kN, overboard bleed 0.85 kg/s.

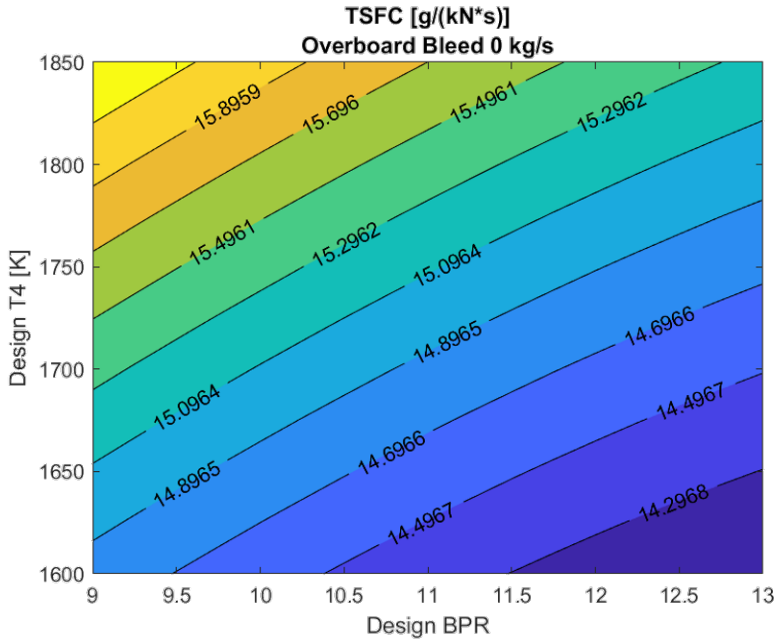

Figure 6.13: ToC SFC contours with respect to different combinations of design BPR and T_4, assuming 0.0 kg/s overboard bleed. With regards to the remaining input: EIS 2015, OPR 55:1, Mach 0.78, altitude 35000 ft, ToC net thrust 25 kN, T/O EoR net thrust 94.0 kN, power off-takes 0.0 kW.

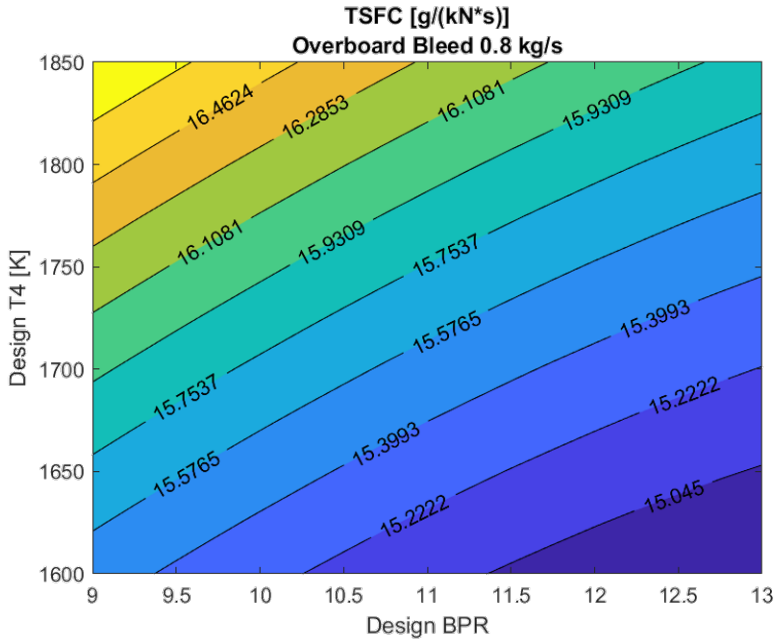

Figure 6.14: ToC SFC contours with respect to different combinations of design BPR and T_4, assuming 0.8 kg/s overboard bleed. With regards to the remaining input: EIS 2015, OPR 55:1, Mach 0.78, altitude 35000 ft, ToC net thrust 25 kN, T/O EoR net thrust 94.0 kN, power off-takes 0.0 kW.

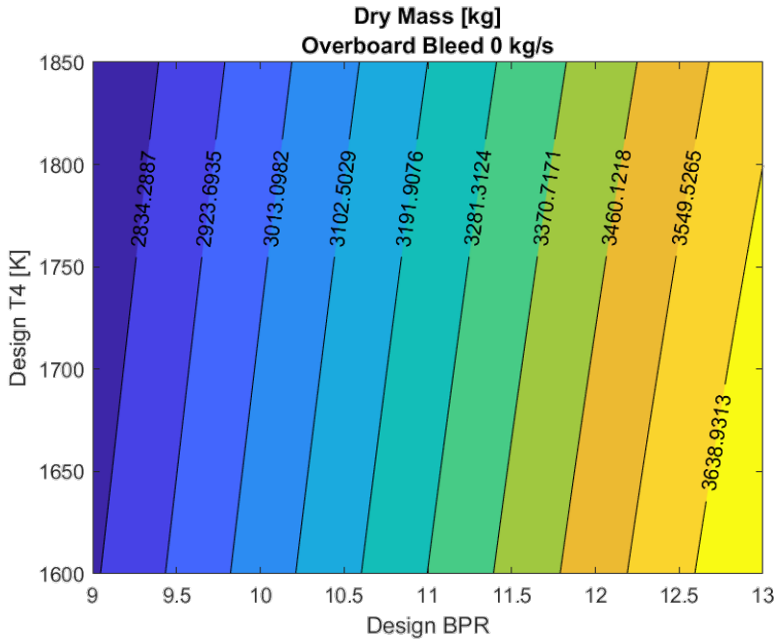

Figure 6.15: Engine dry mass contours with respect to different combinations of design BPR and T_4, assuming 0.0 kg/s overboard bleed. With regards to the remaining input: EIS 2015, OPR 55:1, Mach 0.78, altitude 35000 ft, ToC net thrust 25 kN, T/O EoR net thrust 94.0 kN, power off-takes 0.0 kW.

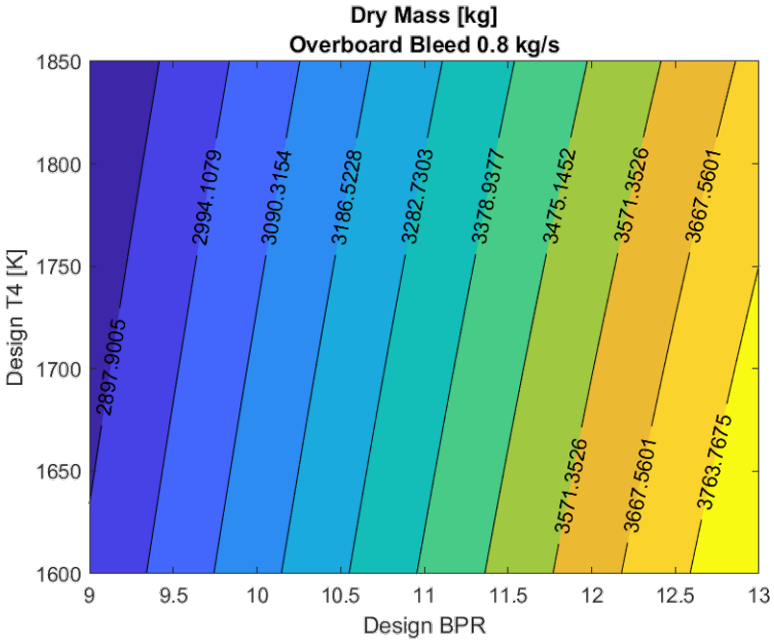

Figure 6.16: Engine dry mass contours with respect to different combinations of design BPR and T_4, assuming 0.8 kg/s overboard bleed. With regards to the remaining input: EIS 2015, OPR 55:1, Mach 0.78, altitude 35000 ft, ToC net thrust 25 kN, T/O EoR net thrust 94.0 kN, power off-takes 0.0 kW.

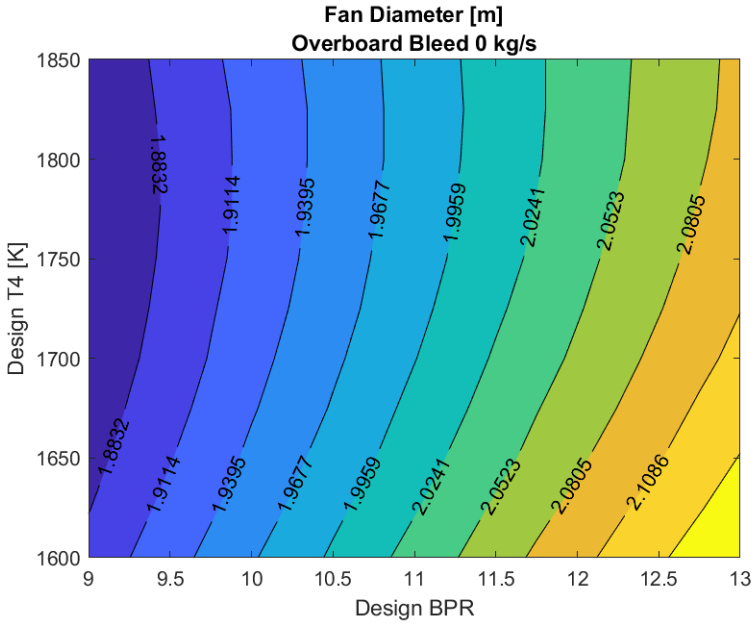

Figure 6.17: Fan diameter contours with respect to different combinations of design BPR and T_4, assuming 0.0 kg/s overboard bleed. With regards to the remaining input: EIS 2015, OPR 55:1, Mach 0.78, altitude 35000 ft, ToC net thrust 25 kN, T/O EoR net thrust 94.0 kN, power off-takes 0.0 kW.

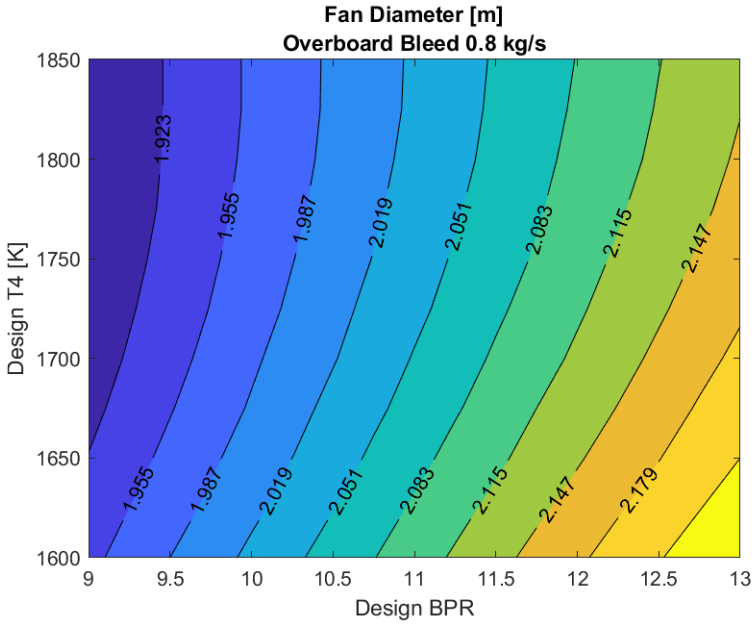

Figure 6.18: Fan diameter contours with respect to different combinations of design BPR and T_4, assuming 0.8 kg/s overboard bleed. With regards to the remaining input: EIS 2015, OPR 55:1, Mach 0.78, altitude 35000 ft, ToC net thrust 25 kN, T/O EoR net thrust 94.0 kN, power off-takes 0.0 kW.

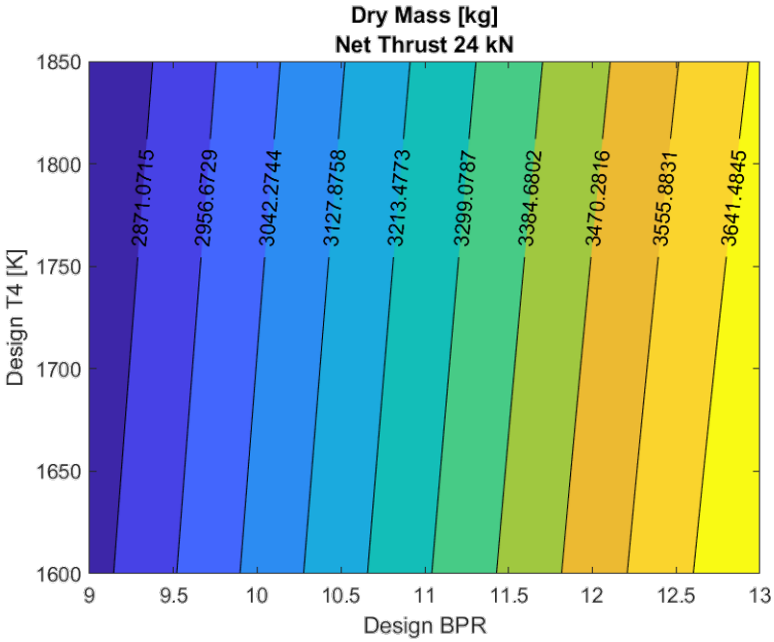

Figure 6.19: Engine dry mass contours with respect to different combinations of design BPR and T_4, assuming a DP net thrust equal to 24.0 kN and a T/O EoR net thrust equal to 94.1 kN. With regards to the remaining input: EIS 2015, OPR 55:1, Mach 0.78, altitude 35000 ft, overboard bleed 0.0 kg/s, power off-takes 0.0 kW.

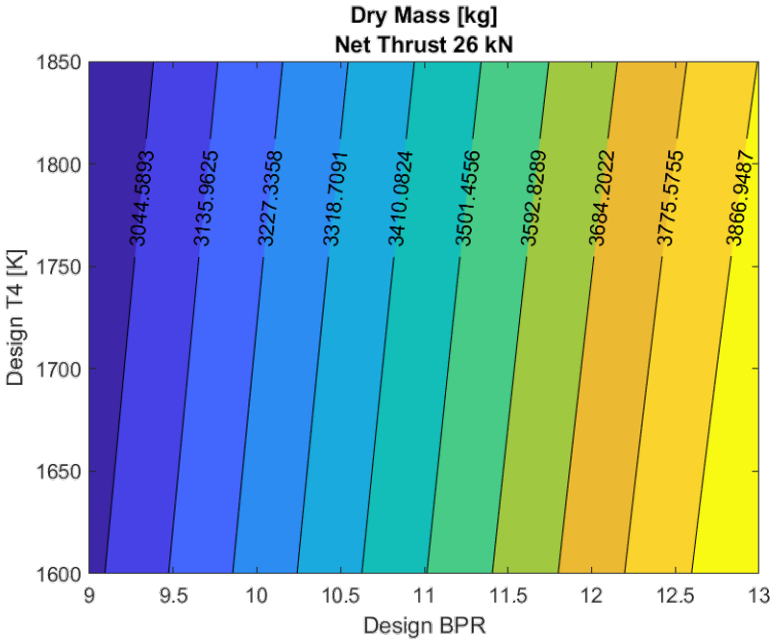

Figure 6.20: Engine dry mass contours with respect to different combinations of design BPR and T_4, assuming a DP net thrust equal to 26.0 kN and a T/O EoR net thrust equal to 102.0 kN. With regards to the remaining input: EIS 2015, OPR 55:1, Mach 0.78, altitude 35000 ft, overboard bleed 0.0 kg/s, power off-takes 0.0 kW.

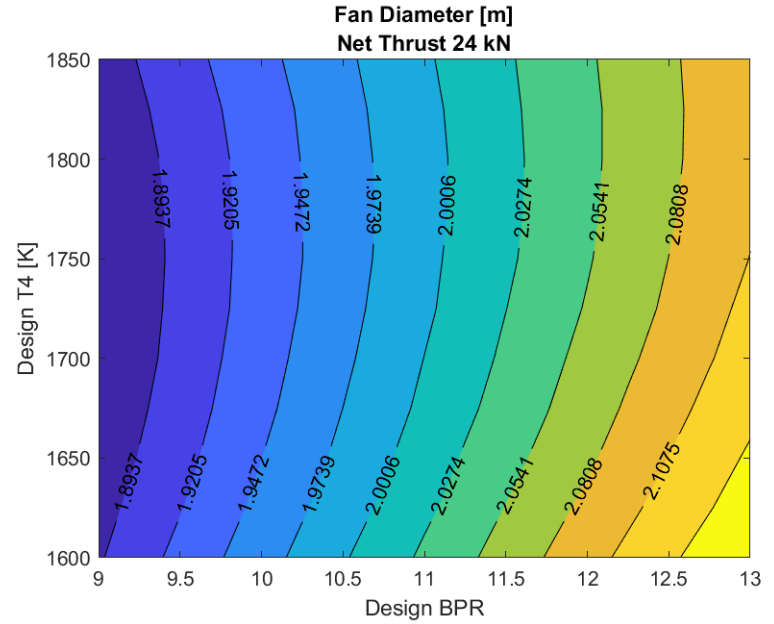

Figure 6.21: Fan diameter contours with respect to different combinations of design BPR and T_4, assuming a DP net thrust equal to 24.0 kN and a T/O EoR net thrust equal to 94.1 kN. With regards to the remaining input: EIS 2015, OPR 55:1, Mach 0.78, altitude 35000 ft, overboard bleed 0.0 kg/s, power off-takes 0.0 kW.

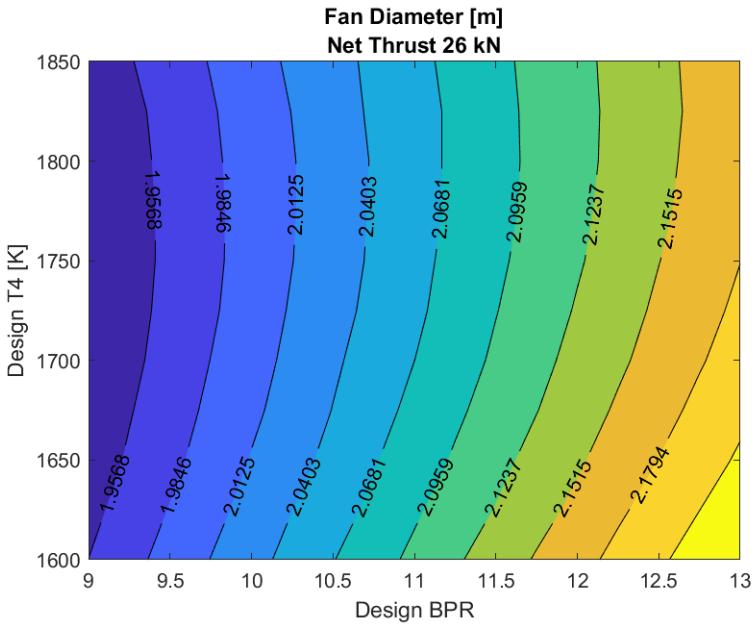

Figure 6.22: Fan diameter contours with respect to different combinations of design BPR and T_4, assuming a DP net thrust equal to 26.0 kN and a T/O EoR net thrust equal to 102.0 kN. With regards to the remaining input: EIS 2015, OPR 55:1, Mach 0.78, altitude 35000 ft, overboard bleed 0.0 kg/s, power off-takes 0.0 kW.

Acknowledgments

The author of this thesis would like to thank Professor Giovanni Torella and Doctor Reinhold Schaber for their support and help during the development of this work.

The ADORNO project has received funding from the Clean Sky 2 Joint Undertaking under the European Union's Horizon 2020 research and innovation program under Grant Agreement ENG ITD n° 821043. The author is grateful to MTU for their contributions and feedback on this research topic. The content of this thesis reflects only the author's view and both the European Commission and the Clean Sky 2 Joint Undertaking are not responsible for any use that may be made of the information it contains.

The GENESIS project has received funding from the Clean Sky 2 Joint Undertaking under Grant Agreement n° 101007968. The JU receives support from the European Union's Horizon 2020 research and innovation program and the Clean Sky JU members other than the Union. The author is grateful to the partners of the GENESIS consortium for their precious feedback. This thesis only reflects the author's view; the JU is not responsible for any use that may be made of the information it contains.

Bibliography

[1] I.H. Abbott and A.E. Von Doenhoff. *Theory of Wing Sections*. Dover Publications, 1959.

[2] M. Achtembosch. Material Flow Analysis: A comparison of manufacturing, use and fate of CFRP-Fuselage components versus Aluminum-Components for commercial airliners. Technical report, Fresenius Environmental Bulletin, 2003.

[3] Federal Aviation Administration. FAA Regulations 14 CFR Appendix B to Part 36. `https://www.ecfr.gov/current/title-14/chapter-I/subchapter-C/part-36`.

[4] AeroContact. ATR 42-500 - Unrivalled performance. Brochure. Accessed: 13/01/2022.

[5] AeroExpo. Airbus family figures - Farnborough 2018 Edition. Brochure, 2018.

[6] Bombardier Aerospace. Bombardier CSeries. Technical report, Bombardier Aerospace, 2017.

[7] Bombardier Aerospace. CSeries: airport planning publication. Technical report, Bombardier Aerospace, 2018.

[8] European Aviation Safety Agency. ICAO Aircraft Engine Emissions Databank. Accessed: 14/01/2022.

[9] European Aviation Safety Agency. Type-certificate data sheet No. E.003 for CFM56-5B and CFM56-5C series engines. Technical report, EASA, 2016.

[10] European Aviation Safety Agency. Type-certificate data sheet No. E.110 for LEAP-1A and LEAP-1C Series Engines. Technical report, EASA, 2016.

[11] European Aviation Safety Agency. Type-certificate data sheet No.EASA.IM.A.570 for BD-500 (A220 Series). Technical report, EASA, 2018.

[12] European Aviation Safety Agency. Type-certificate data sheet No.EASA.IM.E.041 for PW100 series engines. Technical report, EASA, 2018.

[13] European Aviation Safety Agency. Type-certificate data sheet No.IM.E.090 for PW1500G Series Engines. Technical report, EASA, 2018.

[14] European Aviation Safety Agency. Type-certificate data sheet No. IM.E.002 for GE90 Series Engines. Technical report, EASA, 2019.

[15] European Aviation Safety Agency. Type-certificate data sheet No. IM.E.021 for CF34-10E series engines. Technical report, EASA, 2020.

[16] European Aviation Safety Agency. Type-certificate data sheet No. EASA.A.064 for AIRBUS A318 – A319 – A320 – A321. Technical report, EASA, 2021.

[17] B. Aigner, P. Strathoff, and E. Stumpf. Micado: recent developments of models for design and evaluation of electric aircraft propulsion systems. In *Deutscher Luft- und Raumfahrtkongress 2020*, 2020.

[18] Airbus. A220-300: Purpose Built for Efficiency. `https://aircraft.airbus.com/en/aircraft/a220/a220-300`.

[19] Airbus. Airbus Family Figures - June 2017 Edition. Brochure.

[20] Airbus. Airbus A320 - Aircraft characteristics, airport maintenance and planning. Technical report, Airbus, 2020.

[21] International Air Transport Association. Aircraft Technology Roadmap. Technical report, IATA, 2013.

[22] International Air Transport Association. Aircraft Technology Roadmap: Technical Annex. Technical report, IATA, 2013.

[23] International Air Transport Association. Aircraft Technology Roadmap to 2050. Technical report, IATA, 2019.

[24] Air Transport Action Group (ATAG). Climate Change. `https://www.atag.org/our-activities/climate-change.html`, 2008. Accessed: 22/01/2022.

[25] GE Aviation. Cf34-10e turbofan propulsion system. `https://www.geaviation.com/sites/default/files/datasheet-CF34-10E.pdf`. Accessed: 09/03/2022.

[26] GE Aviation. Ge aviation receives orders for cf34-10e engines. `https://www.geaviation.com/press-release/cf34-engine-family/ge-aviation-receives-orders-cf34-10e-engines`, 2011. Accessed: 09/03/2022.

[27] GE Aviation. GE Aviation launches new turboprop engine, 2015. Accessed: 15/01/2022.

[28] F. Baptista. A 0-D Off-Design Performance Prediction Model of the CFM56-5B Turbofan Engine. Technical report, Universidade de Lisboa, 2017.

[29] S.L. Baughcum, T.G. Tritz, S.C. Henderson, and D.C. Pickett. Scheduled Civil Aircraft Emission Inventories for 1992: Database Development and Analysis. Technical report, NASA, 1996.

[30] C. Bayona-Roa, J.S. Solis-Chaves, J. Bonilla, A.G. Rodriguez-Melendez, and D. Castellanos. Computational simulation of pt6a gas turbine engine operating with different blends of biodiesel: A transient-response analysis. *Energies*, 12, 2019.

[31] J. Bijewitz, A. Seitz, and M. Hornung. Architectural comparison of advanced ultra-high bypass ratio turbofans for medium to long range applications. In *Deutscher Luft- und Raumfahrtkongress 2014*, 2014.

[32] J.A. Jr Blackwell. A finite-step method for calculation of theoretical load distributions for arbitrary lifting-surface arrangements at subsonic speeds. Technical note, NASA, 1969.

[33] Boeing. 777-200/300: Airplane Characteristics for Airport Planning. Technical report, Boeing, 2008.

[34] L. Boggero. *Design techniques to support aircraft systems development in a collaborative MDO environment*. PhD thesis, Politecnico di Torino, 2018.

[35] E. Botero, A.D. Wendroff, T. MacDonald, A. Variyar, J.M. Vegh, T. Lukaczyk, J.J. Alonso, T.H. Orra, and C.R. Ilario da Silva. Suave: An open-source environment for conceptual vehicle design and optimization. In *54^{th} AIAA Aerospace Sciences Meeting*, 2016.

[36] A.R. Byerley, A.J. Rolling, and K.W. Van Treuren. Estimating gas turbine engine weight, costs, and development time during the preliminary aircraft engine design process. In *ASME Turbo Expo 2013: Turbine Technical Conference and Exposition*, 2013.

[37] Pratt & Whitney Canada. PW100/PW150 - The Power Behind Regional Airline Turboprops, 2019. Accessed: 13/01/2022.

[38] J.B. Cantwell. The GE90: An Introduction. Technical report, Stanford University, 2011.

[39] D.L. Carter, Osborn R.F., J.A. Hetrick, and S. Kota. The quest for efficient transonic cruise. In *7^{th} AIAA Aviation Technology, Integration and Operations Conference*, 2007.

[40] C. Casale, T. Polito, V. Trifari, M. Di Stasio, P. Della Vecchia, F. Nicolosi, and F. Marulo. Implementation of a noise prediction software for civil aircraft applications. In *AIDAA XXV International Congress*, 2019.

[41] P. Catalano, D. de Rosa, B. Mele, R. Tognaccini, and F. Moens. Effects of riblets on the performances of a regional aircraft configuration in nlf conditions. In *AIAA SciTech Forum*, 2018.

[42] CFM. 2016 CFM orders surpass 2,600 engines. `https://www.cfmaeroengines.com/press-articles/2016-cfm-orders-surpass-2600-engines/`, 2017. Accessed: 21/01/2022.

[43] CFM. Lion group finalizes $5.5 billion U.S. LEAP-1A engine order. `https://www.cfmaeroengines.com/press-articles/lion-group-finalizes-5-5-billion-u-s-leap-1a-engine-order/`, 2018. Accessed: 20/01/2022.

[44] D. Ciliberti, P. Della Vecchia, F. Nicolosi, and A. De Marco. Aircraft directional stability and vertical tail design: a review of semi-empirical methods. *Progress in Aerospace Sciences*, 55:140–172, 2017.

[45] S. Ciornei. *Mach number, relative thickness, sweep and lift coefficient of the wing – An empirical investigation of parameters and equations.* PhD thesis, Hamburg University of Applied Sciences, Department of Automotive and Aeronautical Engineering, 2005.

[46] European Commission. Amended Proposal COM 2002/683 of the European Parliament and the Council for a Directive on the Establishment of a Community Framework for Noise Classification for Civil Subsonic Aircraft of 29.11.2002. Technical report, 2002. https://ec.europa.eu/transparency/documents-register/detail?ref=COM(2002)683&lang=en.

[47] European Civil Aviation Conference. Recommendation ECAC/27-4, NO_x Emission Classification Scheme. Technical report, ECAC, 2003.

[48] E. Coustols and V. Schmitt. Synthesis of experimental riblets studies in transonic conditions. In *45th European Drag Reduction Meeting*, 1990.

[49] N.S. Currey. *Aircraft landing gear design: principles and practices.* AIAA, 1988.

[50] V. Cusati. *Design activities for innovative turboprop aircraft with minimum economic and environmental impact.* PhD thesis, University of Naples Federico II, 2020.

[51] M. Daly. *Jane's Aero Engines.* Jane's Information Group, 2002.

[52] DARcorporation. Advanced Aircraft Analysis (AAA) - Aircraft Design & Analysis. https://www.darcorp.com/wp-content/uploads/2019/05/AAA-Brochure-1.pdf, 2019. Accessed: 24/01/2022.

[53] DARcorporation. Advanced aircraft analysis (aaa). https://www.darcorp.com/advanced-aircraft-analysis-software/, 2022. Accessed: 24/01/2022.

[54] Gobierno de Espana. Incident involving an ATR 72-212 A aircraft, registration EC-MPI, operated by Canarias Airlines at the Tenerife North Airport (GCXO) on 15 October 2019, 2019. Accessed: 13/01/2022.

[55] A. De Marco, M. Di Stasio, P. Della Vecchia, V. Trifari, and F. Nicolosi. Automatic modeling of aircraft external geometries for preliminary design workflows. *Aerospace Science and Technology*, 98, 2020.

[56] P. Della Vecchia, F. Nicolosi, and D. Ciliberti. Aircraft directional stability prediction method by cfd. In *33rd AIAA Applied Aerodynamic Conference*, 2015.

[57] M. Di Stasio, V. Trifari, F. Nicolosi, A. De Marco, S. Fuhrmann, and R. Schaber. Multidisciplinary optimization of a regional jet including advanced airframe and engine technologies. In *AIAA AVIATION Forum 2021*, 2021.

[58] A. Dik, N. Biten, V. Zaccaria, I. Aslanidou, and K.G. Kyprianidis. Conceptual design of a 3-shaft turbofan engine with reduced fuel consumption for 2025. In *9th International Conference on Applied Energy*, 2017.

[59] EASA. Jet aeroplanes noise database. https://www.easa.europa.eu/domains/environment/easa-certification-noise-levels, 2021. Accessed: 26/01/2022.

[60] Embraer. Embraer 190: airport planning manual. Technical report, Embraer, 2021.

[61] Eurocontrol. Aircraft Performance Database - A20N. Accessed: 26/01/2022.

[62] Eurocontrol. Forecasting civil aviation fuel burn and emissions in Europe - Interim Report. Accessed: 14/01/2022.

[63] Copernicus Europe's eyes on Earth. How close are we to reaching a global warming of 1.5°C? https://climate.copernicus.eu/how-close-are-we-reaching-global-warming-15degc, 2021. Accessed: 22/01/2022.

[64] Copernicus Europe's eyes on Earth. Climate Data Store - Global temperature trend monitor. https://cds.climate.copernicus.eu/apps/c3s/app-c3s-global-temperature-trend-monitor?month:float=12&year:float=2021, 2021. Accessed: 22/01/2022.

[65] B. Fehrm. Fundamentals of airliner performance, Part 6; The engine. https://leehamnews.com/2015/01/19/fundamentals-of-airliner-performance-part-6-the-engine/, 2015. Accessed: 20/01/2022.

[66] F. Ferrari. Impact of different subsystem architectures on aircraft engines in terms of specific fuel consumption. Master's thesis, Politecnico di Torino, Italy, 2018.

[67] A. Filippone. *Flight Performance Software FLIGHT*. University of Manchester.

[68] A. Filippone. *Advanced Aircraft Flight Performance*. Cambridge University Press, 2013.

[69] A. Filippone and N. Bojdo. Statistical model for gas turbine engines exhaust emissions. *Transportation Research Part D: Transport and Environment*, 59:451–463, 2018.

[70] M.R. Fink. Airframe noise prediction method. Technical report, FAA, 1977.

[71] M. Fioriti, L. Boggero, A. Mirzoyan, and A. Isyanov. Studies on propulsion and onboard systems matching in agile project distributed collaborative mdo environment applying for advanced regional and medium haul jet. In *31st Congress of the International Council of the Aeronautical Sciences (ICAS)*, 2018.

[72] Advisory Council for Aeronautics Research in Europe. Startegic Research Agenda - Volume I. Technical report, ACARE, 2001.

[73] Advisory Council for Aeronautics Research in Europe (ACARE). Protecting the environment and the energy supply. https://www.acare4europe.org/sria/flightpath-2050-goals/protecting-environment-and-energy-supply-0, 2012. Accessed: 22/01/2022.

[74] N. Gasparovic. Das zweistromtriebwerk bei optimaler und nicht-optimaler auslegung. *Forsch. Ing.-Wesen*, 42(5):157–168, 1976.

[75] J.W. Gauntner. Algorithm for calculating turbine cooling flow and the resulting decrease in turbine efficiency. Technical report, NASA, 1980.

[76] S. Gialanella and Malandruccolo A. *Aerospace Alloys*. Springer Nature, 2019.

[77] V. Grewe, A. Gangoli Rao, T. Gronstedt, C. Xisto, F. Linke, J. Melkert, J. Middel, B. Ohlenforst, S. Blakey, S. Christie, S. Matthes, and K. Dahlmann. Evaluating the climate impact of aviation emission scenarios towards the paris agreement including covid-19 effects. *Nature Communications*, 12, 2021.

[78] H. Grieb. *Projektierung von Turboflugtriebwerken*. Springer Basel, 2004.

[79] S. Gudmundsson. *General Aviation Aircraft Design*. Butterworth-Heinemann, 2013.

[80] M. Guynn, J.J. Berton, K.L. Fisher, W.J. Haller, M.T. Tong, and D.R. Thurman. Refined exploration of turbofan design options for an advanced single-aisle transport. Technical report, NASA, 2011.

[81] J. Heidmann. Improving engine efficiency through core developments. In *AIAA Aero Sciences Meeting 2011*, 2011.

[82] J. Hemmerdinger. GE Aviation lost 1,900 LEAP orders in 12 months. `https://www.flightglobal.com/ge-aviation-lost-1900-leap-orders-in-12-months/143476.article`, 2021. Accessed: 20/01/2022.

[83] H.W. Hilton. *High Speed Aerodynamics*. Longmans, 1951.

[84] R. Horonjeff and F.X. McKelvey. *Planning and Design of Airports*. McGraw-Hill, 1994.

[85] E. Hosking, D.P. Kenny, R.I. McCormick, S.H. Moustapha, P. Sampath, and A.A. Smailys. The pw100 engine: 20 years of gas turbine technology evolution. In *RTO AVT Symposium*, 1998.

[86] D. Howe. *Aircraft conceptual design synthesis*. John Wiley & Sons Inc., 2000.

[87] H.H. Hurt. Aerodynamics for Naval Aviators. Technical report, University of Southern California, 1965.

[88] International Air Transport Association (IATA). Building new technologies. `https://www.iata.org/en/programs/environment/technology-roadmap/`, 2021. Accessed: 22/01/2022.

[89] International Air Transport Association (IATA). Net zero 2050: new aircraft technology. `https://www.iata.org/contentassets/b3783d24c5834634af59148c718472bb/factsheet_newaircrafttechnology.pdf`, 2021. Accessed: 04/03/2022.

[90] International Air Transport Association (IATA). Our commitment to fly net zero by 2050. `https://www.iata.org/en/programs/environment/flynetzero/`, 2021. Accessed: 04/03/2022.

[91] Biofuels International. Turkish Airlines starts using SAF on its flights. https://biofuels-news.com/news/turkish-airlines-starts-using-saf-on-its-flights/, 2022. Accessed: 05/03/2022.

[92] CFM International. CFM International LEAP series. Accessed: 17/01/2022.

[93] CFM International. LEAP Overview. Accessed: 17/01/2022.

[94] Forecast International. The market for aviation turboprop engines: 2010-2019, 2010. Accessed: 15/01/2022.

[95] A.J.B. Jackson. *Optimization of Aero and Industrial Gas Turbine Design for the Environment*. PhD thesis, Cranfield University, 2009.

[96] L. Jenkinson, P. Simpkin, and D. Rhodes. Civil jet aircraft design - data b: engine data file. https://booksite.elsevier.com/9780340741528/appendices/data-b/default.htm, 2001. Accessed: 09/03/2022.

[97] L.R. Jenkinson, P. Simpkin, and D. Rhodes. *Civil Jet Aircraft Design*. Elsevier, 1999.

[98] R.D. Joslin. Overview of Laminar Flow Control. Technical report, NASA, 1998.

[99] V. Karnozov. Aviadvigatel Mulls Higher-thrust PD-14s To Replace PS-90A. https://www.ainonline.com/aviation-news/air-transport/2019-08-19/aviadvigatel-mulls-higher-thrust-pd-14s-replace-ps-90a, 2019. Accessed: 21/01/2022.

[100] I. Kroo. *Aircraft Design: Synthesis and Analysis*. 1999.

[101] A.K. Kundu. *Aircraft Design*. Cambridge University Press, 2012.

[102] J. Kurzke. Performance modeling methodology: efficiency definitions for cooled single and multistage turbines. In *ASME Turbo Expo 2002*, 2002.

[103] J. Kurzke. Achieving maximum thermal efficiency with the simple gas turbine cycle. Technical report, MTU Aero Engines, 2003.

[104] J. Kurzke. How to create a performance model of a gas turbine from a limited amount of information. In *ASME Turbo Expo 2005: Power for Land, Sea and Air*, 2005.

[105] J. Kurzke. *GasTurb 11 - Design and Off-Design Performance of Gas Turbines*. GasTurb GmbH, 2007.

[106] J. Kurzke. Fundamental differences between conventional and geared turbofans. In *ASME Turbo Expo 2009: Power for Land, Sea and Air*, 2009.

[107] K.G. Kyprianidis. Future aero engine designs: An evolving vision. In *IntechOpen*, 2011.

[108] O. Laneckij and A. Raschuk. The Plastic Airplane: a Review of the World's First Bombardier CS300 Airliner. https://en.cfts.org.ua/articles/the_plastic_airplane_a_review_of_the_worlds_first_bombardier_cs300_airliner, 2016. Accessed: 06/01/2022.

[109] R.H. Lange. Application of Hybrid Laminar Flow Control to Global Range Military Transport Aircraft. Technical report, NASA, 1988.

[110] D.S. Lee, D.W. Fahey, A. Skowron, M.R. Allen, U. Burkhardt, Q. Chen, S.J. Doherty, S. Freeman, P.M. Forster, J. Fuglestvedt, A. Gettelman, R.R. De Leon, L.L. Lim, M.T. Lund, R.J. Millar, B. Owen, J.E. Penner, G. Pitari, M.J. Prather, R. Sausen, and L.J. Wilcox. The contribution of global aviation to anthropogenic climate forcing for 2000 to 2018. *Atmospheric Environment*, 244, 2021.

[111] P. Lolis. *Development of a Preliminary Weight Estimation Method for Advanced Turbofan Engines*. PhD thesis, Cranfield University, School of Engineering, 2014.

[112] T. Lukaczyk, A.D. Wendroff, E. Botero, T. MacDonald, T. Momose, A. Variyar, J.M. Vegh, M. Colonno, T.D. Economon, and J.J. Alonso. Suave: An open-source environment for multi-fidelity conceptual vehicle design. In *16th AIAA/ISSMO Multidisciplinary Analysis and Optimization Conference*, 2015.

[113] Z. Lyu and J.R.R.A. Martins. Aerodynamic shape optimization of an adaptive morphing trailing-edge wing. *Journal of Aircraft*, 52(6), 2015.

[114] P. Madden. Clean Sky 2 cleared for take-off with €4.05B budget. https://sciencebusiness.net/news/76201/Clean-Sky-2-cleared-for-take-off-with-%E2%82%AC4.05B-budget, 2013. Accessed: 22/01/2022.

[115] D.R. Martins. Off-Design Performance Prediction of the CFM56-3 Aircraft Engine. Technical report, Universidade de Lisboa, 2015.

[116] MathWorks. Regression learner app, 2021. Accessed: 16/01/2022.

[117] J. Mattingly, H. Heiser, and T. Pratt. *Aircraft Engine Design - 2nd edition*. AIAA, 2002.

[118] B.W. McCormick. *Aerodynamics, Aeronautics, and Flight Mechanics*. John Wiley & Sons Inc., 1995.

[119] J. McGurty. United Airlines launches first commercial flight with 100% SAF. https://www.spglobal.com/commodity-insights/en/market-insights/latest-news/agriculture/120121-united-airlines-launches-first-commercial-flight-with-100-saf, 2021. Accessed: 05/03/2022.

[120] J.D. McLean, D.N. George-Falvy, and P.P. Sullivan. Flight-test of turbulent skin friction reduction by riblets. In *International Conference on Turbulent Drag Reduction by Passive Means*, 1987.

[121] Nathan Meier. Jet Engine Specification Database. Accessed: 14/01/2022.

[122] P. Meyer. Application of HLF Technology to Civil Nacelle. In *CEAS/DragNet European Drag Reduction Conference*, 2001.

[123] United Nations. The Paris agreement. https://unfccc.int/process-and-meetings/the-paris-agreement/the-paris-agreement, 2015. Accessed: 22/01/2022.

[124] BBC News. Europe push for greener aviation. http://news.bbc.co.uk/2/hi/europe/7228054.stm, 2008. Accessed: 22/01/2022.

[125] L. Nicolai and G. Carichner. *Fundamentals of Aircraft and Airship Design*. AIAA, 2013.

[126] F. Nicolosi, D. Ciliberti, and P. Della Vecchia. Aerodynamic design guidelines of aircraft dorsal fin. In *34th AIAA Applied Aerodynamics Conference*, 2016.

[127] F. Nicolosi, D. Ciliberti, P. Della Vecchia, and S. Corcione. Wind tunnel testing of a generic regional turboprop aircraft modular model and development of improved design guidelines. In *AIAA AVIATION Forum 2018*, 2018.

[128] F. Nicolosi, D. Ciliberti, P. Della Vecchia, S. Corcione, and V. Cusati. A comprehensive review of vertical tail design. *Aircraft Engineering and Aerospace Technology*, 89(4):547–557, 2017.

[129] F. Nicolosi, S. Corcione, and P. Della Vecchia. Commuter aircraft aerodynamic design: Wind-tunnel tests and cfd analysis. In *29th ICAS Conference*, 2014.

[130] F. Nicolosi, P. Della Vecchia, and D. Ciliberti. Aerodynamic interference issues in aircraft directional control. *ASCE's Journal of Aerospace Engineering*, 28(1), 2015.

[131] F. Nicolosi, P. Della Vecchia, D. Ciliberti, and V. Cusati. Fuselage aerodynamic prediction methods. *Aerospace Science and Technology*, 55:332–343, 2016.

[132] F. Nicolosi, P. Della Vecchia, and S. Corcione. Design and aerodynamic analysis of a twin-engine commuter aircraft. *Aerospace Science and Technology*, 40:1–16, 2015.

[133] F. Nicolosi, P. Della Vecchia, V. Trifari, M. Di Stasio, F. Marulo, A. De Marco, V. Marciello, and V. Cusati. Noise, emissions and costs trade factors for regional jet platforms using a new software for aircraft preliminary design. In *AIAA AVIATION Forum 2020*, 2020.

[134] G. Norris and G. Thomas. *Boeing 787 Dreamliner - Flying Redefined*. Aerospace Technical Publications, 2005.

[135] RWTH Aachen University Institute of Aerospace Systems. Multidisciplinary Integrated Conceptual Aircraft Design and Optimization Environment. https://www.ilr.rwth-aachen.de/cms/ILR/Forschung/Ausstattung/~hzpwy/MICADO/?lidx=1, 2021. Accessed: 24/01/2022.

[136] Air Transport Association of America. Standard Method of Estimating Comparative Direct Operating Costs of Turbine Powered Transport Airplanes. Technical report, ATA, 1967.

[137] Society of Automotive Engineers. Gas Turbine Exhaust Noise Prediction - ARP-876D. Technical report, SAE, 1994.

[138] Association of European Airlines. AEA Requirements. Technical report, AEA, 1989.

[139] University of Manchester. Aircraft software puts greener, quieter flights on the horizon. https://www.manchester.ac.uk/discover/news/article/?id=6177, 2010. Accessed: 24/01/2022.

[140] University of Manchester. FLIGHT - Improving aircraft performance. http://www.flight.mace.manchester.ac.uk/aircraft-performance-software/index.html, 2022. Accessed: 24/01/2022.

[141] Massachussets Institute of Technology. Design Methodologies for Aerodynamics, Structures, Weight, and Thermodynamic Cycles. Technical report, MIT, 2010.

[142] F. Orefice. *Conceptual Design of Hybrid-Electric Aircraft.* PhD thesis, University of Naples Federico II, 2022.

[143] International Civil Aviation Organization. Annex 16 - Environmental Protection - Volume I - Aircraft Noise (8^{th} edition. Technical report, 2017.

[144] International Civil Aviation Organization. Annex 16 - Environmental Protection - Volume II - Aircraft Engine Emissions (4^{th} edition). Technical report, 2017.

[145] International Civil Aviation Organization. Annex 14 - Aerodromes - Volume I - Aerodromes Design and Operations. Technical report, 2018.

[146] C. Osterheld, W. Heinze, and P. Horst. Preliminary design of a blended wing body configuration using the design tool prado. In *CEAS Conference on Multidisciplinary Aircraft Design and Optimisation*, 2001.

[147] European Parliament. Sustainable aviation fuels. Accessed: 14/01/2022.

[148] W.J.G. Pinsker. The Landing Flare of Large Transport Aircraft. Reports and memoranda, RAE Bedford, 1967.

[149] D. Raymer. *Aircraft Design: A Conceptual Approach, 5^{th} ed.* AIAA, 2012.

[150] R.G. Ribeiro. A comparative study of turbofan engines bypass ratio. Master's thesis, Aeronautics Institute of Technology Sao Jose dos Campos, Brazil, 2013.

[151] K. Risse, E. Anton, T. Lammering, and K. Franz. An integrated environment for preliminary aircraft design and optimization. In *53^{rd} AIAA/ASME/ASCE/AHS/ASC Structures, Structural Dynamics and Materials Conference*, 2012.

[152] H. Ritchie. Climate change and flying: what share of global co_2 emissions come from aviation? https://ourworldindata.org/co2-emissions-from-aviation, 2020. Accessed: 22/01/2022.

[153] J. Roskam. *Airplane Design.* DARCorporation, 1985.

[154] E. Roux. *Modeles Moteur: reacteurs double flux civils et reacteurs militaires a faible taux de dilution avec PC.* PhD thesis, INSA Rouen, SUPAERO, ONERA, 2002.

[155] M. Ruocco. *High-lift and stability issues for innovative transport aircraft configurations in aerodynamic design.* PhD thesis, University of Naples Federico II, 2020.

[156] M. Sadraey. Spoiler Design. Technical report, RAE Bedford.

[157] M. Sadraey. *Aircraft Design: A Systems Engineering Approach.* John Wiley & Sons Inc., 2012.

[158] D.A. Sagerser, S. Lieblein, and R.P. Krebs. Empirical expressions for estimating length and weight of axial-flow components of VTOL powerplants. Technical report, NASA, 1971.

[159] V. Schmitt, J.P. Archambaud, K.H. Horstmann, and A. Quast. Hybrid laminar fin investigations. In *RTO AVT Symposium*, 2000.

[160] D. Scholz, R. Seresinhe, I. Staack, and C. Lawson. Fuel consumption due to shaft power off-takes from the engine. In *AST 2013, Workshop on Aircraft System Technologies*, 2013.

[161] A. Seitz. *Advanced Methods for Propulsion System Integration in Aircraft Conceptual Design.* PhD thesis, Technische Universitat Munchen, 2011.

[162] P. Sforza. *Commercial Airplane Design Principles.* Elsevier, 2014.

[163] Lissys Limited / Dr D. Simos. Piano. `https://www.lissys.uk/index2.html`, 2010. Accessed: 24/01/2022.

[164] Safran SNECMA. GE90 Commercial Aircraft Engines. `http://www.safran-aircraft-engines.com/file/download/fiche_ge90_ang.pdf`. Accessed: 09/03/2022.

[165] C. Soutis. Carbon fiber reinforced plastics in aircraft construction. *Materials Science and Engineering: A*, 412(1-2):171–176, 2005.

[166] K.L. Suder and J.D. Heidmann. Improvement of aeropropulsion fuel efficiency through engine design. In E.S. Nelson and D.R. Reddy, editors, *Green Aviation: Reduction of Environmental Impact Through Aircraft Technology and Alternative Fuels*, chapter 3. CRC Press, 2017.

[167] E. Torenbeek. *Synthesis of subsonic airplane design.* Springer Netherlands, 1982.

[168] E. Torenbeek. *Advanced Aircraft Design: Conceptual Design, Analysis and Optimization of Subsonic Civil Airplanes.* John Wiley & Sons Inc., 2013.

[169] V. Trifari. *Development of a Multi-Disciplinary Analysis and Optimization framework and applications for innovative efficient regional aircraft.* PhD thesis, University of Naples Federico II, 2020.

[170] Clean Sky 2 Joint Undertaking. Clean Sky 2 Joint Undertaking – Development Plan. Technical report, CSJU, 2017.

[171] Engineering Science Data Unit. Evaluation of the attenuation of sound by a uniform atmosphere - ESDU 78002. Technical report, ESDU, 1977.

[172] Engineering Science Data Unit. Estimation of lateral attenuation of air-to-ground jet or turbofan aircraft noise in one-third octave bands - ESDU 82027. Technical report, ESDU, 1982.

[173] Engineering Science Data Unit. Airframe noise prediction - ESDU 90023. Technical report, ESDU, 1990.

[174] Engineering Science Data Unit. Estimation of noise shielding by barriers - ESDU 79011. Technical report, ESDU, 1993.

[175] Engineering Science Data Unit. The correction of measured noise spectra for the effects of ground reflection - ESDU 94035. Technical report, ESDU, 1994.

[176] Engineering Science Data Unit. Prediction of near-field and far-field harmonic noise from subsonic propellers with non-axial inflow - ESDU 95029. Technical report, ESDU, 1996.

[177] Engineering Science Data Unit. Prediction of noise generated by fans and compressors in turbojet and turbofan engines - ESDU 98008. Technical report, ESDU, 1998.

[178] Stanford University. SUAVE. `https://suave.stanford.edu/`, 2022. Accessed: 24/01/2022.

[179] Stanford University. SUAVE - Turbofan modeling tutorial. `https://suave.stanford.edu/tutorials/turbofan.html`, 2022. Accessed: 24/01/2022.

[180] M. Walsh, W. Sellers, and C. McGinley. Riblet drag reduction at flight conditions. In *6^{th} Applied Aerodynamics Conference*, 1988.

[181] P. Walsh and P.P. Fletcher. *Gas Turbine Performance - 2^{nd}*. Blackwell Science, 1998.

[182] M.H. Waters and E.T. Schairer. Analysis of turbofan propulsion system weight and dimensions. Technical report, NASA, 1977.

[183] H. Wemming. Validation and integration of a rubber engine model into a mdo environment. Master's thesis, Linkoping University, Institute of Technology, Sweden, 2010.

[184] C. Werner-Westphal, W. Heinze, and P. Horst. Multidisciplinary integrated preliminary design applied to unconventional aircraft configurations. *Journal of Aircraft*, 45(2), 2008.

[185] Pratt & Whitney. Pratt & Whitney GTF Engine. Accessed: 17/01/2022.

[186] C.H. Wolowicz and R.B. Yancey. Longitudinal aerodynamic characteristics of light, twin-engine, propeller-driven airplanes. Technical report, 1972. `https://ntrs.nasa.gov/citations/19720018356`.

[187] F. Wolters, R.-G Becker, and M. Schaefer. Impact of alternative fuels on engine performance and co_2 emissions. In *ICAS 2012*, 2012.

[188] X.S. Yang. *Nature-inspired Metaheuristic Algorithms*. Luniver Press, 2010.

[189] F. Yin and A. Gangoli Rao. Performance analysis of an aero engine with inter-stage turbine burner. *The Aeronautical Journal*, 121(1245):1605–1626, 2017.

[190] T.M. Young and J.P. Fielding. Flight operational assessment of hybrid laminar flow control (hlfc) aircraft. In *CEAS/DragNet European Drag Reduction Conference*, 2001.

[191] O. Younossi, M.V. Arena, R.M. Moore, M. Lorell, J. Mason, and J.C. Graser. Military Jet Engine Acquisition: Technology Basics and Cost-Estimating Methodology. Technical report, RAND Corporation, 2002.

[192] W.E. Zorumski. Aircraft noise prediction program - Theoretical manual. Technical report, NASA, 1982.